The role of aquaporins in plant responses to drought

Johannes Daniel Scharwies

October, 2017

Thesis submitted for the degree of

Doctor of Philosophy

to the School of Agriculture, Food and Wine,

The University of Adelaide.

THE UNIVERSITY of ADELAIDE

CONTENTS

ABSTRACT

Aquaporins are a family of integral membrane proteins that facilitate transport of water and other small molecules across membranes. Regulation of their expression and/or activity has significant influence on transcellular water flow through changes in membrane permeability. Therefore, they can regulate water flow through plants and control the balance between water uptake from the soil and water loss via transpiration. The aim of this research was to understand aquaporin responses to drought and their relationship to changes in plant physiological parameters. Special attention was given to the role of the TIP2 sub-group of tonoplast localised aquaporins.

In *Arabidopsis thaliana*, drought had significant effects on aquaporin gene expression in leaves, while watering with abscisic acid (ABA), a plant hormone involved in drought signalling, had a different effect. Gene expression of most aquaporin genes was down-regulated during drought, but some isoforms (*AtPIP1;4*, *AtPIP2;4*, and *AtPIP2;5*) were up-regulated, similar to genes involved in abiotic stress responses through ABA. Changes in expression of down-regulated genes *AtPIP1;1*, *AtPIP1;2*, *AtPIP2;2*, and *AtTIP2;2* were observed concomitantly with changes in stomatal conductance in response to soil drying, but earlier than ABA induction.

TIP2 isoforms *AtTIP2;1*, *AtTIP2;2*, and *AtTIP2;3* that were expressed with a C-terminal GFP-tag under the control of a UBQ10 constitutive promoter in Arabidopsis showed tonoplast localisation. Preliminary results indicated significant higher leaf area and a divergent drought response of stomata for an overexpressing line of *AtTIP2;1*. Promoter-GUS lines demonstrated that promoters of *AtTIP2;1*, *AtTIP2;2*, and *AtTIP2;3* were mainly active around vascular tissue and potentially in stomata.

Genome editing was successfully used to create knockout lines for the TIP2 isoforms *AtTIP2;1*, *AtTIP2;2*, and *AtTIP2;3*. One base insertions in the coding sequence of these genes were induced by CRISPR-Cas, which cause frame-shifts that should disrupt protein function. Preliminary observations found a conditional short root phenotype for knockout lines of *AtTIP2;3*.

In the perennial model plant *Vitis vinifera*, differences in hydraulic control during mild water deficit and rehydration were found between the isohydric cultivar Grenache and the anisohydric cultivar Syrah mediated by aquaporins. Grenache showed stronger adjustment of leaf, plant, and root hydraulic conductance to changes in transpiration compared to Syrah. This was associated with stronger correlations between gene expression of some aquaporin isoforms in leaves and roots and plant hydraulic parameters in Grenache. While Grenache responded more readily to changes in soil water availability, Syrah still responded to VPD during mild water deficit.

The results demonstrated that significant relationships exist between aquaporin expression, plant hydraulic parameters, and leaf gas exchange both in the annual model species *Arabidopsis thaliana* and the perennial model species *Vitis vinifera*; even between cultivars difference were reflected by aquaporin expression. Changes in gene expression during drought could not be explained through regulation by ABA, but may be rather controlled by hydraulic signals. Aquaporin isoforms that were induced during drought could be involved in stress signalling. Overexpression of *AtTIP2;1* was associated with a different stomatal response to drought. The uncharacterised isoform *AtTIP2;3* may be involved in root growth.

DECLARATION

I certify that this work contains no material which has been accepted for the award of any other degree or diploma in my name, in any university or other tertiary institution and, to the best of my knowledge and belief, contains no material previously published or written by another person, except where due reference has been made in the text. In addition, I certify that no part of this work will, in the future, be used in a submission in my name, for any other degree or diploma in any university or other tertiary institution without the prior approval of the University of Adelaide and where applicable, any partner institution responsible for the joint-award of this degree.

I give consent to this copy of my thesis, when deposited in the University Library, being made available for loan and photocopying, subject to the provisions of the Copyright Act 1968.

I also give permission for the digital version of my thesis to be made available on the web, via the University's digital research repository, the Library Search and also through web search engines, unless permission has been granted by the University to restrict access for a period of time.

I acknowledge the support I have received for my research through the provision of an Australian Government Research Training Program Scholarship.

Signed.

Date.....13/10/2017.....

ACKNOWLEDGEMENTS

Studying my PhD at The University of Adelaide has been an incredible journey and I would like to take this opportunity to thank all the people that have been involved. First and foremost, I would like to thank my principal supervisor Prof Stephen Tyerman for giving me the opportunity to study my PhD in his laboratory. I'm very grateful for all the good discussions we had, for your encouragement to think outside the box, for giving me the freedom to explore new techniques, for all your help to attend conferences and visit other laboratories, and also for moral support in difficult times. I would also like to thank my co-supervisors Dr Sunita Ramesh, Dr Carlos Rodriguez Lopez, and Prof Matthew Gilliham. Thanks Sunita for all the good discussions, encouragement, and your help in the laboratory. Thanks Carlos for your friendship, for giving me new ideas, and discussing CRISPR-Cas. And thanks Matt for giving guidance and the important bits of advice when needed. I would also like to thank Dr Penny Tricker for her role as my external advisor. Thanks for encouraging me and giving me lots of useful advice. Special thanks goes also to Dr Cameron Grant who helped me with the soil-water-retention curve. I very much enjoyed discussing the theory and conducting the experiment. Thanks also to Drs Everard Edwards and Annette Boettcher from CSIRO for helping to measure abscisic acid concentration in leaf extracts. From our laboratory, I would like to thank Wendy Sullivan for all her help, for organising all the bits that are needed for experiments, and also for making anything possible. Wendy, the lab wouldn't run without you! Thanks also to Dr Rebecca Vandeleur for helping to organise contracts, trips, and equipment around the lab. I'm also very thankful to Dr Stefanie Wege for all her good advice on how to grow the perfect Arabidopsis, Confocal microscopy, any type of experiment, and for being a great lab bench mate. Thanks also to Dr Sam Henderson, Dr Brad Hocking, Asmini Athman, Dr Suzanne Zhao, Dr Rakesh David, Sam McGaughey, Dr Adam Croxford, Dr Jiaen Qiu, and Zeyu Xiao for being good friends in the laboratory and several trips to the local pub to discuss scientific matters. Also, thanks to Siyan Liao, Dr Bo Xu, Yue Qu, Yue Wu, Jonathan Wignes, Dr Stephanie Watts-Williams, Apriadi Situmorang, Ali Mafakheri, and all others from the Tyerman, Gilliham, and Rodriguez Lopez labs for being fantastic lab mates. Thanks to Kate Tepper for coffees and growing Arabidopsis together. I would also like to thank Assoc. Prof David Jeffery for his support as my Postgraduate Coordinator.

A particular rewarding experience was also my collaboration with Dr Silvina Dayer. Thanks Silvina for letting me join your project, for all the great (Skype) meetings, and for your trust. Writing the manuscript together was very enjoyable and a great lesson on collaboration. Thanks also to Dr Vinay Pagay and the other co-authors for great discussions.

I would also like to thank The University of Adelaide and the ARC Centre of Excellence in Plant Energy Biology for scholarships and funding to conduct my PhD research. Without the ARC CoE in PEB this research wouldn't have been possible and I met also many amazing people during the annual Centre retreats. Being part of the Centre has given me lots of opportunities to discuss my research, learn new techniques, meet other students with similar interests, and gain new ideas form hearing about other projects.

While I spent a lot of time at the laboratory during my PhD, I want to thank also all my great friends in Adelaide. Thanks to Markus and Sunny for being great friends and enjoying cake together. Thanks to Bea and Benny, Pedro and Lucia, Amina, Nikita, and Sofia, Antonella, Rowan, and Olivia, Diana and Natalia. Special thanks also to Barry and Kelly for so many fantastic dinners at your place, croquet, and so much support and mentoring. Being with you all in Adelaide makes this a truly special place. I would also like to thank all my friends in Germany for staying in contact with me.

A very special thanks goes to Lina Landinez. Thanks for sharing your life with me while we studied our PhDs. I learned a lot from you and from your family. It was an amazing time together in Adelaide and I will keep you in my heart forever. Thanks also to your family for being so open and sharing everything with me. Te quiero mucho!

Last but not least, I want to thank my family for giving me the freedom and support to be here in Adelaide. I know we are very far apart, but keeping in touch via Skype has helped me a lot and without you this wouldn't have been possible. I look forward to celebrating with you together.

1. INTRODUCTION AND LITERATURE REVIEW

1.1. Motivation

1.1.1. Introduction

Water transport in plants is important for growth, nutrient uptake and distribution, internal translocation of metabolites, and for maintenance of tissue hydration while water is inevitably lost to the atmosphere due to evapotranspiration. Plants first evolved in an aqueous environment (McCourt *et al.* 2004). These algae didn't have any vasculature for transport of water and nutrients. Water flow across membranes in the first simple organisms presumably occurred passively, as it does today for all biological membranes, but a family of channel proteins, called Major Intrinsic Proteins (MIPs), evolved to allow modulation of the permeability of membranes for water (Anderberg *et al.* 2011).

When plants became more complex and adapted gradually to living on the land, they formed waxy cuticles on their leaf surface to prevent water loss and pores on the leaf surface, which evolved into stomata, to regulate gas exchange with the atmosphere. Ultimately, they evolved vascular systems for transport of water, nutrients, and metabolites (Lucas *et al.* 2013).

Water flow from the soil, through the plant, to the atmosphere is largely controlled by the modulation of transpiration through stomata (Jones 1998). The balance between water uptake and water loss will determine the water status of the plant and if water loss is greater than water uptake, the plant will be in water deficit. While closing of stomata can reduce transpiration significantly during periods of limiting soil water supply, this could cause a reduction in carbon gain through photosynthesis, since CO_2 uptake is coupled to stomatal conductance. Therefore, water uptake and water loss needs to be finely tuned.

A major signal for stomatal closure is abscisic acid (ABA), a plant hormone that is produced during biotic and abiotic stress. ABA triggers a cascade of reactions that lead to the closure of stomata. At the same time, hydraulic conductance is reduced inside the plant (Tardieu and Davies 1993). A major regulator of hydraulic conductance are aquaporins, which are water permeable protein channels that belong to the family of major intrinsic proteins (MIPs). They regulate transcellular water flow through modulation of membrane permeability for water (Tyerman *et al.* 1999). It is suggested that they can also influence stomatal conductance via feed-forward control through changes in membrane conductance, for example in the bundle sheath cells (Sade *et al.* 2014b). Hence, both stomatal movement and hydraulic regulation through aquaporins are of major importance to water flow through the soil-plant-atmosphere continuum (Buckley 2005).

1.1.2. Previous research

My research on plant hydraulics started with a Masters by Research in grapevine (*Vitis vinifera*) in the laboratory of Prof. Stephen Tyerman at The University of Adelaide (Scharwies and Tyerman 2016). I investigated pre-harvest berry dehydration disorder in the grape cultivar Syrah. The berries of this cultivar are particularly prone to dehydration during hot and dry conditions just before they reach harvest (McCarthy 1999). This concentrates sugars and makes the juice suboptimal for wine production if high levels of alcohol are to be avoided.

I used plant physiology techniques like the XYL'EM flow meter to measure hydraulic conductance in grape clusters of the two contrasting grape cultivars Syrah and Grenache to understand if water transport was inhibited in Syrah. I observed significant differences in hydraulic conductance between different parts of the grape clusters in the two cultivars (Scharwies and Tyerman 2016). Furthermore, I also observed changes in hydraulic conductance throughout development. Grape clusters from the cultivar Grenache, which is characterised as near-isohydric, had generally higher hydraulic conductance, compared to grape clusters from the cultivar Syrah, which is characterised as anisohydric. While these observations were purely of physical nature, gene expression of aquaporins could have played a significant role in the observed changes of grape cluster hydraulics.

1.1.3. Research topic for my PhD

While investigating the biophysical properties of plant hydraulics in grape clusters for my Masters research degree, I became interested in gaining molecular biology experience and to investigate the contribution of aquaporins in plant hydraulics.

Previous research on drought-rehydration responses in grapevine, which had been conducted in the laboratory of Prof. Stephen Tyerman, showed that the leaf expression of the gene *VvTIP2;1*, which is a tonoplast localised aquaporin, was very well correlated to stomatal conductance during drought and rehydration (Pou *et al.* 2013). Furthermore, research by Sade *et al.* (2009) showed that overexpression of *SlTIP2;2* in tomato increased transpiration in well-watered and drought treated plants. The expression of the gene *TIP2;1* in Arabidopsis, barley, rice, and wheat was identified to be significantly down-regulated during drought stress across species from meta-analysis of microarray data (Shaar-Moshe *et al.* 2015). The only other genes encoding MIPs that were also significantly down-regulated across all species were: *TIP1;1*, *NIP5;1*, and *NIP4;2*. Apart from this, *AtTIP2;1* has also been shown to be important for lateral root emergence (Reinhardt *et al.* 2016) and to function as both a water and ammonia transporter in heterologous expression systems (Loque *et al.* 2005).

This interesting connection between tonoplast localised TIP2 aquaporins and gas exchange during drought stress led to the question about the function of these proteins. Therefore, my PhD research investigated the role of TIP2 aquaporins during drought and rehydration using gene expression and reverse genetic approaches.

During my PhD, I also became involved in a project of a visiting PhD student from Mendoza, Argentina (Silvina Dayer). Dr Dayer came to Adelaide to study the drought and rehydration responses of two grapevine (*Vitis vinifera*) cultivars, Grenache and Syrah, including changes in gene expression of some selected aquaporins. While the experiment itself was conducted by Dr. Dayer and other members of the laboratory, we collaborated on the qPCR analysis of gene expression, analysis of all the data from the project, and joint writing of a manuscript for publication.

1.2. Literature Review

1.2.1. Aquaporins in plants

1.2.1.1. Introduction

Aquaporins are water-conducting transmembrane channel-proteins from the family of major intrinsic proteins (MIPs) and are important for hydraulic regulation in animals and plants (Reizer *et al.* 1993; Tyerman *et al.* 1999). Preston *et al.* (1992) discovered an increased osmotic water permeability of *Xenopus* oocytes that were injected with RNA encoding the protein CHIP28, which is abundant in the plasma membrane of mammalian red blood cells. This water permeability could be inhibited with the water channel blocker mercury chloride. They concluded that CHIP28 (later called aquaporin 1) must be a water channel protein, which with the protein structure and method of water selectivity in the pore earned Peter Agre, the senior author of this research, the 2003 Nobel Prize in Chemistry (Knepper and Nielsen 2004). Interestingly, Preston *et al.* (1992) were not the first to discover water permeability for this protein, which led to some controversy later on (Kuchel 2006). In 1986, the group of Gheorghe Benga published research identifying membrane proteins in red blood cells involved in water transport (Benga *et al.* 1986a; Benga *et al.* 1986b).

In plants, the discovery of aquaporins started with the isolation of an abundant protein of a relative molecular mass M_r = 25,000 from protein body membranes of *Phaseolus vulgaris* L. cotyledons, which was called TP 25 (Pusztai *et al.* 1979). Johnson *et al.* (1989) made an antiserum for this protein and showed that it was present in a wide range of different seeds and was localised to the tonoplast. They hypothesised that it may have a function to protect the integrity of the tonoplast during dehydration-rehydration of seed. Shortly after Preston *et al.* (1992) discovered that aquaporin 1 is a water channel in

red blood cells, Maurel *et al.* (1993) conducted a similar experiment with AtTIP1;1 from *Arabidopsis thaliana* in *Xenopus* oocytes and demonstrated water transport activity for the tonoplast localised protein.

In *Arabidopsis thaliana*, four subfamilies containing 35 MIP encoding genes have been described (Johanson *et al.* 2001); a phylogenetic tree is shown in Figure 1. The largest of these subfamilies are 13 plasma membrane intrinsic proteins (PIPs) and 10 tonoplast intrinsic proteins (TIPs), which are (supposedly) localised in the plasma membrane and tonoplast, respectively. This has been confirmed in most cases, but not all (Barkla *et al.* 1999). The smaller subfamilies are nine Nodulin26-like intrinsic proteins (NIPs), which are localised in both the plasma membrane and endoplasmic reticulum, and three small intrinsic proteins (SIPs), which are localised in the rough endoplasmic reticulum (Maurel *et al.* 2008).

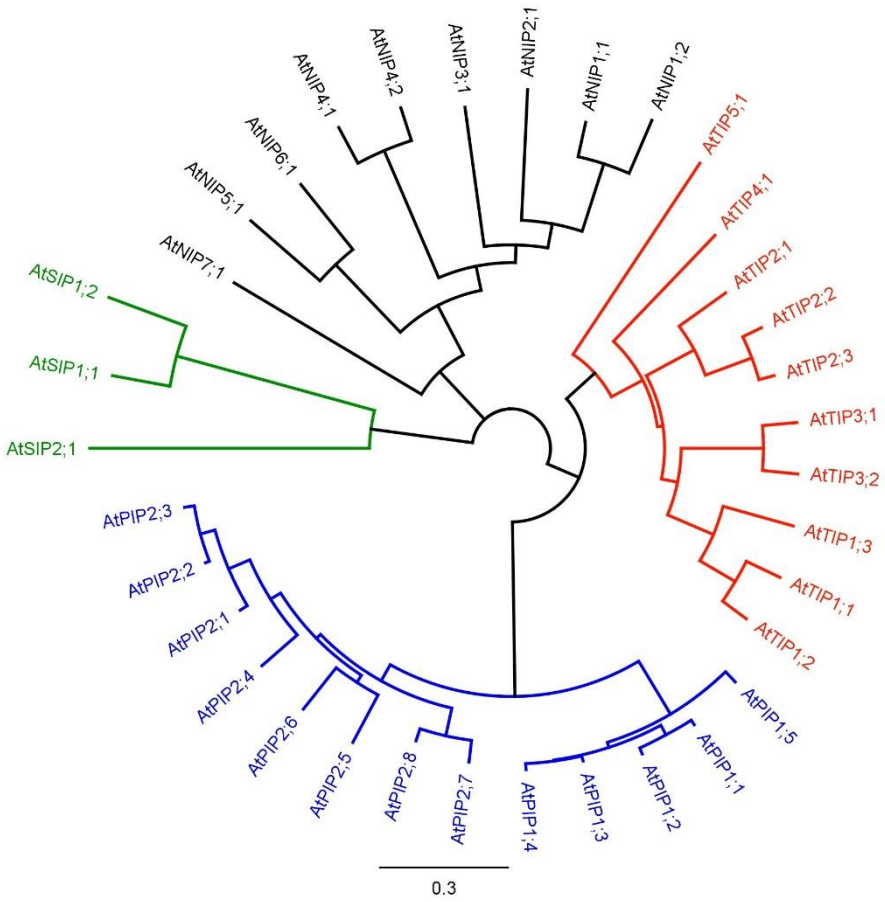

Figure 1. Unrooted phylogenetic tree of the entire family of 35 Major Intrinsic Proteins (MIPs) from *Arabidopsis thaliana*. The phylogenetic tree was constructed from amino acid sequences using Tree Builder in Geneious® 8.1.9 software (Biomatters Ltd.). The distance matrix was calculated as global alignment with free end gaps (Gap open penalty: 12; Gap extension penalty: 3) and a Blosum62 cost matrix. The tree was build using the Jukes-Cantor genetic distance model and the Neighbor-Joining method. All MIPs were divided into four families: plasma membrane intrinsic proteins (PIPs), tonoplast intrinsic proteins (TIPs), NOD26-like intrinsic proteins (NIPs), and small intrinsic proteins (SIPs). The scale bar shows the mean distance of 0.3 changes per amino acid.

Other plant species showed varying numbers of MIPs. In *Physcomitrella patens*, 23 MIPs were identified (Johanson and Danielson 2008). These include three additional subfamilies called X Intrinsic Proteins

(XIPs), Hybrid Intrinsic Protein (HIP), and a GlpF-like intrinsic protein (GIP) (Gustavsson *et al.* 2005). In the crop species *Zea mays*, 36 MIPs were identified (Chaumont *et al.* 2001), while in *Oryza sativa*, 33 MIPs were found (Sakurai *et al.* 2005). In the perennial model species, *Vitis vinifera*, 28 MIPs were identified (Fouquet *et al.* 2008).

Evolutionary studies suggest that members of the MIP family originate from two divergent bacterial paralogues, an aquaporin and a glycerol transporter (Park and Saier 1996). It is not fully known whether this transfer to Eukaryota occurred only via horizontal gene transfer or also by symbiosis (Finn and Cerda 2015). The NIPs may have originated from a single event of horizontal gene transfer from bacteria and have been recruited to transport glycerol due to the lack of aquaglyceroporins in plants (Zardoya *et al.* 2002). Based on the comparison of MIPs from higher plants to MIPs in the moss *Physcomitrella patens*, a bryophyte, Borstlap (2002) argues that MIPs diversified into PIPs, TIPs, NIPs, and SIPs before the divergence of bryophytes into tracheophytes (vascular plants), and even PIPs diversified into PIP1 and PIP2 sub-groups. A higher evolutionary constraint on PIP aquaporins, demonstrated by greater amino acid identity, was also discussed by Soto *et al.* (2012). They hypothesised that the demonstrated interaction between different PIP isoforms, i.e. formation of heterotetramers, could slow the rate of evolution due to necessary coevolution that would need to happen between partners. Based on the differences between *Physcomitrella patens* and higher plants, Borstlap (2002) also argued that TIPs must have diversified into TIP1, TIP2, and TIP3 sub-groups when vascular plants established. Johanson and Danielson (2008) suggested that these sub-groups may have taken over some functions of missing subfamilies that are still present in bryophytes like *Physcomitrella patens* (e.g. HIP, XIPs).

1.2.1.2. Molecular structure of aquaporins

MIPs have a molecular mass of between 26-35 kDa, and are characterised by six membrane-spanning alpha-helix domains (H1-H6) connected by five loops (a-e) (Figure 2). The first crystal structure was solved for the mammalian aquaporin 1 (Sui *et al.* 2001). In plants, crystal structures have been solved for the spinach plasma membrane aquaporin *SoPIP2;1* (Tornroth-Horsefield *et al.* 2006) and the Arabidopsis tonoplast aquaporin *AtTIP2;1* (Kirscht *et al.* 2016). Structural analysis revealed that two of the loops (b, d) are exposed to the cytoplasm, and three loops (a, c, e) are exposed to the extracellular space (Quigley *et al.* 2002). Both the N and C terminal ends are exposed to the cytoplasm. Since transmembrane helices H1-H3 and H4-H6 are similar but of opposite orientation, it is thought that they were created by a tandem, intragenic, duplication event (Reizer *et al.* 1993). For *SoPIP2;1* it was confirmed, that loop D closes the pore from the cytoplasmic side (Tornroth-Horsefield *et al.* 2006). This closure is triggered by the protonation of a conserved histidine (His 193 in *SoPIP2;1*), that can occur during anoxia due to a reduction cytosolic, or by the dephosphorylation of two conserved serine residues (Ser 115 and Ser 274 in SoPIP2;1) during drought stress.

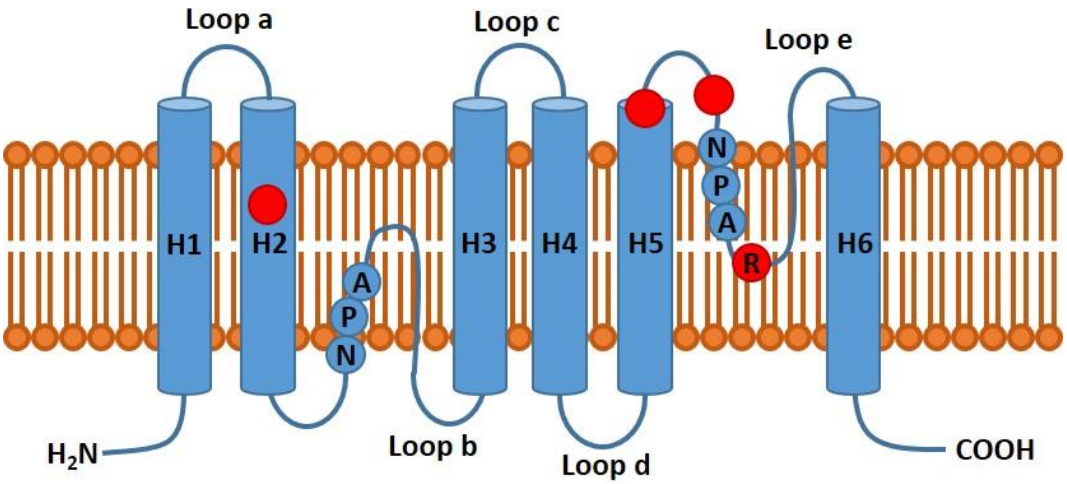

Figure 2. Schematic membrane topology of Major Intrinsic Proteins. Six membrane-spanning alpha-helix domains (H1-H6) are connected by five loops (a-e). Loops b and e, which form the pore, carry conserved Asn-Pro-Ala motifs (NPA motif). The four key residues of the aromatic/Arg filter are located in H2, H5, and loop e (red). The C- and N-terminal ends are exposed to the inside of the membrane (e.g. cytoplasm).

Aquaporins occur as tetramers in membranes and their pore is formed by the loops b and e (Figure 2). These two loops both carry a conserved Asn-Pro-Ala motif (NPA motif), which in addition to an aromatic/Arg filter the main pore constriction for transport of substrates (Reizer *et al.* 1993; Maurel *et al.* 2008). The pore itself is very hydrophobic and water molecules pass through it in a single file (Quigley *et al.* 2002). The asparagine residues within the NPA motifs control the passage of water by forming hydrogen bonds with a single water molecule, preventing the passage of protons (Tajkhorshid *et al.* 2002).

Particular interest has been paid to the structural background of ammonia permeability for *AtTIP2;1* (Kirscht *et al.* 2016). It was revealed that a histidine in loop c is responsible for the ammonia selectivity by interacting with an arginine in the helix of loop e. This pushes the arginine side chain to the side of the pore. Furthermore, the authors speculate about a water filled side pore, which might deprotonate the ammonium ions and improve ammonia permeability.

It has been shown that the C-terminal part of loop e is important for the formation of heterotetramers between PIP1 and PIP2 aquaporins in *Zea mays* (Fetter *et al.* 2004). Also, in PIP2 aquaporins from the same species a LxxxA motif was identified in the transmembrane domain H3, which is necessary for trafficking from the endoplasmic reticulum to the plasma membrane (Chevalier *et al.* 2014).

1.2.1.3. Trafficking and localisation in plant membranes

Aquaporins are made in the endoplasmic reticulum and need to be transported to their destination membrane, i.e. plasma membrane or tonoplast. In their review, Hachez *et al.* (2013) explain how PIP aquaporins are synthesised in the rough endoplasmic reticulum and homo- and heterotetramers (between PIP1 and PIP2 sub-groups) would assemble. They transit through the Golgi apparatus and then the trans-

Golgi network. Once loaded into secretory vesicles, they're shipped to the plasma membrane. In this process, diacidic motifs at the N-terminus of PIP aquaporins are used to route them to the plasma membrane (Zelazny *et al.* 2009). Additionally, the LxxxA motif in the transmembrane helix 3 was identified to be important for localisation to the plasma membrane (Chevalier *et al.* 2014). For tonoplast aquaporins, it was found that they can be trafficked with a Golgi dependent pathway (TIP1;1) or a Golgi independent pathway to the vacuole membrane (Rivera-Serrano *et al.* 2012).

The first MIP in plants was isolated from protein storage vacuoles in *Phaseolus vulgaris* (Pusztai *et al.* 1979; Johnson *et al.* 1989). More MIPs were found in tonoplast fractions and they were called tonoplast intrinsic proteins (TIPs), describing their localisation (Ludevid *et al.* 1992). MIPs that were found to be localised to the plasma membrane were called plasma membrane intrinsic proteins (PIPs) (Weig *et al.* 1997). Different TIP isoforms were used as markers for vacuoles with different functions (Jauh *et al.* 1999). However, a proteomics study on plasma membrane (PM) and tonoplast (TM) fractions of *Mesembryanthemum crystallinum* showed that some MIPs do localise to both PM and TM (Barkla *et al.* 1999). In a review, Wudick *et al.* (2009) show that aquaporins were found to be localised to many different intracellular compartments. Most TIPs were found to be localised to the vacuole membrane, but one study also found some TIPs in the chloroplast envelope (Ferro *et al.* 2003). This localisation remains to be confirmed. The aquaporin McTIP1;2 was observed in endosomes upon osmotic stress (Vera-Estrella *et al.* 2004). Experiments on the effects of salinity also suggested that PIPs and TIPs re-localised into intracellular structures upon stress (Boursiac *et al.* 2005). Therefore, the localisation of some aquaporins may also depend on environmental conditions.

1.2.1.5. Function of aquaporins

Detailed studies of the different aquaporin isoforms have found that many transport also other small molecules besides water (Tyerman *et al.* 2002). These include glycerol, CO_2, ammonia, urea, hydrogen peroxide, boron, and even ions like Na^+ (Weig and Jakob 2000; Uehlein *et al.* 2003; Loque *et al.* 2005; Bienert *et al.* 2007; Yang *et al.* 2015; Byrt *et al.* 2017).

Glycerol transport activity was found for the proteins AtNIP1;1 and AtNIP1;2 in Arabidopsis thaliana (Weig and Jakob 2000). Later it was discussed that this transport function may have been adopted to replace aquaglyceroporins, which are present in bacteria, but not in plants (Zardoya *et al.* 2002). A more exotic GlpF-like intrinsic protein (GIP), identified in the moss *Physcomitrella patens*, showed glycerol transport similar to NIPs (Gustavsson *et al.* 2005).

Transport of a gas, CO_2, was first shown for the aquaporin NtAQP1 from *Nicotiana tabacum* in *Xenopus* oocytes (Uehlein *et al.* 2003). Plants that were deficient or overexpressing NtAQP1 showed that this aquaporin was involved in mesophyll conductance to CO_2 and, hence, very important for the efficiency of

photosynthesis (Flexas *et al.* 2006). In Arabidopsis, AtPIP1;2 was suggested to be of major importance for cellular CO_2 uptake (Uehlein *et al.* 2012).

As well for NtAQP1, transport of glycerol and urea was demonstrated (Otto and Kaldenhoff 2000). In *Arabidopsis thaliana*, the protein AtNIP5;1 was found to transport urea and it was suggested that this might be important for urea uptake by roots (Yang *et al.* 2015).

Heterologous expression of TIP2;1 and TIP2;3 from *Arabidopsis thaliana* and wheat in *Xenopus* oocytes found that both isoforms transport ammonium (Holm *et al.* 2005; Loque *et al.* 2005; Bertl and Kaldenhoff 2007). Recently, the crystal structure of AtTIP2;1 was solved and important residues identified that determine the ammonia selectivity, which is special to TIP2 aquaporins (Kirscht *et al.* 2016). While it has been hypothesised that this transport function might be important for nitrogen-use efficiency, no phenotype has yet been identified in plants (Loque *et al.* 2005).

Another nitrogen source that has been shown to be transported by aquaporins is urea (Yang *et al.* 2015). It was shown that *AtNIP5;1* expression was up-regulated in seedlings grown on media with urea as nitrogen source and that the protein acted as a channel for urea when expressed in *Xenopus* oocytes.

The signalling compound, hydrogen peroxide (H_2O_2), was shown to be transported by the aquaporins AtTIP1;1 and AtTIP1;2 from *Arabidopsis thaliana* in a yeast assay (Bienert *et al.* 2007). Also yeast growth assays with AtPIP2;1, AtPIP2;2, AtPIP2;4, AtPIP2;5, and AtPIP2;7 found potential transport of H_2O_2 (Dynowski *et al.* 2008; Hooijmaijers *et al.* 2012; Tian *et al.* 2016; Rodrigues *et al.* 2017). Therefore, these could be important for stress signal transduction. An *in planta* study of *AtPIP1;4*, a H_2O_2 transporter, showed that gene expression was indeed induced by pathogens and further that apoplastic H_2O_2 was transported into the cytoplasm to trigger stress responses (Tian *et al.* 2016). Similar to this, Rodrigues *et al.* (2017) showed that phosphorylation of AtPIP2;1 during pathogen attack mediated stomatal closure through activation of H_2O_2 transport into guard cells.

A dual water and ion channel function was shown for AtPIP2;1 by Byrt *et al.* (2017). Interestingly, heterotetramers of AtPIP1;2 and AtPIP2;1 showed water permeability but no ion conductance. Ion conductance was sensitive to Ca^{2+} and pH changes. It remains to be shown if this function is related to salinity resistance *in planta*.

Other transport substrates that have been identified to be transported by various aquaporins include acetamide, arsenic, boric acid, formamide, lactic acid, methylammonium, Al citrate complex, and silicon (Maurel *et al.* 2008; Wang *et al.* 2017).

1.2.1.6. Regulation of aquaporin activity

Aquaporin activity, and therefore plant water relations, can be regulated on many different levels; regulation of gene expression, protein synthesis and heteromerization, trafficking, post-translational modification, and also protein turnover and degradation (Chaumont and Tyerman 2014).

Aquaporin gene expression changes throughout plant development and during biotic or abiotic stress. Aquaporins expression has been found to change with time of the day (Harmer *et al.* 2000). During drought stress, some isoforms are upregulated, while other isoforms are downregulated (Alexandersson *et al.* 2010). The expression is often regulated by transcription factors. It was found that the transcription factors *RAP2.4* and *RAP2.4B* regulate the expression of several aquaporin genes (PIP2;1, PIP2;2, PIP2;3, TIP1;1, TIP2;2, TIP2;3) in response to drought (Rae *et al.* 2011). Another transcription factor, TRANSLUCENT GREEN, was suggested to control the internal water balance of plants by binding to the promoters of *AtPIP2;2*, *AtTIP1;1*, and *AtTIP2;3* in *Arabidopsis thaliana* (Zhu *et al.* 2013).

Once aquaporin monomers are made, they assemble into tetramers (Reizer *et al.* 1993). Besides homotetramers, these can also be heterotetramers that appear to modify both membrane targeting and water transport activity based on heterologous expression (Fetter *et al.* 2004). This study showed heteromerization between PIP1 and PIP2 aquaporins from *Zea mays*, which were co-injected in *Xenopus* oocytes. While PIP1 homotetramers had a low water transport activity, heteromers between PIP1 isoforms or between PIP1 and PIP2 isoforms had an increased water transport activity which may be important to regulate their function in membranes. Dual function of water and CO_2 transport were also influenced by heteromerization, as demonstrated for the Tobacco aquaporins NtAQP1 and NtPIP2;1 (Otto *et al.* 2010).

Besides the importance of heteromerization in modulation of water and/or CO_2 transport activity, it seems to have a role in the control of trafficking of aquaporins from the endoplasmic reticulum to the plasma membrane (Zelazny *et al.* 2007). Using FRET imaging in *Zea mays*, they showed that interaction between PIP1 and PIP2 aquaporins is needed for PIP1 transport to the plasma membrane. Another study in *Zea mays* showed that post-Golgi trafficking of ZmPIP2;5 is controlled by SYP121, a syntaxin involved in vesicle trafficking (Besserer *et al.* 2012).

Soon after seed specific TIP aquaporins were discovered, it was also observed that they were phosphorylated (Johnson and Chrispeels 1992) and phosphorylation changed their water transport activity (Maurel *et al.* 1995). When phosphorylated, the channel is in an open state, while dephosphorylation closes the channel (Tornroth-Horsefield *et al.* 2006). Different abiotic stresses and different nutrient treatments changed the phosphorylation status of many aquaporins (Pietro *et al.* 2013; Vialaret *et al.* 2014). A sucrose-induced receptor kinase, SIRK1, was identified in *Arabidopsis thaliana* which phosphorylates PIP aquaporins and may be involved in the response to sucrose-related osmotic

changes in the root environment (Wu *et al.* 2013). Apart from phosphorylation, post-translational modifications also include acetylation, deamidation, and methylation (Pietro *et al.* 2013). As explained before, cytosolic pH and ROS are also involved in gating of aquaporins as occurs under hypoxia and salinity, respectively (Tournaire-Roux *et al.* 2003; Boursiac *et al.* 2008). Hypoxic stress, which causes a decrease in cytosolic pH, results in protonation of a histidine residue in Loop d that closes the pore (Tornroth-Horsefield *et al.* 2006). Cytoplasmic sensing of aquaporins was found to include also the sensing of calcium ions (Gilliham *et al.* 2011). It was found that aquaporins of isolated plasma membrane vesicles from *Beta vulgaris* were sensitive to a dual range of cytoplasmic calcium concentrations allowing a dynamic gating mechanism (Alleva *et al.* 2006). It was shown from the crystal structure solution of the open and closed SoPIP2;1 that Ca^{2+} could bind near loop d and stabilise the closed conformation of the channel (Tornroth-Horsefield *et al.* 2006).

Furthermore, internalisation of aquaporins during abiotic stress like salt was observed (Ueda *et al.* 2016), which is likely related to phosphorylation (Prak *et al.* 2008). During drought stress, trafficking of aquaporins to the plasma membrane was inhibited and proteins were ubiquitinated for subsequent degradation (Lee *et al.* 2009).

Besides gating by protein modification and chemical signals, an influence of mechanical stimuli has been observed for aquaporins. The application of large pressure pulses in cortical cells of young corn roots caused a reduction of hydraulic conductance which could be reversed by the application of abscisic acid (Wan *et al.* 2004). It was proposed that the energy input due to the pressure pulse could cause confirmation changes in the pore of aquaporins resulting in a closure. In another study it was found that solutions of high osmotic strength would cause a reduction of aquaporin mediated water transport, explained by a cohesion/tension model that predicted a collapse of the pore due to high negative pressure inside the pore (Ye *et al.* 2004). However, pressure pulses or osmotic changes could have also been detected by mechano- or osmosensors which could have relayed the signal to aquaporins via phosphorylation or other post-translational mechanisms.

This brief overview of gating mechanisms for aquaporins shows that plants have many means to regulate water flow via aquaporins by opening and closing them in addition to changing their density in different membranes. Therefore, there is no simple on/off mechanism. When analysing expression profiles for aquaporins it is always important to verify if these proteins are made, where they are localised, and if they are active, since many post-translational gating mechanisms exist. Nevertheless, upstream regulation of protein abundance is very important since protein is costly to make.

1.2.2. Aquaporins in plant growth and water relations

1.2.2.1. Introduction to plant water relations

Water in roots and leaves constitute significant pools between the soil and the atmosphere. The rate of water flow between these pools depends on the magnitude of the hydraulic gradients and the conductance for water flow (Dixon and Joly 1895; Tyree 1997).

Leaves need to maintain the right balance between the supply of water from the soil through the roots and stem, and the loss of water due to transpiration. This supply is controlled in part by the roots that sense soil moisture and adjust their hydraulic conductance to the demand of water by the shoot (Steudle and Peterson 1998). Leaves are very prone to dehydration due to their large surface area exposed to the atmosphere; a necessity for light capture for photosynthesis. Water loss from leaves predominantly occurs through open stomata, and to a lesser extent through the leaf epidermis and cuticle. Stomata regulate leaf gas exchange in plants. They control the uptake of carbon dioxide (CO_2) for photosynthesis and water loss via transpiration (Jones 1998). Stomatal regulation is important for plants since they need to maintain the right balance between water loss via transpiration and CO_2 uptake for photosynthesis. As such, much research has been devoted to understanding the components underpinning stomatal control (Hetherington and Woodward 2003).

Recent research has also shown the importance of the control of the leaf water pool by leaf hydraulic conductance (Zwieniecki *et al.* 2007). It was hypothesised that hydraulic conductance of specific tissues in the leaf can be rate limiting and determine characteristics of water use in plants (Tardieu and Simonneau 1998; Schultz 2003). The causes and significance of the generally observed positive correlations between leaf hydraulic conductance and stomatal conductance has been discussed (Shatil-Cohen *et al.* 2011; Dodd 2013; Pantin *et al.* 2013). The factors that control internal leaf hydraulics are much less well understood than that of stomatal control, therefore indicating a pressing research priority.

1.2.2.2. Regulation of plant hydraulics by aquaporins

Water flow in plants occurs along hydraulic gradients as described by the generally accepted cohesion-tension theory (Dixon and Joly 1895). In plants, water can take different pathways through tissues, i.e. apoplastic, symplastic, and transcellular (Steudle and Jeschke 1983; Steudle and Peterson 1998). In the root water can flow in extracellular spaces (apoplastic pathway). In some tissues however extracellular water flow is restricted by hydrophobic coatings of the cell walls such as suberin and lignin. An important example of this is the endodermis in roots that prevents apoplastic water uptake into the stele containing the vascular tissues. Therefore, water has to cross cell membranes with the advantage that this allows selective uptake of minerals to the shoot via the xylem. Water can also flow through intracellular spaces and move between cells via plasmodesmata. This pathway is referred to as the symplastic pathway. A

third pathway, the transcellular pathway, describes water flow through membranes, including the tonoplast.

Cell membranes that have to be crossed in the transcellular pathway are permeable to water but, due to their hydrophobic interior, permeability for water is sometimes much lower than for small uncharged apolar molecules. This can lead to negative reflection coefficients as measured in *Chara coralline* (Steudle and Tyerman 1983). Ray (1960) and Dainty (1963) discussed in their articles the possibility of water permeable pores in membranes, since previous research on osmosis found that water was moving too fast for simple diffusion through the membrane. With the use of mercurial compounds on red blood cells it was established that membrane permeability could be reduced to that of simple lipid bilayers and that the difference must be accounted for by water flow through mercurial sensitive water channels (Macey 1984). Similar to this, protein inhibitors were used in plant cells to test the existence of water channels (Wayne and Tazawa 1990). Finally, as discussed above, the responsible proteins, MIPs, were identified in animal and plant cells (Preston *et al.* 1992; Maurel *et al.* 1993). Since then, extensive research on aquaporins has shown their fundamental role in plant water transport (Chaumont and Tyerman 2014).

Water transport through aquaporins is not only important in tissues that have a restricted apoplastic water flow, but also important for the regulation of the cell water pool. The largest water pool in mature plant cells is the vacuole constituting up to 90% of the cell volume (Taiz 1992). Maintenance of water balance between cytosol and vacuole is important to restrict large volume changes of the cytoplasm that could damage the cytoskeleton and lead to large changes in concentration of metabolites and enzymes (Tyerman *et al.* 1999).

The first plant water channel identified, *AtTIP1;1*, was localised to the tonoplast (Johnson *et al.* 1989). Functional analysis of TIP aquaporins was mainly carried out in heterologous systems like *Xenopus* oocytes (Maurel *et al.* 1993). However in *Xenopus* oocytes, TIPs localise to the plasma membrane since they don't have organelles like the plant vacuole. In plants, it is much harder to investigate the function of TIP aquaporins and their contribution to plant water relations, since the plasma membrane provides the primary initial membrane barrier for water flow. Therefore, changes in tonoplast permeability could be masked by the plasma membrane. Initial measurements on the water permeability of plasma membrane and tonoplast found an about 100-fold higher permeability of the tonoplast and, hence, the tonoplast is often seen as non-limiting to water flow (Kiyosawa and Tazawa 1977; Maurel *et al.* 1997). This could be an important feature to balance volume changes between the cytosol and vacuole as mentioned above (Tyerman *et al.* 1999). However, other experiments in *Chara corallina* using biphasic pressure relaxation curves suggested only a 1.5 to 2.5 fold higher permeability of the tonoplast compared to the plasma membrane (Wendler and Zimmermann 1985a, 1985b). While TIP aquaporins are highly abundant on the

tonoplast and are shown to function as water channels, it still remains to be investigated how much they contribute to the regulation of transcellular water flow.

Hydraulic regulation of root water transport by aquaporins has been studied in several plants (Tyerman *et al.* 1999; Hose *et al.* 2000; Tournaire-Roux *et al.* 2003; Boursiac *et al.* 2005; Vandeleur *et al.* 2014). For grapevine (*Vitis vinifera*), Vandeleur *et al.* (2009) found that the differential expression of *VvPIP1;1*, which interacts with *VvPIP2;2*, may regulate root hydraulic conductance in response to changes in transpiration during drought. Once water reaches the stele in the root, transport to the shoot occurs via the xylem; the main conducting tissue for water flow from the root to the shoot (Taiz and Zeiger 2010). The xylem consists of tracheids and vessel elements; lignified empty cells that are designed to conduct water with high hydraulic conductivity and to resist collapse under high tension (negative pressure). They are surrounded by parenchyma cells and fibres. Xylem hydraulic conductance depends primarily on the number of vessels/tracheids and their diameter (Tyree and Ewers 1991; Steppe and Lemeur 2007). It has been proposed that xylem hydraulic conductance can also be regulated by the shrinking and swelling of pectin in the cellulosic pit membranes that join adjacent vessel elements (Zwieniecki *et al.* 2001). Moreover, embolisms can form in the xylem under highly negative pressures (Sperry *et al.* 1994). Although these are known to be reversible, the mechanisms controlling such reversion are still unclear. There is evidence to indicate that aquaporins may be involved in embolism repair (Secchi *et al.* 2017).

In contrast to xylem vessels and tracheids, the phloem sieve elements are living cells that transport products of photosynthesis and nutrients. Phloem tissue consists of sieve cell elements and their associated companion cells, as well as other parenchyma cells (Taiz and Zeiger 2010). Water serves as a solvent in this vascular tissue for photosynthetic products and nutrients. Transport is from source to sink as described by the Munch pressure flow model (Münch 1930; Patrick 2013). Here aquaporins may be important in clearing phloem derived water from sink tissue. A study in French bean seed found that aquaporins localised to vascular parenchyma cells (Zhou *et al.* 2007). It was hypothesised that aquaporins could regulate water flow from the sieve elements and its subsequent recycling to the xylem. A different study in poplar found PIP2 aquaporins localised to the plasma membrane of sieve elements and it was proposed that these may be important in regulation of water exchange between phloem and xylem (Stanfield *et al.* 2017).

In leaves, water has to move from the xylem to the epidermis and stomata where transpiration occurs. Research on rehydration kinetics of leaves has shown that differences exist between plant species on how well different tissues inside the leaf are hydraulically connected and the pathways for water flow from the xylem to the stomatal cavities (Zwieniecki *et al.* 2007). These differences in hydraulic connection might

create various water pools inside the leaf that could contribute differently to the transpiration stream (Canny *et al.* 2012).

Shatil-Cohen *et al.* (2011) conducted an experiment demonstrating the importance of the bundle-sheath cells as a hydraulic barrier in leaves during drought and ABA treatment. Bundle-sheath cells showed a reduction in osmotic water permeability upon drought or ABA treatment, while mesophyll cells didn't respond. This reduction could also be induced using aquaporin blockers. Hence, they proposed that bundle sheath cells could be a stress sensor in leaves that induce changes in leaf hydraulic conductance by the regulation of aquaporins in response to xylem-born stress signals like ABA. Following this, ABA induced reduction of leaf hydraulic conductance and stomatal closure was observed in an ABA insensitive mutant (*ost2-2*) of *Arabidopsis thaliana* (Pantin *et al.* 2013). It was proposed that stomata were closed by an alternative hydraulic regulatory pathway that could act independently from the biochemical pathway of ABA stress sensing. In this pathway, stomata could be closed via the reduction of leaf hydraulic conductance or decreased turgor in guard cells mediated by aquaporins. Finally, research by Sade *et al.* (2014b) showed that a knock-down of PIP aquaporins in bundle sheath cells caused a reduction of leaf hydraulic conductance. They concluded that aquaporins in the bundle sheath cells may have an important role in the regulation of leaf hydraulic conductance serving as a feed-forward control signal for stomatal conductance. Past the bundle-sheath, it was suggested from calculations that the apoplastic pathway provides the majority of conductance (Buckley 2015), but no direct experimental evidence has been obtained yet. It also remains open, whether TIP aquaporins are involved in regulating leaf hydraulic conductance.

Light-dark transitions and air humidity are also important regulators of aquaporins in leaves. It was found that rosette hydraulic conductance in *Arabidopsis thaliana* was regulated via phosphorylation of *AtPIP2;1* in response to darkness. Moreover, it was observed that low atmospheric relative humidity caused an increase of leaf specific hydraulic conductance in *Arabidopsis thaliana* (Levin *et al.* 2007).

The terminal barrier for water flow from the soil water pool, through the plant, to the atmospheric water pool are the stomatal guard cells. There are differences between plants in how stomata control plant water status such that two extremes can be identified in the degree to which water potential is maintained (Tardieu and Simonneau 1998). Plants that show greater stomatal control and, therefore, maintain higher leaf water potentials under water stress are characterised as isohydric. In contrast, plants that are less conservative in their water usage develop lower leaf water potentials under stress and are characterised as anisohydric. Grapevine (*Vitis vinifera*) is rather unique in this respect since different cultivars can show diverging characteristics; for example. Grenache is considered more isohydric and Syrah more anisohydric (Schultz 2003; Soar *et al.* 2006). While root hydraulic properties linked to aquaporin behaviour

in addition to stomatal control are linked to anisohydric-isohydric behaviour (Vandeleur *et al.* 2009) and a model describing interactions of chemical and hydraulic signals was proposed (Tardieu and Simonneau 1998), a whole plant approach to understand the mechanistic difference is so far missing. As mentioned above, research also highlights the importance of leaf hydraulic conductance in response to changes in vapour pressure deficit of the atmosphere and leaf internal CO_2 conductance which may be linked to stomatal conductance possibly by aquaporins (Shatil-Cohen *et al.* 2011; Flexas *et al.* 2013; Pantin *et al.* 2013).

1.2.2.3. Function of aquaporins in plant growth

When TIP aquaporins were first observed in Arabidopsis, it was also shown that their expression is correlated to cell expansion (Ludevid *et al.* 1992). Experiments on maize plants showed that a reduction of root hydraulic conductance by blocking aquaporins had a significant effect on cell turgor and leaf elongation (Ehlert *et al.* 2009). Altering the expression of the gene *NCED*, which is involved in ABA synthesis had an effect on the expression and protein abundance of PIP aquaporins and root hydraulic conductance, which was also correlated to changes in leaf elongation (Parent *et al.* 2009). Overexpression of *SlTIP2;2* or *NtAQP1* in tomato both had a positive impact on biomass and yield under stress conditions like drought and salinity (Sade *et al.* 2009; Sade *et al.* 2010). Lee *et al.* (2012) showed that overexpression of *AtTIP2;5* in Arabidopsis could mitigate the negative effect of low root temperature on shoot growth. While low root temperature caused a reduction of root cell hydraulic conductivity in wild-type plants, overexpression plants didn't respond to low root temperature. In their review Tardieu *et al.* (2010) also discussed the role of aquaporins on hydraulic conductivity and subsequently leaf growth. They concluded, that increased levels of ABA can have a positive effect on leaf growth under well-watered conditions through increasing hydraulic conductance, but can have an opposite effect under water deficit conditions. Furthermore, Pantin *et al.* (2011) suggested that initial leaf growth is limited by metabolism, while later stages of leaf growth are limited by hydraulics. Therefore, aquaporins could become of major importance for leaf elongation especially in later stages of leaf development.

Mutants of *AtTIP1;3* and *AtTIP5;1* in Arabidopsis showed a negative effect on pollen tube growth (Soto *et al.* 2010). Interestingly, a GFP-AtTIP5;1 line showed localisation of the aquaporin to mitochondria in the pollen tubes. The authors suggested that both genes may be related to nitrogen recycling in pollen tubes.

Aquaporins were also observed to be involved in lateral root emergence. Péret *et al.* (2012) showed that lateral root emergence was delayed in *AtPIP2;1* mutants; both knock-out and overexpression. They suggested that the modified expression interfered with the fine-tuned regulation of water flow by aquaporins during lateral root emergence. Similar to this, Reinhardt *et al.* (2016) observed that a triple

mutant of *AtTIP1;1*, *AtTIP1;2, AtTIP2;1* had a delayed lateral root emergence. The found that especially *AtTIP2;1* was important to restore normal function of lateral root emergence.

These observations show that aquaporins are involved in growth processes in plants through hydraulic regulation and perhaps signalling. The importance of TIP aquaporins in pollen and lateral root growth is particularly interesting, since hydraulic regulation of the vacuole was not seen as limiting to cell expansion previously.

1.2.2.4. Regulation of leaf gas exchange by aquaporins

In the section on regulation of plant hydraulics by aquaporins, research was reviewed on how stomata may be regulated by a hydraulic pathway in leaves, which may provide an additional level of control to that of the direct chemical signalling role of ABA on guard cells. Sade *et al.* (2014b) showed that at least PIP aquaporins in the bundle-sheath cells are involved in this regulation.

However, earlier research from the same group also found that over-expression of *SlTIP2;2*, which is an ortholog to *AtTIP2;1*, in tomato caused an increase in osmotic water permeability of cells and increased transpiration (Sade *et al.* 2009). It was suggested that the overexpression plants became more anisohydric since they maintained a higher transpiration compared to control plants and therefore reached a lower relative water content (ratio between actual water content and maximum water content). Also overexpression of *NtAQP1* in tomato had a similar effect with increased transpiration (Sade *et al.* 2010). In soybean, over-expression of *GmPIP1;6* also caused an increase in transpiration and higher root hydraulic conductivity during salt stress treatment (Zhou *et al.* 2014). This suggests that low root hydraulic conductivity could be limiting to stomatal conductance during salt stress. Interestingly, a good correlation between the expression of *VvTIP2;1* and leaf hydraulic and stomatal conductance was found in grapevine during a drought-rehydration experiment (Pou *et al.* 2013). Additionally, a significant correlation between *VvPIP2;1* expression and leaf hydraulic conductance was found, which, however, was not correlated to stomatal conductance. A cross-species meta-analysis of gene expression also found TIP1;1 and TIP2;1 to be significantly down-regulated during drought stress in Arabidopsis, barley, rice, and wheat (Shaar-Moshe *et al.* 2015). This suggests that TIP aquaporins may also be important regulators for plant hydraulics and/or gas exchange.

As mentioned above, the expression of some TIPs and a PIP (*AtTIP1;1*, *AtTIP2;3*, and *AtPIP2;2*) in *Arabidopsis thaliana* was found to be regulated by the transcription factor TRANSLUCENT GREEN which increased drought tolerance when over-expressed (Zhu *et al.* 2013). Over-expression lines showed a vitrified leaf phenotype which pointed to a disruption in leaf water balance and gave the transcription factor its name. Hence, it was proposed that this transcription factor could control the water balance of leaves.

Direct influence of aquaporins on guard cell movement was shown by Grondin *et al.* (2015). They found that AtPIP2;1 was phosphorylated by OST1 in response to ABA which increased guard cell permeability to water. This was necessary for ABA triggered stomatal closure. Subsequently Rodrigues *et al.* (2017) demonstrated, that AtPIP2;1 mediated stomatal responses to pathogen attack by facilitating hydrogen peroxide transport into guard cells. It would be possible that also TIP aquaporins are involved to synchronise water movement to and from the vacuole in guard cells. Further research is needed on this topic.

1.2.3. Aquaporins during biotic & abiotic stress

1.2.3.1. Abiotic stress responses

Changes in the expression of aquaporin encoding genes in response to different abiotic stresses have been measured in the model plant *Arabidopsis thaliana* and many other species (Jang *et al.* 2004; Hachez *et al.* 2012; Liu *et al.* 2013; Shaar-Moshe *et al.* 2015). Each stress triggers a different response and the expression of some aquaporin isoforms might be up-regulated whereas others are down-regulated for a particular stress.

In *Arabidopsis thaliana*, most MIP isoforms were down-regulated in leaves under drought stress (Alexandersson *et al.* 2005; Alexandersson *et al.* 2010). Only *AtPIP1;4* and *AtPIP2;5* were found to be up-regulated and *AtPIP2;6* didn't show any change. The general down-regulation could be important to reduce plant hydraulic conductance and water flow through the plant, while up-regulated genes could be involved in stress signalling, e.g. *AtPIP1;4* was shown the facilitate hydrogen peroxide transport (Tian *et al.* 2016).

Much research has been done on how aquaporins respond salinity since salinity causes significant yield losses in agriculture and can be easily applied in a laboratory setting. Boursiac *et al.* (2005) found that gene expression of most PIP and TIP isoforms was down-regulated in Arabidopsis upon salt stress. The use of general antibodies against PIP1, PIP2, and TIP1 isoforms confirmed also a reduction in protein abundance. Moreover, intracellular re-localisation of the AtTIP1;1 isoform from the vacuole to spherical structures, possibly intravacuolar invaginations, was observed using GFP labelled protein. Internalization was also found for AtPIP2;1 upon salinity stress (Ueda *et al.* 2016). The down-regulation of PIP isoforms was confirmed by Lee and Zwiazek (2015). Proteomic studies also showed that phosphorylation of aquaporins changed in response to salinity. Vialaret *et al.* (2014) observed rapid dephosphorylation of PIP2;2 and PIP2;7 at the C-terminus during NaCl treatment. Also for *AtPIP2;1*, changes in phosphorylation at the C-terminus in response to salinity were found (Prak *et al.* 2008). These were related to changes in intracellular localisation.

Some responses to stress have been found to be mediated via abscisic acid (ABA). It was shown that ABA has a strong effect on hydraulic conductance in roots and leaves. The accumulation of ABA caused by drought stress was related to an increase of root hydraulic conductivity in maize roots (Hose *et al.* 2000). It was suggested that the increase in hydraulic conductance could be due to the activation of aquaporins. However, other research on drought stress in grapevine showed a decrease of root hydraulic conductance and even increased suberisation of roots which may help to reduce water loss to the soil (Vandeleur *et al.* 2009). In *Nicotiana tabacum* it was observed that the application of ABA to hydroponically grown plants caused an increase in root hydraulic conductance and an increased gene expression and protein abundance of some PIP isoforms (Mahdieh and Mostajeran 2009). In tomato, the overproduction of ABA in mutant plants under well-watered conditions increased total plant performance presumably as a result of the observed reduced stomatal conductance and a higher root hydraulic conductance (Thompson *et al.* 2007). A strong influence of ABA on hydraulic conductance and also aquaporin activity was found and a general regulation of plant water status via ABA-mediated aquaporin activity was proposed (Parent *et al.* 2009), but the details of this regulation are still not known. In the case of *AtPIP1;2*, ABA had an effect on the expression via transcription factors (Kaldenhoff *et al.* 1996). Further research is needed to understand the influence of ABA on aquaporins under well-watered versus drought conditions, since previous research showed conflicting results.

Even though the level of expression can give some indication of the activity of particular aquaporin isoforms, the actual protein abundance in membranes and their activity is crucial for their influence on plant hydraulics. Expression profiles should be interpreted with caution since differences between aquaporin gene expression and actual protein abundance in membranes was found in some cases (Monneuse *et al.* 2011). Therefore, it is important to remember that gene expression is not equal to protein abundance.

1.2.3.2. Biotic stress responses

Compared to abiotic stress, much less is known of the role of aquaporins in biotic stress responses. After Eybishtz *et al.* (2009) found that *SlTIP1;1* was significantly up-regulated in tomato plants that were resistant to *Tomato yellow leaf curl virus* (TYLCV) upon infection, Sade *et al.* (2014a) investigated TYLCV resistance in *tip1;1* null mutants in *Arabidopsis thaliana* and found that they were more susceptible to TYLCV than the wild-type. Moreover, they tested a *SlTIP2;2* constitutive expression line in tomato that showed decreased susceptibility to TYLCV. They suggested that this increased resistance was due to a link between TIP aquaporins, lower abscisic acid in leaves, and increased salicylic acid signalling. Further research is needed to explain how TIP aquaporins influence hormone homeostasis.

Research by Tian *et al.* (2016) on *AtPIP1;4* found that it acted to transduce hydrogen peroxide (H_2O_2) stress signalling. Yeast cells expressing *AtPIP1;4*, were able to translocate externally applied H_2O_2 into the cytoplasm. A null mutant of *pip1;4* in *Arabidopsis thaliana* showed increased susceptibility to *Pseudomonas syringae* pv *tomato* infection compared to the wild-type. Complementation with *AtPIP1;4* could rescue the phenotype. They concluded that *AtPIP1;4* was important for H_2O_2 signal transduction into the cytoplasm to induce disease immunity. Similar to this, transport of H_2O_2 into guard cells by AtPIP2;1 was shown to mediate stomatal responses during pathogen attack (Rodrigues *et al.* 2017). Since several other PIP and TIP aquaporins were also shown to transport H_2O_2 (Bienert *et al.* 2007; Dynowski *et al.* 2008; Hooijmaijers *et al.* 2012), it would be interesting to understand their role in disease immunity.

1.2.4. Emerging roles of tonoplast aquaporins

While a TIP aquaporin was the first water channel to be characterised (Maurel *et al.* 1993), the majority of research on the impact of plant aquaporins on water transport has concerned PIP isoforms of aquaporins due to their localisation on the plasma membrane and, hence, perceived stronger impact on cell water permeability. However, interesting functions of TIP aquaporins have been found in substrate transport, growth and even leaf gas exchange.

Unlike any PIP isoform, some TIP isoforms (TIP2;1 and TIP2;3) have been found to transport ammonia (Holm *et al.* 2005; Loque *et al.* 2005). While the crystal structure for *At*TIP2;1 was solved to understand how ammonia is transported (Kirscht *et al.* 2016), no conclusive evidence about their function in ammonia transport *in planta* has yet been found. Kirscht *et al.* (2016) suggested that *At*TIP2;1 may help to trap ammonia in the vacuole as ammonium (NH_4^+) during transient periods of photorespiration and, therefore, reduce losses of nitrogen (as volatile ammonia, NH_3) from the plant. Photorespiration occurs during abiotic stress such as drought and salinity (Voss *et al.* 2013). However, gene expression of TIP isoforms is known to be down-regulated during drought and salinity (Alexandersson *et al.* 2005; Boursiac *et al.* 2005). Therefore, the NH_3 permeability of the tonoplast could decrease rather than increase during photorespiration. Interestingly, NH_3 served as a volatile signal in yeast colonies causing growth repression in neighbouring colonies to the NH_3 emitters (Palkova *et al.* 1997). When *Brassica oleracea* plants were exposed to atmospheric NH_3, they also showed growth repression at certain concentrations (Castro *et al.* 2006). Ammonia might also serve as a volatile signal between plants during stress, when NH_3 is produced during photorespiration. Down-regulation of TIP aquaporins could reduce NH_3 entrapment and exchange with the vacuole under these conditions.

TIP isoforms were also related to growth phenotypes of pollen tubes and lateral roots (Soto *et al.* 2010; Reinhardt *et al.* 2016). Soto *et al.* (2010) found that pollen from single and double mutants of *AtTIP1;3* and *AtTIP5;1* would have slower pollen tube growth compared to the wild-type on media without nitrogen.

They concluded that those TIP isoforms may be involved in nitrogen recycling during pollen tube growth. A direct role in lateral root emergence was found for *AtTIP1;1*, *AtTIP1;2*, and *AtTIP2;1* by (Reinhardt *et al.* 2016). A triple knock-out mutant showed significantly delayed lateral root emergence, which could be rescued by the expression of *AtTIP2;1* under its native promoter. They concluded that the spatiotemporal expression of the TIP aquaporins was important for correct lateral root emergence.

Other functions of TIP isoforms include the control of water movement during seed development and desiccation, as indicated for *Hv*TIP3;1 in barley (Utsugi *et al.* 2015). Or in conferring salinity resistance, as exampled by the transgenic expression of *SlTIP2;2* from tomato in Arabidopsis (Xin *et al.* 2014). Also, a role in biotic stress tolerance to *Tomato yellow leaf curl virus* was shown for *TIP1;1* and *TIP2;2* (Sade *et al.* 2014a). While the authors suggested a role of TIP aquaporins in hormonal balance, stress signalling via hydrogen peroxide could also play a role, since *TIP1;1* has been shown to transport hydrogen peroxide (Bienert *et al.* 2007). Since most TIP isoforms, and indeed PIP isoforms, have multiple transport substrates it is difficult to conclude from the available evidence the exact mechanism of how these aquaporins confer advantage under stress conditions.

Interestingly, the overexpression of *SlTIP2;2*, which is most similar to *AtTIP2;1*, in tomato caused increased transpiration and converted plant behaviour from isohydric to more anisohydric during drought (Sade *et al.* 2009). The authors suggested that overexpression, which increased osmotic permeability of protoplasts, could increase the capacitance of vacuoles for hydraulic buffering during drought stress. The increase of osmotic permeability of protoplasts is, however, surprising, since water channels on the plasma membrane, the primary hydraulic barrier, were not modified. In the study, *SlTIP2;2* expression was driven by the constitutive promoter 35S. It is possible that high promoter activity could have caused TIP2;2 to localise to other membranes, or even have a negative effect on expression. Further research is needed to confirm whether overexpression also affected the expression of other aquaporin isoforms and if altered subcellular localisation of the overexpressed TIP2;2 plays a role. Expression of TIP isoforms were however also correlated with stomatal conductance and drought in other studies which examined expression patterns. Pou *et al.* (2013) found a very good correlation between the expression of *VvTIP2;1* and changes in stomatal conductance during drought and rehydration on leaves of grapevine. Similarly, TIP2;1 (and TIP1;1) were found to be significantly down-regulated in a cross-species meta-analysis of gene expression during drought in Arabidopsis, barley, rice, and wheat (Shaar-Moshe *et al.* 2015). These indicators of a role of TIP aquaporins in plant gas exchange regulation require further research.

1.2.5. Conclusion

This review of the literature on aquaporins and their role in plant water relations reveals that aquaporins are a large and highly diverse group of channel proteins with the feature that most of them are permeable to water. Besides water, many isoforms have also special transport functions for glycerol, carbon dioxide, ammonium, urea, hydrogen peroxide, other small molecules, and even ions (Weig and Jakob 2000; Tyerman *et al.* 2002; Loque *et al.* 2005; Bienert *et al.* 2007; Uehlein *et al.* 2012; Byrt *et al.* 2017). Gene expression studies also showed that aquaporins were significantly differentially regulated during abiotic and biotic stresses. During drought and salinity stress the expression of most isoforms was down-regulated (Alexandersson *et al.* 2005; Boursiac *et al.* 2005).

Most studies have focused on PIP isoforms and their role in plant hydraulic regulation. Hydraulic regulation by PIP aquaporins has been investigated in roots of grapevine (Vandeleur *et al.* 2009) and in leaves of Arabidopsis during drought (Sade *et al.* 2014b) suggesting significant regulatory influence. However, a molecular and physiological comparison of different Arabidopsis accession failed to find correlation between PIP aquaporin expression and root hydraulic conductivity (Sutka *et al.* 2011). This indicates that post-translational mechanism may be more important than simply gene expression.
The role of many TIP isoforms in plant hydraulics, however, remains unknown. Some research indicated that the tonoplast membrane has a higher water permeability compared to the plasma membrane (Kiyosawa and Tazawa 1977; Wendler and Zimmermann 1985b; Maurel *et al.* 1997) and, therefore, should not be limiting to water flow. However, experimental procedure like the use of certain bathing solutions or isolation protocols for protoplasts may have introduced errors to those measurements. Also, the more recent evolutionary diversification of TIP aquaporins into sub-groups may indicate that they don't underlay the same evolutionary constraints as PIP aquaporins and may have redundant functions (Borstlap 2002). Indeed, research by Reinhardt *et al.* (2016) on the role of TIP aquaporins in lateral root emergence showed that only a triple mutant of *tip1;1*, *tip1;2*, and *tip2;1* showed a significant delay of lateral root emergence. This could indicate redundancy between isoforms. Interestingly, several studies have pointed at a role of TIP2 aquaporins in leaf gas exchange (Sade *et al.* 2009; Pou *et al.* 2013; Shaar-Moshe *et al.* 2015). So far, no experimental evidence has been found as to how these aquaporins could influence, for example, stomatal conductance. Moreover, the question remains as to how this is connected to their function as ammonia transporters.

1.3. Research questions and aims

From the literature review it appeared that there is still very little is known about the role of TIP aquaporins. In particular, the observation that overexpression of the TIP isoform *SlTIP2;2* had a significant effect on transpiration and hydraulic behaviour of tomato plants (Sade *et al.* 2009) is interesting, since no adequate explanation has been provided so far. This observation was supported by results from gene expression studies in grapevine and other crop species, which have pointed to a significant role of TIP2;1 during drought and rehydration (Pou *et al.* 2013; Shaar-Moshe *et al.* 2015). For some TIP isoforms, ammonia transport activity was found (Loque *et al.* 2005), but no phenotype in plants has been identified yet. The following research questions therefore arise:

- Considering that the correlation between *VvTIP2;1* expression and stomatal conductance was found in grapevine, does this also translate to the model plant Arabidopsis and are there other isoforms whose expression is correlated to stomatal conductance during drought and rehydration?
- Abscisic acid (ABA) is well known as a signal mediating stomatal closure during drought. Is aquaporin expression also regulated by ABA which would explain the correlation to stomatal conductance?
- Overexpression of *SlTIP2;2* in tomato caused an increase in transpiration and more anisohydric character of transgenic plants. Would constitutive expression of TIP2 isoforms in Arabidopsis cause the same phenotype?
- If overexpression causes an increase in transpiration, would null mutants of TIP2 aquaporins show a decrease of transpiration?

1.3.1. Aquaporin expression profiling during drought and rehydration in *Arabidopsis thaliana*

Aquaporin gene expression during drought and rehydration has been profiled in *Arabidopsis thaliana* before (Alexandersson *et al.* 2005). While those results showed that not only TIP2 aquaporins were down-regulated during drought, no physiological parameters were assessed in the experiment, which could have been correlated against gene expression as was the case by Pou *et al.* (2013). Moreover, the effect of abscisic acid, instead of drought, has not been tested yet. Therefore, the aims are as follows:

- Develop a standard drought-rehydration experiment for *Arabidopsis thaliana* with a sufficient dry-down phase to assess changes in gene expression and measured plant physiological parameters

- Develop an equivalent abscisic acid watering experiment, to induce stomatal closure similar to the drought experiment, in *Arabidopsis thaliana* and assess changes in gene expression and measure plant physiological parameters
- Measure soil water content, leaf water content, abscisic acid concentration in leaves, and stomatal conductance to compare against changes in gene expression
- Use co-expression analysis to detect patterns and groups from gene expression profiles which may be linked to physiological changes

1.3.2. Constitutive expression of *AtTIP2* aquaporins in *Arabidopsis thaliana*

Constitutive expression of *SlTIP2;2* in tomato caused an increase in transpiration and more anisohydric character of transgenic plants (Sade *et al.* 2009). While transgenic expression of *SlTIP2;2* in *Arabidopsis thaliana* conveyed salinity tolerance (Xin *et al*. 2014), no effects of constitutive expression of native AtTIP2 aquaporins in the model plant *Arabidopsis thaliana* are known. Moreover, it is not known whether specific isoforms of TIP2 aquaporins affect transpiration, or if it's a general feature. Hence, the project had the following aims:

- Constitutive expression of *AtTIP2;1*, *AtTIP2;2*, and *AtTIP2;3* driven by a UBQ10 promoter in *Arabidopsis thaliana* ecotype Col-0; two versions: 1) only native protein and 2) protein tagged with GFP fluorescent label on C-terminal end
- Confirmation of tonoplast localisation for constitutive expression lines of *AtTIP2;1*, *AtTIP2;2*, and *AtTIP2;3* by confocal microscopy
- Test constitutive expression lines in the previously developed drought-rehydration experiment and assess changes in stomatal conductance compared to the wild-type
- Construction of promoter::GUS lines for promoters of *AtTIP2;1*, *AtTIP2;2*, and *AtTIP2;3* in *Arabidopsis thaliana* ecotype Col-0
- Colorimetric localisation of *AtTIP2;1*, *AtTIP2;2*, and *AtTIP2;3* promoter activity using promoter::GUS lines

1.3.3. Null mutants of *AtTIP2* aquaporins in *Arabidopsis thaliana*

A triple knock-out mutant of *tip1;1*, *tip1;2*, and *tip2;1* in *Arabidopsis thaliana* showed a significant delay of lateral root emergence (Reinhardt *et al.* 2016). While expression of *AtTIP2;1* under control of its native promoter was able to rescue the phenotype of the triple knock-out mutant, no experiments were done on the single *tip2;1* null mutant line. In particular, no research is published on the effect of TIP2 null mutants

on plant gas exchange. At the time the project was conceived, the single *tip2;1* null mutant line was not known to us. Also, no suitable T-DNA lines for *AtTIP2;2*, and *AtTIP2;3* were found which were likely to show reduced of absent expression of those aquaporins. Hence, genome editing by CRISPR-Cas was used to develop the desired null mutants. The research aims are as follows:

- Use CRISPR-Cas to induce InDels in the coding region of the genes *AtTIP2;1*, *AtTIP2;2*, and *AtTIP2;3* in *Arabidopsis thaliana* ecotype Col-0
- Develop appropriate screening techniques to find homozygous null mutants
- Out-cross CRISPR-Cas to obtain null mutants with "clean" background
- Assess phenotype of null mutants

1.3.4. Comparison of isohydric grape cultivar Grenache to anisohydric cultivar Syrah during drought-rehydration

Comparison of the grape (*Vitis vinifera*) cultivars Grenache and Syrah showed their divergent behaviour in drought adaption (Schultz 2003). The cultivar Grenache behaves more conservative (isohydric) by their stomata responding more readily to declining soil water availability that prevents the occurrence of low leaf water potentials. In contrast, Syrah behaves more towards the anisohydric behaviour by maintaining higher stomatal conductance at a similar water potential, leading generally to lower leaf water potentials. Dr. Silvina Dayer conducted a drought-rehydration experiment to compare the response of both cultivars and study changes in plant hydraulic conductance and aquaporin gene expression. I joined the experiment to analyse aquaporin gene expression using real-time quantitative PCR, investigate the data obtained from the experiment, and write a manuscript with Dr Dayer. The project aims are as follows:

- Analyse aquaporin gene expression from leaves and root samples of *Vitis vinifera* using real-time quantitative PCR
- Data analysis in R using (multiple) linear regression and advanced correlation analysis
- Write a manuscript for publication

1.4. Significance of the research

Plant hydraulic behaviour and stomatal regulation are interesting breeding targets, since water availability is restricted in many areas of crop production and the need for irrigation is a big challenge in agriculture (Rosegrant *et al.* 2009; Langridge and Reynolds 2015). Aquaporins have significant roles in controlling plant water relations through modification of membrane permeability for water and other small solutes (Chaumont and Tyerman 2014). Much research has been done on PIP aquaporins and their role in plant hydraulics, since they are localised to the plasma membrane, which is the primary barrier for symplastic and transcellular water flow (Steudle and Peterson 1998; Martre *et al.* 2002; Hachez *et al.* 2013; Sade *et al.* 2014b). In contrast, much less is known about the role of TIP aquaporins, which are mainly localised to the tonoplast. Here I aim to provide some base work to investigate the role of TIP2 aquaporins in the model species *Arabidopsis thaliana* during drought. Additionally, I collaborated on some research investigating hydraulic regulation and the role of aquaporins in the contrasting *Vitis vinifera* cultivars Grenache (near-isohydric) and Syrah (anisohydric) during drought and rehydration.

Previous research showed that overexpression of the TIP2 aquaporin isoform *SlTIP2;2* in tomato increased transpiration in transgenic plants (Sade *et al.* 2009). Moreover, significant regulation of TIP2 aquaporin expression was found during drought across multiple species (Shaar-Moshe *et al.* 2015) and a strong correlation to stomatal conductance was shown in grapevine (Pou *et al.* 2013). While a direct link between *At*PIP2;1 and stomatal regulation was found by Grondin *et al.* (2015), no experimental evidence for TIP aquaporins has been found as yet.

Research outcomes from this study will improve our understanding how plants respond to drought and rehydration and the role of aquaporins in this process. Generation of a collection of TIP2 aquaporin overexpression and knock-out mutant lines will provide a valuable resource for research even after this PhD project. Comparison between the model species *Arabidopsis thaliana* and the crop species *Vitis vinifera* will offer knowledge on how well results from one species translate to another. In future, new breeding targets could be identified based on TIP2 aquaporin function in plants to improve water use efficiency of crops and reduce the need for irrigation in farming leading to a more sustainable agriculture.

2. CO-EXPRESSION LINK AQUAPORIN GENE EXPRESSION TO PHYSIOLOGICAL PARAMETERS DURING DROUGHT AND REHYDRATION IN *ARABIDOPSIS THALIANA*

2.1. Introduction

Plants need to balance water uptake from the soil and water loss via transpiration to avoid desiccation. The primary response of plants during drought is to reduce stomatal conductance in order to reduce transpiration (Tardieu and Davies 1993). Declining soil water availability triggers a hydraulic signal within the plant, inducing stomatal closure through the action of the stress hormone abscisic acid (ABA). While this is the general description of the response, the actual sequence and different pathways involved are still under debate. There is ample evidence for ABA being a trigger for stomatal closure (Finkelstein 2013). While early reports indicated that ABA was being produced both in the root and in leaves in response to drying (Walton *et al.* 1976; Pierce and Raschke 1981), it was hypothesized that ABA is translocated from the root to the shoot to close stomata during soil water deficit (Zhang *et al.* 1987). However, other evidence suggests that ABA that is produced in the leaves itself induces the closure of stomata (Manzi *et al.* 2015; McAdam *et al.* 2016). Christmann *et al.* (2013) hypothesized that a hydraulic signal could originate from the root and be transmitted to the shoot where it is transduced into a chemical signal like ABA. Aquaporins could be involved in the transmission and/or transduction of this hydraulic signal and, hence, have an influence on stomatal control (Chaumont and Tyerman 2014; Yaaran and Moshelion 2016).

In *Arabidopsis thaliana*, 35 aquaporin isoforms have been found (Johanson *et al.* 2001). Most of them belong either to the subfamily of plasma membrane intrinsic proteins (PIPs), considered to be principally localized to the plasma membrane, or to the subfamily of tonoplast intrinsic proteins (TIPs), which are considered to be localized to the tonoplast membrane. Indeed some aquaporins are used as membrane markers. Aquaporins facilitate passive water transport and are often also permeable to other small molecules (Tyerman *et al.* 2002). They can be actively gated by phosphorylation or protonation (Tornroth-Horsefield *et al.* 2006).

The role of aquaporins in plant water relations has been extensively reviewed (Chaumont and Tyerman 2014; Maurel *et al.* 2015; Moshelion *et al.* 2015). Increased aquaporin expression or activity can increase the water permeability of membranes and may speed the recovery from drought, as shown for PIP aquaporins (Martre *et al.* 2002). This change in water permeability of the plasma membrane alters the hydraulic conductance of tissues. Postaire *et al.* (2010) demonstrated the importance of aquaporins in plant hydraulics by showing that a single aquaporin isoform *AtPIP1;2*, highly expressed in leaves, could account for up to 20% of the rosette hydraulic conductance in Arabidopsis. There are other examples, like

AtPIP2;1, which was shown to mediate the total increase of rosette hydraulic conductance in response to darkness in Arabidopsis (Prado *et al.* 2013). Changes in hydraulic conductance can have strong effects on both water potential gradients and flow rates. Therefore, changes in conductance as a result of changes in aquaporin activity could transmit or amplify pressure signals. Interestingly, (Pantin *et al.* 2013) found that ABA was able to induce stomatal closure in ABA-insensitive mutants of Arabidopsis when applied to intact plants instead of epidermal peals. They concluded that ABA may influence aquaporin expression or activity and create a hydraulic signal that subsequently controls stomatal aperture instead of a direct control by ABA. This work was complemented by observations from (Sade *et al.* 2014b) that PIP aquaporin expression in the bundle sheath could control water flow along the bundle sheath – mesophyll – continuum and potentially create a hydraulic feed-forward signal for stomatal control in leaves. It remains to be shown whether hydraulic signals arise due to changes in expression or activity of aquaporins and if these changes are triggered by ABA or if alternative pathways exist. Fern and lycophyte stomata, for example, were shown to be regulated mainly by passive hydraulic signals, rather than ABA (McAdam and Brodribb 2012).

While most of this research has focused on PIP aquaporins, which control water flow across the plasma membrane, some research has also indicated a close connection between TIP aquaporins, presumed localized to the tonoplast, and stomatal regulation. Sade *et al.* (2009) showed that the overexpression of *SlTIP2;2* in tomato plants had a significant effect on transpiration. Overexpression lines transpired more and for longer during drought. The authors considered that this made the plants more anisohydric, which is characterized by more open stomata and more negative water potentials in response to water deficit. While it was speculated that the overexpression increased hydraulic conductivity and therefore water flow through the plants, which may have affected stomatal conductance, no conclusive data was provided. In line with this, research on drought and rehydration in grapevine (*Vitis vinifera*) showed that gene expression of a particular tonoplast aquaporin *VvTIP2;1*, to be highly correlated to changes in stomatal conductance and also leaf hydraulic conductivity (Pou *et al.* 2013). A cross-species meta-analysis on changes in gene expression during drought in Arabidopsis, barley, rice, and wheat also showed that *TIP1;1* and *TIP2;1* gene expression was significantly down-regulated in all four species (Shaar-Moshe *et al.* 2015). Usually, less emphasis is given to TIP aquaporins in the control of plant hydraulics, even though they are presumed to influence water permeability of the tonoplast that surrounds the vacuole constituting approximately 90% of cell volume of a mature plant cell (Taiz 1992). Traditionally, it is understood that the tonoplast conductance for water flow is about 100-fold larger than that of the plasma membrane, which may serve an important function in keeping the balance between the volume of the cytoplasm and the vacuole (Tyerman *et al.* 1999). However it is since considered that these earlier estimates of the difference between plasma membrane and tonoplast water permeabilities may have been in error due to the underestimation of the plasma membrane permeability. Very high water permeabilities have been

recorded for the plasma membrane when the membrane has been more carefully fractionated (Alleva *et al.* 2006). Hence, it is not known how much TIP aquaporin expression and activity may influence plant hydraulics. Clearly lateral root emergence in Arabidopsis was dependent on *AtTIP1;1*, *AtTIP1;2*, and *AtTIP2;1* (Reinhardt *et al.* 2016). The authors suggested that the timing and location of activity of these aquaporins was important for coordinated cell growth and expansion during lateral root emergence.

So far, multiple studies have measured changes in gene expression during drought in the model plant *Arabidopsis thaliana* (Jang *et al.* 2004; Alexandersson *et al.* 2005). Alexandersson *et al.* (2005) presented the most comprehensive study of changes in gene expression of all aquaporin isoforms during drought and rehydration. They found that gene expression of most aquaporin isoforms were down-regulated during drought, except for *AtPIP1;4*, *AtPIP2;5*, *AtPIP2;6*, and *AtSIP1;1*. Judging from the expression profiles and their co-expression matrix (Alexandersson *et al.* 2010), changes in gene expression of down-regulated genes looked very similar. While in grapevine a very good correlation between gene expression of a particular aquaporin and stomatal conductance was found (Pou *et al.* 2013), this seemed less likely in Arabidopsis. However, studies on gene expression changes during drought in Arabidopsis did not include any physiological water relations or gas exchange parameters, making it difficult to assess the relationship to the actual plant response to drought. Hence, it would be useful to collect data on gene expression and plant physiological responses under drought to determine if particular aquaporin isoforms could have an important role in stomatal control. Knowledge about changes in soil water availability, soil water potential, and ABA signaling would give a more comprehensive picture on the response to drought.

In this study, I carried out drought and rehydration experiments on potted plants of *Arabidopsis thaliana* to study the stomatal responses while monitoring the change in water availability in the soil and concentration of ABA in the leaves. At the same time, changes in gene expression in the leaves were measured to relate to physiological responses. To exclude hydraulic signals from the soil and study purely ABA as a chemical signal in drought responses, an ABA watering experiment was conducted as well with the aim to trigger a similar stomatal response compared to the drought-rehydration experiment. Likewise, changes in gene expression were measured to find out if these are triggered by ABA or rather the hydraulic component of drought stress. I expected to find isoforms with expression that correlated to stomatal responses and potential ABA concentrations in the leaves. Parallel measurements of changes in soil water availability, modelling of soil hydraulic characteristics, and ABA biosynthesis in the leaves would give insides on the trigger of drought responses and in which sequence those responses are activated. During the course of these experiments it was noted that control plants under a continuous water regime also showed a reduction in stomatal conductance in parallel to the droughted plants grown in the same growth room. Thus some examination of the possibility of volatile signals from droughted plants that influenced the control plants was examined taking care to assess the changes in air VPD

during the drought treatment, which is well known to influence stomatal conductance (McAdam and Brodribb 2015).

2.2. Material and Methods

2.2.1. Plant Material and Growth Conditions

Arabidopsis (*Arabidopsis thaliana*) ecotype Col-0 seed were sown on solid, half-strength Murashige and Skoog medium (Murashige and Skoog 1962). After vernalisation at 4°C for 3 days in the dark, plates were transferred to a walk-in growth chamber at The Plant Accelerator® Adelaide, Australia (34° 58' 17'' S, 138° 38' 23'' E). Plants were grown under short-day conditions (10 h light/ 14 h dark, PAR ~150 µmol m^{-2} s^{-1}, 21°C) for 7 d until they were transferred to soil. Plastic pots (170 cm^3) were filled with 92 g soil mixture (85 % (v/v) Seedling Substrate Plus+, Bord na Móna; 15 % (v/v) Horticultural Sand, Debco Pty Ltd) to a packing density of 0.54 g/cm^3 and drenched with 0.05 g/L Confidor® (Bayer). Plants were grown for another 5 weeks under short-day conditions until the experiments. A week before the experiment, the soil in each pot was covered by white plastic granules to reduce evaporation from the soil and achieve a uniform drying during the drought treatment. Plants were also selected for good health and similar size. A day before the start of the experiment, five mature leaves of equal size were selected on each plant and marked with solvent free liquid paper (Liquid Paper). Plants were split into two groups (treatment/control). Trays of 12 plants from different groups were placed side-by-side on the shelves.

2.2.2. Drought and abscisic acid treatment

For the drought – rehydration experiment, watering was withheld for plants from the treatment group from day 1 till day 7 when plants started wilting. After measurements were performed on day 7, these plants were rehydrated by flooding the trays overnight. Plants from the control group were watered to field capacity by flooding the trays each day for 30 minutes.

For the ABA experiment, a 50 mM stock solution of abscisic acid (Sigma Aldrich) in ethanol was prepared. To water the plants, this stock solution was diluted with RO water to defined concentrations. A mock was produced by adding the same volume of ethanol without ABA.

In a trial, 10 mL of five different concentrations of ABA (0, 1, 10, 25, 50 µM) were applied repeatedly to six plants each over five consecutive days. The solutions were applied to each pot onto the soil at 9 am. Additionally, plants were allowed to take up RO water supplied into their saucers for one hour.

For the proper ABA experiment, increasing concentrations of ABA (0.1, 1, 2, 4, 8, 16, 50 µM) were applied to plants of the treatment group over seven consecutive days. The control group was watered with the mock solution. To each pot, 30 mL of solution was applied, which was just slightly more than the daily consumption of the plants. After day 7, plants from the treatment group were also watered with the mock solution for recovery.

2.2.3. Physiology measurements

Physiology measurements and sampling were conducted each day from 1-3 pm. Five plants per group were randomly selected from different trays. Stomatal conductance (g_s) was measured on leaves 1-4 using an AP4 leaf Porometer (Delta-T Devices). Afterwards they were immediately frozen in liquid nitrogen. Leaves 1 and 2 were frozen in individual 2 mL Eppendorf tubes for gene expression analysis, while leaves 3 and 4 were combined for ABA measurements. Leaves 5 and 6 were collected to determine water content (WC) and relative water content (RWC), calculated as follows:

$$WC = \frac{FW - DW}{DW} \quad (1)$$

$$RWC = \frac{FW - DW}{TW - DW} \quad (2)$$

Fresh weight (FW) of leaves was determined immediately after abscission on a precision balance (MS403S, precision: 1 mg, Mettler Toledo). Subsequently, leaves were rehydrated to full turgid weight (TW) in tap water overnight and weighed the next morning after removing excess liquid with paper towel. Dry weight (DW) was determined on a precision balance (E12140, precision: 0.1 mg, OHAUS) after drying at 60 °C for one week. The remaining rosette was frozen in liquid nitrogen for future analysis. Gravimetric soil water content (θ_g) of the whole soil in the pots was calculated from fresh soil weight (M_{wet}) and dry soil weight (M_{dry}) after drying the soil at 105 °C till no further weight change.

$$\theta_g = \frac{M_{wet} - M_{dry}}{M_{dry}} \quad (3)$$

Temperature (*T*) and relative humidity (*rH*) were recorded inside the growth chambers using a QP6014 Temperature & Humidity Datalogger (DIGITECH). The vapour pressure deficit (VPD in Pa) was estimated by an exponential function (Fishman and Genard 1998):

$$VPD = 0.008048 \times e^{0.0547 \times T} \times \frac{100 - rH}{100} \quad (4)$$

2.2.4. ABA analysis

Frozen leaf samples were ground into a fine powder in liquid nitrogen using a mortar and pestle. Approximately 100-150 mg of frozen powder was transferred to pre-chilled Eppendorf tubes and the exact fresh weight was recorded on a precision balance (MS403S, Mettler Toledo). To each sample, 500 µL of 20 % methanol was added. The samples were mixed by vortex and refrigerated (5 °C) overnight. Next morning, samples were mixed by vortex and centrifuged at 10,000 rpm for 3 min. The supernatant was collected in a new Eppendorf tube and the pellet resuspended in 500 µL of 20 % methanol. This was centrifuged again and both supernatants combined. 300 µL of deuterated internal standard (analogues of ABA, phaseic acid, and dihydrophaseic acid; each at 100 ng/mL) were added and mixed by pipetting.

Strata™-X 33 µm Polymeric Reversed Phase columns (1 mL, Phenomenex) were prepared. These were inserted in 15 mL Falcon tubes and loaded with 1 mL of 100 % methanol; then centrifuged at 2500 rpm for 5 min. The Discard flowthrough was discarded and then the column was loaded with 1 mL Millipore H_2O and centrifuged at 2500 rpm for 5 min.

Samples were loaded onto columns and centrifuged at 2500 rpm for 5 min. The flowthrough was discarded. The column was washed with 1 mL 20 % methanol and centrifuged at 2500 rpm for 5 min., again discarding the flowthrough. The sample then eluted with 1 mL 90 % methanol and centrifuged at 2500 rpm for 5 min. The flowthrough was transferred to a 2 mL Eppendorf tube. These samples were dried in a Centrivap Concentrator (LABCONCO) at room temperature in darkness. The dried samples were stored at -20 °C till further analysis.

The dried samples were dissolved in 30 µL 70 % methanol then centrifuged for 5 min. at 13,000 rpm and 20 µL aliquoted into LC/MS tubes. The samples were measured by LC-MS/MS [Agilent 6410 QQQ LC-MS/MS with Agilent 1200 series HPLC (Agilent Technologies, Santa Clara, CA, USA)] using a Phenomenex C18 column [75mm × 4.5mm × 5 µm (Phenomenex, Torrance, CA, USA)] with a column temperature of 40 °C. Solvents were nanopure water and acetonitrile, both with 0.05 % acetic acid. The samples were eluted with a linear gradient from 10 % to 90 % acetonitrile in 15 min. Compounds were identified by retention times and mass/charge ratio.

2.2.5. Soil water retention curve

Soil mixture made for the drought-rehydration and ABA experiments was filled in 150 rings (r = 15 mm, h ≈ 10 mm) made from polyvinyl chloride (PVC) pipe. The rings were filled with a homogenous mixture of the soil to a packing density of 0.54 g/cm^3.

To measure gravimetric water content of the soil at 0.005 m of matric head, five rings were fitted with a base made from cloth. The rings were submerged in RO water up to their rim and their wet weight

recorded several times. Afterwards the rings were filled with the soil according to the instructions above and, again, submerged in RO water. Wet weights of the rings with soil were recorded several times. Afterwards the soil from each ring was quantitatively washed out into individual pre-weighed weighing dishes, which were dried in an oven at 105 °C overnight. Dry weights were recorded the following day. Gravimetric water content was calculated as per equation (3).

Six Extractor 0675 Ceramic Plates [4 × 1 bar, 1 × 5 bar, 1 × 15 bar (ICT International)] were pre-soaked in RO water. On each plate, 25 rings with soil were evenly distributed. The setup is shown in Table 1; data from levels with red shading were excluded since the samples were measured before equilibrium was reached. Ceramic plates, which were used for determining gravimetric water content at lower levels of matric potential head, were connected to a hanging water column, while plates for higher levels of matric potential head were enclosed in pressure extractors (ICT International). Once equilibrium was achieved at the set level of matric potential head, five samples were collected from the plate with a spatula and the soil was immediately enclosed in pre-weighed weighing containers. After fresh weight was recorded, the soil was dried in an oven at 105 °C overnight. Dry weights were recorded the following day. Gravimetric water content was calculated as per equation (3).

Table 1. List of Ceramic Plate setup showing levels of matric head measured with each plate and what method was used. Data for all levels shown were recorded to understand the shape of the soil-water-retention curve, but only levels with green shading were used for the calculation of the soil-water-retention models, since they were evenly distributed along the log range of matric head values. Levels with red shading were excluded (measurement errors).

Plate #	Levels of matric head, *h* (m)					Method
1	0.005	0.01	0.02	0.03	0.04	Hanging water column
2	0.04	0.05	0.06	0.07	0.08	Hanging water column
3	0.08	0.09	0.10	0.11	0.12	Hanging water column
4	0.12	0.13	0.14	0.15	0.16	Hanging water column
5	0.16	0.2	0.3	0.5	1.0	Pressure Plate
6	1.0	2.5	5.0	10	15	Pressure Plate

A selection of levels, which were equally distributed along the soil-water-retention curve, were chosen to fit a model to the curve (green shading Table 1). Two model equations were used to fit the soil-water-retention curve to estimate soil water potential (Ψ_{soil}) from θ_g data collected in the drought – rehydration experiment. The widely used Van Genuchten model (5) (Van Genuchten 1980) and the newer Groenevelt-Grant soil water retention model (6) (Grant *et al.* 2010) were used to fit to the data, respectively:

$$\theta_g(h) = \theta_r + \frac{\theta_s - \theta_r}{[1 + (\alpha h)^n]^m} \quad (5)$$

$$\theta_g(h) = \theta_s - k_1 \, exp\left[-\left(\frac{k_0}{h}\right)^n\right] \quad (6)$$

The Van Genuchten model uses residual moisture content (θ_r), saturated moisture content (θ_s), alpha α (inverse of air entry potential), levels of matric head potential (h), index n for pore-size distribution, and scaling parameter m, which is also related to the pore-size distribution. Similar to the Van Genuchten model, the Groenevelt-Grant soil water retention model uses θ_s. Additionally it has three fitting parameters: k_0, k_1, and n; k_0 is related to the air entry potential similar to α.

Fitting parameters for the Van Genuchten model were determined using the *SSvgm* function from the HydroMe R package (Omuto and Gumbe 2009) and a custom made function was used for the Groenevelt-Grant soil water retention model in the program R (R Core Team 2017).

Relative hydraulic conductivity of the soil (K_r) was calculated according to Grant *et al.* (2010) and as elaborated on by Chahal (2010). Fitting parameters from the Groenevelt-Grant soil water retention model were used to calculate relative water contents for the soil that were anchored to the oven dry matric suction of $10^{6.9}$ cm (θ_{rL}):

$$\theta_{rL} = 1 - \frac{1}{\lambda} exp\left[-\left(\frac{k_0}{10^{6.9}}\right)^n\right] \quad (7)$$

In this equation λ was defined as:

$$\lambda = \frac{\theta_s}{k_1} \quad (8)$$

The shape of the hydraulic conductivity function was described by an incomplete gamma function:

$$M(h) = \frac{1}{\lambda} \cdot \left[\Gamma\left[\xi + 1, [-\ln[\lambda(1 - \theta_{rL})]]\right] - \Gamma\left[\xi + 1, \left[-\ln\left[\lambda\left[1 - \left[1 - \frac{1}{\lambda} exp\left[-\left(\frac{k_0}{h}\right)^n\right]\right]\right]\right]\right]\right] \quad (9)$$

Which includes ξ = β/n, where the parameter β = 1 is to accommodate the Mualem model. With this, the relative hydraulic conductivity (K_r) was calculated, where M(0) is the incomplete gamma function at saturation:

$$K_r(h) = \left[1 - \frac{1}{\lambda} exp\left[-\left(\frac{k_0}{h}\right)^n\right]\right]^{0.5} \left(\frac{M(h)}{M(0)}\right)^2 \quad (7)$$

2.2.6. RNA extraction and cDNA synthesis

Individual frozen leaf samples were ground into a fine powder using two 3 mm steel grinding balls in each 2 mL Eppendorf tube. The tubes with leaf samples and steel grinding balls were kept in liquid nitrogen until grinding the samples twice (different orientations) for 30 sec at 1500 strokes/min into a fine powder using the Geno/Grinder® (SPEX®SamplePrep). Afterwards, samples were immediately cooled again in liquid nitrogen and transferred to -80 °C until further processing.

Extraction of total RNA was done using the Spectrum™ Plant Total RNA Kit (Sigma Aldrich) and the On-Column DNase I Digestion Set (Sigma Aldrich) according to Kit instructions. Briefly, 500 µL of Lysis Solution/2-ME Mixture was added to 50-100 mg frozen fine powder of leaf tissue. Samples were immediately mixed using the Geno/Grinder® for 30 sec at 1500 strokes/min and incubated for 5 min at 56 °C. Solids were separated from the lysate using the filtration column and 750 µL binding Solution was added to the lysate. Nucleic acids were captured using the binding column and washed with 300 µL Wash Solution 1. Samples were incubated with 80 µL of DNase digestion mixtures for 15 min at room temperature. Afterwards, columns were washed with 500 µL of Wash Solution 1 and Wash Solution 2 in subsequent steps. Total RNA was eluded in 50 µL Elution Solution. Quantification of total RNA yield was done using the NanoDrop™ 1000 Spectrophotometer (Thermo Fisher Scientific). Total RNA quality was assessed by gel electrophoresis of 500 ng total RNA which was denatured at 70 °C for 10 min, and immediately cooled on ice for 3 min. Samples were run at 60 V for 60 min in a 1.2 % (w/v) agarose gel in 0.5 x TAE buffer with GelRed™ DNA stain (Biotium). Nucleic acids were visualised in a ChemiDoc Imaging Systems (Bio-Rad). Samples were stored at -80 °C until further processing.

Subsequently, cDNA synthesis was done using the iScript™ Reverse Transcription Supermix for RT-qPCR (Bio-Rad). Briefly, 4 µL iScript RT Supermix was added to 1 µg of total RNA and adjusted to 20 µL total reaction volume with nuclease-free water. The reverse transcription reaction was carried out in a G-Storm Thermal Cycler GS1 (Gene Technologies Ltd): 5 min at 25 °C, 30 min at 42 °C, 5 min at 85 °C. No-RT controls were included to check for genomic DNA contamination. Samples were stored at -20 °C until further processing.

2.2.7. OpenArray® gene expression analysis

Relative gene expression of the full set of Arabidopsis MIPs and some ABA signalling and drought stress responsive genes (

Supplementary Table S2) was measured using custom designed TaqMan® OpenArray® Real-Time PCR Plates (56 assay format) (Thermo Fisher Scientific) that were run on a QuantStudio® 12K Flex Real-Time PCR System (Thermo Fisher Scientific).

For each OpenArray® plate, 48 samples of cDNA were prepared in 6 µL multi-reaction pre-mixes (Supplementary Table S3); final cDNA concentration of 24 ng/µL. Each pre-mix was prepared in a 96-well PCR plate on ice. After careful mixing and centrifugation, 5 µL of each pre-mix was transferred to 384-well PCR plate using a multichannel pipette according to manufacturer's instructions. Samples were transferred from the 384-well PCR plate automatically to the OpenArray® plate using the OpenArray™ AccuFill™ System (Thermo Fisher Scientific). Immediately after the transfer, OpenArray® plates were sealed and filled with QuantStudio™ Immersion Fluid (Thermo Fisher Scientific) according to manufacturer's instructions. Subsequently, OpenArray® plates were run on a QuantStudio® 12K Flex Real-Time PCR System. After the runs, gene amplification data were retrieved as *.csv files and further analysis was performed in the program R (R Core Team 2017).

2.2.8. Data analysis

All data was processed and analysed in the program R (R Core Team 2017). Data clean-up and wrangling was done using functions from the *tidyverse* collection of R packages (Wickham 2017). Plotting of figures was carried out using the *ggplot2* package from the *tidyverse* collection of R packages unless stated otherwise.

Gene expression analysis was performed using relative threshold cycles (C_{rt}) from the QuantStudio® 12K Flex Real-Time PCR System output. Data was augmented with sample information and genes with missing or low expression (average C_{rt} > 30) were excluded. The most suitable reference genes for normalisation of gene expression were chosen from the set of available references genes (*AtACT2*, *AtELF*, *AtGAPC2*, *AtTUB5*, *AtUBQ10*) using the packages *ReadqPCR* and *NormqPCR* (Perkins *et al.* 2012). These suggested *AtACT2* and *AtGAPC2* as most stable expressed genes (Supplementary Figure S4, Supplementary Figure S6), which were subsequently used for normalisation of gene expression. Normalised gene expression was calculated according to Pfaffl (2001) as $\Delta C_{rt} = \bar{x}(C_{rt,ACT2}, C_{rt,GAPC2}) - C_{rt,GOI}$, where $\bar{x}(C_{rt,ACT2}, C_{rt,GAPC2})$ is the arithmetic mean of the relative threshold cycles of the reference genes and $C_{rt,GOI}$ is the relative threshold cycle of the 'gene of interest', e.g. *AtPIP1;1*. Normalised expression of genes was compared between leaf 1 and 2 sampled from each plant during the experiment as internal control (Supplementary Figure S5, Supplementary Figure S7). Relative changes in gene expression ($\log_2$ ratio) between the well-watered control plants and drought-rehydration treated plants was calculated for each time-point of the experiment as $\Delta\Delta C_{rt} = \bar{x}(\Delta C_{rt,drought\text{-}rehydration}) - \bar{x}(\Delta C_{rt,well\text{-}watered})$, where $\bar{x}(\Delta C_{rt,drought\text{-}rehydration})$ is the arithmetic mean of normalised gene expression from all samples of the

drought-rehydration treatment per time-point and $\bar{x}(\Delta C_{rt,well\text{-}watered})$ is the arithmetic mean of normalised gene expression from all samples of the well-watered plants per time-point. Whether genes were significantly differentially expressed ($p \leq 0.05$) was tested by ANOVA with Bonferroni post-tests comparing $\Delta C_{rt,well\text{-}watered}$ and $\Delta C_{rt,drought\text{-}rehydration}$.

Cluster analysis of gene expression was carried out by construction of a correlation matrix using Pearson correlation coefficients. Coefficients that were not significant ($p > 0.05$) were excluded. Genes were clustered into modules by hierarchical clustering (average linkage clustering) using the function *hclust* on a distance matrix of the correlation coefficients. Modules were inferred from the dendrogram tree of *hclust* using the function *cutreeHybrid* from the R package *dynamicTreeCut* (Langfelder *et al.* 2008). Co-expression of genes and clusters were visualised using the R package *heatmap3* (Zhao *et al.* 2014).

Correlation analysis between gene expression and plant physiological parameters was conducted using Pearson correlation coefficients. Coefficients which were not significant ($p > 0.05$) were excluded. Correlations were visualised using the R package *corrplot* (Wei and Simko 2016).

2.3. Results

2.3.1. Application of drought stress and ABA treatments

Two separate experiments were carried out to compare plants subjected to 1) drought and rehydration and 2) ABA watering treatment.

Measurements of the gravimetric soil water content (θ_g) in the drought-rehydration experiment showed an almost linear decline for plants which had their watering withheld (Figure 3a). Since θ_g was measured for the entire soil in each pot after the plant material was sampled, these results represent a pot average. Soil from pots in the well-watered group had an average θ_g of 1.69 ± 0.01 g g^{-1}, while soil from the wilting plants on day 7 had an average θ_g of 0.27 ± 0.05 g g^{-1}.

To induce stomatal closure similar to the drought-rehydration experiment, increasing concentrations of ABA were applied in the watering solution in the second experiment (Figure 3b). Preliminary experiment (Supplementary Figure S2) showed that the application of increasing concentrations of ABA was more effective in mimicking stomatal closure during drought than repeated application of the same concentration.

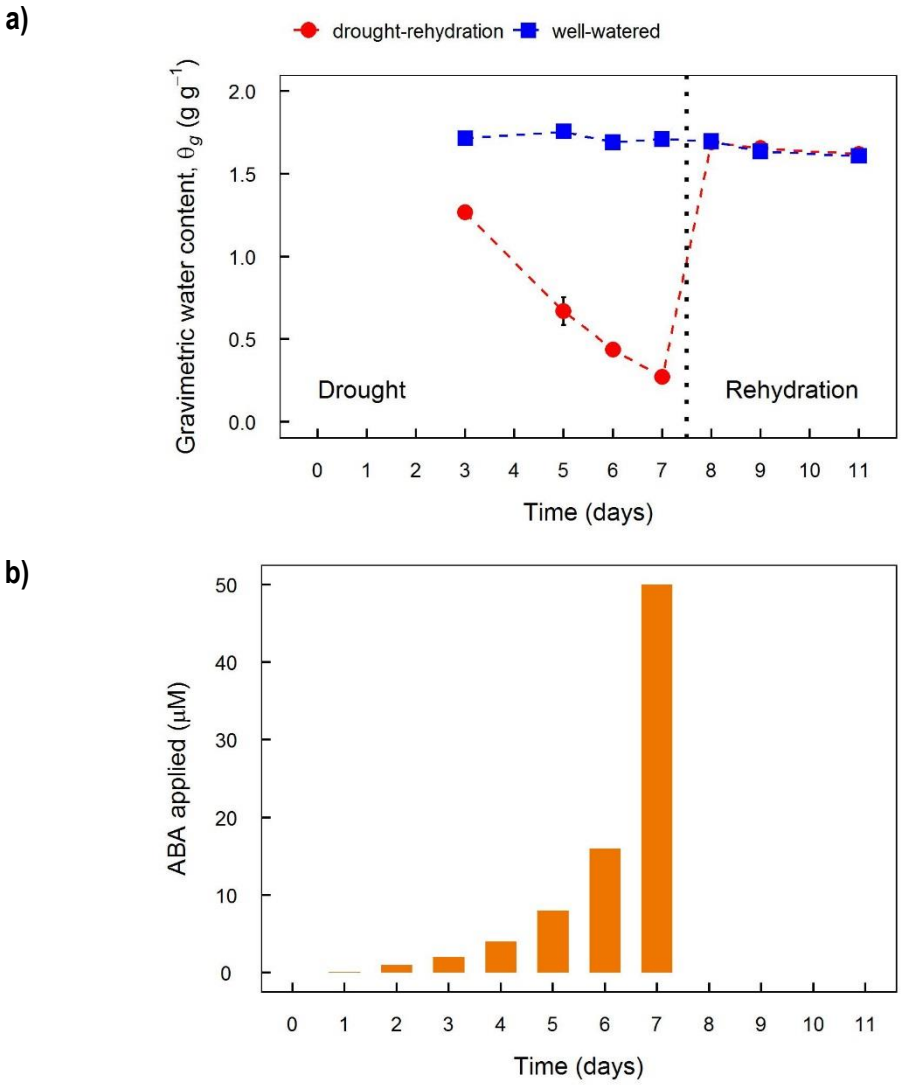

Figure 3. Application of drought stress and ABA treatments in the drought-rehydration and ABA experiments, respectively. a) Gravimetric water content (θ_g) of soil samples from the drought – rehydration experiment. For the "drought – rehydration" group (solid red circles) watering was withheld from day 1 till day 7 (wilting point), after which watering to field capacity was resumed. The "well – watered" group (solid blue squares) was watered to field capacity each day of the experiment. Soil of the entire pot was collected after sampling plants for experiments. Each point represents the mean ± SE of four or five pots. b) ABA concentration in watering solution for the ABA treatment. Each plant was watered with 30 mL of solution in the morning of each day of the experiment. ABA concentration was increased from day 1 till 7 (0.1, 1, 2, 4, 8, 16, 50 µM). On day 0 and day 8 till 11, a mock solution without ABA was applied. Likewise, mock-control plants were watered with a mock solution without ABA but containing ethanol (0.0002-0.1 %).

2.3.2. Plant responses to drought – rehydration and ABA treatment

Both drought and ABA treatment caused a decrease in stomatal conductance (g_s) compared to the well-watered or mock-control plants (Figure 4).

In the drought-rehydration experiment, plants which were not watered maintained the same g_s compared to the well-watered controls until day 4 (Figure 4a). Afterwards g_s declined rapidly till day 7 and was significantly lower compared to the controls. On day 7 wilting was observed for most plants. Upon

rewatering, which was done after the measurements on day 7, plants recovered and g_s increased again albeit not recovering to the average g_s measured at the beginning of the experiment.

Notably, also well-watered control plants showed variations in g_s during the experiment. On day 6, g_s of well-watered plants dropped significantly and remained low until day 10. A similar observation was made in a drought and rehydration trial experiment, which was conducted before this study (Supplementary Figure S3). In the trial, stomatal conductance of well-watered control plants decrease concomitantly with the drought treated plants and increased again after re-watering of the droughted plants.

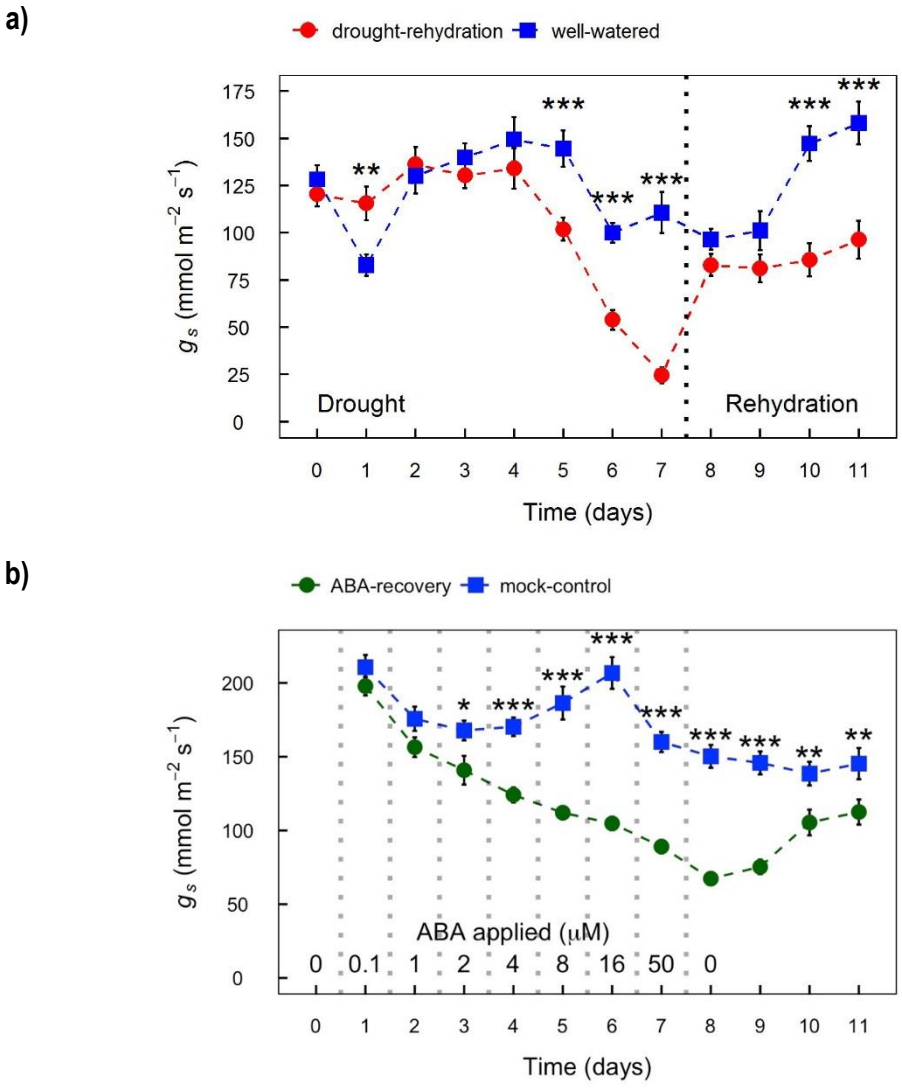

Figure 4. Stomatal conductance (g_s) measured on leaves of Arabidopsis plants (*Arabidopsis thaliana*) ecotype Col-0 used in the drought – rehydration and ABA watering experiments. Each point represents the mean ± SE of five independent plants on which g_s was measured on four leaves each. Significant differences between the treated and control groups by ANOVA with Bonferroni post-tests are marked: * for P ≤ 0.05, ** for P ≤ 0.01 or *** for P ≤ 0.001. a) Drought – rehydration: For plants of the "drought – rehydration" group (solid red circles) watering was withheld from day 1 till day 7 (wilting point), after which watering to field capacity was resumed. Plants of the "well – watered" group (solid blue squares) were watered to field capacity each day of the experiment. b) ABA watering: Plants of the "ABA recovery" group (solid green circles) were watered with ABA

solution of increasing concentrations (annotation above x-axis) till day 7; afterwards mock – control solution was applied for recovery. Plants of the "mock-control" group (solid blue squares) were only watered with the mock – control solution each day.

Similar to the drought-rehydration experiment, watering with solutions of increasing ABA concentrations was effective in closing stomata of treated plants (Figure 4b). On day 3, when solution with 2 µM ABA was applied, g_s of the treated plants was significantly lower compared to the mock-control plants. Each day higher concentrations of ABA were applied, the g_s declined further. From day 8 plants from the treated group were watered with the mock-control solution for recovery and g_s started to increase again albeit not reaching the same value as control plants till day 11. The mock-control plants also showed changes in g_s during the course of the experiment.

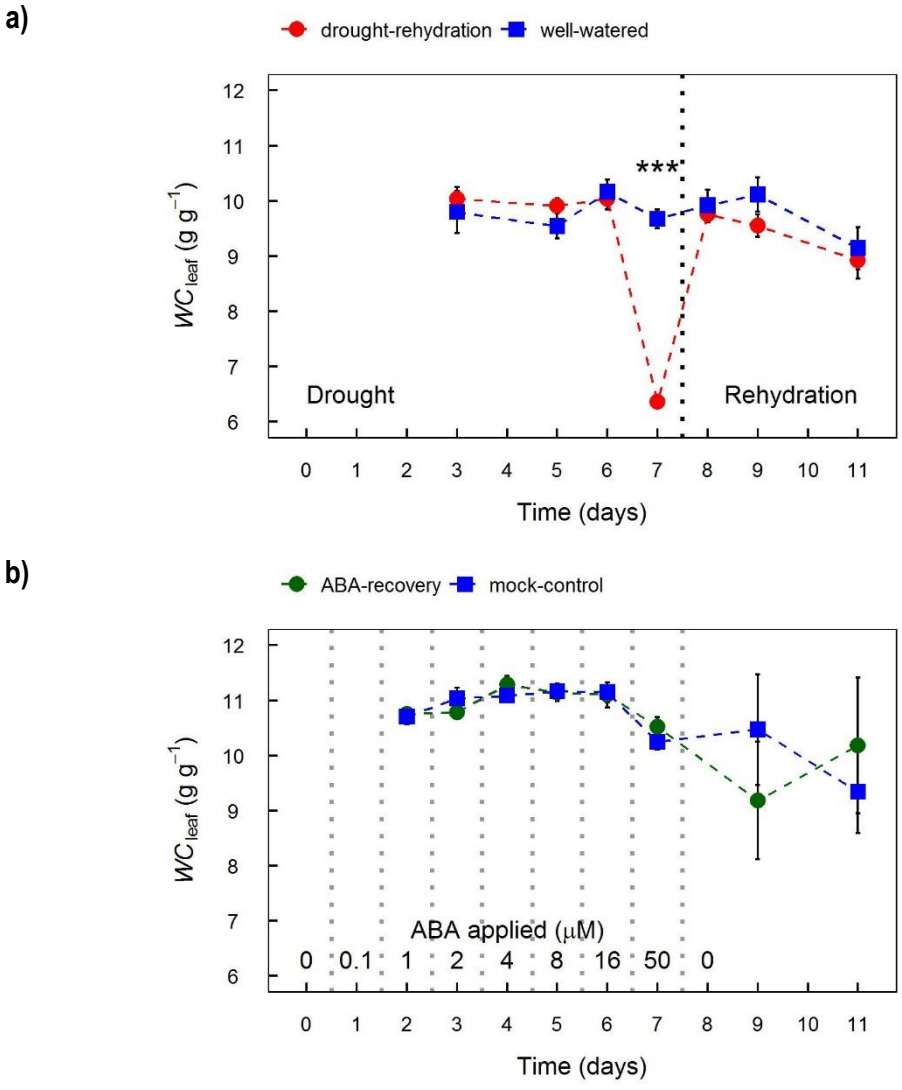

Figure 5. Absolute leaf water content (WC_{leaf}) of leaves of Arabidopsis plants (*Arabidopsis thaliana*) ecotype Col-0 collected in the drought-rehydration and ABA watering experiments. Each point represents the mean ± SE of five independent plants on which WC_{leaf} was measured on two leaves each. Significant differences between the treated and control groups by ANOVA with Bonferroni post-tests are marked: *** for P ≤ 0.001. a) Drought – rehydration: For plants of the "drought – rehydration" group (solid red circles) watering was withheld from day 1 till day 7 (wilting point), after which watering to field capacity was resumed. Plants of the "well – watered" group (solid blue squares) were watered to field capacity each day of the experiment.

b) ABA watering: Plants of the "ABA recovery" group (solid green circles) were watered with ABA solution of increasing concentrations (annotation above x-axis) till day 7; afterwards mock – control solution was applied for recovery. Plants of the "mock-control" group (solid blue squares) were only watered with the mock – control solution each day.

Absolute leaf water content (WC_{leaf}), which reflects the water to dry weight ratio in a leaf, was very stable for plants in the drought-rehydration experiment, except on day 7 when plants from the drought group showed a significant lower leaf water content compared to plants from the well-watered group (Figure 5a). At the same time wilting was observed for these plants. Once re-watered, WC_{leaf} recovered immediately to the level of well-watered plants.

Plants from the ABA watering experiment (Figure 5b) had, on average, a higher WC_{leaf} (10.6 g g^{-1}) compared to the drought-rehydration experiment (9.8 g g^{-1}). While there was no significant difference in WC_{leaf} between the ABA treated group and the mock-control group at any time, WC_{leaf} dropped on day 7 and showed a higher variance on days 9 and 11.

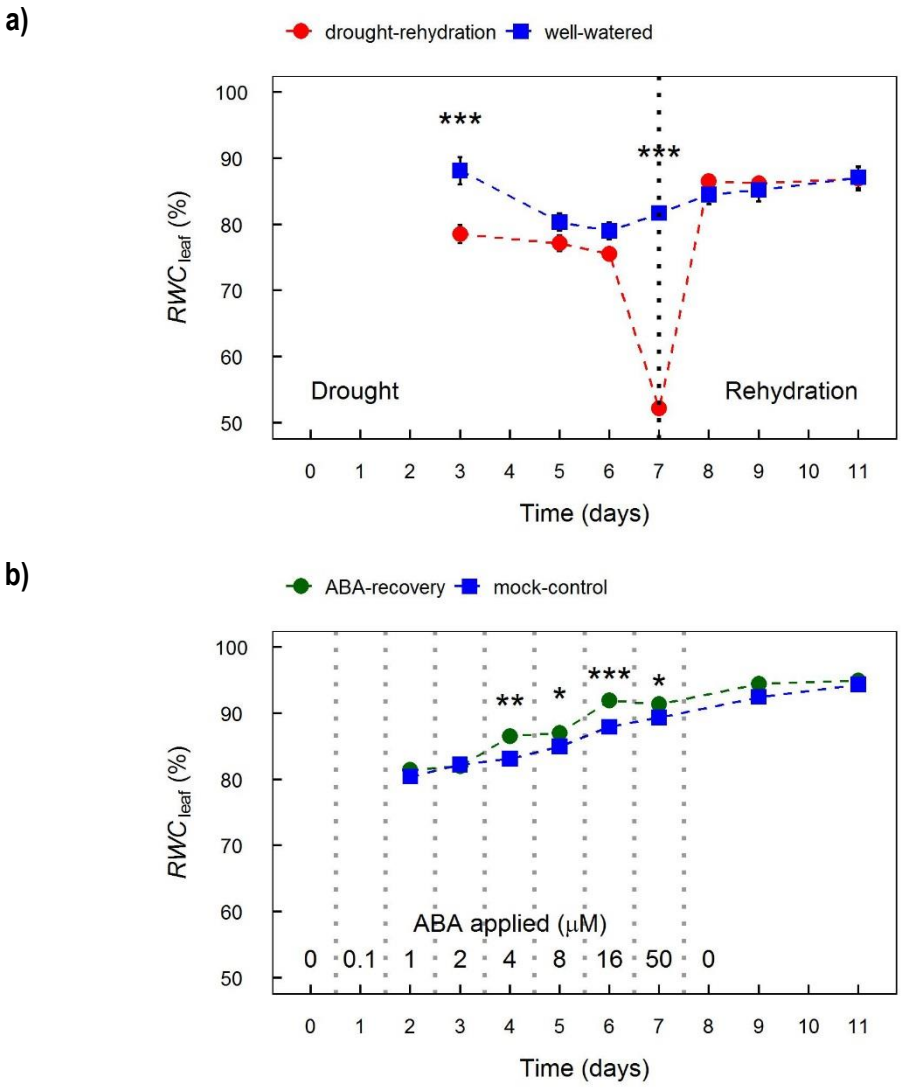

Figure 6. Relative water content (RWC_{leaf}) of leaves of Arabidopsis plants (*Arabidopsis thaliana*) ecotype Col-0 collected in the drought-rehydration and ABA watering experiments. Each point represents the mean ± SE of five independent plants on

which RWC_{leaf} was measured on two leaves each. Significant differences between the treated and control groups by ANOVA with Bonferroni post-tests are marked: * for P ≤ 0.05, ** for P ≤ 0.01 or *** for P ≤ 0.001. a) Drought – rehydration: For plants of the "drought – rehydration" group (solid red circles) watering was withheld from day 1 till day 7 (wilting point), after which watering to field capacity was resumed. Plants of the "well – watered" group (solid blue squares) were watered to field capacity each day of the experiment. b) ABA watering: Plants of the "ABA recovery" group (solid green circles) were watered with ABA solution of increasing concentrations (annotation above x-axis) till day 7; afterwards mock – control solution was applied for recovery. Plants of the "mock-control" group (solid blue squares) were only watered with the mock – control solution each day.

In contrast to WC_{leaf}, the relative leaf water content (RWC_{leaf}) was significantly lower in the drought treated group on day 3 compared to the well-watered controls in the drought-rehydration experiment (Figure 6a). RWC_{leaf} is considered to be proportional to turgor, if turgor is above zero and the elastic modulus remains the same (Jones and Turner 1978). On days 5 and 6 this difference was not significant, since RWC_{leaf} also decreased in the well-watered control plants. Similar to the WC_{leaf}, there was a strong, significant drop of RWC_{leaf} on day 7. After re-watering, drought treated plants recovered completely to the same level of RWC_{leaf} compared to the well-watered controls.

In the ABA watering experiment, ABA treated plants had a higher RWC_{leaf} compared to the mock-control plants, which was significant on days 4 to 7 (Figure 6b). While the average RWC_{leaf} was similar between the drought-rehydration and ABA watering experiment, a trend of increasing RWC_{leaf} was observed in the ABA watering experiment.

a)

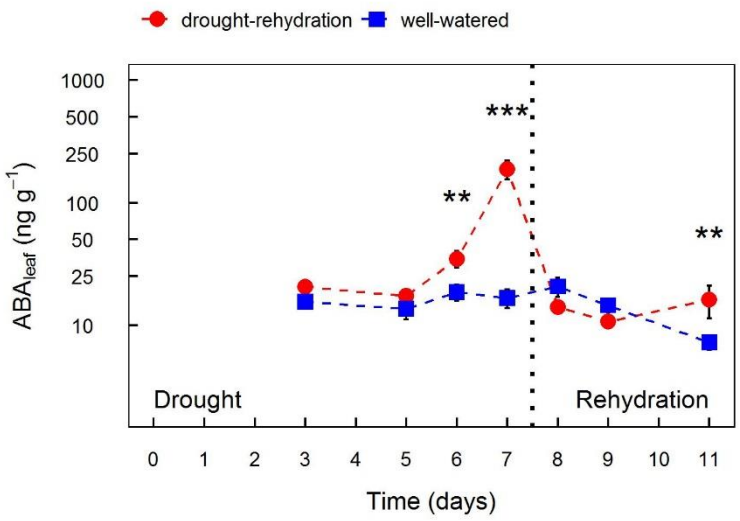

b)

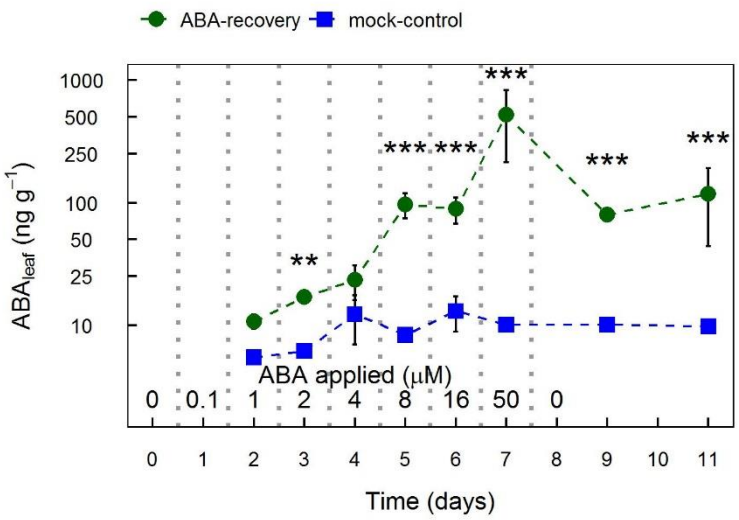

Figure 7. ABA concentrations (ABA_{leaf}) of leaves of Arabidopsis plants (*Arabidopsis thaliana*) ecotype Col-0 collected in the drought-rehydration and ABA watering experiments. Each point represents the mean ± SE of five independent plants from which two leaves each were collected and pooled for ABA_{leaf} measurement. Significant differences between the treated and control groups by ANOVA with Bonferroni post-tests are marked: ** for P ≤ 0.01 or *** for P ≤ 0.001. a) Drought – rehydration: For plants of the "drought – rehydration" group (solid red circles) watering was withheld from day 1 till day 7 (wilting point), after which watering to field capacity was resumed. Plants of the "well – watered" group (solid blue squares) were watered to field capacity each day of the experiment. b) ABA watering: Plants of the "ABA recovery" group (solid green circles) were watered with ABA solution of increasing concentrations (annotation above x-axis) till day 7; afterwards mock – control solution was applied for recovery. Plants of the "mock-control" group (solid blue squares) were only watered with the mock – control solution each day.

Leaf abscisic acid concentration (ABA_{leaf}) was similar and stable for drought treated and well-watered plants till and including day 5 in the drought-rehydration experiment (Figure 7a). On day 6, a significant increase of ABA_{leaf} was measured in drought treated plants, which comes after the initial decrease of g_s (Figure 4a). From day 6 to day 7, there was a very strong increase, up to an average of 188 ng ABA g^{-1} FW (Figure 7a). Upon re-watering, ABA_{leaf} immediately declined to values similar to the well-watered controls. On day 11, plants from the re-watered group had again a significant higher ABA_{leaf} compared to the well-watered control plants. This difference could also be due to a drop in ABA_{leaf} in the well-watered control plants towards the end of the experiment.

In comparison to the drought-rehydration experiment, plants from the ABA experiment had a lower ABA_{leaf} at the beginning of the experiment (Figure 7b). Watering the plants with solutions of increasing ABA concentrations, was effective in increasing the ABA_{leaf}. From day 3 the ABA_{leaf} was significantly higher in the ABA treated plants, compared to the mock-controls. The average maximum ABA_{leaf}, which was measured on day 7, was 523 ng ABA g^{-1} FW. When plants from the ABA group were watered with mock-control solution from day 8, ABA_{leaf} declined slightly but still remained very high. The mock-control plants showed an increase in ABA_{leaf} from day 1 to 4, but remained stable thereafter.

2.3.3. Changes in gene expression in response to drought – rehydration and ABA treatment

Measurements of gene expression in leaves from plants of the drought-rehydration and ABA treatment experiment showed significant differences.

Many genes were significantly differentially expressed in droughted compared to well-watered plants (Figure 8a). In particular, on day 7, when the drought was most severe, gene expression was significantly up- or down-regulated. Most aquaporin genes were significantly down-regulated. The gene which was most strongly down-regulated was *AtTIP2;2*, which showed about a 25-fold reduction in expression compared to the expression in leaves of well-watered plants. Other tonoplast localised aquaporins (*AtTIP1;1*, *AtTIP1;2*, *AtTIP2;1*) also showed a strong reduction in gene expression. From the sub-family of plasma membrane localised aquaporins, *AtPIP2;2* showed the strongest reduction in expression; by about 20-fold. Interestingly, some aquaporin genes were also up-regulated. The plasma membrane localised aquaporins *AtPIP1;4*, *AtPIP2;4*, and *AtPIP2;5* were about 5-fold up-regulated. This was very similar to the genes *AtNCED3* and *AtABI1* which are involved in ABA synthesis and signalling. The gene *AtNCED3* was already more than 2-fold up-regulated on day 6 and the gene *AtPIP2;4* remained up-regulated from day 7 until day 9.

In contrast, only a few genes were significantly differentially expressed in plants subjected to the ABA treatment (Figure 8b). Only *AtSYP122* and *AtTIP2;1* were more than 2-fold up- or down-regulated on day 5, respectively. More genes were about 1.5-fold significantly up- or down-regulated, but no trend was visible such as genes were differentially expressed on certain days of the experiment.

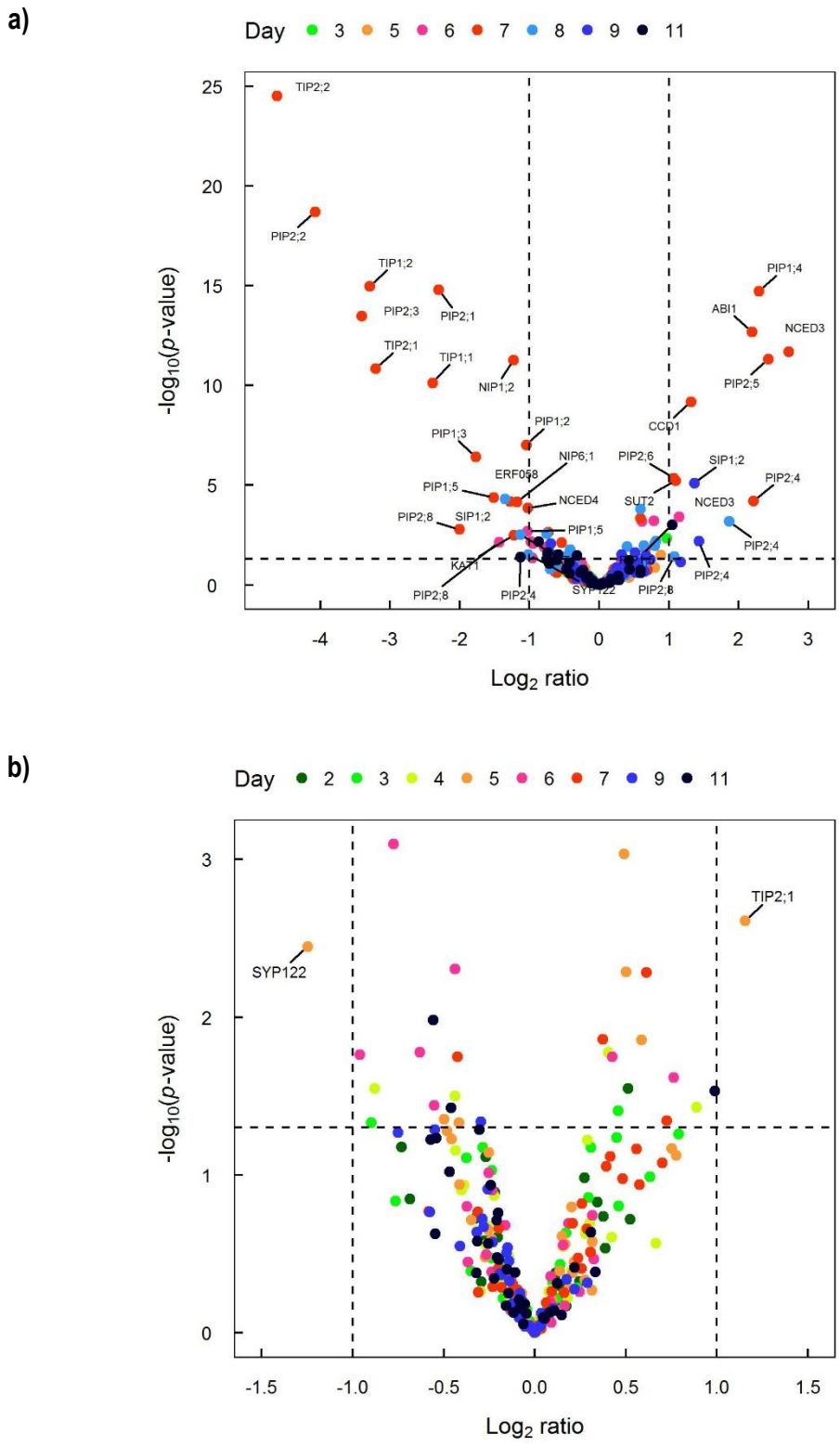

Figure 8. Volcano plot representation of differentially expressed genes in leaves of *Arabidopsis thaliana* during the a) drought-rehydration and b) ABA treatment experiments. Log_2 ratios are shown as difference between the mean expression of drought treated versus well-watered plants or ABA treated versus mock-control plants. Vertical dashed lines indicate 2 fold changes in expression. *P*-values were calculated by ANOVA with Bonferroni post-tests. The horizontal dashed line shows the significance cut-off at $p \leq 0.05$. Gene expression from different days is colour coded. Labels with gene names are given for genes that were significantly differentially expressed ($p \leq 0.05$) and at least 2-fold up- or down-regulated.

Gene co-expression was investigated for leaf samples from drought treated and subsequently rehydrated plants and from plants which were watered with ABA solutions by cluster analysis to find similar patterns of gene expression.

Three major clusters (blue+yellow, brown, turquoise) of gene co-expression were found for samples from drought treated and subsequently rehydrated plants (Figure 9a). The largest cluster (blue+yellow) comprised mainly aquaporin genes that were up-regulated during drought, as shown in Figure 8a. This cluster was divided into two modules: blue and yellow. The yellow module contained mainly PIP1 aquaporin genes. In particular, gene expression of *AtPIP1;1*, *AtPIP1;2* and *AtPIP1;3* were highly correlated. In contrast to genes in the yellow module, genes in the blue module were negatively correlated to genes in the brown module. In the blue module, some PIP2 and all TIP aquaporins were found and were strongly correlated. The brown module contained genes related to ABA synthesis and stress signalling like *AtNCED3*, *AtCCD1*, and *AtABI1*, a sucrose transporter *AtSUT2*, and also four aquaporin genes *AtPIP1;4*, *AtPIP2;5*, *AtPIP2;6*, and *AtSIP1;1*. These genes were shown to be up-regulated during drought stress as seen in Figure 8a. The turquoise module contained the remaining genes. Expression of *AtRAP2.4*, a transcription factor, and *AtKAT1*, a potassium channel involved in stomatal opening, were positively correlated to most genes from the blue+yellow module. The transcriptional repressor *AtMYB2* was found to be negatively correlated to expression of aquaporin genes in the blue module.

In contrast to gene expression affected by drought, samples from ABA treated plants showed significantly different patterns of co-expression (Figure 9b). Most aquaporin genes don't group anymore together in modules. Compared to the hierarchical clustering for the drought-rehydration samples, lower linkage was found for gene expression from the ABA treated samples. Expression of some genes like *AtPIP2;1*, *AtTIP1;1*, and *AtTIP1;2* still showed a good correlation as seen in the blue module. Also *AtSYP122*, *AtMYB2*, *AtERF058*, and *AtSIP2;1* did still group together in the turquoise module similar to the drought-rehydration experiment in Figure 9a.

a)

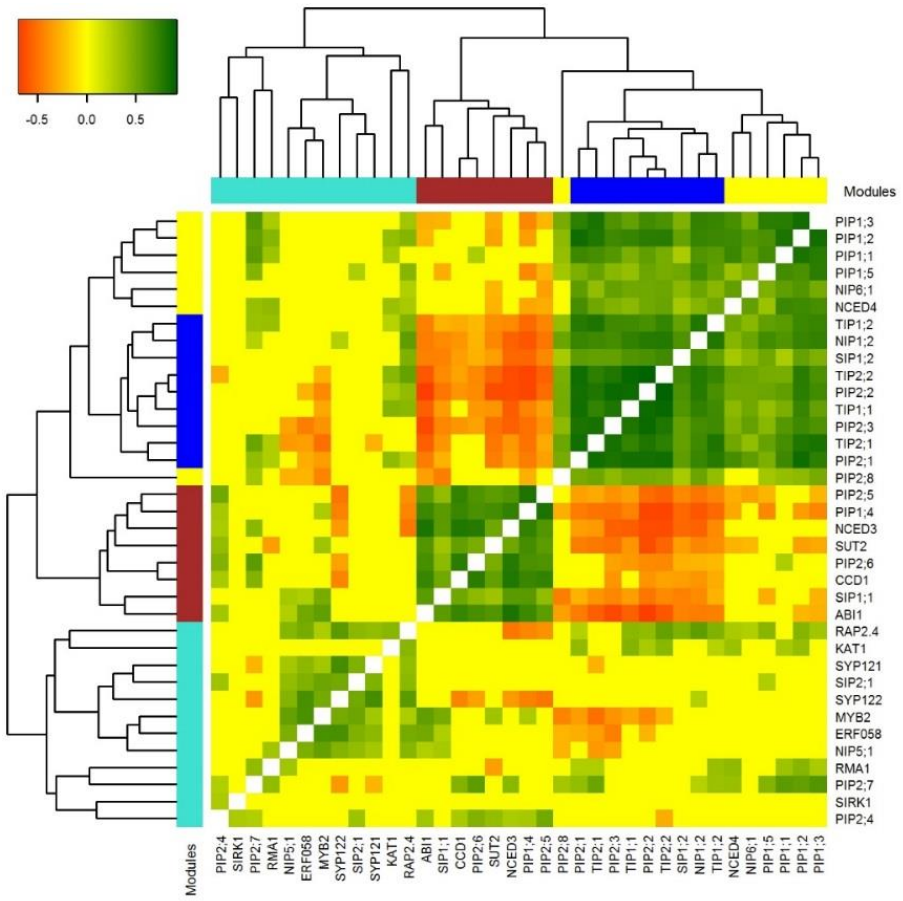
-0.5
0.0
0.5
Modules
PIP1;3
PIP1;2
PIP1;1
PIP1;5
NIP6;1
NCED4
TIP1;2
NIP1;2
SIP1;2
TIP2;2
PIP2;2
TIP1;1
PIP2;3
TIP2;1
PIP2;1
PIP2;8
PIP2;5
PIP1;4
NCED3
SUT2
PIP2;6
CCD1
SIP1;1
ABI1
RAP2.4
KAT1
SYP121
SIP2;1
SYP122
MYB2
ERF058
NIP5;1
RMA1
PIP2;7
SIRK1
PIP2;4
Modules
PIP2;4
SIRK1
PIP2;7
RMA1
NIP5;1
ERF058
MYB2
SYP122
SIP2;1
SYP121
KAT1
RAP2.4
ABI1
SIP1;1
CCD1
PIP2;6
SUT2
NCED3
PIP1;4
PIP2;5
PIP2;8
PIP2;1
TIP2;1
PIP2;3
TIP1;1
PIP2;2
TIP2;2
SIP1;2
NIP1;2
TIP1;2
NCED4
NIP6;1
PIP1;5
PIP1;1
PIP1;2
PIP1;3

b)

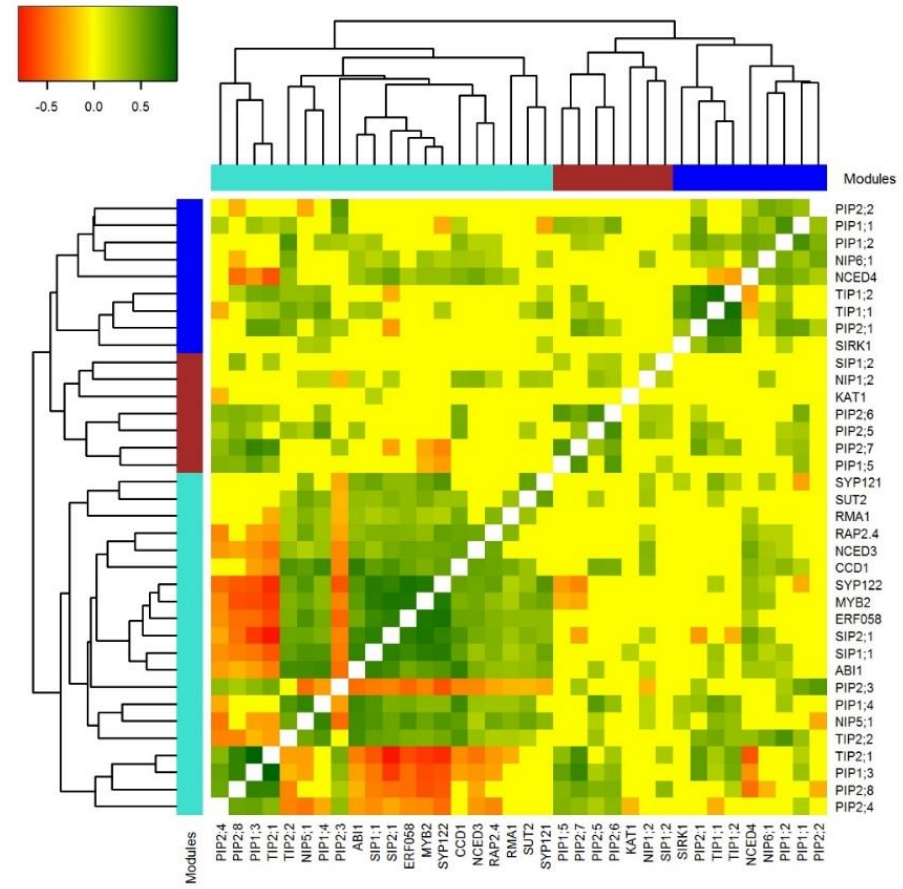
-0.5
0.0
0.5
Modules
PIP2;2
PIP1;1
PIP1;2
NIP6;1
NCED4
TIP1;2
TIP1;1
PIP2;1
SIRK1
SIP1;2
NIP1;2
KAT1
PIP2;6
PIP2;5
PIP2;7
PIP1;5
SYP121
SUT2
RMA1
RAP2.4
NCED3
CCD1
SYP122
MYB2
ERF058
SIP2;1
SIP1;1
ABI1
PIP2;3
PIP1;4
NIP5;1
TIP2;2
TIP2;1
PIP1;3
PIP2;8
PIP2;4
Modules
PIP2;4
PIP2;8
PIP1;3
TIP2;1
TIP2;2
NIP5;1
PIP1;4
PIP2;3
ABI1
SIP1;1
SIP2;1
ERF058
MYB2
SYP122
CCD1
NCED3
RAP2.4
RMA1
SUT2
SYP121
PIP1;5
PIP2;7
PIP2;5
PIP2;6
KAT1
NIP1;2
SIP1;2
SIRK1
PIP2;1
TIP1;1
TIP1;2
NCED4
NIP6;1
PIP1;2
PIP1;1
PIP2;2

Figure 9. Cluster analysis of gene co-expression in leaves from *Arabidopsis thaliana* plants a) exposed to drought stress and rehydrated and b) watered with ABA solutions. For each set of gene expression data, a matrix of Pearson's correlation coefficients was calculated. Significant correlation coefficients ($p \leq 0.05$) are shown as colour gradient from green (positive correlation) to red (negative correlation); yellow represents no correlation. Genes were clustered into modules by hierarchical clustering using a distance matrix of the significant correlation coefficients. The modules are shown as horizontal and vertical colour bars with their corresponding dendrogram.

The expression of most genes in leaves from plants, which were droughted and rehydrated (D-R) was significantly ($p \leq 0.05$) positive or negative correlated to the measured plant physiological parameters like stomatal conductance (g_s), abscisic acid concentration in leaves (ABA), absolute water content of leaves (WC), and relative water content of leaves (RWC) across the whole time of the experiment (all days) (Figure 10). The gene expression of *AtABI1*, *AtCCD1*, *AtNCED3*, *AtERF058*, *AtPIP1;4*, *AtPIP2;5*, *AtPIP2;6*, *AtSIP1;1*, and *AtSUT2* were positive correlated to ABA concentration in the leaves. Interestingly, gene expression of the aquaporins *AtNIP5;1* and *AtPIP2;7* was not correlated to any of the physiological parameters. Also *AtPIP2;4* and *AtSIP2;1* showed only a weak negative correlation to absolute water content of the leaf. Stomatal conductance was highest positive correlated to *AtPIP2;2* ($r = 0.79$), followed by *AtPIP2;3* ($r = 0.78$), *AtTIP2;1* ($r = 0.73$), and *AtTIP2;2* ($r = 0.71$); the highest negative correlation was to *AtABI1* ($r = -0.78$). Dissecting the correlations (samples from droughted and rehydrated plants only) for the experiment into different periods showed that significant positive correlations between gene expression of *AtPIP1;1*, *AtPIP1;2*, *AtPIP2;2, and AtTIP2;2* and stomatal conductance appeared consistently from day 5 (< day 6), when the stomata started to respond to the water deficit. Significant positive correlations between ABA biosynthesis genes *AtNCED3*, *AtCCD1* and aquaporin *AtPIP1;4* and leaf ABA concentration appeared from day 6 (< day 7). The highest positive correlation to ABA for the whole time of the experiment (all days) was found for *AtABI1* ($r = 0.85$), followed by *AtCCD1* ($r = 0.79$), *AtPIP1;4* ($r = 0.79$), and *AtNCED3* ($r = 0.75$). Overall, the highest (positive or negative) correlation coefficient was found between the gene expression of *AtTIP2;2* and RWC ($r = 0.91$). Gene expression which was positive correlated to g_s was usually also positive correlated to WC and RWC, but negative correlated to ABA_{leaf}.

In contrast, fewer significant correlations were found between gene expression in leaves from plants in the ABA treatment group and plant physiological parameters measured on leaves of the ABA treatment experiment for the whole time of the experiment (all days). The overall highest correlation found for this data was a positive correlation between *AtSIP2;1* and RWC ($r = 0.83$); this correlation was not found in the drought-rehydration experiment. Contradictory coefficients were shown for most correlations to RWC between the two experiments. Almost no correlations were found between gene expression and ABA concentration in the leaf and WC.

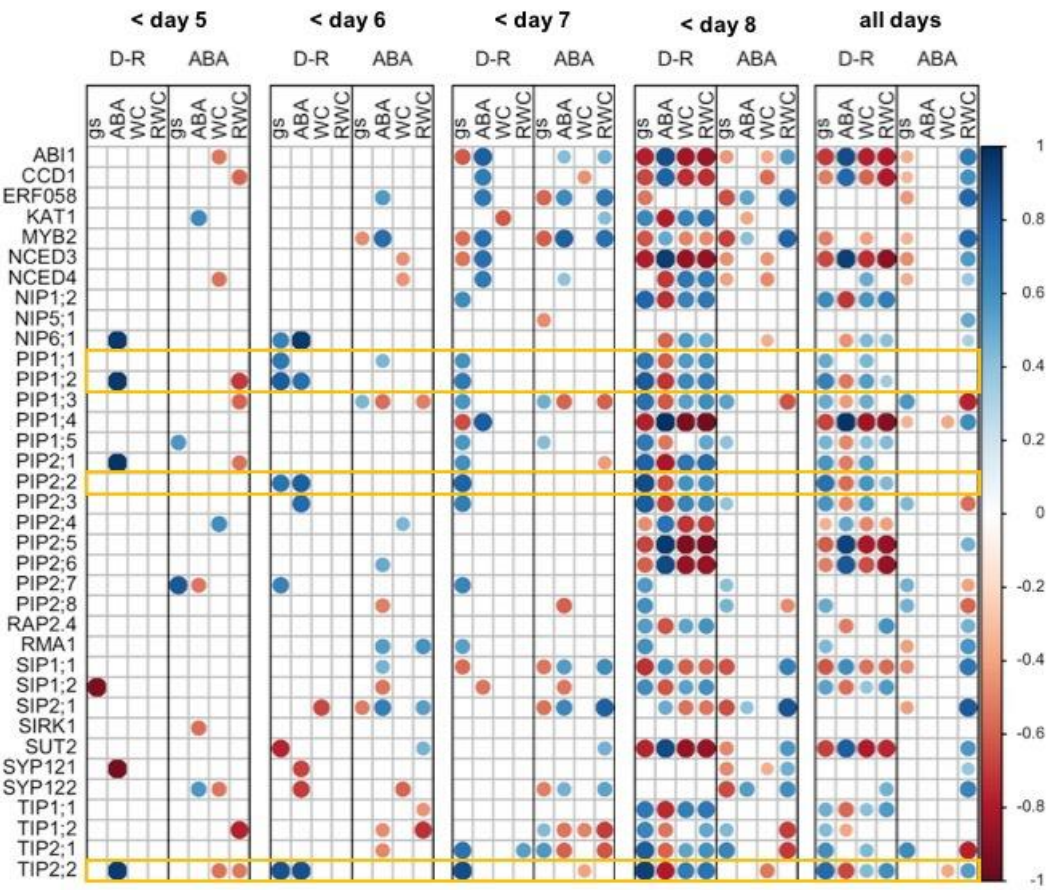

Figure 10. Pearson correlation matrices between plant physiological parameters and gene expression in leaves of *Arabidopsis thaliana*, which were droughted and rehydrated (D-R) or watered with ABA solutions (ABA). Correlation coefficients were calculated and non-significant ($p > 0.05$) correlations excluded (blank spaces). Positive correlations are shown in blue, while negative correlations are shown in red. The colour hue and size of the dot indicate the strength of the correlation. Correlation matrices are shown for data from different time periods of the experiment to demonstrate for which part of the experiment significant correlations were found.

Analysis of the correlations found between stomatal conductance and expression of the genes *AtPIP2;2* and *AtTIP2;2* in leaves from droughted and rehydrated plants by linear regression showed that the regression lines have a y-intercept close to zero (Figure 11). Excluding data from the rehydration period of the experiment (day 8 till 11) reduced the scatter around the regression lines and increased the coefficients of determination, R^2 (Figure 11 inserts).

a)

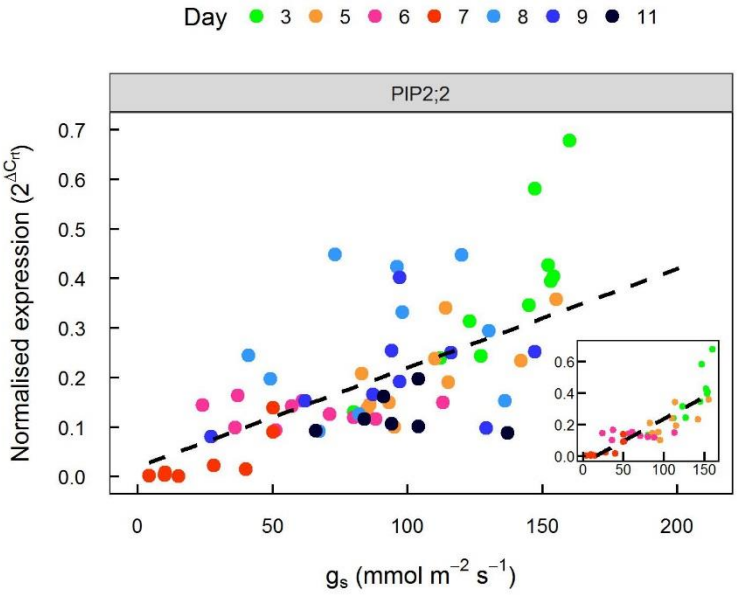

b)

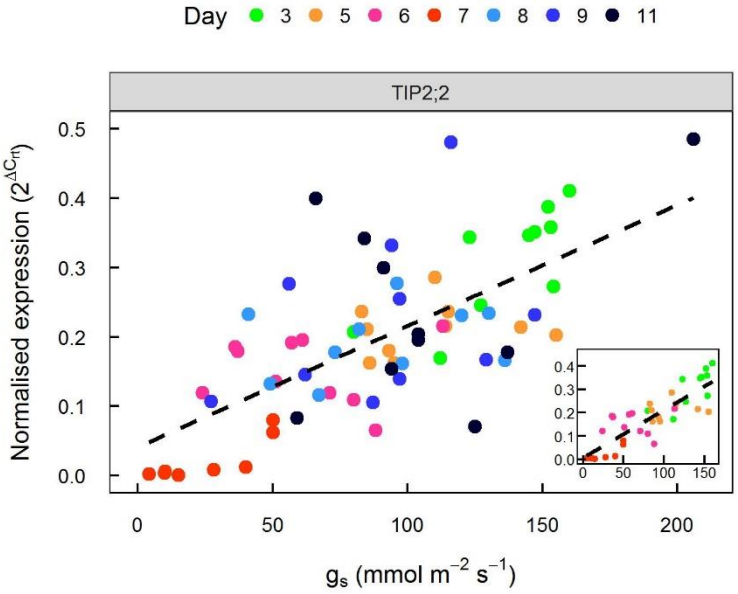

Figure 11. Linear regressions between stomatal conductance (g_s) and normalised expression (NRQ) of the aquaporin genes (a) *AtPIP2;2* and (b) *AtTIP2;2* in leaves of *Arabidopsis thaliana* plants which have been droughted and rehydrated as part of the drought and rehydration experiment. Each point shows data from individual leaves. Different colours indicate data collected on different days of the experiment. Watering was withheld from day 1 till day 7 (wilting point), after which watering to field capacity was resumed (day 8 till 11). While the main figures show regressions for data from all days (drought and rehydration), inserts show regressions only for data from day 3 till 7 (drought). Linear regressions: a) main figure NRQ ($2^{\Delta Crt}$) = 0.001997 ± 0.0003174*g_s (mmol m^{-2} s^{-1}) + 0.02036 ± 0.03187, R^2 = 0.3857; insert NRQ ($2^{\Delta Crt}$) = 0.002788 ± 0.0002861*g_s (mmol m^{-2} s^{-1}) - 0.04246 ± 0.02796, R^2 = 0.7251; b) main figure NRQ ($2^{\Delta Crt}$) = 0.001745 ± 0.000235*g_s (mmol m^{-2} s^{-1}) + 0.04124 ± 0.02345, R^2 = 0.4553; insert NRQ ($2^{\Delta Crt}$) = 0.002043 ± 0.0002087*g_s (mmol m^{-2} s^{-1}) + 0.006638 ± 0.0204, R^2 = 0.7269.

2.3.4. Soil water potential and relative hydraulic conductivity

Changes in soil water potential and relative hydraulic conductivity of the soil were investigated as triggers for the activation of drought stress responses. For the soil mixture used in the drought-rehydration

experiment, a soil water retention curve was recorded (Figure 12b). The experimental data was interpolated by two different models, the Groenevelt-Grant (blue line) and Van Genuchten (red line) equations, to convert measured gravimetric water content into matric head (h) or soil water potential (Ψ_s). The summaries of the nonlinear model fit for the Groenevelt-Grant and Van Genuchten equations are shown in Table 2.

While both models visually provide a close fit to the experimental data (Figure 12), the Van Genuchten model has a lower residual standard error (RSE = 0.046) compared to the Groenevelt-Grant model (RSE = 0.059). Hence, the Van Genuchten model was used for the calculation of soil water potentials. The horizontal dashed lines in Figure 12a show the average θ_g for samples that were collected during the drought-rehydration experiment on different days. Since the average θ_g for the drought group on day 7 was lower compared to the model, no soil water potentials could be calculated for these samples and, hence, they are assumed to be lower than -1 MPa (Figure 12b).

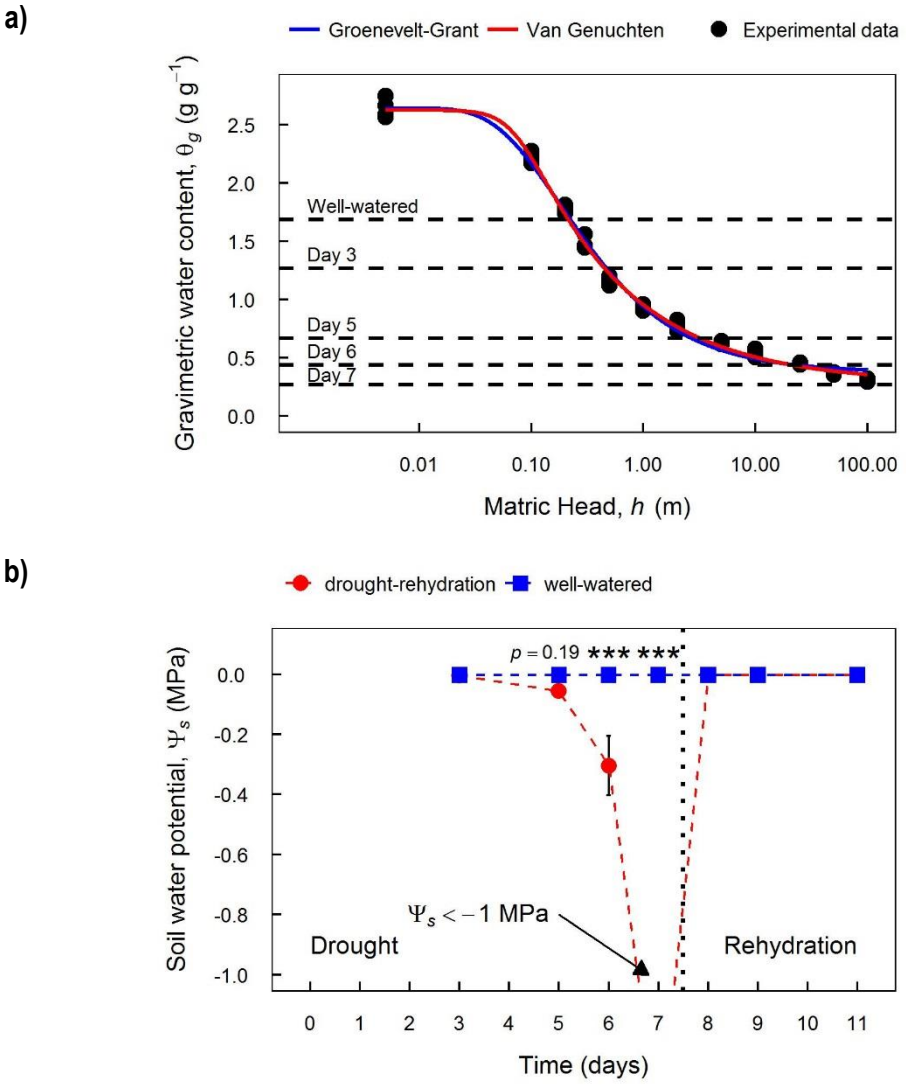

Figure 12. Soil water retention curve and calculated soil water potential (Ψ_s) for soil samples from the drought – rehydration experiment. a) Soil water retention for a soil mixture (85% (v/v) Seedling Substrate Plus+, Bord na Móna; 15% (v/v) Horticultural

Sand, Debco Pty Ltd) used in the drought – rehydration and ABA experiments was measured on small samples (approx.. 4 g) using the hanging water column and pressure plate method. For each step-change in gravimetric water content, five samples were measured (solid circles). Models by Groenevelt-Grant (blue line) (Eq. () and Van Genuchten (red line) (Eq. () were fitted to the data using nonlinear least square methods. Average gravimetric water content measured for the well-watered group and the drought group (days 3 – 7) from the drought-rehydration experiment are shown as horizontal dashed lines. b) Soil water potentials were calculated using predictions from the Van Genuchten model. Since soil water content on day 7 for the drought group was lower than the range of the soil water retention curve no predictions other than Ψ_s < -1 MPa could be made. Mean ± SE are shown. Significant differences between the drought-rehydration and well-watered groups by ANOVA with Bonferroni post-tests are marked: *** for P ≤ 0.001. On day 5, an almost significant difference was detected.

The calculated Ψ_s in Figure 12b show that Ψ_s of the drought treated plants dropped significantly below the well-watered controls only from day 6. On day 5, the average Ψ_s was lower in the drought treated pots than in the well-watered pots, but the difference was not significant. Once the drought treated pots were re-watered, the Ψ_s recovered back to that of the well-watered pots immediately.

Table 2. Summary of non-linear model fit parameters of the Groenevelt-Grant (Eq. 6) and Van Genuchten (Eq. 5) equations to the soil water retention curve. Soil water content (SWC) and matric head (MatricHead) were taken from the experimental data of the soil water retention curve. The Van Genuchten equation was fitted using the *SSvgm* function from the *HydroMe* R package (Omuto and Gumbe 2009).

Model: Groenevelt-Grant			
Parameter	**Estimate**	**Std. Error**	***p*-value**
θ_s	2.646406	0.025976	< 0.0001 ***
k_1	2.270783	0.032204	< 0.0001 ***
k_0	0.183207	0.006897	< 0.0001 ***
n	0.736099	0.026089	< 0.0001 ***
Residual standard error: 0.05861 on 61 degrees of freedom			
Model: Van Genuchten			
Parameter	**Estimate**	**Std. Error**	***p*-value**
θ_r	0.28417	0.02347	< 0.0001 ***
θ_s	2.63087	0.02062	< 0.0001 ***
α	13.48305	1.00262	< 0.0001 ***
n	3.23562	0.81597	0.000198 ***
m	0.14837	0.04360	0.001194 **
Residual standard error: 0.04606 on 60 degrees of freedom			

Changes in the relative hydraulic conductivity of the soil during the drought experiment were estimated through integration of the Groenevelt-Grant model with Mualem restriction (Grant *et al.* 2010). The relative hydraulic conductivity decreased exponentially with increasing matric head suction (Figure 13a). When matric head suction is transformed into gravimetric soil water content, it becomes clear that relative hydraulic conductivity declines steeply once gravimetric soil water content drops below 1 g g^{-1} (Figure 13b); this happened between day 3 and 5 as indicated by the dashed vertical lines.

A comparison of the relative hydraulic conductivity of soil from well-watered plants and droughted plants showed only a 10-fold difference on day 3, but a 800-fold difference on day 5, and a 10^6-fold difference on day 6 (Figure 13c). This emphasizes the steep decline of relative hydraulic conductivity of soil from droughted plants after day 3.

a)

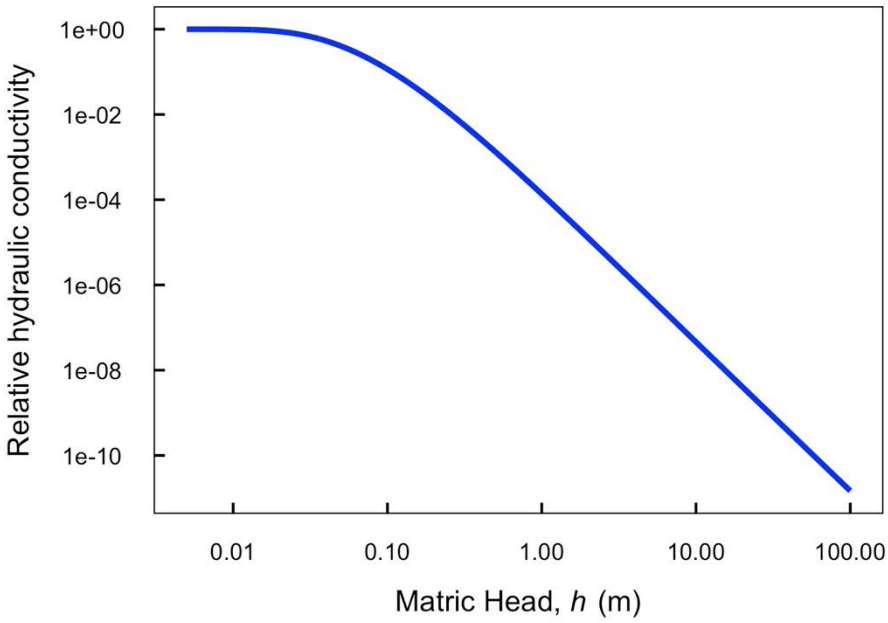

b)

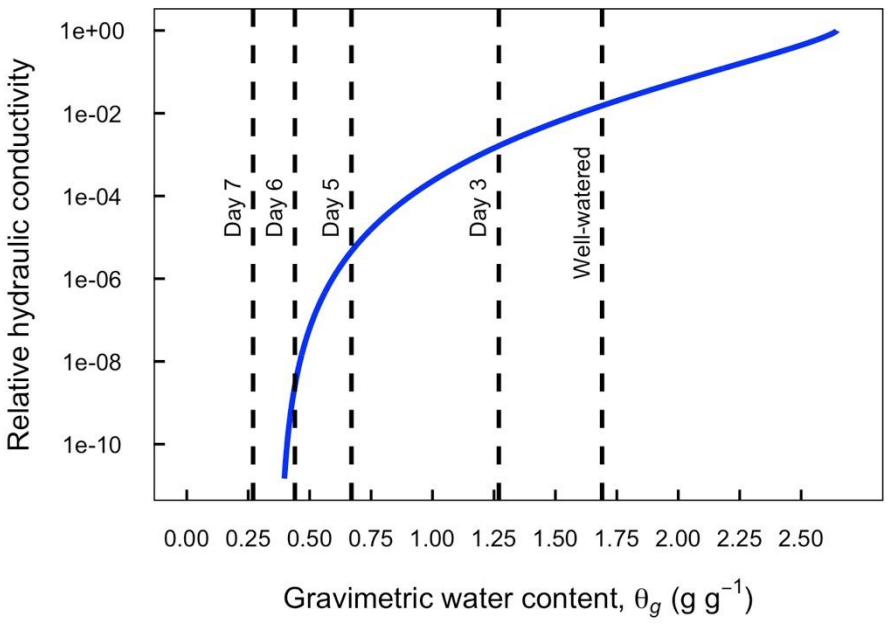

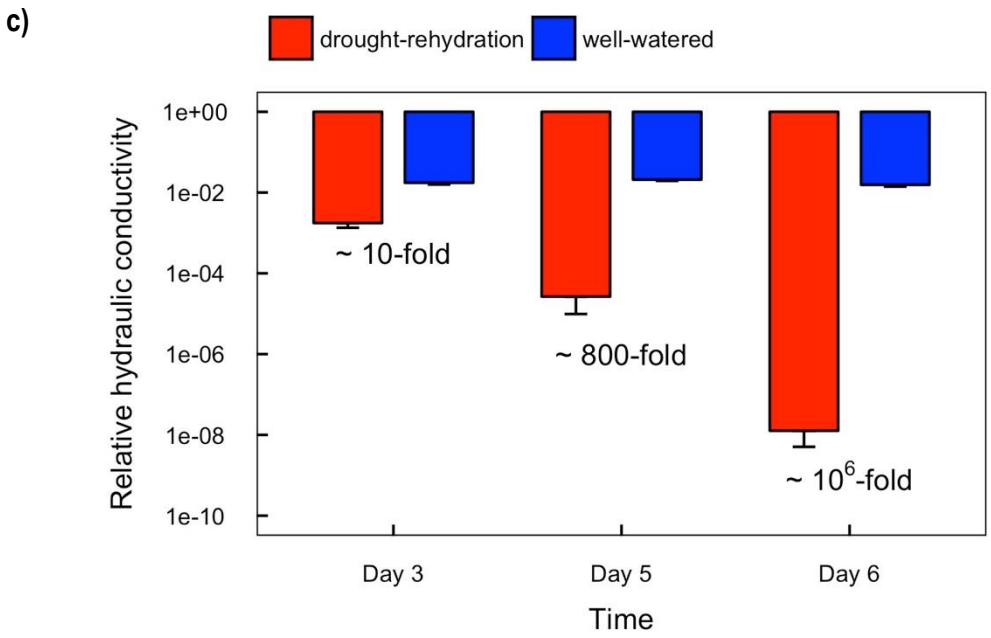

Figure 13. Relative hydraulic conductivities (relative to saturated hydraulic conductivity) predicted for soil samples from the drought – rehydration experiment. a) Based on the Groenevelt-Grant water retention model for the soil mixture (85% (v/v) Seedling Substrate Plus+, Bord na Móna; 15% (v/v) Horticultural Sand, Debco Pty Ltd) used in the drought-rehydration and ABA experiments, relative hydraulic conductivity of the soil was predicted as a function of Matric head (h) through integration and introduction of the Mualem model. b) Relative hydraulic conductivity shown as a function of soil water content (θ_g). Average gravimetric water content measured for the well-watered group and the drought group (days 3 – 7) from the drought-rehydration experiment are shown as horizontal dashed lines. c) Comparison of relative hydraulic conductivity between drought treated and well-watered controls for days 3, 5, and 6. Mean ± SE and approximate fold differences are shown.

2.3.2. Trigger and signalling for drought stress responses

Relationships between gravimetric soil water content (θ_g), soil water potential (Ψ_s), stomatal conductance (g_s) and abscisic acid concentration in leaves (ABA_{leaf}) were investigated to understand how changes in soil water availability trigger stress response through ABA and influence stomatal conductance.

A positive exponential relationship was found between θ_g and g_s (Figure 14a). The relationship shows that g_s declined most rapidly when $\theta_g \leq 0.5$ g g^{-1}. An extrapolation of the curve shows, that the x – intercept [$g_s(\theta_g) = 0$] is $\theta_g = 0.2$ g g^{-1}, which is close to the estimated residual soil moisture content (Table 2: $\theta_r = 0.28$ g g^{-1}) predicted by the Van Genuchten model (Figure 12a). Data for θ_g and g_s after re-watering (days > 7) didn't fit the same relationship.

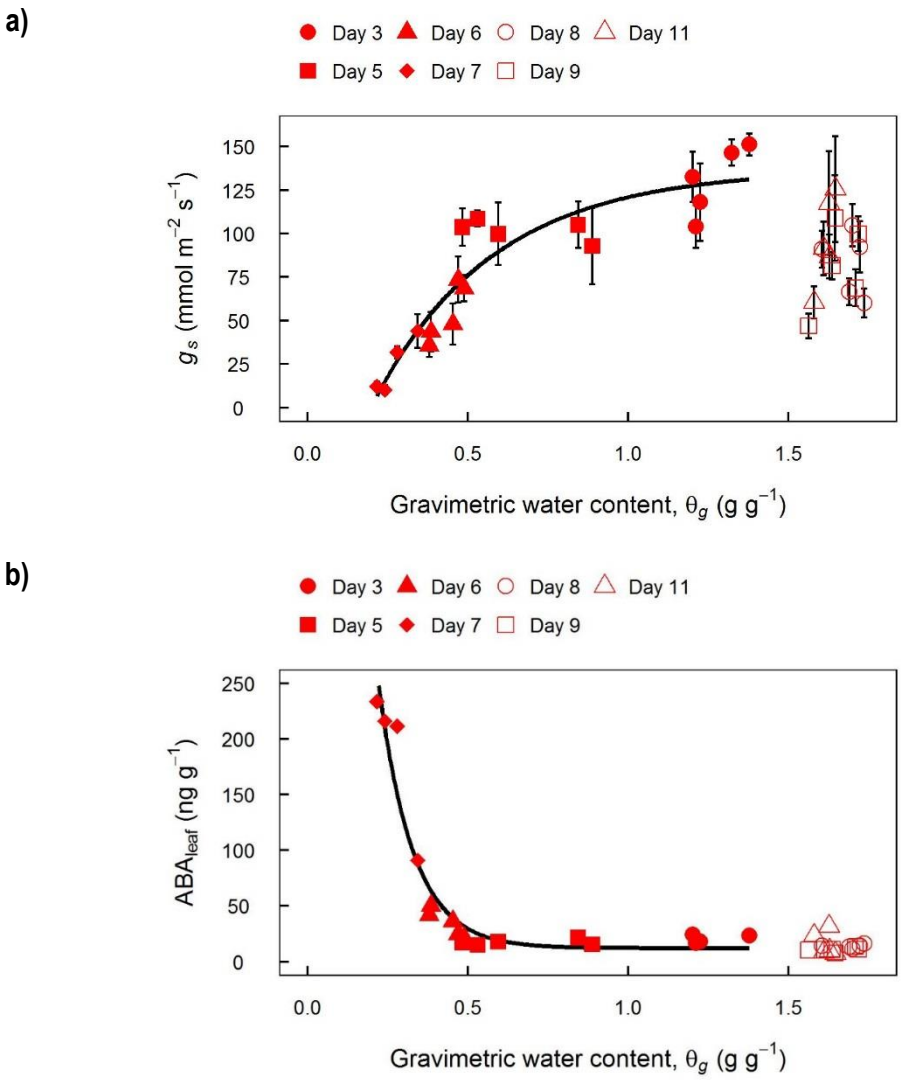

Figure 14. Relationship between gravimetric soil water content (θ_g) and stomatal conductance (g_s) or ABA concentrations (ABA_{leaf}) of leaves from drought treated Arabidopsis plants (*Arabidopsis thaliana*) ecotype Col-0 collected in the drought-rehydration experiment on days 3 (solid circles), 5 (solid squares), 6 (solid triangles), and 7 (solid diamonds). Data for re-watered plants are shown for days 8 (open circles), 9 (open squares), and 11 (open triangles). a) For each day, the average g_s ± SE per plant are shown. An exponential regression (solid black line) was fitted to days 3 – 7 (drought period) using nonlinear least-squares estimates (g_s (mmol m^{-2} s^{-1}) = -95.52 ± 47.90 + (136.87 ± 12.33 + 95.52 ± 47.90) * [1 – exp(– 2.68 ± 0.78 * θ_g (g g^{-1}))], r = 0.93). b) Data points represent individual plants; no error bars are shown. An exponential regression (solid black line) was fitted to days 3 – 7 (drought period) using nonlinear least-squares estimates (ABA_{leaf} (ng g^{-1}) = (1889.02 ± 623.50 – 11.93 ± 7.77) * exp(– 9.32 ± 1.42 * θ_g (g g^{-1})) + 11.93 ± 7.77, r = 0.97).

In contrast, the exponential relationship found between θ_g and ABA_{leaf} is negative (Figure 14b). Similar to the relationship with g_s, ABA_{leaf} increased rapidly when $\theta_g \leq 0.5$ g g^{-1}. In contrast to the relationship $g_s \sim \theta_g$, data for θ_g and ABA_{leaf} after re-watering (days > 7) would still fit the same relationship.

Similar to the relationships between θ_g and g_s or ABA_{leaf} (Figure 14), exponential relationships were also found to be the best fit between Ψ_s and g_s or ABA_{leaf} (Figure 15). Due to the fact that Ψ_s is close to zero at high θ_g, many points cluster around zero and a lower separation was achieved compared to using θ_g.

In particular, data from plants during the rehydration phase (> day 7) does not fit the exponential regressions. Figure 15a shows that data from day 3 and 5 already separated due to lower g_s and lower Ψ_s. On day 6, three plants didn't show a strong decline in Ψ_s yet, while two plants had a much lower Ψ_s.

An exponential relationship was also found for Ψ_s and ABA_{leaf} (Figure 15b), however, ABA_{leaf} only changed on day 6 (also shown in Figure 7), while Ψ_s already changed on day 5.

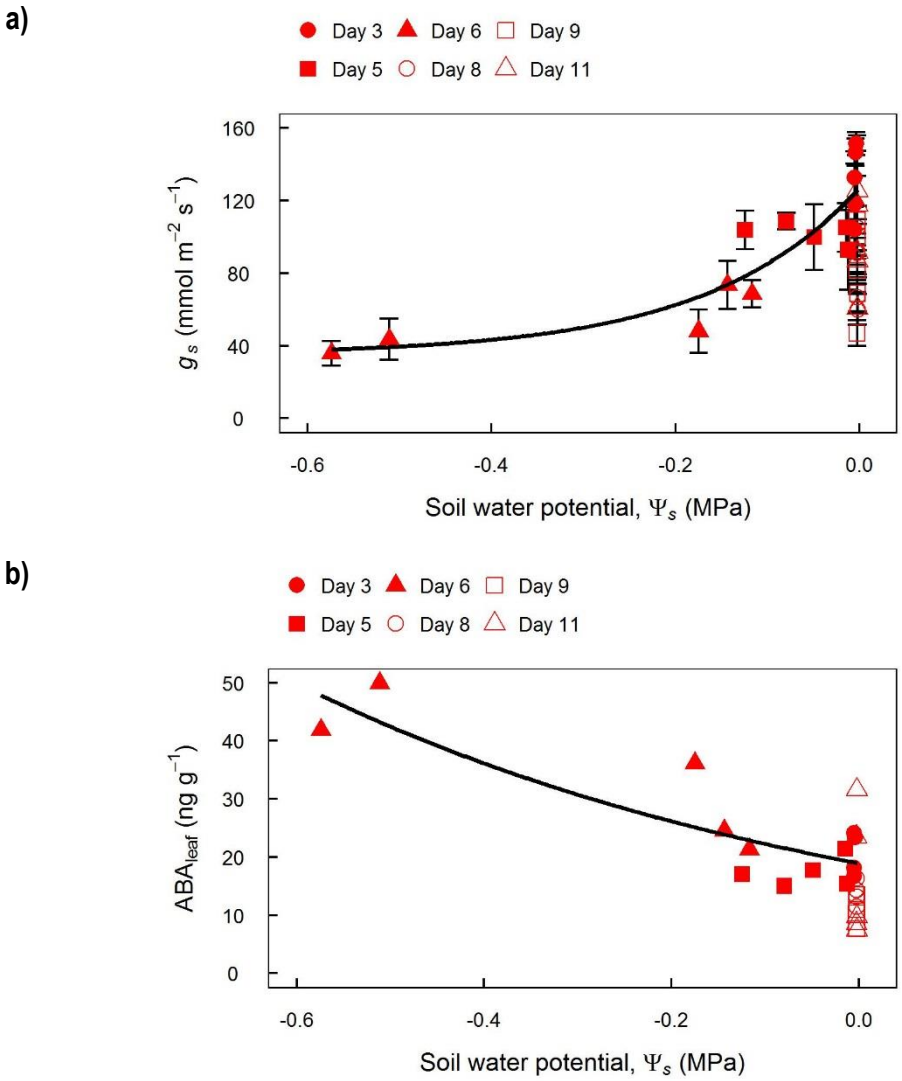

Figure 15. Relationship between calculated soil water potential (Ψ_s) and stomatal conductance (g_s) or ABA concentrations (ABA_{leaf}) of leaves from drought treated Arabidopsis plants (*Arabidopsis thaliana*) ecotype Col-0 collected in the drought-rehydration experiment on days 3 (solid circles), 5 (solid squares), and 6 (solid triangles). Data for re-watered plants are shown for days 8 (open circles), 9 (open squares), and 11 (open triangles). No day 7 is shown, since Ψ_s couldn't be calculated for that time point.). a) For each day, the average g_s ± SE per plant are shown. An exponential regression (solid black line) was fitted to days 3 – 6 (drought period) using nonlinear least-squares estimates (g_s (mmol m^{-2} s^{-1}) = (126.61 ± 7.72 – 34.93 ± 17.39) * exp(6.01 ± 2.77 * Ψ_s (MPa)) + 34.93 ± 17.39, r = 0.88). b) Data points represent individual plants; no error bars are shown. An exponential regression (solid black line) was fitted to days 3 – 6 (drought period) using nonlinear least-squares estimates (ABA_{leaf} (ng g^{-1}) = 18.97 ± 1.64 * exp(– 1.61 ± 0.23 * Ψ_s (MPa)), r = 0.87).

Comparisons between the relationship of ABA_{leaf} and changes in g_s for both experiments suggested a stronger response of g_s to changes in ABA_{leaf} during the drought-rehydration experiment compared to the ABA-recovery experiment (Figure 16). While higher maximum stomatal conductance and maximum ABA concentration in leaves were measured in the ABA-recovery experiment, g_s was reduced much more in the drought-rehydration experiment.

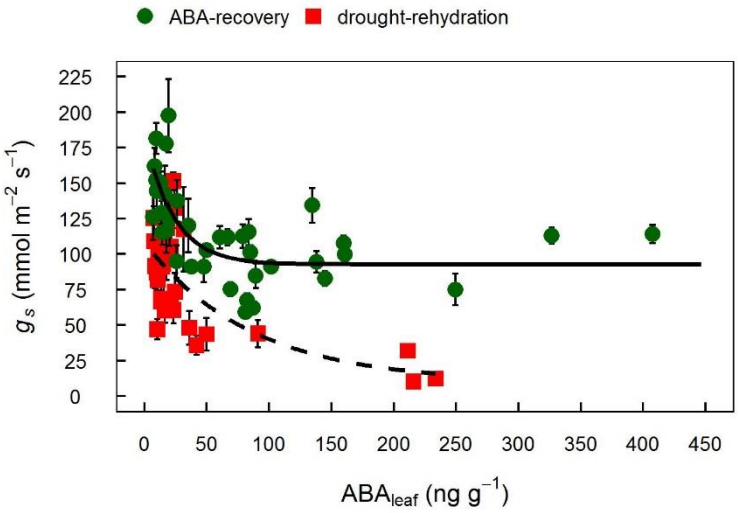

Figure 16. Relationship between ABA concentrations (ABA_{leaf}) and stomatal conductance (g_s) of leaves from Arabidopsis plants (*Arabidopsis thaliana*) ecotype Col-0 collected in the ABA experiment (solid green circles) and drought-rehydration experiment (solid red squares). Each point represents the average g_s ± SE measured on two leaves per plant and the ABA concentration from these two leaves measured as a pooled sample. Exponential regression lines were fitted to data from each experiment separately using nonlinear least-squares estimates: ABA experiment (solid line): g_s (mmol m^{-2} s^{-1}) = 91.18 ± 22.44 * exp(– 0.043 ± 0.020 * ABA_{leaf} (ng g^{-1})) + 92.75 ± 6.27, r = – 0.34 ; Drought-rehydration experiment (dashed line): g_s (mmol m^{-2} s^{-1}) = 99.25 ± 22.76 * exp(– 0.012 ± 0.009 * ABA_{leaf} (ng g^{-1})) + 9.24 ± 27.10, r = – 0.97. Both regressions are predicted to be significantly different ($P \leq 0.001$).

2.4. Discussion

2.4.1. Significant changes in aquaporin gene expression related to drought but not to extended exogenous ABA application

Hydraulic and chemical signals are involved in regulating stomatal responses to water deficit in plants (Tardieu and Davies 1993; Buckley and Mott 2013). The biosynthesis of the phytohormone abscisic acid during stress is known to be a trigger for stomatal closure, which helps the plant to conserve water when the soil is drying (Zhang *et al.* 1987; Christmann *et al.* 2007). Studies on gene expression of aquaporins in *Arabidopsis thaliana* comparing drought and exogenous ABA application found different responses (Jang *et al.* 2004; Parent *et al.* 2009). Jang *et al.* (2004) found that most genes encoding PIP aquaporins were down-regulated during drought, but the same genes were often up-regulated in response to

exogenous ABA exposure. A comprehensive study on gene expression of all aquaporins in *Arabidopsis thaliana* during drought showed that gene expression was down-regulated for all aquaporins except for *AtPIP1;4*, *AtPIP2;5*, *AtPIP2;6*, and *AtSIP1;1* (Alexandersson et al. 2005; Alexandersson et al. 2010).

The drought-rehydration and ABA watering experiments demonstrated that both drought and ABA were effective in triggering stomatal closure, but had a very different effect on leaf hydration and gene expression. While most aquaporin genes were down-regulated and most ABA synthesis and signaling genes were up-regulated during drought, almost no significant changes in gene expression were found during the ABA watering experiment (Figure 8). The observed changes in gene expression during drought and rehydration match with the observations by Alexandersson *et al.* (2005). The aquaporin isoforms *AtPIP1;4*, *AtPIP2;4*, and *AtPIP2;5* were about 5-fold up-regulated on day 7 of the drought stress (Figure 8a), when stomatal conductance was the lowest and plants started wilting (Figure 4a). The expression of *AtPIP2;4* remained also significantly elevated on days 8 and 9, after plants had been re-watered. For all three aquaporin isoforms, hydrogen peroxide (H_2O_2) permeability was observed in yeast assays (Hooijmaijers *et al.* 2012; Tian *et al.* 2016). Tian *et al.* (2016) showed that *AtPIP1;4* is involved in the transport of H_2O_2 from the apoplast into the symplast during the activation of disease immunity pathways. Likewise, H_2O_2 is important for signalling during ABA mediated stomatal closure (Pei *et al.* 2000). The co-expression analysis also showed very good correlations between the expression of *AtPIP1;4* and *AtPIP2;5* and *AtNCED3* and *AtCCD1*, which are involved in ABA biosynthesis (Figure 9a). Hence, up-regulation of these isoforms could be important for H_2O_2 transport as a signalling compound. A two-fold up-regulation was also observed for the isoform *AtPIP2;6*, while Alexandersson *et al.* (2005) reported this gene as constitutively expressed. Previous research indicated that *AtPIP2;6*, which is expressed around the vasculature in leaves, is important for the regulation of leaf hydraulic conductivity (Prado *et al.* 2013). Other significantly up-regulated genes included *AtABI1*, a phosphatase involved in ABA signalling (Merlot *et al.* 2001), and *AtSUT2*, a sucrose transporter important for abiotic stress tolerance, which is induced by ABA (Gong *et al.* 2015).

Surprisingly, none of the genes up-regulated during drought were found to be up-regulated at least 2-fold in response to the ABA watering (Figure 8b). The only gene that was found to be up-regulated about 2-fold was *AtTIP2;1* on day 5. Previous research had shown that gene expression of PIP aquaporins in Arabidopsis was up-regulated in response to exogenous ABA exposure (Jang *et al.* 2004) and even elevated levels of endogenous ABA in transgenic plants (Parent *et al.* 2009). Measurements of the leaf ABA concentration showed that even higher levels of ABA were achieved by ABA watering compared to drought (Figure 7). Therefore, it is confirmed that ABA was transported to the shoot. The results on 100 µM exogenous ABA application on two-weeks old hydroponically grown Arabidopsis by Jang *et al.* (2004) indicated that gene expression of PIPs was initially up-regulated, but between 12 to 24 hours after the

treatment expression started to decline again. Compared to their study, the maximal concentration applied in this study was only 50 μM ABA. However, this was enough to achieve the maximal ABA inducible closure of stomata, as shown in Figure 16. Moreover, ABA concentrations measured in the leaves in response to ABA watering were even higher than under drought stress (Figure 7). It is not known whether application of ABA at higher concentrations, as in the study by (Jang *et al.* 2004), would trigger responses that are not connected to the mode of action ABA has during drought stress. On the other hand, it is possible that the extended exposure to ABA in this study also activated responses in the plant that antagonized the transcriptional activation by ABA. Further research is necessary to understand why this study found a lack of transcriptional response, while other studies showed transcriptional activation of aquaporins by ABA.

Gene expression of most PIP and TIP aquaporins detected in leaves was down-regulated by drought (Figure 8a). The strongest effect was found on the expression of *AtTIP2;2* and *AtPIP2;2* which were 25 and 20 fold down-regulated, respectively. This matches the results by (Alexandersson *et al.* 2005). Both genes also showed a strong correlation in gene expression (Figure 9). A co-expression network constructed by Alexandersson *et al.* (2010) showed a similar result. Since transcellular water flow depends on a coordination of water permeability of the plasma membrane and tonoplast, co-expression between PIPs and TIPs could indicate which isoforms are regulated in parallel. Gene expression of similar isoforms like *AtPIP2;1, AtPIP2;3*, *AtTIP1;1*, *AtTIP1;2*, and *AtTIP2;1* were also strongly down-regulated during drought. Both *TIP1;1* and *TIP2;1* were found in a cross-species meta-analysis of gene expression during drought to be significantly down-regulated in Arabidopsis, barley, rice, and wheat alike (Shaar-Moshe *et al.* 2015). It is interesting that such a strong connection between gene expression of tonoplast localised aquaporins and drought stress responses was found. Water permeability of the tonoplast controls water flow in and out of the vacuole, which can make up to 90% of the cell volume (Taiz 1992), but since the plasma membrane is the primary barrier for transcellular water flow, it doesn't seem necessary to make changes to the tonoplast water permeability. Some studies even measured about a 100-fold higher water permeability of the tonoplast compared to the plasma membrane and, hence, concluded that the tonoplast resistance is non-limiting to water flow (Kiyosawa and Tazawa 1977; Maurel *et al.* 1997). However, measurements of the plasma membrane permeability in these studies could have been erroneous (too low) due to the isolation procedure used, since other studies found higher permeabilities (Alleva *et al.* 2006). Nevertheless, Tyerman *et al.* (1999) argued that higher conductance of the tonoplast could be an important feature to balance volume changes between the cytosol and vacuole. In the case of PIP aquaporins, which are localised to the plasma membrane, studies have shown their influence on leaf hydraulics (Martre *et al.* 2002; Laur and Hacke 2014; Sade *et al.* 2015). Sade *et al.* (2015) showed that knock-down plants for PIP aquaporins in the bundle sheath showed reduced leaf hydraulic conductance and suggested that PIP aquaporin activity could control the bundle sheath –

mesophyll continuum for water flow in leaves. It remains to be tested whether TIP aquaporins have a significant influence on leaf hydraulics similar to this.

Furthermore, it would be important to investigate different gene expression patterns in PIP1 aquaporins compared to PIP2 and TIP aquaporins to find out more about their function during drought. While gene expression of PIP1, PIP2, and TIP aquaporins was well correlated as shown in the co-expression matrix (Figure 9a), PIP1 aquaporins showed no significant correlations to ABA biosynthesis genes *AtNCED3* and *AtCCD1*. In contrast, PIP2 and TIP aquaporins showed a significant negative correlation. This could indicate that changes in gene expression are differently timed and may have different functions.

The transcription factor *AtRAP2.4* showed also a significant positive correlation to many PIP and TIP aquaporins (Figure 9a). In knock-out mutant plants for this transcription factor, gene expression of many aquaporin genes was significantly down-regulated (Rae *et al.* 2011). Hence, this transcription factor may also have an important role in regulating gene expression of aquaporins during drought.

Significant differences between the co-expression matrices from the drought-rehydration experiment compared to the ABA watering experiment suggest that ABA may not be the primary regulator for gene expression changes during drought (Figure 9). While early modelling of drought responses assumed an ABA signal from the root to the shoot (Tardieu and Davies 1993), research now suggests that a hydraulic signal from the root to the shoot may trigger ABA biosynthesis in the leaves (Christmann *et al.* 2007). According to Christmann *et al.* (2013), hydraulic sensors in leaves could potentially sense changes in turgor pressure. Hence, it could be possible that aquaporin gene expression is regulated in response to these signals. Further research is needed to identify potential sensors and understand their influence on aquaporin expression.

2.4.2. Good correlations between changes in stomatal conductance and gene expression of some aquaporin genes

Research on changes of aquaporin gene expression during drought and rehydration in grapevine found a very good correlation between the expression of *VvTIP2;1* and changes in stomatal conductance (Pou *et al.* 2013). Likewise a cross-species meta-analysis of gene expression during drought in Arabidopsis, barley, rice, and wheat also pointed at a significant role of TIP2;1 (Shaar-Moshe *et al.* 2015).

As pointed out above, gene expression of all four TIP aquaporins that were detected in leaves (*AtTIP1;1*, *AtTIP1;2*, *AtTIP2;1*, and *AtTIP2;2*) in the drought-rehydration experiment was significantly down-regulated (Figure 8a). The correlation matrix in Figure 10 showed, that *AtPIP1;1*, *AtPIP1;2*, *AtPIP2;2, and AtTIP2;2* showed consistently good correlations to changes in stomatal conductance during the drought-rehydration experiment. From the point when stomatal conductance significantly decreased on day 5, a

significant positive correlation between gene expression of these four aquaporin isoforms and stomatal conductance was observed (< day 6). This link preceded the induction of ABA biosynthesis on day 6 (Figure 7). Linear regression analysis between stomatal conductance and gene expression of *AtPIP2;2* and *AtTIP2;2* also showed that both intersect close to 0:0 (Figure 11). This result matches with findings by Pou *et al.* (2013), who also observed that stomatal conductance and gene expression of *VvTIP2;1* in grapevine intersected at 0:0. While their research found the best correlation for *VvTIP2;1* to stomatal conductance, the isoform *AtTIP2;2* is very closely related to *AtTIP2;1*. In fact, also *AtTIP2;1* showed a good correlation, but it was better for *AtTIP2;2*. In tomato, overexpression of *SlTIP2;2* had a significant effect on transpiration through changes in stomatal conductance (Sade *et al.* 2009). The correlation between gene expression and stomatal conductance that we also found in Arabidopsis does not prove any direct link, but it suggests that *AtPIP1;1*, *AtPIP1;2*, *AtPIP2;2* are good candidates to investigate further. The early response as soon as stomatal conductance dropped suggests a strong relationship through regulation. Perhaps, gene expression of these aquaporin isoforms is regulated by hydraulic rather than chemical signals, since ABA related genes showed a later induction and also ABA concentration in the leaves increased only afterwards (Figure 7). Better correlations between stomatal conductance and gene expression for data from the drought phase of the experiment (Figure 11 inserts) indicate that during the rehydration phase other factors may play a role as well. Tombesi *et al.* (2015) concluded from their study in grapevine, that stomatal responses during drought were induced by hydraulic signals and later maintained by ABA. The delayed induction of ABA in our study also supports this hypothesis, however, local effects of ABA inside guard cells cannot be excluded.

Likewise, gene expression of *AtPIP1;4* showed a good correlation to ABA concentration in leaves similar to the ABA biosynthesis genes *AtNCED3* and *AtCCD1*. Further research on *AtPIP1;4* could uncover potential involvement in stress signalling. Like *AtPIP2;1*, which has been shown to facilitate hydrogen peroxide import into guard cells (Rodrigues *et al.* 2017), *AtPIP1;4* could have a similar function, since hydrogen peroxide transport by this isoform was also shown in response to pathogen attack (Tian *et al.* 2016).

2.4.3. Well-watered plants mimic stomatal response of drought stressed plants

The significant drop in stomatal conductance in well-watered plants during the drought period from day 6 till day 9 was also observed in a similar drought-rehydration experiment, which was conducted as a trial (Supplementary Figure S3). While measurements of the soil water content showed no changes for well-watered plants during the experiment (Figure 3a), changes in vapour pressure deficit (VPD) are known to affect stomatal conductance (Tardieu and Simonneau 1998; Levin *et al.* 2007). The drying plants reduced their transpiration during the drought phase of the experiment, which could have caused of drop in humidity and increase of VPD in the growth chamber. However, calculated VPD didn't show any pattern

and significant changes that could explain the observed drop in stomatal conductance (Supplementary Figure S8). From day 5 to day 6, VPD didn't change significantly.

In herbivory, the emission of volatile signals from attacked plants to their neighbors is well known (Paré and Tumlinson 1999). However, no research is known on volatile signaling during abiotic stress like drought and whether plants could communicate drought stress to their neighbors. Previously, stomatal regulation by vapour-phase ions has been suggested by Mott *et al.* (2014) after they observed stomatal responses in isolated epidermis when suspended over solutions with different pH. This may indicate that some sort of volatile communication may exist. During drought, gene expression of *AtTIP2;1*, which is known to transport ammonia (Loque *et al.* 2005; Kirscht *et al.* 2016), is down-regulated. Under normal conditions ammonia is trapped in the acidic vacuole by an acid-trap mechanism. During abiotic stress like drought photorespiration occurs, which produces ammonia (Voss *et al.* 2013). If the tonoplast permeability for ammonia is decreased, ammonia cannot be efficiently trapped and will be lost to the atmosphere as gas. Interestingly, it was observed that ammonia served as a volatile signal in yeast colonies causing growth repression in neighbouring colonies to emitters (Palkova *et al.* 1997). When *Brassica oleracea* plants were exposed to atmospheric ammonia, they also showed growth repression at certain concentrations (Castro *et al.* 2006). This observed growth repression may indicate that the plants were in a mode of stress. In this sense, ammonia might also serve as a volatile signal between plants during stress. To answer this question, it would be necessary to conduct an experiment, which excludes the possibility of changes in VPD and tests of the existence of a volatile signal.

2.4.4. Stomatal control by ABA and responses to soil drying

The control of stomatal conductance has been a matter of debate for some time. Tardieu and Davies (1993) discussed how stomata are controlled by hydraulic and chemical signals. In their model, ABA acts as a chemical signal transported from the root to the shoot. However, the use of grafted plants with roots that cannot produce ABA indicated that ABA may also be produced in the shoot, since those plants still closed their stomata during drought (Holbrook *et al.* 2002). A hydraulic root to shoot signal was proposed for Arabidopsis that would convey the stress signal to the leaves (Christmann *et al.* 2007).

The difference in sensitivity of stomata to measured endogenous levels of ABA in leaves between the drought-rehydration and ABA watering experiments supports the idea, that ABA is not the sole control mechanism of stomatal conductance (Figure 16). A combination of hydraulic and chemical control may determine the degree of stomatal closure. In the case of ABA watering, no hydraulic signals would have been involved in the stomatal response, since there was no water deficit. While leaf turgor and water potential have not been measured, measurements of the relative leaf water content, which indicates turgor changes, suggested that only on day 7 a significant drop in turgor occurred (Figure 6a). Indeed, on day 7

wilting of droughted plants was observed. However, leaf water potential may have changed much earlier and initiated stomatal responses.

Tombesi *et al.* (2015) even suggested that stomatal closure is mainly controlled by passive hydraulic mechanisms in grapevine. In their view, stomatal responses were initiated by hydraulic signals and maintained by ABA. Estimates of the soil water potential (Figure 12b), using the soil-water-retention curve (Figure 12a), showed no significant change until day 6, while stomata already responded on day 5 (Figure 4a). Therefore, changes in soil water potential may not be the primary trigger of drought responses. However, a significant drop in relative hydraulic conductivity of the soil between days 3 and 5 may have caused a reduction of water flow to the root and subsequently a drop in root water potential (Figure 13). This could have initiated stomatal closure. ABA concentration in the leaves also only increased significantly on day 6 (Figure 7a), after the initiation of stomatal responses to drought. These findings indicate, that hydraulic signals may play an important role in the control of stomata during drought in *Arabidopsis thaliana*. Further research on changes of water potentials and plant hydraulic conductance will be needed to gain a better understanding about the hydraulic control of stomata.

2.4.5. Conclusion

The research presented here shows that exogenous ABA treatment did not trigger the same plant physiological and gene expression responses as drought. Therefore, aquaporin gene expression may be controlled by a different pathway. While gene expression of most aquaporin genes was down-regulated during drought, some isoforms (*AtPIP1;4*, *AtPIP2;4*, and *AtPIP2;5*) were up-regulated, similar to genes involved in abiotic stress responses through ABA. These may have a role in hydrogen peroxide stress signalling. The down-regulated genes *AtPIP1;1*, *AtPIP1;2*, *AtPIP2;2, and AtTIP2;2* showed a very good correlation to changes in stomatal conductance. Linear regressions between stomatal conductance and gene expression of *AtPIP2;2, and AtTIP2;2* during drought and rehydration also showed that the relationship intersected at 0:0. Changes in gene expression were observed concomitantly with changes in stomatal conductance in response to soil drying, but earlier than ABA induction. This could point at drought response initiation by hydraulic rather than chemical signalling. Further research could investigate the role of these aquaporin isoforms in hydraulic signalling during drought stress. Observed changes of stomatal conductance in well-watered plants during drought phase raises the question whether stress signalling could occur from drought treated plants to their well-watered neighbours. Changes in relative soil hydraulic conductivity may trigger hydraulic signals inside the plant initiating stomatal responses to drought.

3. TONOPLAST LOCALISATION AND DROUGHT PHENOTYPES OF *At*TIP2 ISOFORMS OVEREXPRESSED IN ARABIDOPSIS

3.1. Introduction

Tonoplast intrinsic proteins (TIPs) are a sub-family of the major intrinsic proteins (MIPs) superfamily. MIPs are integral membrane proteins that are permeable to water and other small molecules and, therefore, often called aquaporins. The first aquaporin identified in plants was the TIP isoform *At*TIP1;1 from *Arabidopsis thaliana*, which was expressed in *Xenopus* oocytes to test for osmotic water permeability (Maurel *et al.* 1993). The protein was found to be highly abundant on the tonoplast membrane in seeds (Johnson *et al.* 1989). In Arabidopsis, 35 MIP isoforms have been identified (Johanson *et al.* 2001). Due to their function in water permeability of membranes, many studies have investigated the role of aquaporins in plant water relations (Chaumont and Tyerman 2014). For example, knockout mutants of *At*PIP2;2, which belongs to the MIP sub-family of plasma membrane intrinsic proteins (PIPs), showed a significant decrease of hydraulic conductivity of root cortex cells and osmotic hydraulic conductivity of intact roots in *Arabidopsis thaliana* (Javot *et al.* 2003). In leaves, the aquaporins *At*PIP1;2, *At*PIP2;1, and *At*PIP2;6 were found to regulate rosette hydraulic conductivity (Prado *et al.* 2013). Phosphorylation of *At*PIP2;1 was essential to increase rosette hydraulic conductivity in darkness. When the expression of several *At*PIPs was silenced by the use of microRNAs, a decrease in leaf hydraulic conductance was observed that negatively affected transpiration (Sade *et al.* 2014b).

Whilst the first identified water conducting channel in plants, *At*TIP1;1, is localised to the tonoplast (Johnson *et al.* 1989), most studies investigating the effect of aquaporins on plant hydraulics focus on PIPs, which are localised to the plasma membrane. Due to its location, the plasma membrane provides the primary barrier for symplastic water transport. Hence, changes in plasma membrane hydraulic conductance should have larger effects compared to changes in tonoplast hydraulic conductance and changes in tonoplast hydraulic conductance could be masked by the plasma membrane. However, the vacuole with the tonoplast as its barrier takes up a large volume inside the cell, which can be up to 90 % of the total cell volume (Taiz 1992). Measurements of the tonoplast conductance for water flow found a significantly higher conductance compared to that of the plasma membrane (about 100-fold) and, hence, the tonoplast is often seen as non-limiting to water flow (Kiyosawa and Tazawa 1977; Maurel *et al.* 1997). However, model calculations also suggest that this higher conductance of the tonoplast could be particularly important to balance changes in cytoplasmic volume and avoid damages to cellular machinery (Tyerman *et al.* 1999).

Recently, research findings have also reported phenotypes for plants with increased or decreased expression of TIPs. One early study on RNAi suppressed expression of *AtTIP1;1* suggested that the loss of this aquaporin would be lethal (Ma *et al.* 2004). However, further studies that used a knockout line of *AtTIP1;1*, which was shown to be devoid of the protein, found no significant effect on plant health and suggested off-target effects by RNAi could have led to wrong conclusions in the previous study (Schüssler *et al.* 2008; Beebo *et al.* 2009). Heterologous overexpression of *PgTIP1* from *Panax ginseng* in *Arabidopsis thaliana* showed significant beneficial effects on plant growth with longer roots, higher dry and fresh weight of shoots, and increased seed size (Lin *et al.* 2007). Experiments on abiotic stress tolerance of these overexpression lines found an increased salinity tolerance by elevated sodium accumulation in the shoot, changes in drought tolerance depending on the growing conditions, and decreased cold acclimation ability (Peng *et al.* 2007). Similar to this, *SlTIP2;2* from tomato (*Solanum lycopersicum*), which is most similar to *AtTIP2;1* from Arabidopsis, was overexpressed in its native background and also in *Arabidopsis thaliana* under the control of a 35S promoter (Sade *et al.* 2009). The transgenic tomato plants showed an increased biomass, fruit yield, and transpiration under normal conditions. Salt and drought treatments found that *SlTIP2;2* overexpression plants transpired for longer and had an increased fruit yield compared to wild-type controls. Heterologous overexpression in Arabidopsis also improved salinity tolerance. Later it was found that increased expression of both *SlTIP1;1* and *SlTIP2;2* conferred resistance against *Tomato yellow leaf curl virus* (TYLCV) in tomato (Sade *et al.* 2014a). In research from a different group, *SlTIP2;2* was overexpressed under the control of its endogenous promoter in Arabidopsis (Xin *et al.* 2014). Like 35S driven overexpression, these plants showed increased salinity tolerance. Interestingly, the study found that *SlTIP2;2* was down-regulated in salt stressed roots, but upregulated in shoots in wild-type tomato. The same pattern was also observed for heterologous expression in Arabidopsis. In the earlier research, Sade *et al.* (2009) presented an *in silico* analysis of gene expression in tomato that suggested a general overexpression of *SlTIP2;2* in roots under abiotic stress. In contrast to this, heterologous expression of *TaTIP2;2* from wheat in *Arabidopsis thaliana* reduced osmotic and salinity stress tolerance in seedlings leading to bleaching and reduced root growth (Xu *et al.* 2013). In *Arabidopsis thaliana*, a transcription factor, TRANSLUCENT GREEN (TG), was identified that interacts with the promoters of *AtTIP1;1*, *AtTIP2;3*, and *AtPIP2;2* (Zhu et al. 2013). Overexpression lines of TG also showed an increased expression of *AtTIP2;2*, but no interaction with the promoter was found. When *AtTIP1;1* was overexpressed under the control of a 35S promoter, a phenotype with vitrified leaves was observed. More exotically, the heterologous overexpression of *TsTIP1;2* from the halophyte *Thellungiella salsuginea* in *Arabidopsis thaliana* increased the tolerance to drought, salinity, and oxidative stress (Wang *et al.* 2014). Most recently, *AtTIP1;1*, *AtTIP1;2*, and *AtTIP2;1* were identified to facilitate lateral root emergence (Reinhardt *et al.* 2016). In particular, a triple knockout

mutant of these genes showed significant reduced numbers of lateral roots. Interestingly the phenotype could be rescued by expressing just *AtTIP2;1* under the control of its native promoter.

These results from previous research suggest that TIP aquaporins have important roles in conferring stress tolerance, in particular under drought and salinity, and are connected to growth both in total plant biomass and specifically lateral root emergence. Their role in the adaption to drought and osmotic stress is particularly interesting, since this could be connected to their role in regulating water flow in and out of the vacuole through changes in tonoplast hydraulic conductance. As discussed above, the effect of changes in tonoplast hydraulic conductance could easily be masked by the primary resistance provided by the plasma membrane, so an investigation is needed to understand their impact on plant hydraulics. Interestingly, a study on aquaporin gene expression in grapevine leaves (*Vitis vinifera*) during drought-rehydration events pointed to a very high correlation between the expression of *VvTIP2;1* and stomatal conductance (Pou *et al.* 2013). In fact, the linear regression predicted close to zero expression of *VvTIP2;1*, when stomatal conductance was zero. Likewise, a drought experiment in *Malus prunifolia* (Willd.) Borkh. showed a decline in *TIP2;1* gene expression when watering was withheld (Liu *et al.* 2013). In a cross-species meta-analysis of gene expression for Arabidopsis, Barley, Rice, and Wheat, *TIP1;1* and *TIP2;1* were identified as significantly down-regulated during drought stress in all species. In Arabidopsis alone, most MIP genes were found to be down-regulated during drought in leaves, but *AtTIP2;1* was the earliest responding gene and showed a very strong down-regulation (Alexandersson *et al.* 2005). Likewise, *AtTIP2;2* was also very significantly down-regulated. A low relative humidity experiment in Arabidopsis showed a seven-fold increase of *AtTIP2;3* expression in roots which was the highest expressed of all aquaporins (Levin *et al.* 2009). In Rice, the expression of *OsTIP1;1*, *OsTIP1;2*, *OsTIP2;1*, and *OsTIP2;2* was induced at lower humidity compared to a high humidity treatment both for long and short term exposure (Kuwagata *et al.* 2012). Additionally, *AtTIP2;1* and *AtTIP2;2* have been shown to transport ammonia (Holm *et al.* 2005; Loque *et al.* 2005; Kirscht *et al.* 2016). Overexpression of *AtTIP2;1* in Arabidopsis found no conclusive change in ammonium accumulation in roots compared to wild-type when plants from hydroponic culture with nitrate were supplied with ammonium (Loque *et al.* 2005). Apart from the function as nitrogen source, ammonia could also be important in signalling. In yeast experiments, ammonia was suggested to be a gaseous signal between colonies, which causes growth inhibition in neighbouring colonies (Palkova *et al.* 1997). Experiments in *Brassica oleracea*, also found an influence of atmospheric ammonia on biomass production (Castro *et al.* 2006).

So far, no comprehensive study exists that investigates the effects of overexpression of each of the three TIP2 (*AtTIP2;1*, *AtTIP2;2*, and *AtTIP2;3*) aquaporin isoforms. While several studies investigated the function of *AtTIP2;1*, less is known about *AtTIP2;2* and *AtTIP2;3*. The aim here was to create a complete set of transgenic lines that express the genes *AtTIP2;1*, *AtTIP2;2*, and *AtTIP2;3* individually under the

control of the endogenous UBQ10 (ubiquitin) promoter (Grefen *et al.* 2010) in *Arabidopsis thaliana* with or without C-terminal fluorescent GFP tag. The GFP tagged lines were used to confirm the localisation of the proteins to the tonoplast. Later they may be used to study protein movement between different cellular compartments in response to abiotic stresses. The lines for constitutive expression of the proteins without GFP will be primarily used to examine phenotypes in plants that are subjected to drought stress. Since *AtTIP2;1* is the closest homologue to *SlTIP2;2* (Sade et al. 2009) and primarily expressed in leaves, we hypothesise that constitutive expression of the protein will change their response to drought stress. Constitutive expression of *AtTIP2;2* and *AtTIP2;3* will provide information if they have similar functions compared to *AtTIP2;1*. Additionally, promoter-GUS fusion lines were created for the same set of genes to understand their native expression patterns.

3.2. Materials and Methods

3.2.1. Cloning of CDS into pUB-DEST and pUBC-GFP-DEST

Blunt-end PCR products of the coding sequences from the genes *AtTIP2;1*, *AtTIP2;2*, and *AtTIP2;3* were amplified by PCR with a four-nucleotide adaptor sequence on the 5' end (5' CACC … 3') for directional TOPO® cloning into the entry vector pENTR/D-TOPO (ThermoFisher Scientific). The coding sequences were either amplified in full length, or without the last three nucleotides on the 3' end, which encode for the stop codon. Sequences without the stop codon were paired with a GFP sequence for GFP tagging of the proteins on their C terminus. For *AtTIP2;2* and *AtTIP2;3*, the full-length cDNA clones U12229 and S63513 in pUNI vectors were obtained from the Arabidopsis Biological Resource Center (The Ohio State University) as templates for PCR amplification. For *AtTIP2;1*, a full-length cDNA clone (U17252) in pENTR vector was also available, but sequence comparison to the *Arabidopsis thaliana* TAIR10 reference genome found a single nucleotide variance in the clone. Hence, cDNA, synthesised from *Arabidopsis thaliana* Col0 wild-type mRNA, was used as template for PCR amplification. PCR amplification was done using gene specific primers (Supplementary Table S4) for *AtTIP2;1* (TIP21_CACC-FL_F, TIP21_FL_R or TIP21_FL-STOP_R), *AtTIP2;2* (TIP22_CACC-FL_F, TIP22_FL_R or TIP22_FL-STOP_R), and *AtTIP2;3* (TIP23_CACC-FL_F, TIP23_FL_R or TIP23_FL-STOP_R) and Phusion® High-Fidelity DNA Polymerase (New England Biolabs); pipetting instructions are shown in Supplementary Table S5. The cycling conditions were 3 min at 98°C initial denaturation, followed by 35 cycles of 10 sec at 98 °C denaturation, 30 sec at 68 (*AtTIP2;1*), 62 (*AtTIP2;2*), 70 (*AtTIP2;3*) °C annealing, 30 sec at 72 °C extension, and 10 min at 72 °C final extension. Amplified PCR products were examined by gel electrophoresis at 100 V for 45 min in a 1.2 % (w/v) agarose gel in 0.5 x TAE buffer with GelRed™ DNA stain (Biotium) and purified using the GenElute PCR Clean-Up Kit (Sigma-Aldrich).

Directional TOPO® cloning of the PCR products into the entry vector pENTR/D-TOPO was performed using the pENTR™/D-TOPO™ Cloning Kit (ThermoFisher Scientific) according to the manufacturer's instructions. Pipetting instructions are shown in Supplementary Table S6. Briefly reactions were incubated for 30 min at room temperature and stored at 4°C overnight. The reactions were transformed into *E. coli* DH5α competent cells (Supplementary Methods) and plated onto selective LB plates (50 µg/mL Kanamycin = Kan) and incubated at 37°C overnight. Five colonies per construct were grown in 5 mL liquid LB (Luria Bertani medium) + Kan (50 µg/mL) at 200 rpm shaking and 37°C overnight. Plasmid DNA was extracted using the GenElute™ Plasmid Miniprep Kit (Sigma-Aldrich) and approx. 100 ng plasmid DNA from each transformant was digested using the restriction enzyme *Nhe*I (New England Biolabs) for two hours at 37°C. Restriction digests were examined by gel electrophoresis at 100 V for 45 min in a 1.2 % (w/v) agarose gel in 0.5 x TAE buffer with GelRed™ DNA stain (Biotium) to find plasmids with inserts. Subsequently, Sanger Sequencing was performed at AGRF (PD service, www.agrf.org.au) using M13 primers (Supplementary Table S4) to confirm the correct sequence of the inserts.

LR reactions (Supplementary Table S7) between entry vectors (pENTR+insert) and the destination vectors pUB-DEST or pUBC-GFP-DEST (Supplementary Figure S9) were performed using LR Clonase II enzyme (ThermoFisher Scientific) according to the manufacturer's instructions. Briefly, after incubation overnight at room temperature, the LR reaction was stopped by Proteinase K treatment (0.5 µL/reaction, 10 min at 37 °C). The total reactions were transformed into Stellar™ Competent Cells (Clontech) as per manufacturer's instructions and cultures were grown on selective LB plates (100 µg/mL Spectinomycin = Spec) at 37 °C overnight. Three colonies per construct were grown in 5 mL liquid LB + Spec (100 µg/mL) cultures at 200 rpm in a shaking incubator at 37 °C overnight. Plasmid DNA was extracted using the GenElute™ Plasmid Miniprep Kit (Sigma-Aldrich). Approximately 100 ng plasmid DNA from the each of the transformants was digested using the restriction enzymes *EcoR*I + *Sbf*I (New England Biolabs) at 37°C overnight. Restriction digests were examined by gel electrophoresis at 100 V for 45 min in a 1.2 % (w/v) agarose gel in 0.5 x TAE buffer with GelRed™ DNA stain (Biotium) to find plasmids with inserts.

3.2.2. Cloning of promoter sequences into pMDC162

Predicted promoter sequences for *AtTIP2;1*, *AtTIP2;2*, and *AtTIP2;3* were retrieved from the Arabidopsis Gene Regulatory Information Server (Davuluri *et al.* 2003) and primers for the full length of these predicted promoters (*AtTIP2;1*: 2277 bp, *AtTIP2;2*: 3060 bp, *AtTIP2;3*: 1271 bp upstream of start codon) were designed in NCBI Primer-BLAST (Ye *et al.* 2012). The sequences were amplified by PCR from genomic DNA of *Arabidopsis thaliana* Col0 wild-type with a four-nucleotide adaptor sequence on the 5' end (5' CACC … 3') for directional TOPO® cloning into the entry vector pENTR/D-TOPO (ThermoFisher Scientific). PCR amplification was done using gene specific primers (Supplementary Table S4) for

AtTIP2;1 (pTIP21_CACC_F, pTIP21_R), *AtTIP2;2* (pTIP22_CACC_F, pTIP22_R), and *AtTIP2;3* (pTIP23_CACC_F, pTIP23_R) and Phusion® High-Fidelity DNA Polymerase (New England Biolabs); pipetting instructions are shown in Supplementary Table S5. The cycling conditions were 3 min at 98 °C initial denaturation, followed by 35 cycles of 10 sec at 98 °C denaturation, 30 sec at 62 (*AtTIP2;1*), 64 (*AtTIP2;2*), 63 (*AtTIP2;3*) °C annealing, 1 min at 72°C extension, and 5 min at 72 °C final extension. PCR products were examined by gel electrophoresis at 100 V for 45 min in a 1.2 % (w/v) agarose gel in 0.5 x TAE buffer with GelRed™ DNA stain (Biotium) and purified using the GenElute PCR Clean-Up Kit (Sigma-Aldrich).

Directional TOPO® cloning of the PCR products into the entry vector pENTR/D-TOPO was performed using the pENTR™/D-TOPO™ Cloning Kit (ThermoFisher Scientific). Reaction setup was performed according to the manual and as mentioned above. Approximately 100 ng plasmid DNA from each of the transformants was digested using different combinations of restriction enzymes (New England Biolabs): pENTR/pAtTIP2;1 (*EcoR*V + *Noc*I), pENTR/pAtTIP2;2 (*Avr*II + *EcoR*V), pENTR/pAtTIP2;3 (*Avr*II + *Afl*II). Restriction digests were incubated at 37 °C overnight and examined by gel electrophoresis at 100 V for 45 min in a 1.2 % (w/v) agarose gel in 0.5 x TAE buffer with GelRed™ DNA stain (Biotium) to find plasmids with insert. Subsequently, Sanger Sequencing was performed at AGRF (PD service, www.agrf.org.au) using M13 and SP1-8 primers (Supplementary Table S4) to confirm the correct sequence of the inserts.

Since both the entry vector (pENTR+insert) and destination vector (pMDC162) contain kanamycin resistance, pENTR+insert were cut by restriction enzyme to linearize the plasmid prior to LR reactions. This made sure to avoid selecting bacteria that had taken up the entry vector. For linearization, a total of approx. 500 ng pENTR+insert and the following combinations of restriction enzymes (New England Biolabs) were used: pENTR+pAtTIP2;1 (*EcoR*V + *Nhe*I), pENTR+pAtTIP2;2 (*Bbs*I + *EcoR*V), pENTR+pAtTIP2;3 (*BsrB*I + *Nhe*I). Restriction digests were incubated at 37 °C for 2 hours and subsequently purified using the MinElute Reaction Cleanup Kit (Qiagen). LR reactions (Supplementary Table S7) between linearized pENTR+insert and the destination vector pMDC162 (Supplementary Figure S10) were performed using LR Clonase II enzyme (ThermoFisher Scientific) according to the manufacturer's instructions and as mentioned above. Approximately 100 ng plasmid DNA from each of the transformants was digested using the following restriction (New England Biolabs) at 37 °C overnight: pMDC162+pAtTIP2;1 (*Hind*III + *Nar*I), pMDC162+pAtTIP2;2 (*Nhe*I), pMDC162+pAtTIP2;3 (*BamH*I + *Nhe*I). Restriction digests were examined by gel electrophoresis at 100 V for 45 min in a 1.2 % (w/v) agarose gel in 0.5 x TAE buffer with GelRed™ DNA stain (Biotium) to find plasmids with insert.

3.2.2. Plant Material

Arabidopsis (*Arabidopsis thaliana*) ecotype Col-0 seed from the laboratory stock were sown on solid, half-strength Murashige and Skoog's medium (Murashige and Skoog 1962) (Supplementary Table S16). After vernalisation at 4 °C for 3 days in the dark, plates were transferred to a walk-in growth chamber at The Plant Accelerator® Adelaide, Australia (34° 58' 17.00'' S, 138° 38' 23.00'' E). Plants were grown under long-day conditions (16 h light/ 8 h dark, PAR ~150 µmol m^{-2} s^{-1}, 21 °C) for 7 d until they were transferred to soil (85 % (v/v) Seedling Substrate Plus+, Bord na Móna; 15 % (v/v) Horticultural Sand, Debco Pty Ltd). For floral dip transformations, 3 – 5 plants were grown per pot. Once flowering started, initial inflorescences were cut after one week to induce more inflorescences. At the peak of flowering, floral dip transformations were performed (Clough and Bent 1998).

3.2.3. Agrobacterium transformation for overexpression lines

Constructs of pUB-DEST+insert and pUBC-GFP-DEST+insert were transformed into chemically-competent *Agrobacterium tumefaciens* cells as outlined in the Supplementary Methods. Transformations were grown on 2YT plates (Supplementary Table S16) + Rifampicin = Rif (50 µg/mL) + Spec (100 µg/mL) for 2 – 3 days at 28 °C.

Three colonies per construct were grown in 5 mL 2YT Broth + Rif (50 µg/mL) + Spec (100 µg/mL) overnight at 28 °C and 200 rpm. Constructs in *Agrobacterium* were evaluated by liquid culture PCR (Supplementary Table 11) using the gene specific primers (Supplementary Table S4). The cycling conditions were 3 min at 98 °C initial denaturation, followed by 35 cycles of 10 sec at 98 °C denaturation, 30 sec at 68 (*AtTIP2;1*),62 (*AtTIP2;2*),70 (*AtTIP2;3*) °C annealing, 30 sec at 72 °C extension, and 10 min at 72 °C final extension. PCR products were examined by gel electrophoresis at 100 V for 45 min in a 1.2 % (w/v) agarose gel in 0.5 x TAE buffer with GelRed™ DNA stain (Biotium). Nucleic acids were visualised in a ChemiDoc Imaging Systems (Bio-Rad).

For floral dip transformations, 250 mL 2YT Broth + Rif (25 µg/mL) + Spec (100 µg/mL) were inoculated with 4 mL of the starter culture and grown overnight in a shaking incubator at 28 °C and 200 rpm. Floral dip transformation was carried out as per Supplementary Methods. For each construct, four pots with 3-5 plants were dipped.

Plants were grown to seed and seeds were collected when mature (T_1).

3.2.4. Selection procedure of overexpression lines

For selection of transformed T_1 plants, about 200 mg T_1 seed were uniformly sown on soil in a tray (30 x 40 cm) and vernalised at 4 °C for 3 days in the dark. A control with *Arabidopsis thaliana* Col-0 wild-type seed was included. Subsequently, trays were transferred to a walk-in growth chamber at The Plant

Accelerator® Adelaide, Australia (as above). Plants were grown under long-day conditions (as above) for 5 days under a cover. Selection was carried out using Basta® herbicide (Bayer Crop Science) at a working concentration of 300 µM according to Weigel and Glazebrook (2006). Seedlings were sprayed three times at a three-day interval. Effectiveness of selection was evaluated by observing the response of *Arabidopsis thaliana* Col-0 wild-type seedlings. Twenty five survivors from each line were transplanted into the ARASYSTEM (BETATECH) and grown to seed (T_2).

For selection of transformed T_2 plants with single locus T-DNA, a subsample of seed from 16 T_1 lines was screened at first; there was no need to screen more lines since enough lines with single locus T-DNA were identified. T_2 seed were sterilised with chlorine gas according to Supplementary Methods. For each line, about 150 seed were sown on solid, half-strength Murashige and Skoog medium (Murashige and Skoog 1962) (Supplementary Table S16) supplemented with 10 mg/L (50 µM) glufosinate ammonium (Sigma-Aldrich). After vernalisation at 4 °C for 3 days in the dark, plates were transferred to the Plant Accelerator® Adelaide and grown under long-day conditions for 7 days, or until selection was clearly visible. The ratio of resistant to sensitive seed was evaluated for each line. Only lines which had a 3:1 ratio (resistant:sensitive), and hence most likely only a single insertion of the T-DNA, were used for further selection. Ten seedlings for each selected line were transplanted to the ARASYSTEM and grown to seed (T_3).

For selection of homozygous T_3 plants, T_2 seed were sterilised with chlorine gas according to Supplementary Methods. For each line, about 100 seed were sown on solid, half-strength Murashige and Skoog medium (Murashige and Skoog 1962) (Supplementary Table S16) supplemented with 10 mg/L (50 µM) glufosinate ammonium (Sigma-Aldrich). After vernalisation at 4 °C for 3 days in the dark, plates were transferred to the Plant Accelerator® Adelaide and grown under long-day conditions for 7 days, or until selection was clearly visible. Lines which showed 100% survival were considered homozygous for the T-DNA insert. Five seedlings per homozygous line were transplanted into a single pot and grown to seed.

3.2.5. Agrobacterium transformation for GUS lines

Constructs of pMDC162+pAtTIP2;1, pMDC162+pAtTIP2;2, and pMDC162+pAtTIP2;3 were transformed into chemically-competent *Agrobacterium tumefaciens* cells as outlined in the Supplementary Methods. Transformations were grown on 2YT plates (Supplementary Table S15) + Rif (50 µg/mL) + Kan (50 µg/mL) for 2 – 3 days at 28 °C.

Four colonies per construct were grown in 5 mL 2YT Broth + Rif (50 µg/mL) + Kan (50 µg/mL) overnight at 28 °C and 200 rpm. Constructs in *Agrobacterium* were evaluated by liquid culture PCR (Supplementary Table S11) using primers towards the 3' end of the promoters (Supplementary Table S4): pMDC162+pAtTIP2;1 (SP3 + pTIP21_R), pMDC162+pAtTIP2;2 (SP7 + pTIP22_R),

pMDC162+pAtTIP2;3 (SP8 + pTIP23_R). The cycling conditions were set to an annealing temperature of 55°C for 30 sec and 35 cycles; expected product sizes were pMDC162+pAtTIP2;1 (903 bp), pMDC162+pAtTIP2;2 (992 bp), and pMDC162+pAtTIP2;3 (830 bp).

For floral dip transformations, 250 mL 2YT Broth + Rif (25 µg/mL) + Kan (50 µg/mL) were inoculated with 4 mL of the starter culture and grown overnight at 28 °C and 200 rpm. Floral dip transformation was carried out as per Supplementary Methods. For each construct, four pots with 3-5 plants were dipped.

Plants were grown to seed and seeds were collected when mature (T_1).

3.2.6. Selection procedure of GUS lines

For selection of T_1 transformants, seeds were sterilised with chlorine gas (Supplementary Methods). For each line, seed were densely sown on four square plates (10 cm x 10 cm) on solid, half-strength Murashige and Skoog's medium (Murashige and Skoog 1962) (Supplementary Table S16) supplemented with 20 mg/L hygromycin (AG Scientific) and 100 mg/L cefotaxime sodium salt (Sigma-Aldrich). After vernalisation at 4 °C for 3 days in the dark, plates were transferred to a long-day growth chamber in the Plant Accelerator® Adelaide for a rapid screening by differences in hypocotyl elongation (Harrison *et al.* 2006). Briefly, plates were exposed to light for 6 hours and subsequently wrapped in aluminum foil for 2 days. Afterwards, plates were unwrapped and seedlings grown for a further 24 hours in light. Seedlings with hygromycin resistance showed significantly longer hypocotyls. From these, 25 seedlings per line were transplanted to the ARASYSTEM (BETATECH) and grown to seed. No further selection was carried to this stage.

3.2.7. Confocal microscopy

Seeds from multiple homozygous transgenic T_3 lines of *Arabidopsis thaliana* Col0 expressing the constructs pUBC-AtTIP2;1-GFP, pUBC-AtTIP2;2-GFP, and pUBC-AtTIP2;3-GFP were sown in rows on square plates with solid, half-strength Murashige and Skoog's medium (Murashige and Skoog 1962) (Supplementary Table S16). After vernalisation at 4 °C for 3 days in the dark, plates were transferred to the Plant Accelerator® Adelaide and grown vertically under long-day conditions for 7 - 14 days. Plates were wrapped for 16 hours in aluminum foil before confocal microscopy. Whole seedlings were mounted in half-strength liquid MS medium and immediately observed with a Nikon A1R Laser Scanning Confocal microscope using either a 20X Plan Apochromat Lambda dry objective or two different water immersion objectives (40X Apo LWD WI λS; 60X Plan Apo VC WI) at the Adelaide Microscopy Waite Facility. The plasma membrane staining dye FM 4-64 (Vida and Emr 1995) was used for some samples. For this, whole seedlings were incubated for 10 – 15 min in a 1:1000 dilution of 2 mM FM 4-64 and subsequently

mounted in half-strength liquid MS medium. GFP was excited at 488 nm and detected at 525 nm. FM 4-64 was excited at 561.1 nm and detected at 595 nm. Images were acquired with a DS-Ri1 CCD camera.

3.2.8. GUS staining and microscopy

GUS staining of leaves and roots from T_1 transformants was conducted according to a protocol by Bomblies and Franks (2007). Leaves and roots of 4-week old plants were harvested into 90 % cold acetone on ice. Samples were transferred into a vacuum chamber and a vacuum of 25 cmHg was applied for 10 min at room temperature. Afterwards, samples were fixed at room temperature for 30 min. Meanwhile, Staining Buffer without X-Gluc (Supplementary Table S8) was prepared with cold solutions on ice. After fixing, tissue was transferred to the Staining Buffer without X-Gluc by paintbrush. Samples were transferred into a vacuum chamber and a vacuum of 25 cmHg was applied for 10 min on ice. Meanwhile, Staining Buffer with X-Gluc (Supplementary Table S8) was prepared with cold solutions on ice; final concentration of 2 mM X-Gluc i.e. 0.2 ml 0.1 M X-Gluc to 10 mL of Staining Buffer. Samples were transferred to the Staining Buffer with X-Gluc by paintbrush, sealed into a vacuum chamber and a vacuum of 25 cmHg was applied for 20 min on ice. Vacuum was released slowly to check if samples sunk indicating full infiltration; if not, vacuum was repeated. Afterwards, samples were incubated in the dark at 37 °C overnight.

The next day, samples were taken successively through clearing solutions of 20 %, 35 %, and 50 % ethanol and incubated for 30 min in each at room temperature. Afterwards, samples are incubated for 30 min in FAA fixative (Supplementary Table S8) at room temperature. Samples were transferred into 70 % ethanol and stored at 4 °C.

GUS staining was observed and images were taken using a stereo Nikon SMZ dissecting microscope 800 (Nikon Co.) and a Zeiss AxioPhot fluorescent microscope (ZEISS Australia) under brightfield illumination with TOUPCAM™ UCMOS05100 KPA (ProSciTech).

3.2.9. Drougth – rehydration experiments

T_3 seeds of the homozygous transgenic lines for constitutive expression of *AtTIP2;1*, *AtTIP2;2*, and *AtTIP2;3* with or without C-terminal GFP fluorescent tag and wild-type seed were sown on solid, half-strength Murashige and Skoog's medium (Murashige and Skoog 1962) (Supplementary Table S16). After vernalisation at 4°C for 3 days in the dark, plates were transferred to a walk-in growth chamber at The Plant Accelerator® Adelaide, Australia (as above). Plants were grown under short-day conditions (10 h light/ 14 h dark, PAR ~150 µmol m^{-2} s^{-1}, 21 °C) for 7 d until they were transferred to soil. Plastic pots (170 cm^3) were filled with 92 g soil mixture (85 % (v/v) Seedling Substrate Plus+, Bord na Móna; 15 % (v/v) Horticultural Sand, Debco Pty Ltd) to a packing density of 0.54 g/cm^3 and drenched with 0.05 g/L

Confidor® (Bayer). Plants were grown for another 5 weeks under short-day conditions until the experiments. A week before the experiment, the soil in each pot was covered by white plastic granules to reduce evaporation from the soil and achieve a uniform drying during the drought treatment. Plants were randomly split into two groups (well-watered/drought-rehydration). Trays were filled with 12 plants from different lines and trays of different groups (well-watered/drought-rehydration) were placed side-by-side on the shelves.

Photographs of 4 or 6 weeks old plants were taken to compare leaf area by image analysis in ImageJ (Schneider et al. 2012).

When plants were 6-7 weeks old, watering was withheld for plants from the drought group until plants started wilting. For the first experiment, plants were rehydrated by flooding the trays overnight once the wilting point was reached (day 7). In the second experiment, measurements were terminated once the wilting point was reached (day 10). Plants from the control group were watered to field capacity by flooding the trays each day for 30 minutes to about 2/3 of the pot height.

Stomatal conductance (g_s) was repeatedly measured on one mature leaf for each plant using an AP4 leaf Porometer (Delta-T Devices) throughout the experiment. For the rehydration assay, six leaves were harvested per line from different plants and rehydrated with the petiole in RO water in a closed petri dish. Excess water was carefully wiped from each leaf before measuring fresh weight (FW) on a precision balance (precision = 0.1 mg, E12140, OHAUS) repeatedly. Turgid weight (TW) was measured after 24 hours rehydration.

For the second experiment, the leaf, which was used to measure stomatal conductance, was harvested for RNA on day 10, when the stress was most severe, and immediately frozen in liquid nitrogen.

3.2.10. Determination of *AtTIP2;1* overexpression by semiquantitative RT-PCR

Frozen leaf samples were ground into a fine powder using two 3 mm steel grinding balls in each 2 mL Eppendorf tube. The tubes with leaf samples and steel grinding balls were kept in liquid nitrogen until grinding the samples twice (different orientations) for 30 sec at 1500 strokes/min into a fine powder using the Geno/Grinder® (SPEX®SamplePrep). Afterwards, samples were immediately cooled again in liquid nitrogen and transferred to -80 °C until further processing.

Extraction of total RNA was done using the Spectrum™ Plant Total RNA Kit (Sigma Aldrich) and the On-Column DNase I Digestion Set (Sigma Aldrich) according to Kit instructions. Briefly, 500 µL of Lysis Solution/2-ME Mixture was added to 50-100 mg frozen fine powder of leaf tissue. Samples were immediately mixed using the Geno/Grinder® for 30 sec at 1500 strokes/min and incubated for 5 min at

56 °C. Solids were separated from the lysate using the filtration column and 750 µL binding Solution was added to the lysate. Nucleic acids were captured using the binding column and washed with 300 µL Wash Solution 1. Samples were incubated with 80 µL of DNase digestion mixtures for 15 min at room temperature. Afterwards, columns were washed with 500 µL of Wash Solution 1 and Wash Solution 2 in subsequent steps. Total RNA was eluded in 50 µL Elution Solution. Quantification of total RNA yield was done using the NanoDrop™ 1000 Spectrophotometer (Thermo Fisher Scientific). Total RNA quality was assessed by gel electrophoresis of 500 ng total RNA which was denatured at 70 °C for 10 min, and immediately cooled on ice for 3 min. Samples were run at 60 V for 60 min in a 1.2 % (w/v) agarose gel in 0.5 x TAE buffer with GelRed™ DNA stain (Biotium). Nucleic acids were visualised in a ChemiDoc Imaging Systems (Bio-Rad). Samples were stored at -80 °C until further processing.

Subsequently, cDNA synthesis was done using the iScript™ Reverse Transcription Supermix for RT-qPCR (Bio-Rad). Briefly, 4 µL iScript RT Supermix was added to 1 µg of total RNA and adjusted to 20 µL total reaction volume with nuclease-free water. The reverse transcription reaction was carried out in a G-Storm Thermal Cycler GS1 (Gene Technologies Ltd): 5 min at 25 °C, 30 min at 42 °C, 5 min at 85 °C. Samples were stored at -20 °C until further processing.

Semiquantitative reverse transcription PCR was performed with the KAPA Taq PCR Kit (KAPABIOSYSTEMS) in a 10 µL reaction volume containing 1 µL cDNA, 1 µL KAPA Taq Buffer w/loading dye (10X), 0.2 µL KAPA dNTP Mix (10 mM each), 0.5 µL gene specific primer mix for *AtACT2* and *AtTIP2;1* (10 µM) (Supplementary Table S4), and 0.04 µL KAPA Taq DNA Polymerase (5 U/µL). The cycling conditions were 3 min at 95 °C, then 26 cycles of 30 sec at 95 °C, 30 sec at 64 °C, and 30 sec at 72 °C, followed by 30 sec at 72 °C.

PCR products were examined by gel electrophoresis at 80 V for 1 h in a 1.2 % (w/v) agarose gel in 0.5 x TAE buffer with GelRed™ DNA stain (Biotium). Nucleic acids were visualised in a ChemiDoc Imaging Systems (Bio-Rad).

Relative quantities were calculated from band intensities using Image Lab software, version 5.2 (Bio-Rad Laboratories).

3.3. Results

3.3.1. Generation of overexpression and promoter-GUS lines

Sequence alignments showed a single base mismatch between the cDNA clone U17252 and the *AtTIP2;1* reference sequence (TAIR10 genome) at position 677 in the DNA coding sequence with an adenosine

instead of a guanine (Figure 17). Translation of the sequences showed that this difference would lead to a change in the amino acid sequence at position 226 with glutamic acid instead of glycine (Figure 17b).

Sequences of the cDNA clones U12229, for *AtTIP2;2*, and S63513, for *AtTIP2;3*, showed 100 % identity to the *AtTIP2;2* and *AtTIP2;3* reference sequences (TAIR10 genome), respectively.

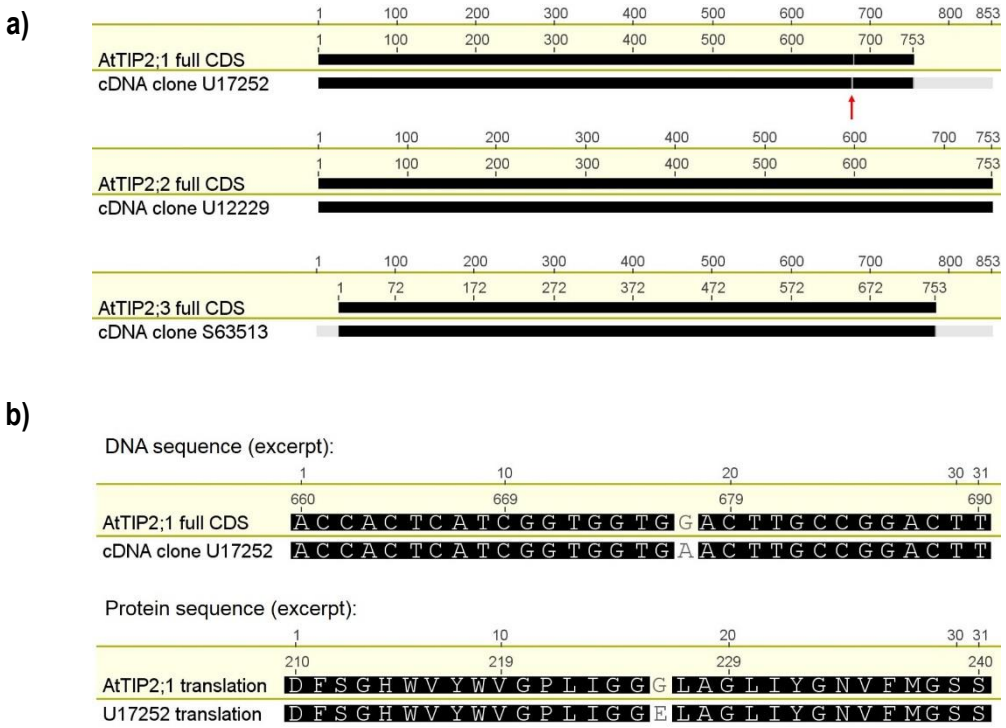

Figure 17. Sequence alignments between TAIR10 reference genome and cDNA clones for genes *AtTIP2;1*, *AtTIP2;2*, and *AtTIP2;3*. a) DNA sequence alignments with the cDNA clones U17252, U12229, and S63513 form the Arabidopsis Biological Resource Center (The Ohio State University). Black fill indicates identical sequences, while white shows dissimilarity. A red arrow points at a single base mismatch between U17252 and the *AtTIP2;1* reference sequence. b) Excerpts of DNA and protein sequences to show mismatch between U17252 and the *AtTIP2;1* reference sequence.

The coding sequences of *AtTIP2;1*, *AtTIP2;2*, and *AtTIP2;3* were either amplified full length or without the last three bases at the 3' end, which encode for the stop codon; gel electrophoresis showed that they had all the correct size of 757 bp (with adaptor and stop) or 751 bp (with adaptor, without stop) (Figure 18).

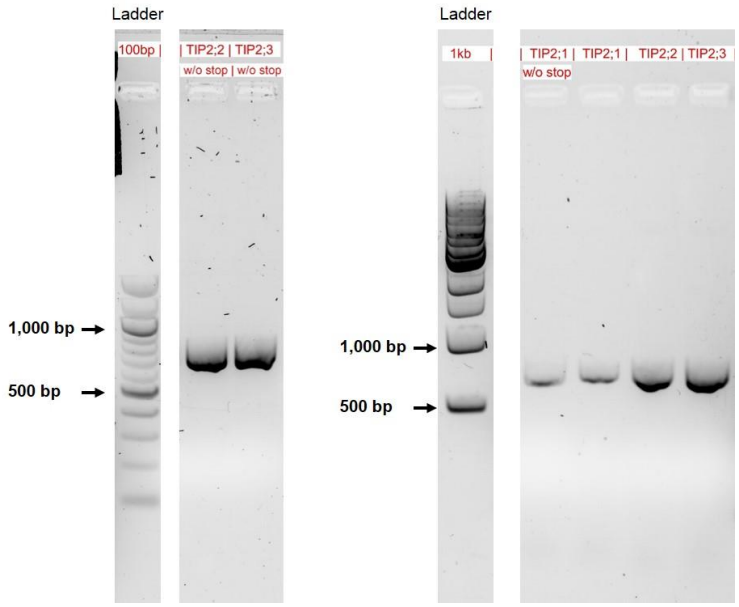

Figure 18. Gel electrophoresis of PCR amplified coding sequences from the genes *AtTIP2;1*, *AtTIP2;2*, and *AtTIP2;3* with adaptors for directional TOPO® cloning. The PCR products were run on two different gels and additional lanes between the ladders and PCR products were removed by cropping. For the left gel a 100 bp DNA ladder (New England Biolabs) was used and for the right gel a 1 kb DNA ladder (New England Biolabs).

The predicted promoter sequences obtained from the Arabidopsis Gene Regulatory Information Server (AGRIS) had a length of 2122 bp for *AtTIP2;1*, 2938 bp for *AtTIP2;2*, and 1118 bp for *AtTIP2;3*. Primers to amplify these promoters did span a slightly larger segment of DNA to make them specific (Figure 19a). Gel electrophoresis of the amplified promoter sequences showed the expected size differences with pmAtTIP2;3 being the shortest and pmAtTIP2;2 being the longest (Figure 19b).

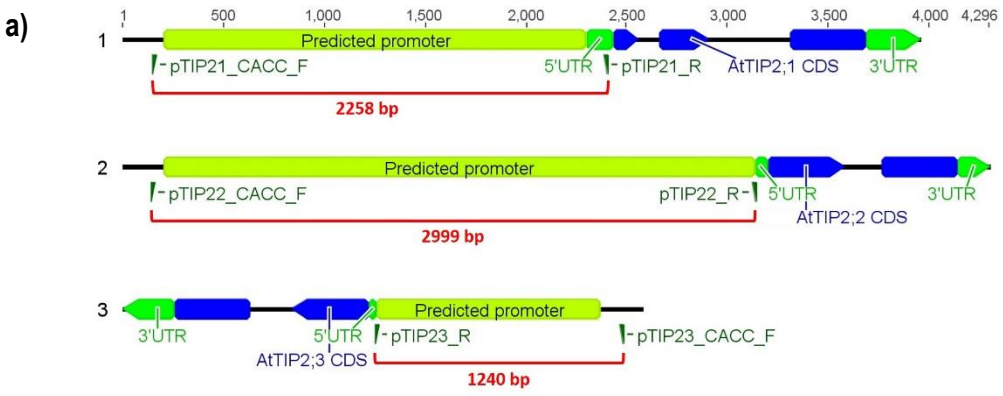

b)

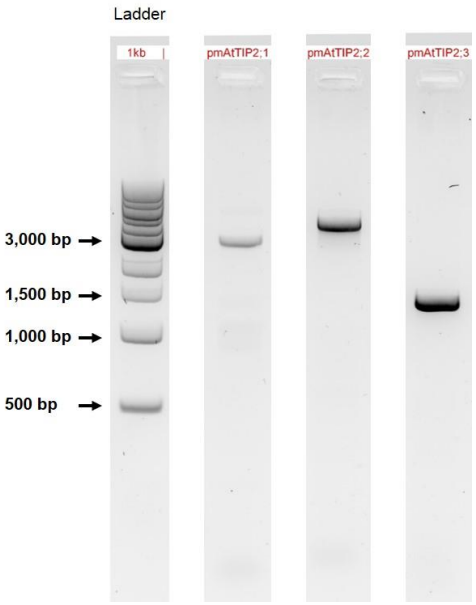

Figure 19. Schematic representation of predicted promoter sequences upstream of the genes *AtTIP2;1*, *AtTIP2;2*, and *AtTIP2;3* and visualisation of these PCR amplified promoter by gel electrophoresis. a) Predicted promoter sequences (light green) were obtained from the Arabidopsis Gene Regulatory Information Server and primers (dark green below scheme) were designed to amplify the full length promoters. In some cases, the primer pairs also amplify a short part of sequence upstream of the predicted promoter and/or some part of the 5' UTR. The product length is indicated by a red bracket. b) Gel electrophoresis of the PCR amplified promoter sequences with adaptors for directional TOPO® cloning. The PCR products were run on the same gel, but additional lanes with other products were remove by cropping. A 1 kb DNA ladder (New England Biolabs) was used as size reference.

Sanger sequencing showed that the coding and promoter sequences of *AtTIP2;1*, *AtTIP2;2*, and *AtTIP2;3* were successfully cloned into pENTR (Figure 20 and Figure 21). While all the cloned coding sequences matched the references 100% (Figure 20), two bases of adenosine immediately downstream of the coding sequence of *AtTIP2;3* were missing in the backbone of pENTR according to the sequencing results (Figure 20c).

a)

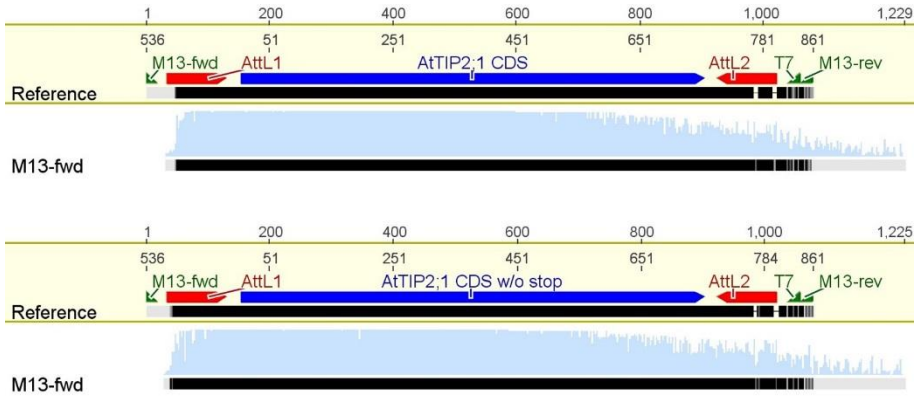

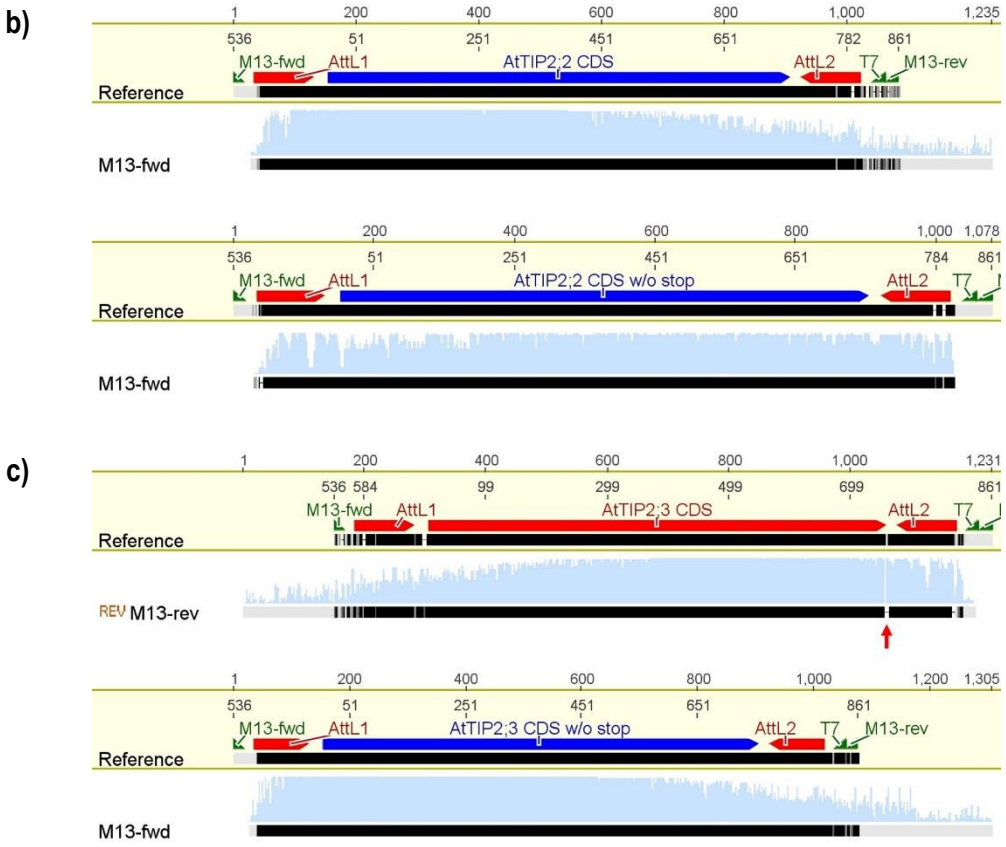

Figure 20. Confirmation of correct sequence for coding sequences of (a) *AtTIP2;1*, (b) *AtTIP2;2*, and (c) *AtTIP2;3* with or without the last three bases for the stop codon cloned into pENTR. The reference sequence shows part of the pENTR vector with the relevant insert between the M13 primer sites. M13 forward or reverse primers (dark green) were used to amplify plasmid DNA during Sanger Sequencing. The light blue area above the Sanger Sequencing trace shows the quality of base calling. Below, the similarity between reference and sequencing trace is shown in black for match, or grey for mismatch. A vertical red arrow indicates two missing adenosine bases immediately after the full length CDS of *AtTIP2;3* (c).

Likewise, clones with the correct insertions of promoter from *AtTIP2;1*, *AtTIP2;2*, and *AtTIP2;3* were confirmed (Figure 21). Multiple primers were used to cover the full length of each insert, since the promoters were substantially longer than the coding sequences. This allowed also to have a high sequencing quality of base calling all along the sequenced inserts.

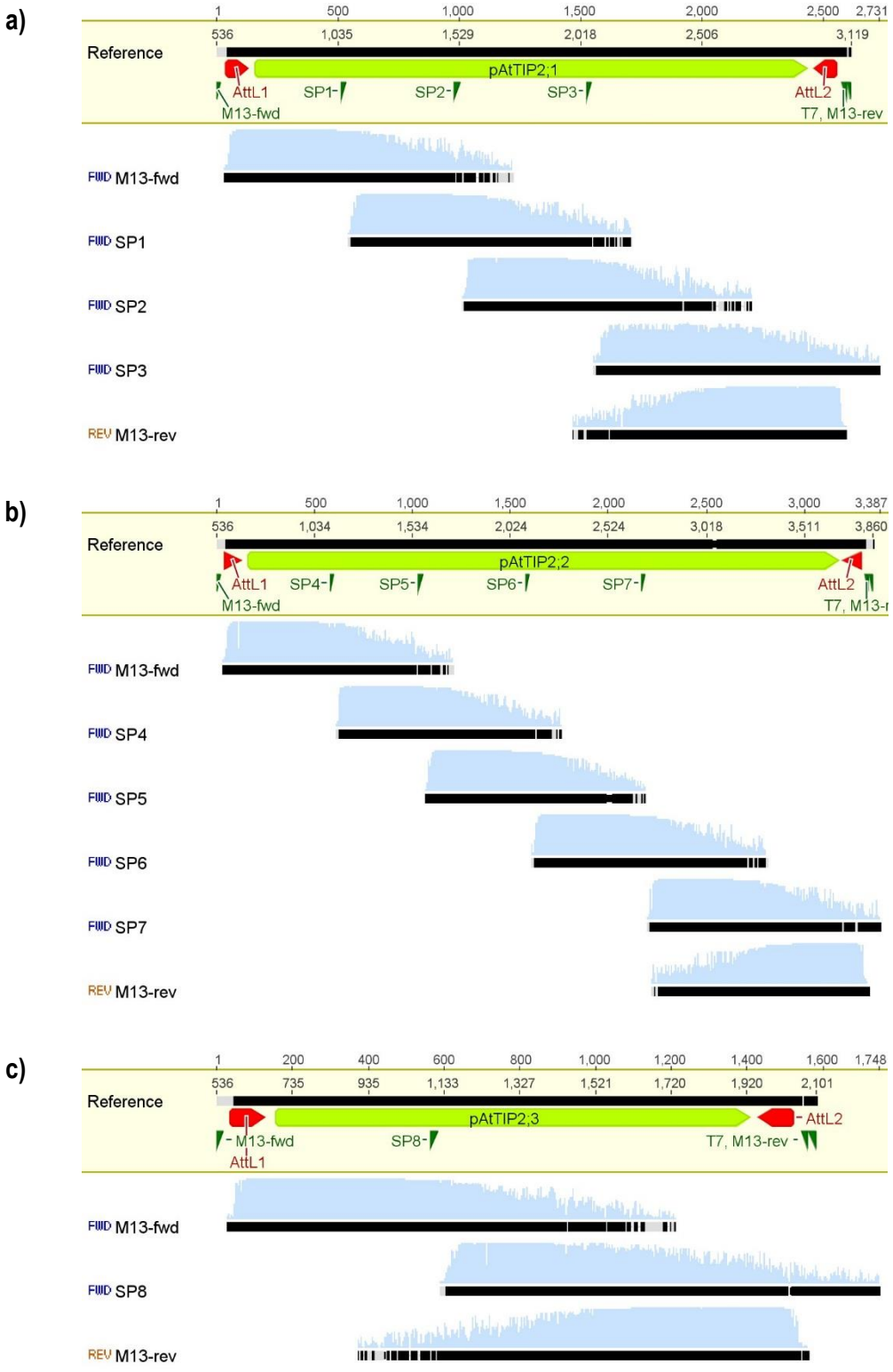

Figure 21. Confirmation of correct sequence for promoters of (a) *AtTIP2;1*, (b) *AtTIP2;2*, and (c) *AtTIP2;3* cloned into pENTR. The reference sequence shows part of the pENTR vector with the relevant insert between the M13 primer sites. M13 forward, reverse, and additional sequencing (SP1-8) primers (dark green) were used to amplify plasmid DNA during Sanger Sequencing. Sequencing traces from several primers were layered to cover the full length of the inserts. The light blue area above the Sanger Sequencing traces shows the quality of base calling. Below, the similarity between reference and sequencing trace is shown in black for match, or grey for mismatch.

After coding and promoter sequences were subcloned from pENTR to their destination vectors by LR reaction, restriction digests were preformed to confirm whether subcloning was successful (Figure 22). The destination vectors pUB-DEST and pUBC-GFP-DEST with inserts were cut with the restriction enzymes EcoRI and SbfI after subcloning (Figure 22a). Since the empty destination vectors have two sites for EcoRI, of which one is located within the recombination site, restriction digest of empty vectors would produce three fragments instead of two. Separation of the fragments from the subclones by gel electrophoresis showed that two fragments were produced consistent with the predicted sizes shown by a virtual digest.

Similar, the destination vector pMDC162 was cut using different combinations of restriction enzymes after subcloning the promoter sequences of *AtTIP2;1*, *AtTIP2;2*, and *AtTIP2;3* into it (Figure 22b). The empty pMDC162 vector has a single restriction site for both NarI and NheI, no site for HindIII, and three sites for BamHI, of which two are located within the recombination site. The promoter sequence of *AtTIP2;1* has one restriction site for HindIII, which should produce two fragments with NarI. However, NarI is a multi-site enzyme, which needs more than one restriction site to function at its full capacity (Broek *et al.* 2006). The enzyme forms loops with two restriction sites during digest. Therefore, three fragments can be expected, with one being the linearized vector. The promoter sequence of *AtTIP2;2* has a restriction site for NheI as well, apart from the site in pMDC162, which also makes two fragments if subcloning was successful. Thirdly, insertion of the promoter of *AtTIP2;3*, which has no restriction site for either BamHI or NheI, into pMDC162 would remove two sites for BamHI, leaving only two fragments if subcloning was successful. For *AtTIP2;2* and *AtTIP2;3*, clones with two fragments were found which confirms successful subcloning. For *AtTIP2;1*, three fragments were found: one large fragment, which made a strong band and two smaller fragments with similar but fainter bands. The strong band is supposedly the linearized vector produced by HindIII alone, while the faint band are the fragments produced by HindIII and NarI.

a)

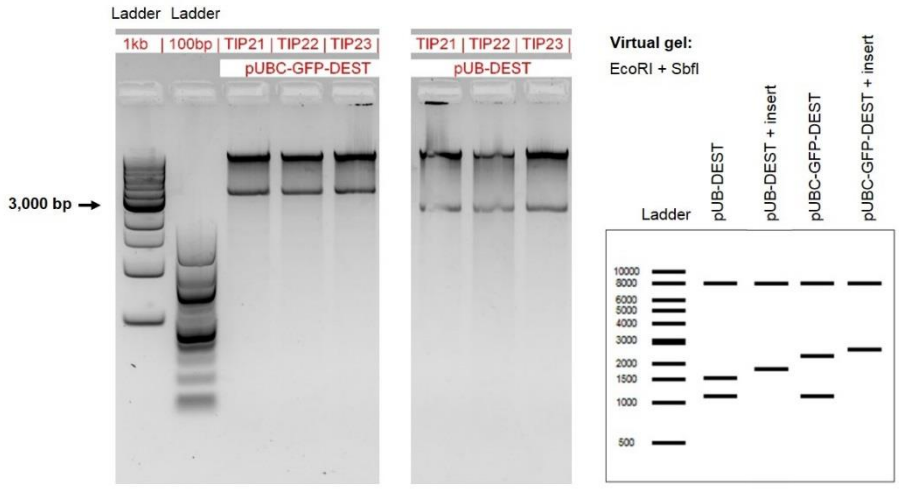

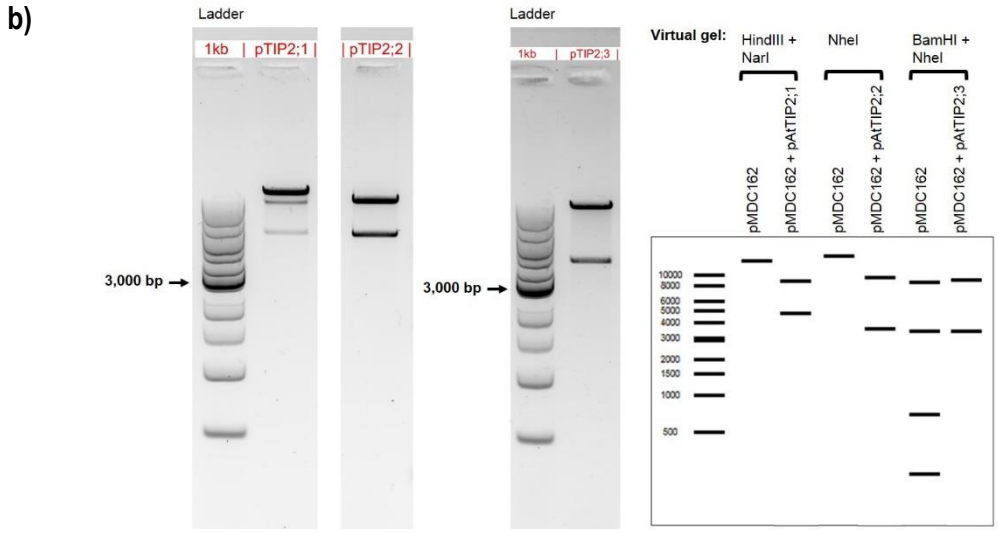

Figure 22. Restriction digest of destination vector constructs with inserts of the coding sequences or promoters for genes *AtTIP2;1*, *AtTIP2;2*, and *AtTIP2;3*. A virtual digest of both destination vectors with and without the inserts are shown on the right. a) Destination vectors pUB-DEST and pUBC-GFP-DEST with inserts of the coding sequences for *AtTIP2;1*, *AtTIP2;2*, and *AtTIP2;3* were cut by restriction enzymes EcoRI and SbfI (New England Biolabs). Two ladders (100 bp and 1 kb by New England Biolabs) are shown as size reference. All digests were run on the same gel, but additional lanes were removed by cropping. b) Destination vector pMDC162 with inserts of the promoter sequences for *AtTIP2;1*, *AtTIP2;2*, and *AtTIP2;3* were cut by different combinations of restriction enzymes (New England Biolabs): promoter *AtTIP2;1* (HindIII + NarI), promoter *AtTIP2;2* (NheI), and promoter *AtTIP2;3* (BamHI + NheI). A 1 kb ladder (New England Biolabs) is shown as size reference. Restriction digests were run on two different gels. Additional lanes were removed by cropping.

With all coding sequences and promoters successfully subcloned into the destination vectors, a group of overexpression and promoter GUS constructs were then available to explore the functions and expression localisation of *AtTIP2;1*, *AtTIP2;2*, and *AtTIP2;3* (Figure 23). For overexpression, the coding sequences of all three genes were driven by an ubiquitin 10 promoter (pUBQ10) and selection could be achieved using the glufonisate resistance (BarR) (Figure 23a). Additionally, a sequence for a GFP fluorescent tag with no stop codons was attached to the genes.

For studying the promoter activity, predicted promoter sequences should be driving expression of the gusA gene (Figure 23b). Selection of these constructs could be achieved by hygromycin resistance (HygR).

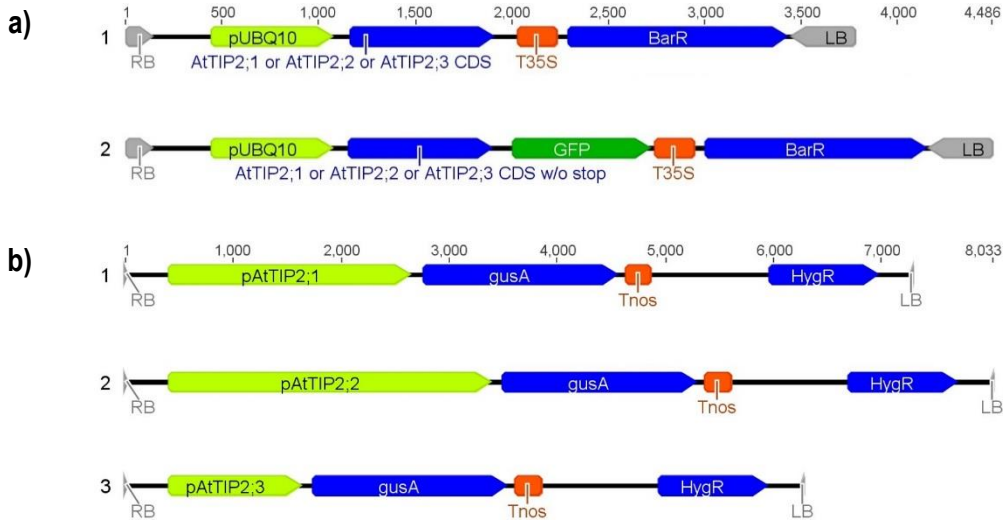

Figure 23. Schematic representation of T-DNA constructs for a) the overexpression of *AtTIP2;1*, *AtTIP2;2* and *AtTIP2;3* with and without fluorescent GFP tag and b) the expression of the *gusA* reporter gene driven by promoter sequences of either *AtTIP2;1*, *AtTIP2;2* or *AtTIP2;3*. The T-DNA constructs for overexpression (a) were created within the vectors pUB-DEST, for construct 1, and pUBC-GFP-DEST, for construct 2. The genes are driven by a UBQ10 promoter (light green) and terminated by a 35S terminator (orange). The bar gene (dark blue) serves as selection marker by conferring glufosinate resistance. Construct 1 contains the full coding sequence (without introns) of either of the three aquaporin genes, while construct 2 contains the full coding sequences without stop and the fluorescent GFP tag (dark green). The GUS reporter T-DNA constructs (a) were created within the vector pMDC162 which contains a hygromycin resistance gene (dark blue) as selection marker. The expression of *gusA* is driven by promoter sequences of the aquaporin genes (*AtTIP2;1*: 2258 bp; *AtTIP2;2*: 2999 bp; *AtTIP2;3*: 1240 bp) and terminated by a nos terminator.

The segregation analysis of overexpressors, to find lines with T-DNA insertions in a single locus, identified between approx. 20 – 60 % of T_1 lines that had T-DNA insertions only in one locus. This included several lines from two independent transformation events. These heterozygous lines were then grown to seed to find homozygous offspring.

Promoter – Gus lines were only grown to T_1 generation and no segregation analysis was carried out.

Table 3. Single locus frequency of overexpression construct inserts observed for T_1 lines. Segregation ratios are determined in T_2 offspring germinated on medium with glufosinate ammonium.

Line	Lines tested	Lines with 1:3 segregation	Single locus freq. (%)
pUB-AtTIP2;1	16	10	62.5
pUBC-AtTIP2;1-GFP	16	3	18.8
pUB-AtTIP2;2	16	8	50.0
pUBC-AtTIP2;2-GFP	16	6	37.5
pUBC-AtTIP2;3	16	7	43.8
pUBC-AtTIP2;3-GFP	16	10	62.5

Multiple homozygous overexpression lines were detected upon T_3 segregation analysis (Table 4). Frequencies of approx. 20 – 40 % homozygous lines were observed in populations of 40.

Table 4. Frequency of homozygous T_2 lines, detected by segregation analysis of T_3 offspring. T_3 offspring with 100 % germination on selective plates with glufosinate ammonium were assumed to originate from homozygous T_2 lines.

Line	Lines tested	100 % germination	Homozygous freq. (%)
pUB-AtTIP2;1	40	14	35.0
pUBC-AtTIP2;1-GFP	40	9	22.5
pUB-AtTIP2;2	40	13	32.5
pUBC-AtTIP2;2-GFP	40	7	17.5
pUBC-AtTIP2;3	40	17	42.5
pUBC-AtTIP2;3-GFP	40	16	40.0

3.3.2. Protein localisation

Confocal microscopy of homozygous T_3 seedlings expressing pUBQ10 promoter driven coding sequences of *AtTIP2;1*, *AtTIP2;2* or *AtTIP2;3* combined with a GFP fluorescent tag in *Arabidopsis thaliana* Col0 showed that all three genes were expressed in cotyledons and roots.

Seedlings expressing the AtTIP2;1-GFP constructs showed GFP fluorescence in both cotyledons and roots (Figure 24). Pavement cell in cotyledons were clearly lined by a membrane labelled with the fluorescently labelled proteins (Figure 24a). The labelled membranes were distinctively separated in different cells. Especially at the meeting points of three cells this was univocally observable. The GFP tagged AtTIP2;1 proteins were also localised to a membrane in the guard cells of stomata (Figure 24b). Fluorescent structures inside the guard cells looked like cytoplasmic strands or fragmented vacuoles. Chloroplasts which were also in the focal place are shown in red.

Likewise, GFP fluorescence was also detected in the roots (Figure 24c, d). An overview of the root tip showed that fluorescence could be detected in almost every cell (Figure 24c). Observations of root cortex cells in the meristematic zone showed the GFP fluorescence localised to a membrane within the cells that also had invaginations (Figure 24d).

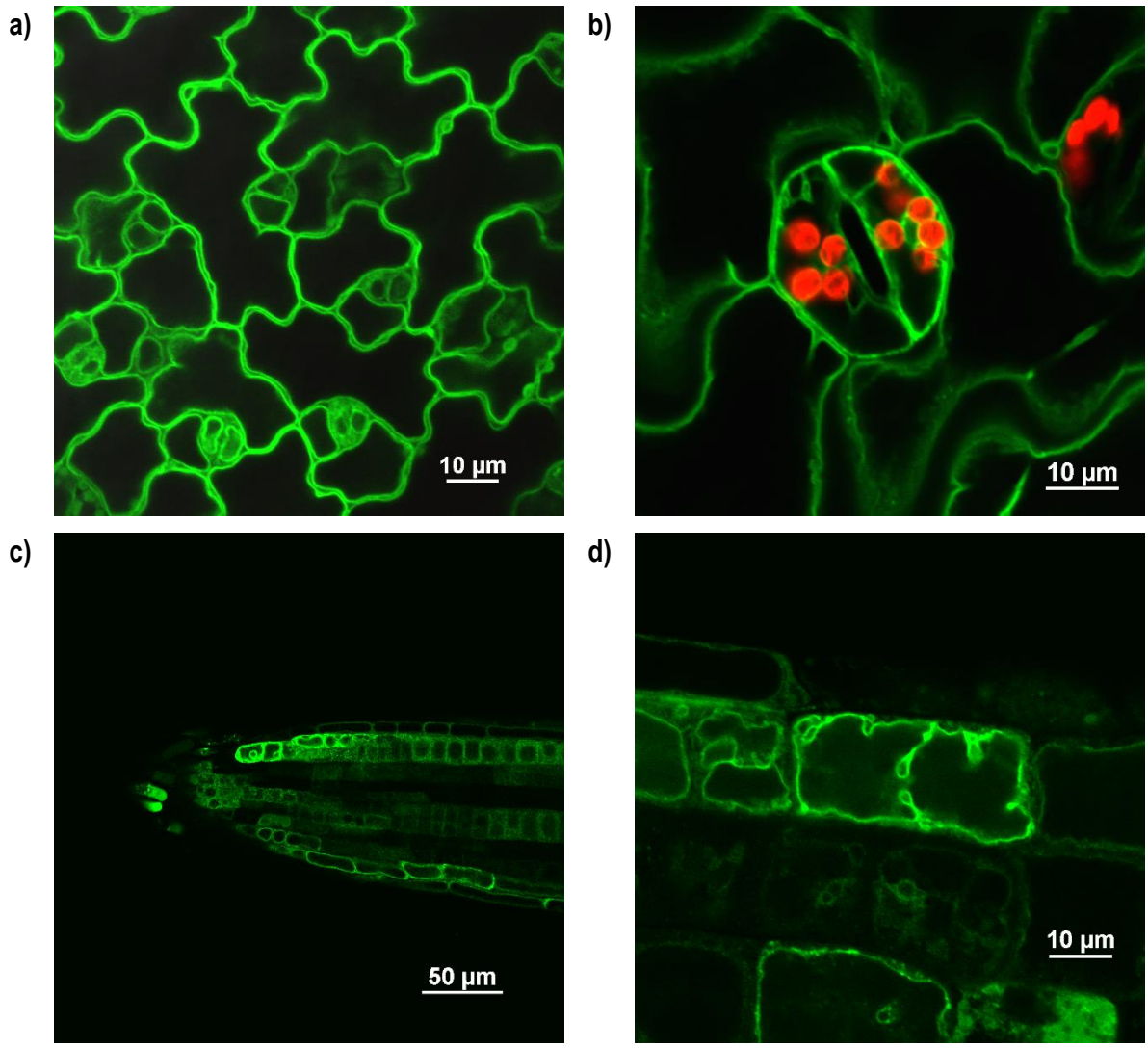

Figure 24. Localisation of AtTIP2;1-GFP observed by confocal microscopy of cotyledons and roots from *Arabidopsis thaliana* Col0 plants expressing pUBQ10 promoter driven *AtTIP2;1* linked to a GFP fluorescent tag. a) Pavement cells, b) close-up of guard cells with chloroplasts (red), c) root tip, and d) close-up of root cortex cells within the meristem zone.

The fluorescent plasma membrane dye FM4-64 helped to distinguish the tonoplast localisation of the GFP fluorescence by AtTIP2;1-GFP from the plasma membrane (Figure 25). In particular, the separation of the plasma membrane from the tonoplast by cell organelles like the nucleus showed that FM4-64 and the GFP signal did not overlay (Figure 25a). When the channels were split, the dent in the tonoplast membrane caused by the nucleus could still be observed (Figure 25b), while the plasma membrane was straight (Figure 25c). The nucleus itself could not be observed in this particular case (Figure 25d), which may be due to the focal plane.

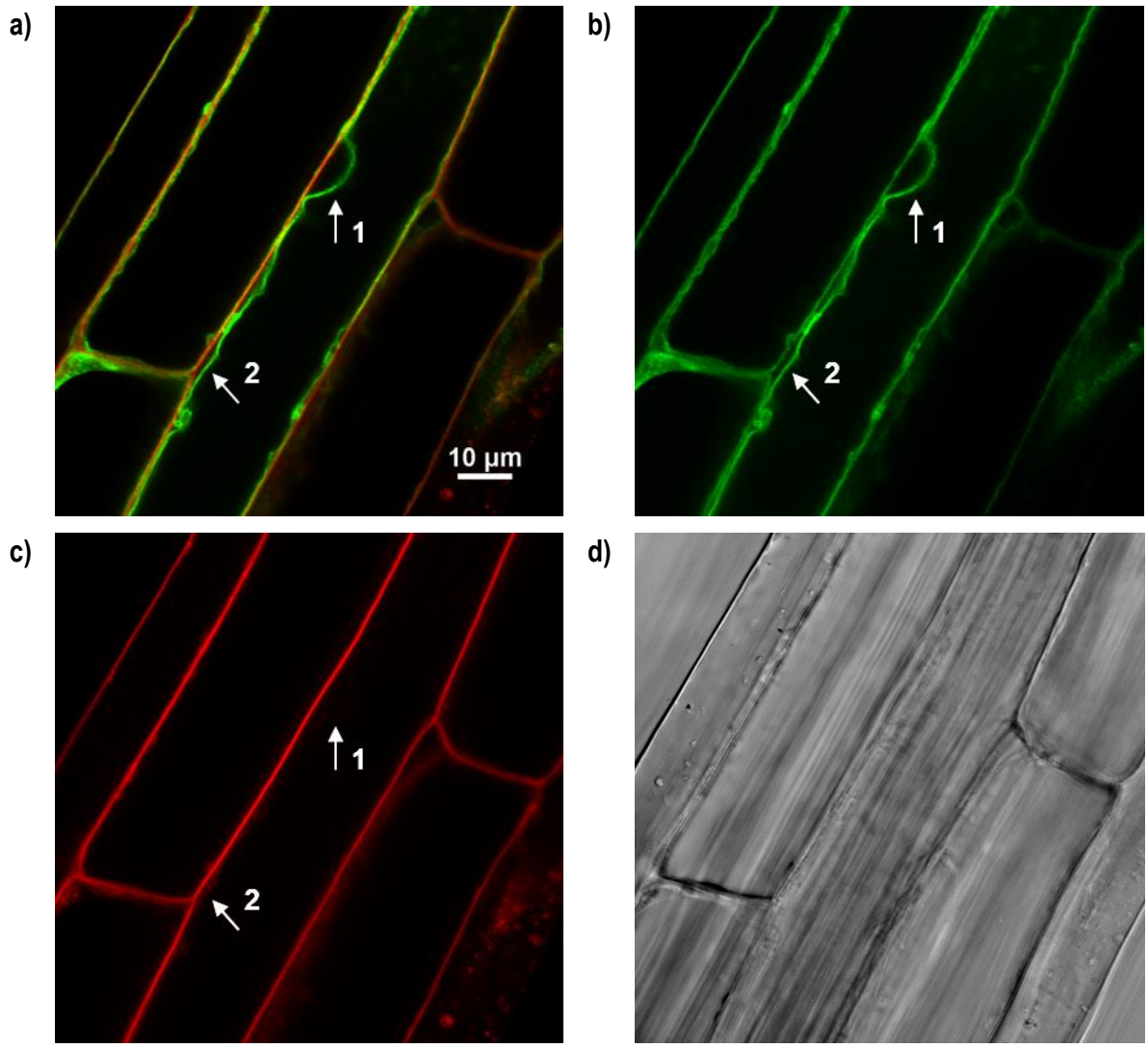

Figure 25. Tonoplast localisation of AtTIP2;1-GFP observed in comparison to the plasma membrane staining dye FM4-64 by confocal microscopy root cortical cells from *Arabidopsis thaliana* Col0 plants expressing pUBQ10 promoter driven *AtTIP2;1* linked to a GFP fluorescent tag. The arrows indicate areas where the tonoplast membrane is clearly separated from the plasma membrane. Arrow 1 points at the nucleus. a) Merged image, b) GFP fluorescence, c) FM4-64 dye fluorescence, and d) bright field image. The scale of all four images is the same as indicated in the first image.

Similarly, the tonoplast localisation of AtTIP2;2-GFP (Figure 26) and AtTIP2;3-GFP (Figure 27) could be distinguished from the plasma membrane by the use of the FM4-64 dye. Several nuclei were observed (Figure 26d, Figure 27d) that clearly separated the fluorescence of the FM4-64 dye on the plasma membrane (Figure 26c, Figure 27c), from the GFP signal on the tonoplast membrane (Figure 26b, Figure 27b).

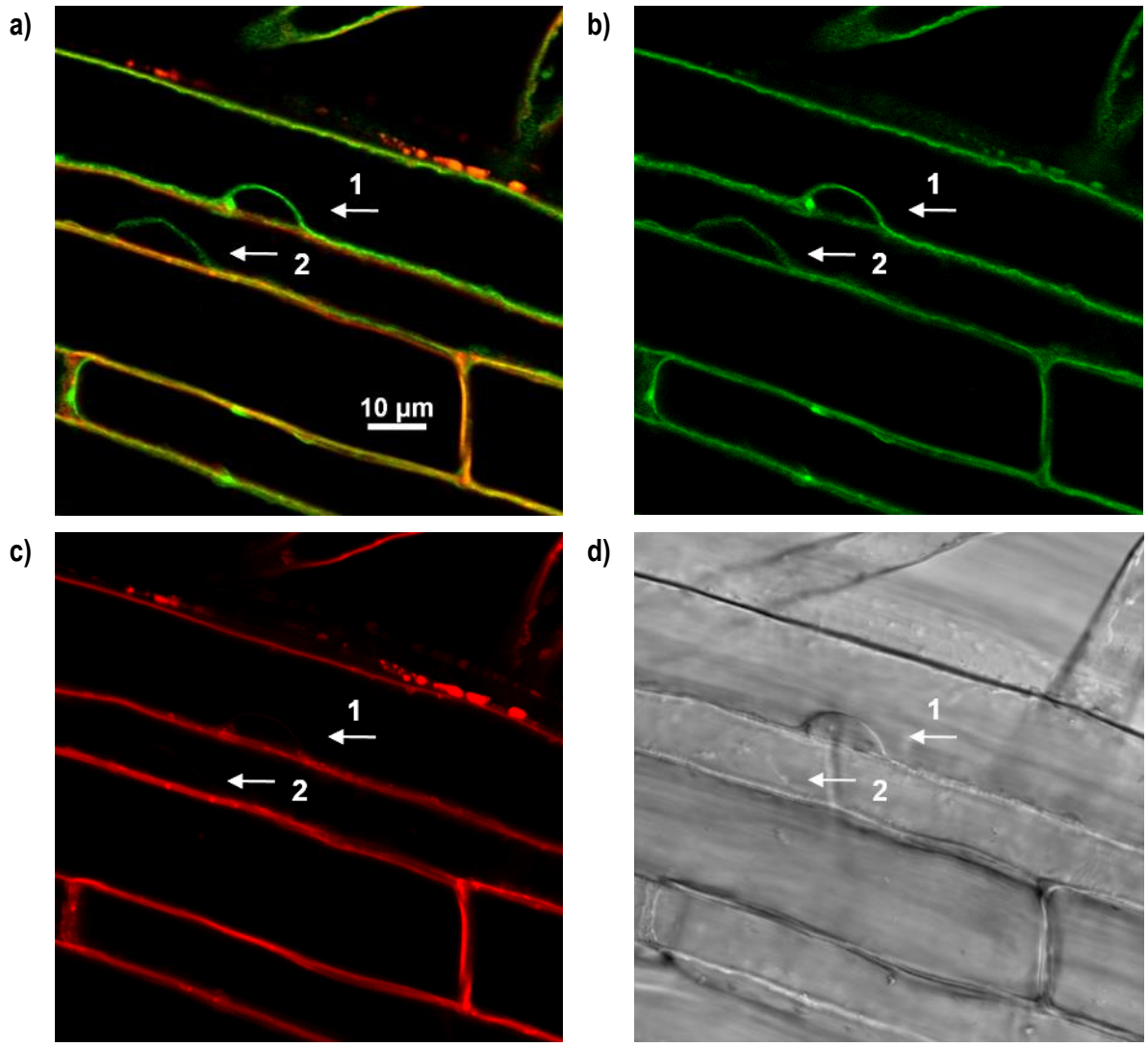

Figure 26. Tonoplast localisation of AtTIP2;2-GFP observed in comparison to the plasma membrane staining dye FM4-64 by confocal microscopy root cortical cells from *Arabidopsis thaliana* Col0 plants expressing pUBQ10 promoter driven *AtTIP2;2* linked to a GFP fluorescent tag. The arrows indicate areas where the tonoplast membrane is clearly separated from the plasma membrane by the nucleus. a) Merged image, b) GFP fluorescence, c) FM4-64 dye fluorescence, and d) bright field image. The scale of all four images is the same as indicated in the first image.

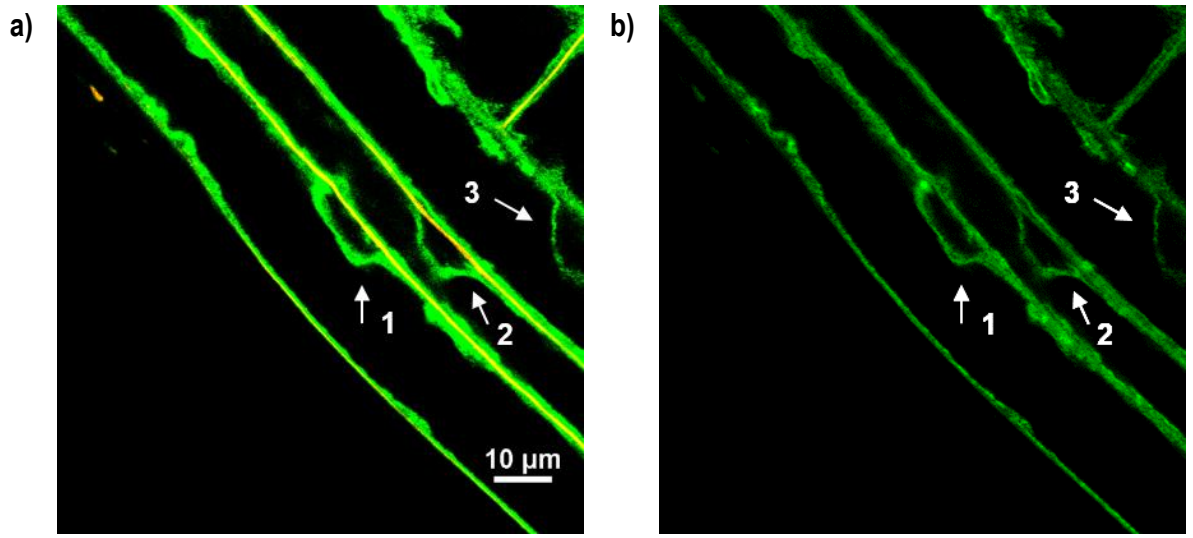

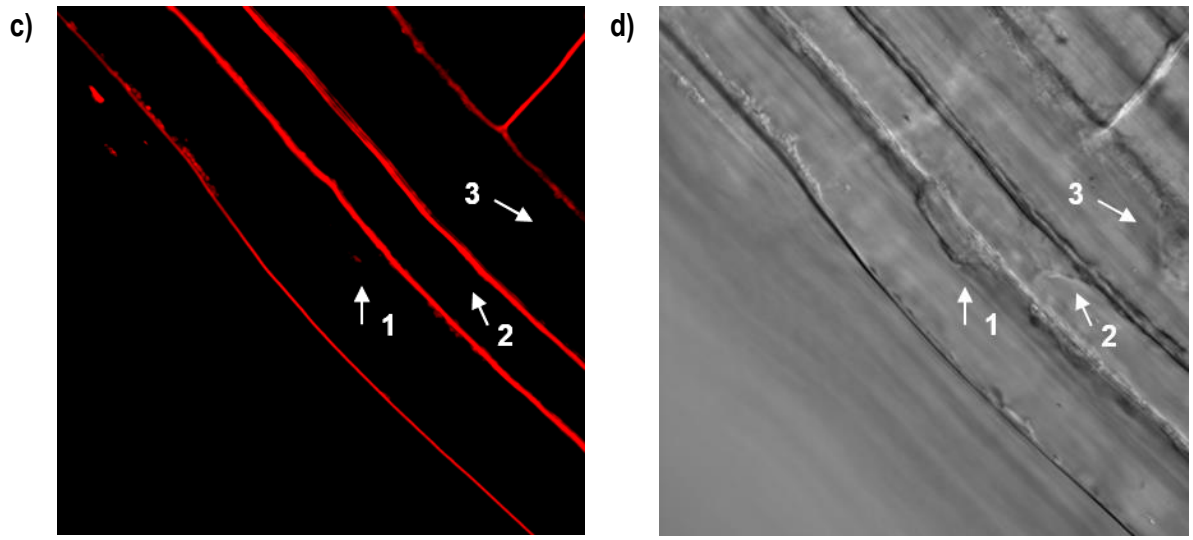

Figure 27. Tonoplast localisation of AtTIP2;3-GFP observed in comparison to the plasma membrane staining dye FM4-64 by confocal microscopy root cortical cells from *Arabidopsis thaliana* Col0 plants expressing pUBQ10 promoter driven *AtTIP2;3* linked to a GFP fluorescent tag. The arrows indicate areas where the tonoplast membrane is clearly separated from the plasma membrane by the nucleus. a) Merged image, b) GFP fluorescence, c) FM4-64 dye fluorescence, and d) bright field image. The scale of all four images is the same as indicated in the first image.

3.3.3. Promoter activity

The expression patterns of *AtTIP2;1*, *AtTIP2;2* or *AtTIP2;3* were visualised by using the predicted promoter sequences of these genes to drive the expression of *gusA*. Histochemical staining (GUS assay) of plant tissue, expressing these constructs, with X-Gluc produces a blue precipitate (chloro-bromoindigo), when X-Gluc is broken down by the protein β-glucuronidase which is encoded by *gusA*.

Tissue from wild-type *Arabidopsis thaliana* Col0 showed no staining in the GUS assay (Figure 28).

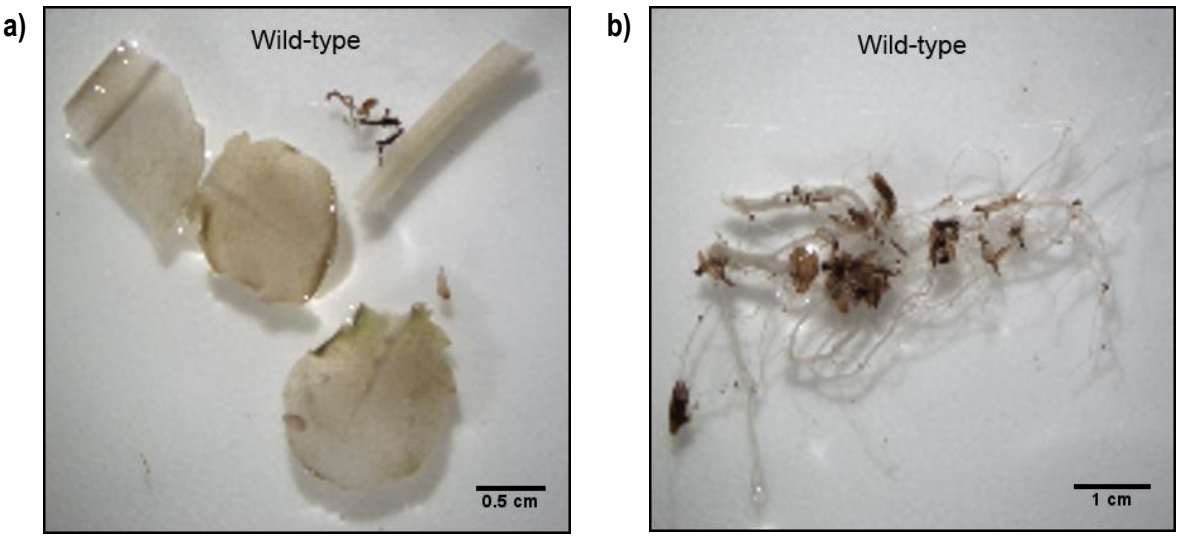

Figure 28. Negative controls of *Arabidopsis thaliana* Col0 wild-type leaves (a) and roots (b) stained in the GUS assay.

In contrast, transgenic lines expressing the pAtTIP2;1-GUS construct showed strong staining around the vasculature in leaves (Figure 29a). At higher magnification, staining in particular in guard cells could be observed (Figure 29b). In roots, staining could be observed in the stele and pericycle (Figure 29c, d). While the root cap was strongly stained, no stain was observed in basal meristem (Figure 29c). Apart from the stele and pericycle, the base of the lateral root primordia was also stained (Figure 29d).

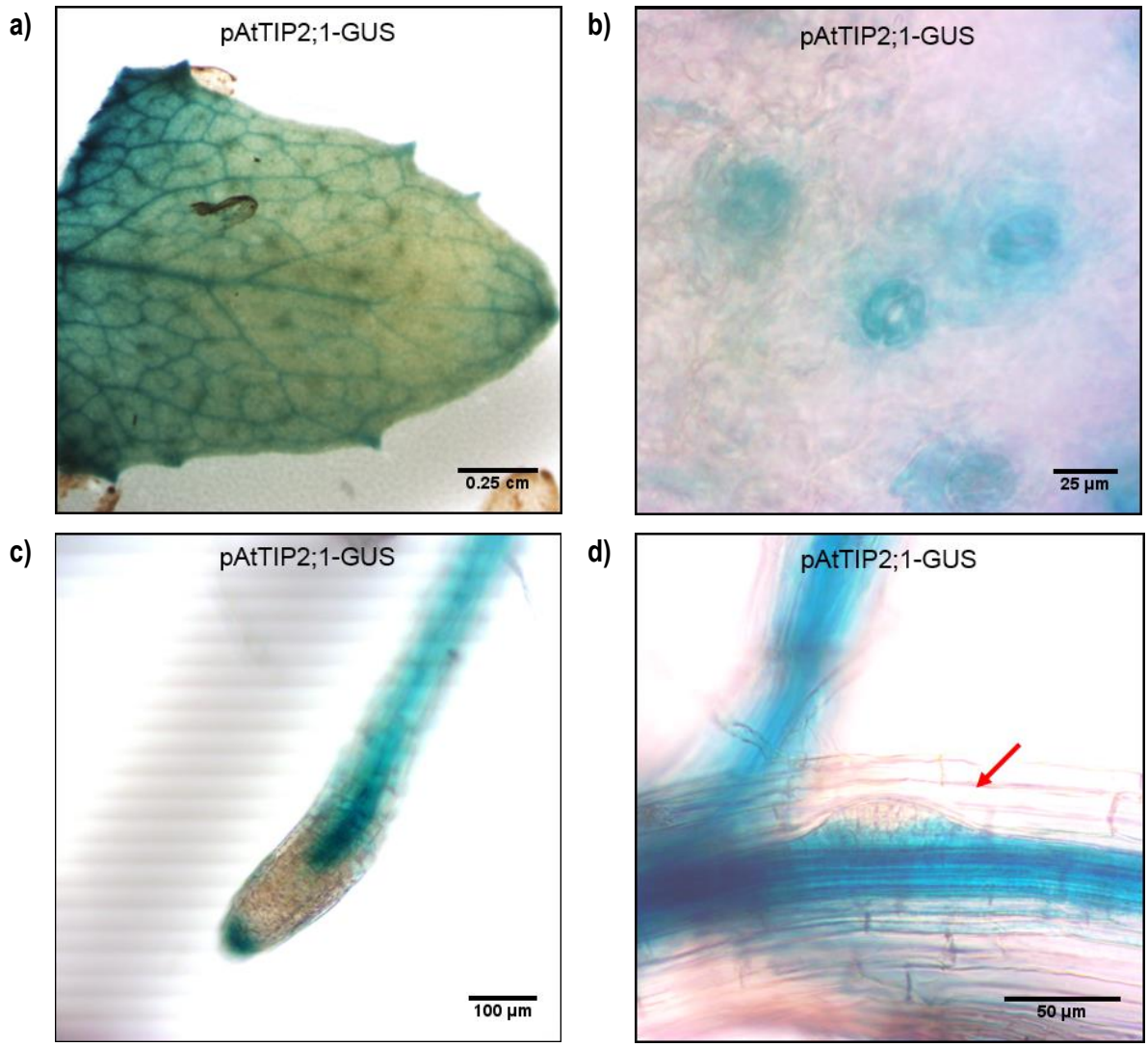

Figure 29. Activity of the *AtTIP2;1* promoter visualised by histochemical staining in a) leaves, b) stomata, c) roots, and d) lateral root primordia. Lateral root primordia pointed out by red arrow.

Similarly, transgenic lines expressing the pAtTIP2;2-GUS construct also showed staining of the vasculature in leaves (Figure 30a). Compared to pAtTIP2;1-GUS, there seemed less staining in spaces between the veins. Additionally, staining around the hydathodes was clearly visible. In roots, staining in the stele and root cap was observed, while no stain was found in the meristem (Figure 30b).

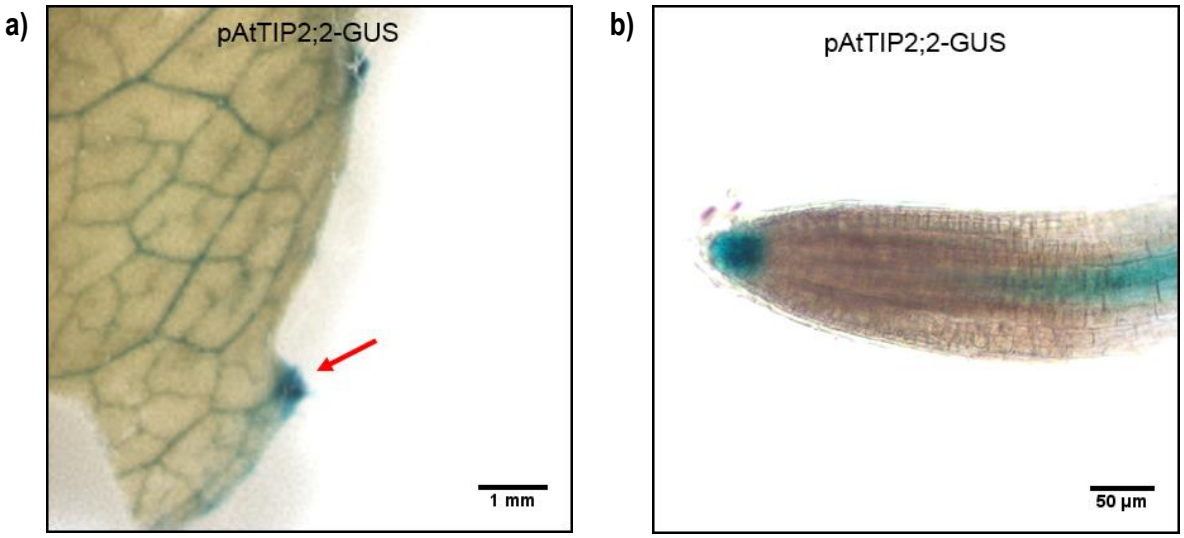

Figure 30. Activity of the *AtTIP2;2* promoter visualised by histochemical staining in a) leaves and b) roots. Hydathode pointed out by red arrow.

Transgenic lines expressing the pAtTIP2;3-GUS construct also showed staining of the vasculature in leaves and some staining between the veins (Figure 31a). In contrast to both other promoters, no staining was observed in the root cap, while similar staining was found in the stele and pericycle (Figure 31b). In contrast to pAtTIP2;1-GUS, no staining was observed at the base of lateral root primordia (Figure 31c).

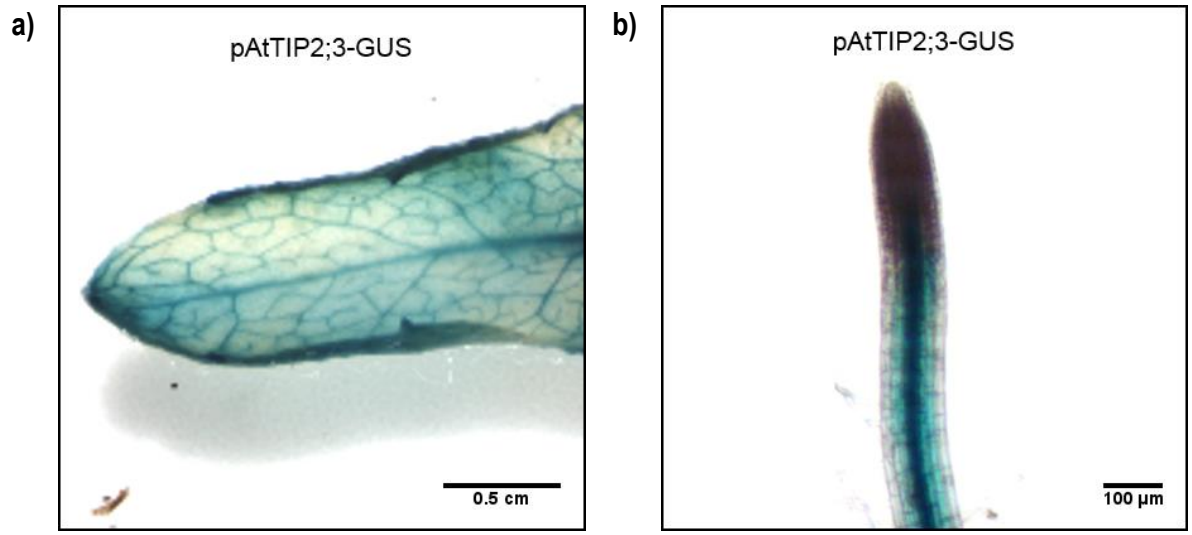

c)

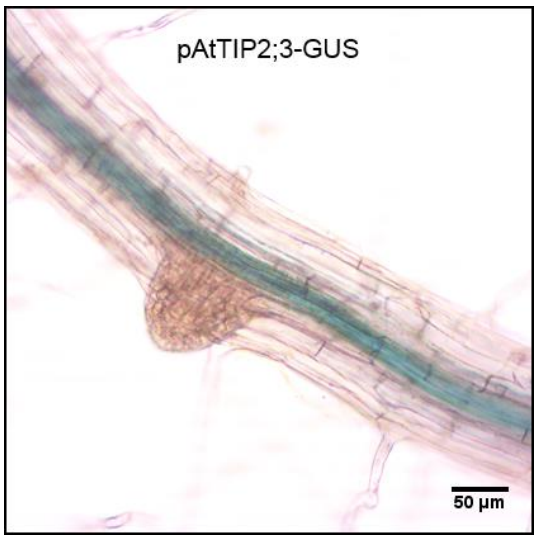

Figure 31. Activity of the *AtTIP2;3* promoter visualised by histochemical staining in a) leaves, b) roots, and c) lateral root primordia.

3.3.4. Drought-rehydration assessment of homozygous transgenic lines for constitutive expression of *AtTIP2* isoforms

Studies were carried out with some homozygous transgenic lines in the T_3 generation to assess the influence of constitutively expressed TIP2 aquaporins in *Arabidopsis thaliana* during drought-rehydration events.

3.3.4.1. First experiment: Mixed selection of transgenic AtTIP2 lines during drought and rehydration

For a first experiment, a mix of homozygous transgenic plants, which had T-DNA insertions for constitutive expression of the genes *AtTIP2;1*, *AtTIP2;2*, and *AtTIP2;3* coupled with or without a c-terminal GFP fluorescent tag, were grown. The plants showed no obvious differences in morphology or growth compared to Col-0 wild-type plants, which were used as controls (Figure 32). All plants were healthy and developed similar to the wild-type controls.

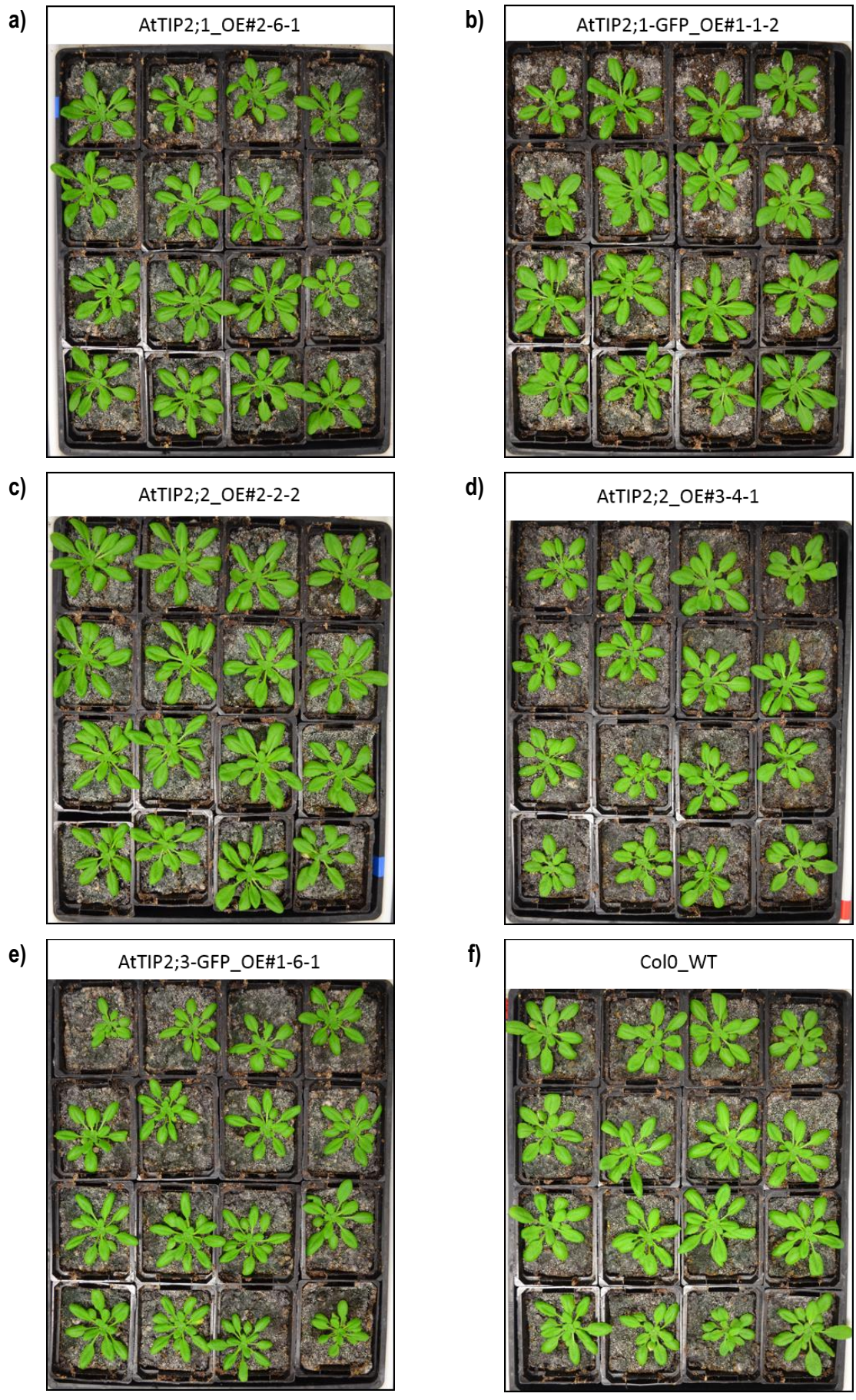

Figure 32. Visual comparison between transgenic *Arabidopsis thaliana* plants, expressing TIP2 aquaporins under the control of a constitutive UBQ10 promoter, and the Col0 wild-type. Plants were grown under short-day conditions (10 h light/ 14 h

dark,PAR ~150 µmol m^{-2} s^{-1}, 21°C) for four weeks. All transgenic plants are offspring from homozygous single locus T_2 plants. a) *AtTIP2;1* overexpressor line, b) *AtTIP2;1* overexpressor line with c-terminal GFP fluorescent tag, c) *AtTIP2;2* overexpressor line, d) *AtTIP2;2* overexpressor line, e) *AtTIP2;3* overexpressor line with c-terminal GFP fluorescent tag, and f) Col0 wild-type plants.

Image analysis showed that 4-weeks old plants from the line AtTIP2;2_OE#2-2-2 had a significant larger leaf area compared to the Col0_WT, while there were no significant differences between the other lines and the wild-type (Figure 33).

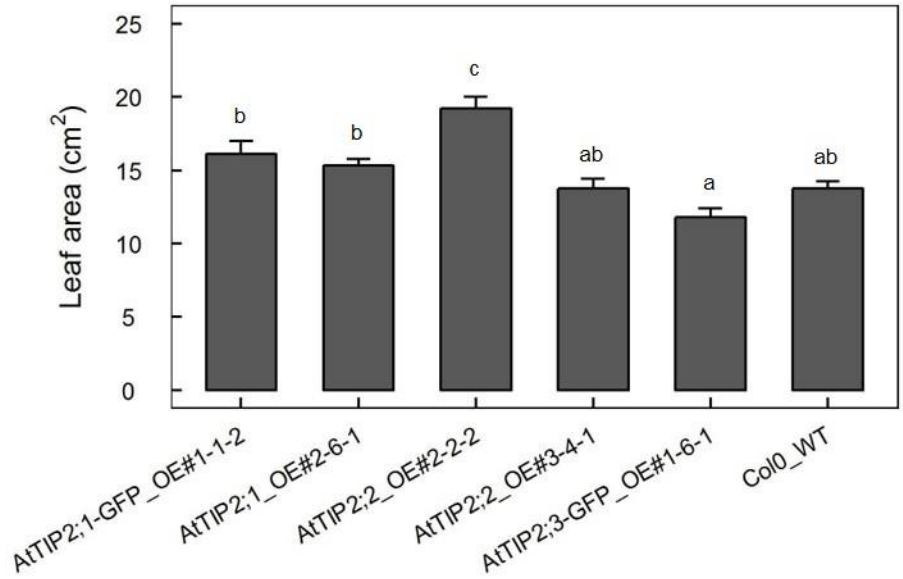

Figure 33. Comparison of leaf area between 4-weeks old transgenic *Arabidopsis thaliana* plants, expressing TIP2 aquaporins under the control of a constitutive UBQ10 promoter, and the Col0 wild-type. Bars show the mean ± SEM for n = 16 (transgenic lines) or n = 47 (Col0 wild-type) plants. Comparisons were carried out by one-way ANOVA with Bonferroni post-hoc test. Different letters indicate significant differences at $p \leq 0.05$.

A drought-rehydration experiment was performed, once the plants were 7-weeks old. Measurements of stomatal conductance (g_s) showed significantly lower g_s in drought treated wild-type plants (Col0_WT) on days 6 and 7 compared to well-watered plants (Figure 34). Even on day 8, when plants were re-watered, the previously drought treated plants still had a significantly lower g_s compared to well-watered control plants. This was similar for plants from the transgenic line AtTIP2;2_OE#2-2-2. Interestingly, plants from the transgenic AtTIP2;1 lines (AtTIP2;1-GFP_OE#1-1-2, AtTIP2;1_OE#2-6-1) only showed a significant difference in g_s between the well-watered and drought treated group on day 7 when plants started wilting. Once they were re-watered, no difference was found compared to the well-watered controls. For the transgenic line AtTIP2;2_OE#3-4-1, no significant difference in g_s was found between drought treated and well-watered plants on day 6, but the average g_s of the drought treated plants was lower. For the transgenic line AtTIP2;3-GFP_OE#1-6-1, well-watered and rehydrated plants had the same g_s on day 8. Interestingly, also well-watered plants showed a drop in g_s from day 3 to day 6.

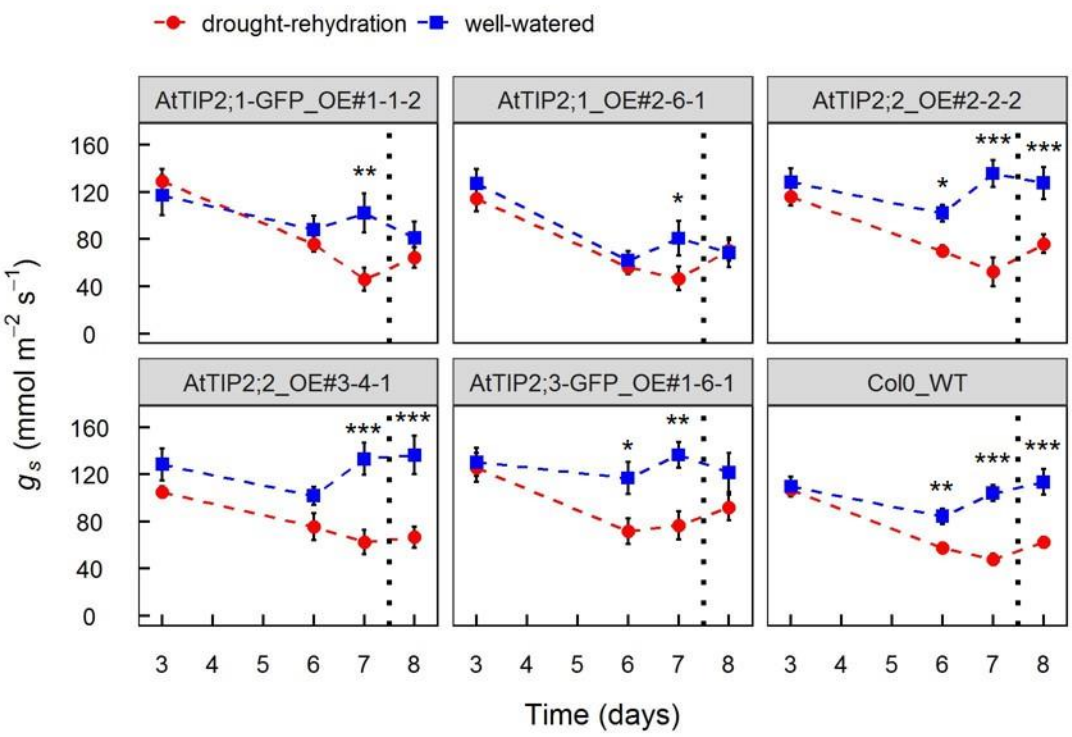

Figure 34. Stomatal conductance (g_s) measured on leaves of Arabidopsis plants (*Arabidopsis thaliana*) ecotype Col-0 used in a drought – rehydration experiment. Plants were either transgenic, expressing TIP2 aquaporins under the control of a constitutive UBQ10 promoter, or Col-0 wild-type. Each point represents the mean ± SE of six independent plants on which g_s was measured on one leaf each. Significant differences between the treated and control groups by ANOVA with Bonferroni post-tests are marked: * for P ≤ 0.05, ** for P ≤ 0.01 or *** for P ≤ 0.001. A vertical dotted line indicates when plants were re-watered.

The observed differences in behaviour compared to the wild-type control were not reflected by significant differences in g_s between lines within the well-watered or drought treated groups (Figure 35) during the drought period (up to day 7). Well-watered plants of the transgenic lines AtTIP2;2_OE#2-2-2, AtTIP2;2_OE#3-4-1, and AtTIP2;3-GFP_OE#1-6-1 had on average a higher g_s compared to the wild-type Col0_WT throughout the experiment, but this was not significant. In contrast, well-watered plants of the line AtTIP2;1_OE#2-6-1 had on average a lower g_s compared to the wild-type Col0_WT from day 6 – 8, which was also not significant. For drought treated plants, the differences were smaller. Only drought treated plants of the line AtTIP2;3-GFP_OE#1-6-1 had on average a higher g_s compared to the wild-type Col0_WT. This difference was significant on day 8 when plants were rehydrated.

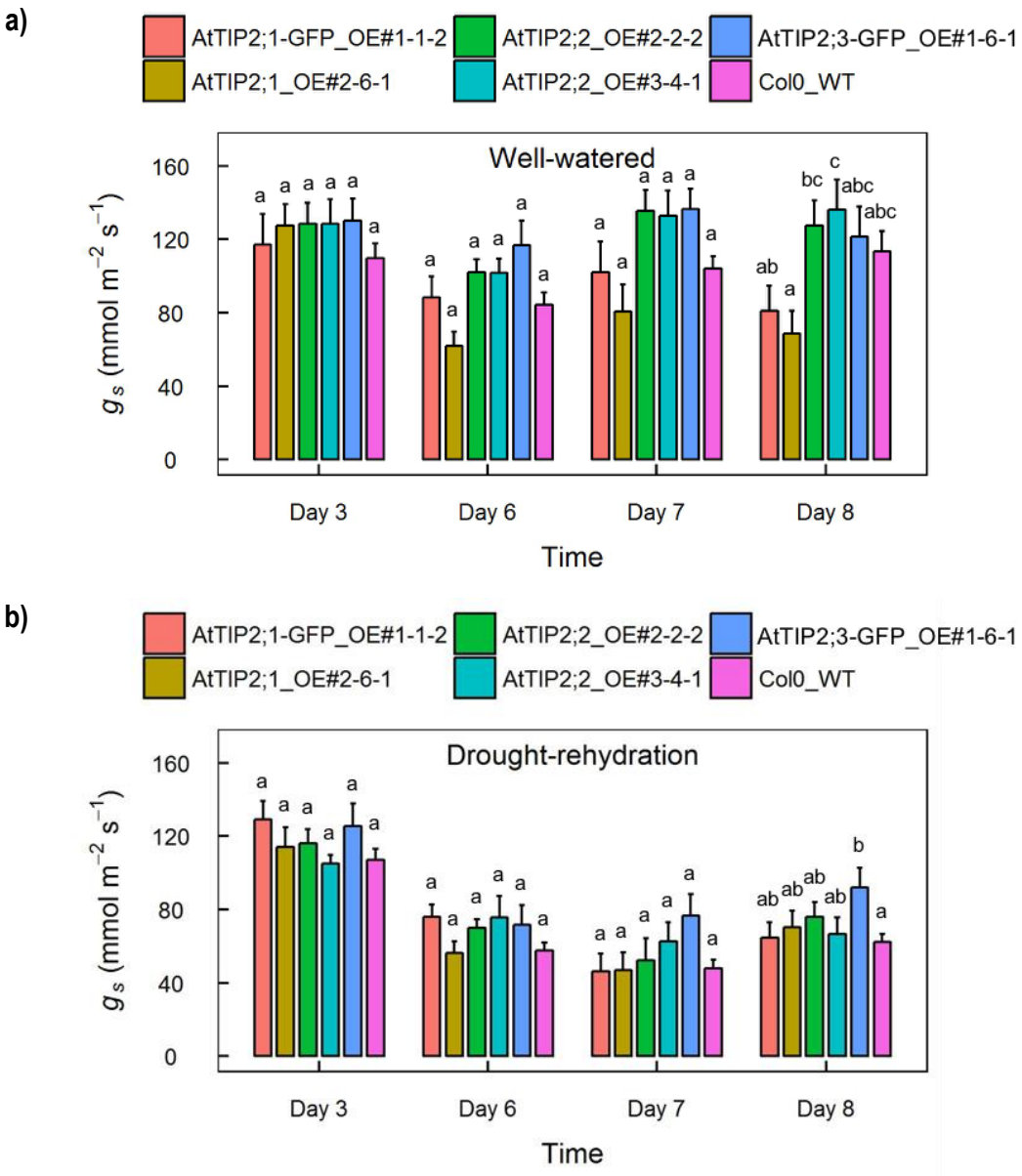

Figure 35. Comparison of stomatal conductance (g_s) between multiple transgenic lines of *Arabidopsis thaliana* and the wild-type (WT) during different days of a drought – rehydration experiment. Well-watered plants (a) and plants in the drought-rehydration group (b) were compared separately. For the drought-rehydration group, watering was withheld for seven days and plants were rehydrated before day 8. Plants were either transgenic, expressing TIP2 aquaporins under the control of a constitutive UBQ10 promoter, or Col-0 wild-type. Bars show the mean ± SEM of six independent plants on which g_s was measured on one leaf each. Comparisons were carried out by one-way ANOVA with Bonferroni post-hoc test. Different letters indicate significant differences at $p \leq 0.05$ per day.

Wilted leaves were sampled from transgenic and wild-type plants to test their rehydration kinetics. Instead of line AtTIP2;2_OE#3-4-1, the line AtTIP2;2-GFP_OE#1-3-3 was used and additional TIP2;3 lines (AtTIP2;3_OE#3-6-1) was used. Leaves had different degrees of dehydration to start with, but rehydrated to about the same level (Figure 36).

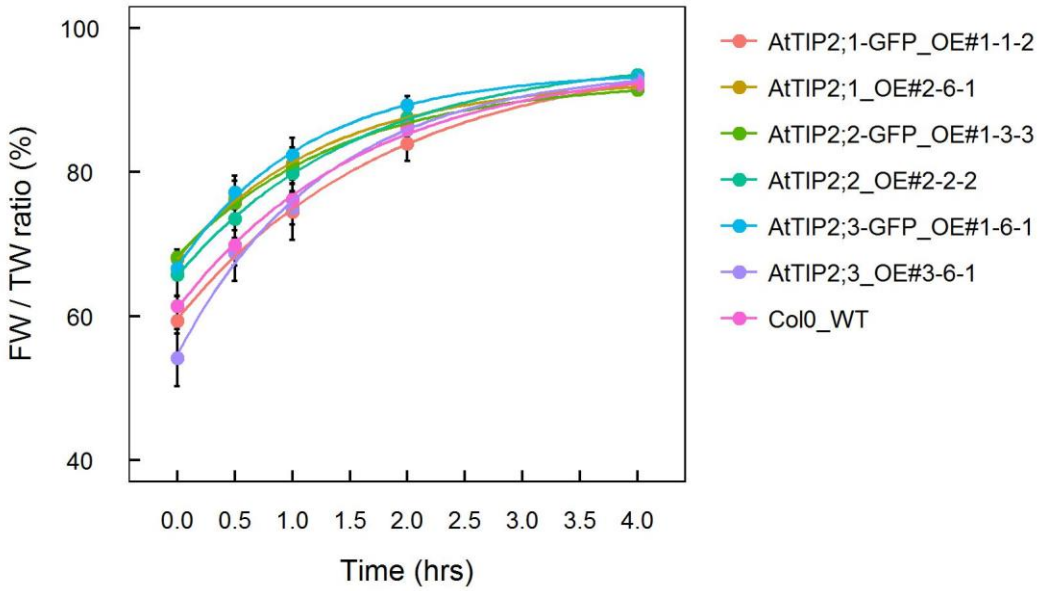

Figure 36. Comparison of rehydration kinetics between wilted leaves from transgenic *Arabidopsis thaliana* plants expressing TIP2 aquaporins under the control of a constitutive UBQ10 promoter and the Col0 wild-type. Rehydration was calculated as percentage ratio of actual fresh weight (FW) at consecutive time points during rehydration relative to the maximum turgid weight (TW) when leaves were fully hydrated. Data are shown as mean ± SEM of six leaves from independent plants. One phase exponential association kinetics (solid lines) were calculated for each line according to the following equation: Y=Y0 + (Plateau-Y0)*(1-exp(-K*x)).

Comparisons of the rehydration rate constant showed no significant differences between the different lines, since the confidence intervals were rather large (Table 5). However, leaves from the wild-type Col0_WT had the lowest rate constant K = 0.1295, while all transgenic lines had higher rate constants.

Table 5. Confidence intervals for rate constant K, calculated for the rehydration kinetics of wilted leaves from multiple *Arabidopsis thaliana* lines (Figure 36). Rehydration kinetics were calculated using a one phase exponential association equation: Y=Y0 + (Plateau-Y0)*(1-exp(-K*x)).

Line	K	95 % CI (lower)	95 % CI (upper)
AtTIP2;1-GFP_OE#1-1-2	0.1841	0.1297	1.038
AtTIP2;1_OE#2-6-1	0.2077	0.4278	1.218
AtTIP2;2-GFP_OE#1-3-3	0.1628	0.3984	1.096
AtTIP2;2_OE#2-2-2	0.2035	0.244	1.113
AtTIP2;3-GFP_OE#1-6-1	0.1985	0.5205	1.381
AtTIP2;3_OE#3-6-1	0.1612	0.4606	1.155
Col0_WT	0.1295	0.3724	0.8995

3.3.4.2. Second experiment: Transgenic AtTIP2;1 lines during drought

In a second experiment, more transgenic lines expressing AtTIP2;1 under the control the constitutive promoter UBQ10 were grown to be compared with the wild-type Col0_WT in a drought experiment.

Comparison of leaf area for 6-weeks old plants showed that one transgenic line had a significant smaller leaf area (AtTIP2;1_OE#3-6-7) and one transgenic line a significant larger leaf area (AtTIP2;1_OE#2-3-6) compared to the wild-type (Figure 37). The transgenic line AtTIP2;1_OE#2-6-1, which was grown in the previous experiment as well, showed no difference to the wild-type as in the previous experiment (Figure 33).

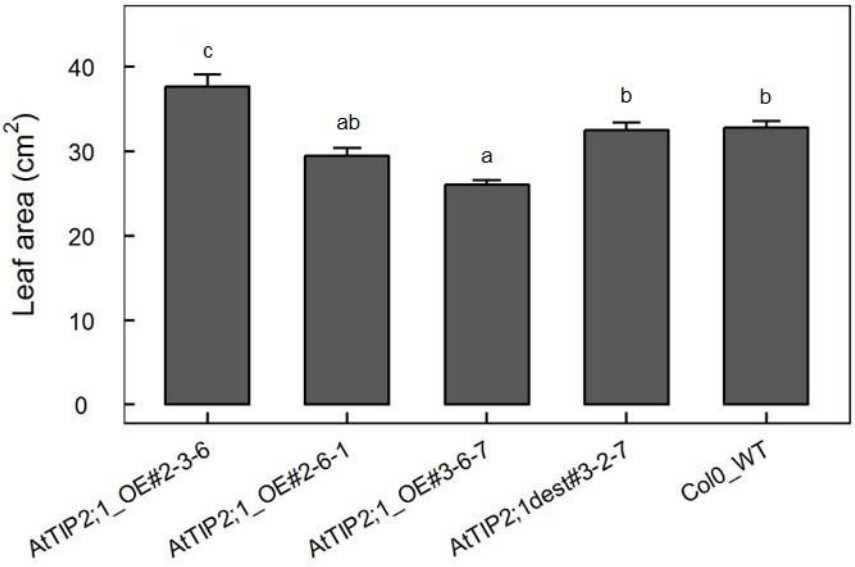

Figure 37. Comparison of leaf area between 6-weeks old transgenic *Arabidopsis thaliana* plants, expressing AtTIP2;1 aquaporins under the control of a constitutive UBQ10 promoter, and the Col0 wild-type. Bars show the mean ± SEM for n = 12 (transgenic lines) or n = 24 (Col0 wild-type) plants. Comparisons were carried out by one-way ANOVA with Bonferroni post-hoc test. Different letters indicate significant differences at $p \leq 0.05$.

In a drought experiment for these plants, watering was stopped for 10 days when the plants started to wilt (Figure 38); no rehydration was done as in contrast to the previous experiment. Compared to the previous experiment (Figure 34), dehydration to wilting took longer and significant differences in g_s between well-watered and drought treated wild-type Col0_WT plants were only observed from day 8 (Figure 38). Stomatal conductance of well-watered and droughted plants from the transgenic line AtTIP2;1_OE#2-3-6 showed clear differences, which were significant from day 7. While g_s of the well-watered plants didn't change much throughout the experiment, g_s of the droughted plants declined from about day 4. As well, Col0_WT plants, which served as a control, showed significant differences in g_s between the well-watered and droughted plants. However, the difference wasn't as strong compared to the transgenic line AtTIP2;1_OE#2-3-6. Moreover, well-watered control plants showed variable g_s with a large drop from day 4 to 6. This drop in g_s of well-watered plants was also observed in transgenic lines AtTIP2;1_OE#2-6-1

and AtTIP2;1_OE#3-6-7. At appeared that g_s of well-watered plants tracked g_s of droughted plants in all lines (including Col0_WT) except AtTIP2;1_OE#2-3-6. Interestingly, no difference in g_s was found between well-watered and droughted plants from the transgenic lines AtTIP2;1_OE#2-6-1, AtTIP2;1_OE#3-2-7, and AtTIP2;1_OE#3-6-7 despite that the droughted plants started wilting on day 10. While transgenic line AtTIP2;1_OE#2-3-6 showed a clearly different behaviour with on average higher g_s in well-watered plants and lower g_s in droughted plants, no significant difference was found when comparing g_s between all lines divided into well-watered and droughted plants for each day (like Figure 35).

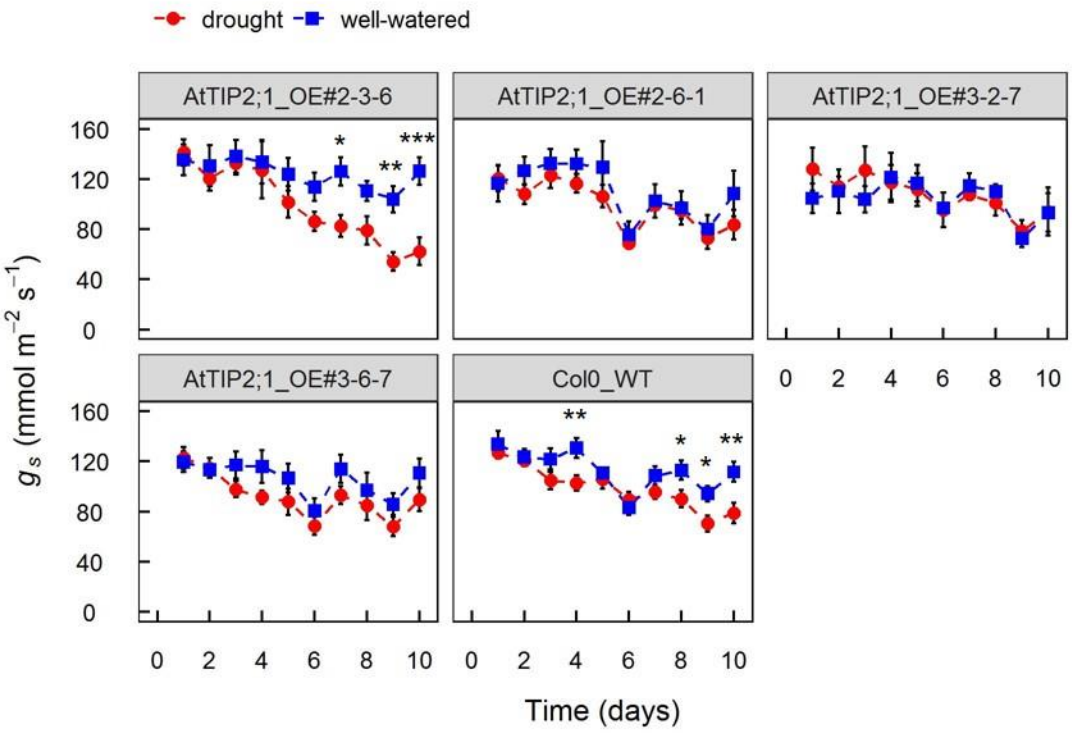

Figure 38. Stomatal conductance (g_s) measured on leaves of Arabidopsis plants (*Arabidopsis thaliana*) ecotype Col-0 used in a drought experiment. Plants were either transgenic, expressing AtTIP2;1 aquaporins under the control of a constitutive UBQ10 promoter, or Col-0 wild-type. Each point represents the mean ± SE of 12 (transgenic lines) or 24 (wild-type) independent plants on which g_s was measured on one leaf each. Significant differences between the treated and control groups by ANOVA with Bonferroni post-tests are marked: * for P ≤ 0.05, ** for P ≤ 0.01 or *** for P ≤ 0.001. No rehydration was performed.

Semiquantitative RT-PCR on leaf samples from three selected lines, which were collected on day 10 of the experiment, showed that *AtTIP2;1* was only overexpressed in line AtTIP2;1_OE#2-3-6 (Figure 39). Interestingly, expression of *AtTIP2;1* appeared to be even higher in leaves from droughted plants compared to well-watered plants for this line. In contrast, Col0_WT, which served as a control, showed lower expression of *AtTIP2;1* in leaves from droughted plants. Gene expression of *AtTIP2;1* was similar in the transgenic line AtTIP2;1_OE#2-6-1 compared to Col0_WT. The difference in expression between leaves from droughted and well-watered plants wasn't that strong in line AtTIP2;1_OE#2-6-1, however.

The housekeeping gene *AtACT2* was used to normalise against (Figure 39a). Below the band for the gene-specific PCR products primer-dimers were observed.

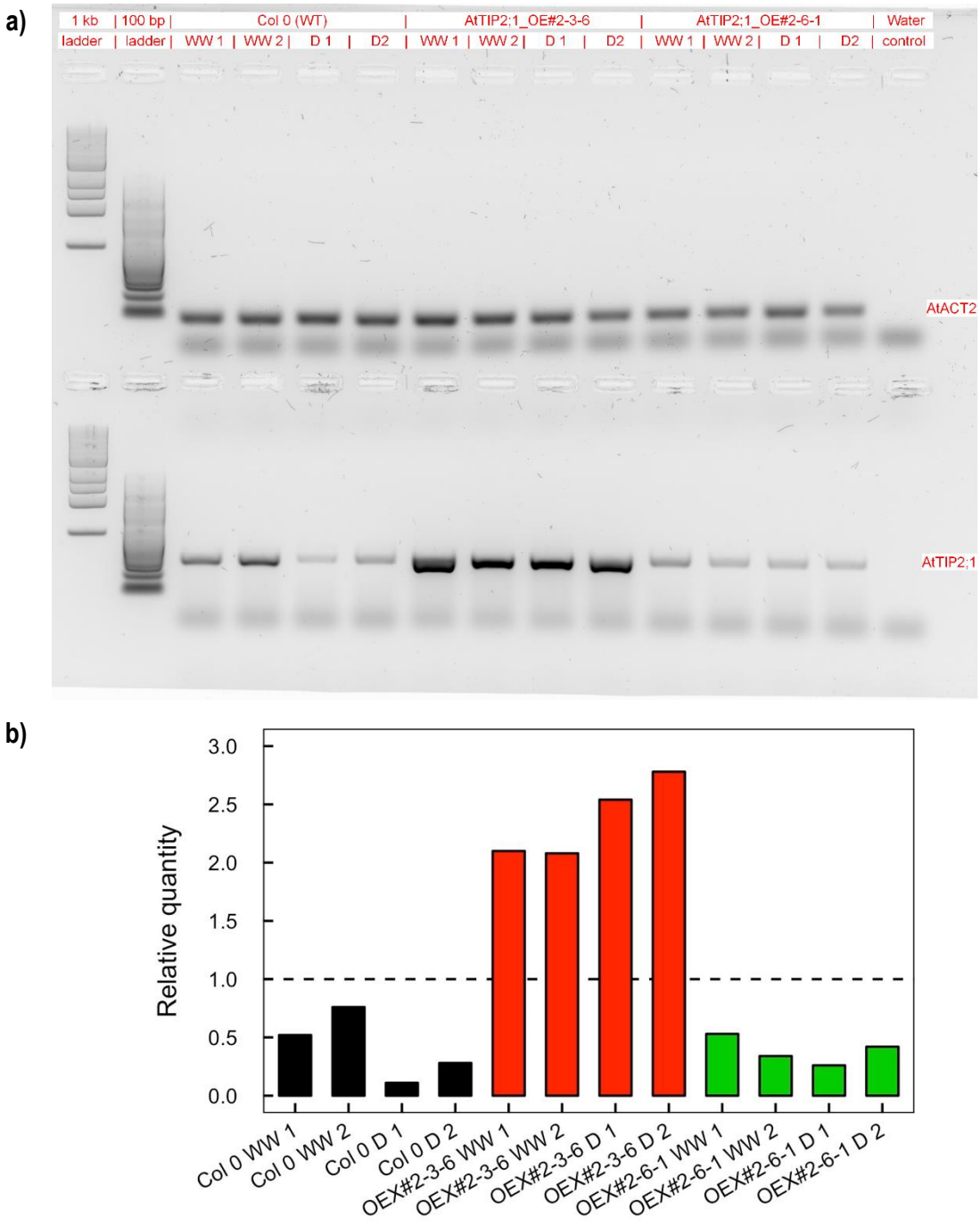

Figure 39. Relative gene expression of *AtTIP2;1* measured in leaf samples from droughted (D) and well-watered (WW) plants on day 10 of the drought experiment by semiquantitative RT-PCR. a) Agarose gel electrophoresis of PCR products for the genes *AtACT2* (top row) and *AtTIP2;1* (bottom row) amplified from cDNA. Products in the same column were amplified from the same cDNA sample with the same amount of cDNA as template. Each replicate (1, 2) is from a different plant. Negative controls (water instead of cDNA) were included for both genes. b) Quantification of *AtTIP2;1* relative to *AtACT2* based on the fluorescence intensities from the agarose gel image. The horizontal dashed line indicates the relative level of *AtACT2* expression.

Linear regressions between stomatal conductance of well-watered and droughted plants recorded throughout the second drought-rehydration experiment for the lines tested by semiquantitative RT-PCR showed a significant (p = 0.0176) different behaviour between the overexpression line AtTIP2;1_OE#2-3-6 and the wild-type like and wild type control lines AtTIP2;1_OE#2-6-1 and Col0_WT (Figure 40). In the wild-type like and wild type control lines AtTIP2;1_OE#2-6-1 and Col0_WT, g_s of the well-watered plants followed closely the g_s of the droughted plants and regression lines were not significantly different (p > 0.05) from a simple linear regression with a slope of 1 and an intercept of 0,0. In contrast, g_s of the well-watered plants remained high while g_s of the droughted plants declined in the overexpressor line AtTIP2;1_OE#2-3-6. The linear regression was significantly different (p = 0.0349) to a simple linear regression with a slope of 1 and an intercept of 0,0.

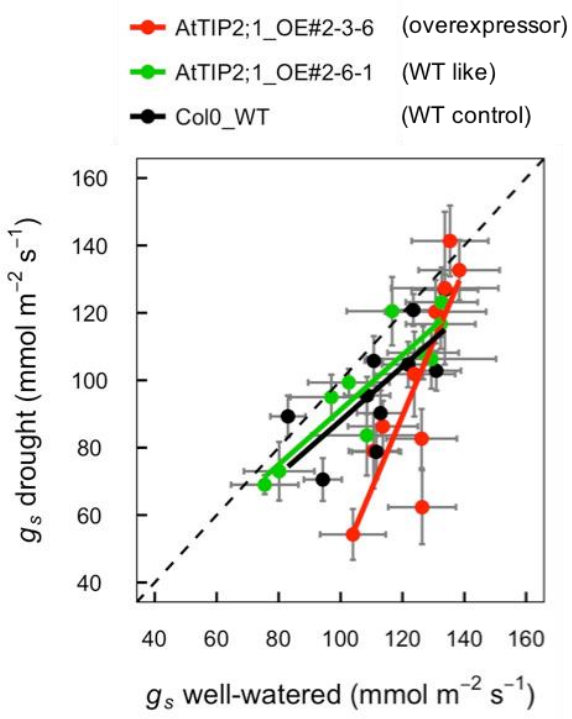

Figure 40. Linear regressions between stomatal conductance (g_s) of well-watered and droughted plants recorded throughout the second drought-rehydration experiment. Data are shown as mean ± SE of 12 (AtTIP2;1_OE#2-3-6, AtTIP2;1_OE#2-6-1) or 24 (Col0_WT) independent plants on which g_s was measured repeatedly on one leaf each. Linear regressions: AtTIP2;1_OE#2-3-6 g_s drought (mmol m^{-2} s^{-1}) = 2.187 ± 0.5467 * g_s well-watered (mmol m^{-2} s^{-1}) - 173 ± 68.19; AtTIP2;1_OE#2-6-1 g_s drought (mmol m^{-2} s^{-1}) = 0.8129 ± 0.1443 * g_s well-watered (mmol m^{-2} s^{-1}) + 9.941 ± 16.16; Col0_WT g_s drought (mmol m^{-2} s^{-1}) = 0.803 ± 0.2726 * g_s well-watered (mmol m^{-2} s^{-1}) + 7.705 ± 31.1. The dashed line shows a simple linear regression with a slope of 1 and an intercept of 0,0.

3.4. Discussion

Aquaporins from the TIP2 subgroup of tonoplast intrinsic proteins have been linked to drought and salinity resistance (Sade *et al.* 2009), transport of ammonia (Loque *et al.* 2005; Kirscht *et al.* 2016), and lateral root emergence (Reinhardt *et al.* 2016). Constitutive expression of *SlTIP2;2* in tomato has shown to cause increased transpiration of transgenic plants (Sade *et al.* 2009). So far, the effects of constitutive expression of any TIP2 aquaporin isoform on leaf gas exchange have not been investigated in the model plant Arabidopsis. To fill this gap, a comprehensive set of TIP2 overexpression and promoter lines was generated and used to investigate their function during drought.

3.4.1. A comprehensive set of *At*TIP2 overexpression and promoter lines

While coding sequences of *AtTIP2;2*, and *AtTIP2;3* were amplified from cDNA clones deposited at the Arabidopsis Biological Resource Center (The Ohio State University), the cDNA clone for *AtTIP2;1* (Clone: U17252) didn't match the TAIR10 reference sequence (Figure 17). A search in the 1001 Proteomes database (Joshi *et al.* 2012) revealed no natural accessions with this non-synonymous single-nucleotide polymorphisms (adenosine instead of guanine) that leads to a change in the protein sequence at position 226 from glycine to glutamic acid. This points to a random mutation having occurred. Due to unpredictable consequences that this mutation may cause, the coding sequence of *AtTIP2;1* was amplified from cDNA of *Arabidopsis thaliana* ecotype Col-0 instead. After PCR amplification (Figure 18) and cloning into the Gateway™ Entry vector pENTR/D-TOPO™, Sanger sequencing confirmed the correct sequences in pENTR/D-TOPO™ (Figure 20). While a 100 % match was confirmed for both *AtTIP2;1* and *AtTIP2;2*, two missing adenosine bases were detected immediately downstream of the full length coding sequence of *AtTIP2;3* (Figure 20c); which were initially not noticed. The two missing bases, which may have been cleaved during TOPO® cloning, should not have any influence on gene expression and protein translation since they are outside the coding sequence. After sub-cloning into the destination vectors pUB-DEST and pUBC-GFP-DEST (Grefen *et al.* 2010), correct insertion was demonstrated by restriction digest (Figure 22a). Constitutive expression driven by the endogenous UBQ10 promoter from Arabidopsis (Figure 23a) instead of the traditional 35S promoter may have the benefit of reduced mislocalisation of the target gene and decreased suppression of promoter activity due to a more moderate expression activity, as explained by Grefen *et al.* (2010). Since multiple copy numbers of the T-DNA in transgenic plant lines has been implicated with increased silencing of the transgene (Hobbs *et al.* 1990; Tang *et al.* 2007), transgenic lines with insertion(s) at a single locus were selected by 3:1 Mendelian segregation (

Table 3). While this increased the chance of selecting lines with a single copy of the T-DNA, multiple insertions at the same locus remained a possibility and may have led to silencing (De Buck *et al.* 2001; De Paepe *et al.* 2009). Other techniques like Southern blot could have been used to verify copy number

definitively (Głowacka *et al.* 2016). Multiple homozygous lines were found in the T_3 generation (Table 4) that were used for protein localisation studies and in drought-rehydration experiments, as discussed below.

Promoter sequences of *AtTIP2;1*, *AtTIP2;2*, and *AtTIP2;3* were successfully amplified from genomic DNA of *Arabidopsis thaliana* ecotype Col-0 (Figure 19) and Sanger sequencing confirmed 100 % match between the promoter inserts of all three genes in pENTR and the reference sequences (Figure 21). TIP2 aquaporin promoter fusion lines with GFP, YFP, or GUS have been described before in the literature (Hunter *et al.* 2007; Gattolin *et al.* 2009; Zhu *et al.* 2013). Most of these studies used promoter fusions with GFP or YFP to study the localisation of gene expression. Hunter *et al.* (2007) fused a 2.5 kb segment of genomic DNA, including the 5' promoter and gene sequence of *AtTIP2;1*, to the fluorescent reporter YFP. From this, the total length to the promoter was 1240 bp, while in this study we used the predicted promoter of 2102 bp (Figure 19). The most comprehensive study was done by Gattolin *et al.* (2009), who studied the expression pattern of all three *AtTIP2* aquaporin isoforms in roots. They used the same construct as Hunter *et al.* (2007) for *AtTIP2;1*. For *AtTIP2;2*, a 1322 bp segment of the promoter was used which is shorter compared to the predicted promoter of 2942 bp in our study (Figure 19). For *AtTIP2;3*, they used the same promoter sequence (1125 bp) as was used here. While fusions with fluorescent proteins like GFP and YFP have the benefit that they can be observed *in vivo*, gene expression localisation *in vitro* by GUS reporter assay can produce results with less background signal and specimens can be kept for longer periods of time (de Ruijter *et al.* 2003). Zhu *et al.* (2013) used promoter-GUS fusions for *AtTIP2;2* and *AtTIP2;3*, but sequences were 506 bp and 708 bp long, which is much shorter than the predicted promoter sequences used here. While previous studies, may show the correct expression patterns, longer promoter sequences and the use of GUS fusions in this study may give additional information. Restriction digest confirmed successful sub-cloning of the promoter sequences into the destination vector pMDC162 (Figure 22).

3.4.2. Tonoplast localisation of *At*TIP2 aquaporin isoforms

Confocal microscopy demonstrated that c-terminal GFP-tagged aquaporins *At*TIP2;1-GFP, *At*TIP2;2-GFP, and *At*TIP2;3-GFP were localised to the tonoplast (Figure 24 - Figure 27). Tonoplast localisation of TIPs was first discovered based on proteomic studies (Pusztai *et al.* 1979; Johnson *et al.* 1989). Later, antibodies raised against different isoforms of TIPs were used to distinguish vacuoles with different functions (Jauh *et al.* 1999). Soon after, fluorescent tagging of proteins with GFP was developed in plants and GFP::TIP2;1 constructs were used as a tonoplast marker (Cutler *et al.* 2000). Gattolin *et al.* (2009) conducted the most comprehensive study of TIP localisation and analysis of expression patterns in roots of *Arabidopsis thaliana*. They found that TIPs would localise mainly to the membrane of the central vacuole and structures called vascular bulbs. These results align with the findings here. All three TIP2

aquaporins were localised to the membrane of the central vacuole (Figure 25 - Figure 27). Careful staining with the fluorescent dye FM4-64 was used to distinguish the tonoplast from the plasma membrane, which was especially evident when the plasma membrane and tonoplast were separated by a nucleus attached to the side of the cell. The FM4-64 dye can penetrate the cell wall and is incorporated into the plasma membrane (Vida and Emr 1995). Upon membrane internalization, dye is also incorporated into the endomembrane system like the tonoplast. Hence, we chose a short time of staining and rapid imaging to achieve distinguishable staining of the plasma membrane only. Additionally to the tonoplast localisation observed in cortex cells of roots, we observed tonoplast localised GFP fluorescence in pavement cells of cotyledons and guard cells (Figure 24a, b). These images are similar compared to confocal fluorescence micrographs by Hunter *et al.* (2007). In contrast to Hunter *et al.* (2007) and Gattolin *et al.* (2009), not many GFP labelled vascular bulbs were observed. TIP2 localisation to these structures may be conditional and depend on the age of the plant and growing conditions. Ferro *et al.* (2003) also found *AtTIP1;1* and *AtTIP2;1* in a chloroplast enriched fraction during proteomic characterisation. They hypothesised that these were contaminants, however, a potential chloroplast localisation is still in debate (Wudick *et al.* 2009). Images obtained of guard cells show the tonoplast localisation of AtTIP2;1-GFP and auto-fluorescence of the chloroplasts (Figure 24b), but no chloroplast localisation could be concluded from these images. Future experiments could aim to release chloroplasts from protoplasts to examine them separately. The observed tonoplast localisation for all three TIP2s confirm the expected localisation and hence a similar localisation can be expected for the overexpression constructs without GFP tag.

3.4.3. *At*TIP2 promoter activity predominant around vascular tissues

Promoter-GUS fusions for *AtTIP2;1*, *AtTIP2;2*, and *AtTIP2;3* showed promoter activity in both leaves and roots (Figure 29 - Figure 31). In leaves, stronger staining was observed around the vascular bundles (Figure 29a, Figure 30a, Figure 31a), which may indicate a role in leaf hydraulic regulation. Similar observations were made for *AtTIP1;1* (Beebo et al. 2009). Silencing of gene expression for PIP aquaporins in bundle sheath cells reduced leaf hydraulic conductance significantly (Sade *et al.* 2014b). Interestingly, staining was also found in guard cells of pAtTIP2;1-GUS lines (Figure 29b). This has not been reported before. Expression activity of *AtTIP2;1* in the guard cells could be connected to the observation that changes in expression of this TIP isoform were significantly correlated to changes in stomatal conductance during the drought-rehydration experiment presented in Chapter 2. In grapevine a similar correlation was found (Pou *et al.* 2013) and it was also associated to drought in several other plant species (Shaar-Moshe *et al.* 2015). The overexpression of *Sl*TIP2;2, which is very similar to *At*TIP2;1, increased transpiration in tomato plants compared to controls (Sade *et al.* 2009). Gene expression for *AtTIP2;1* was detected in guard cells in previous studies (Leonhardt *et al.* 2004; Wang *et al.* 2011), however, it appeared to be lower compared to mesophyll cells. Further investigation is needed to confirm

high promoter activity for *AtTIP2;1* in guard cells. Surprisingly, we also found promoter activity for *AtTIP2;3* in leaves (Figure 31a). Previous studies have shown that *AtTIP2;3* is very lowly expressed in leaves (Alexandersson *et al.* 2005) and a GUS fusion with a short piece of the *AtTIP2;3* promoter also showed no staining in leaves (Zhu *et al.* 2013). This may indicate that despite promoter activity not many transcripts of *AtTIP2;3* are being made, or the nature of this artificial system lead to an erroneous expression. We exclude staining which is not related to GUS activity, since negative controls did not show any staining (Figure 28). Further research is needed to confirm the promoter activity of *AtTIP2;3* in leaves.

GUS staining in roots was mainly detected in the stele (Figure 29c, d; Figure 30b; Figure 31b, c). For pAtTIP2;1-GUS, staining was also observed at lateral root primordia (Figure 29d), which matches previous observations (Gattolin *et al.* 2009). This was in contrast to no staining in lateral root primordia for pAtTIP2;3-GUS (Figure 27c). While Gattolin *et al.* (2009) did not observe AtTIP2;1 in other cell types than lateral root primordia in the root, Hunter *et al.* (2007) reported AtTIP2;1 in mature root cells. The observation by Gattolin *et al.* (2009), later led to the conclusion that AtTIP2;1 is important in lateral root emergence by Reinhardt *et al.* (2016). Different promoter activity patterns may also be explainable due to the different developmental stage of plants. Here material from mature plants was used, compared to week-old seedlings that were used by studies in the literature. Comparison between different developmental stages could improve knowledge in this area. Similar to previous studies (Hunter *et al.* 2007; Gattolin *et al.* 2009), no promoter activity was found in root meristematic cells for promoters of all three TIP2 isoforms (Figure 29c; Figure 30b; Figure 31b). However, for promoters of *AtTIP2;1* and *AtTIP2;2*, significant staining was observed in the columella (Figure 29c; Figure 30b), which has only been reported for *AtTIP1;2* (Gattolin *et al.* 2009). The observed staining for promoter activity of all three TIP2s showed that they were mostly active around vascular tissue in the leaves and roots indicating that they could be regulating hydraulic conductivity. The activity of the *AtTIP2;1* promoter in guard cells fits with previous observations that expression of this gene is highly linked to drought and recovery, stomatal conductance, and transpiration. Further research will be needed to document changes in promoter activity throughout plant development.

3.4.4. Stomatal behaviour of overexpression lines during drought and rehydration

Based on observations of *SlTIP2;2* overexpression in tomato (Sade *et al.* 2009), higher biomass, stomatal conductance (g_s) and transpiration in overexpression plants would be expected compared to the wild-type.

A mixed selection of homozygous transgenic lines for constitutive expression of *AtTIP2;1*, *AtTIP2;2*, or *AtTIP2;3* during the first drought-rehydration experiment didn't show any lines that had significantly higher g_s compared to the wild-type throughout the experiment (Figure 34 and Figure 35). Only one line,

AtTIP2;2_OE#2-2-2, was identified with significantly higher leaf area compared to the wild-type (Figure 33). Also, transgenic lines didn't show any obvious growth and/or leaf phenotype (Figure 32). It is important to point out that gene expression was not assessed during the experiment and, hence, it is not known whether these lines had an increased expression. Gene expression of *AtTIP2;1* in leaves of the transgenic line AtTIP2;1_OE#2-6-1, which was measured in the second drought experiment (Figure 39), was not different to the wild-type. This points at silencing of the T-DNA, which was reported to be an issue of constitutive expression experiment (Hobbs *et al.* 1990; Tang *et al.* 2007). Other transgenic lines used in the first drought-rehydration experiment could have also had their T-DNA silenced. Interestingly, gene expression of *SlTIP2;2* was also not measured in the transgenic lines used by (Sade *et al.* 2009), which leads to the question as to how *SlTIP2;2* expression was modified. A leaf rehydration assay showed that leaves from transgenic lines rehydrated faster than leaves from the wild-type, but these differences were not significant (Figure 36). Leaves from plants of the line AtTIP2;1_OE#2-6-1 showed the fastest rehydration albeit no difference in gene expression of *AtTIP2;1* compared to the wild-type as shown in Figure 39. Hence, no conclusion could be drawn from these observations.

In contrast to the first experiment, the second experiment focused only on homozygous transgenic lines for constitutive expression of *AtTIP2;1*. The transgenic line AtTIP2;1_OE#2-3-6 was identified to have a significantly higher expression of *AtTIP2;1* compared to the wild-type, while no difference was found for the transgenic line AtTIP2;1_OE#2-6-1 (Figure 39). This showed that gene silencing of the T-DNA was still an issue, despite using the UBQ10 promoter which was suggested to be less prone to silencing compared to a 35S promoter (Grefen *et al.* 2010). The confirmed overexpressor line AtTIP2;1_OE#2-3-6 had a significant larger leaf area compared to the wild-type and other transgenic lines (Figure 37), which is in line with observations of constitutive expression of *SlTIP2;2* in tomato (Sade *et al.* 2009). While Sade *et al.* (2009) also observed higher transpiration in well-watered and droughted transgenic tomato plants, this was not observed in plants from the overexpressor line AtTIP2;1_OE#2-3-6. A more stable g_s of well-watered plants of the overexpressor line AtTIP2;1_OE#2-3-6 suggests a stronger influence of the overexpression on well-watered compared to droughted plants (Figure 38, Figure 40). While g_s of well-watered wild-type plants mimicked changes in g_s of droughted plants, g_s of well-watered plants of the overexpressor line AtTIP2;1_OE#2-3-6 remained higher when g_s of droughted plants declined (Figure 40). This response of wild-type plants was similar to observations in the drought-rehydration experiment in Chapter 2. It appears as if the overexpression of *AtTIP2;1* made the well-watered plants less susceptible to what causes the decline in g_s that was repeatedly observed during the drought phase of the experiments. Similar to the wild-type, well-watered plants from the transgenic line AtTIP2;1_OE#2-6-1, which didn't show overexpression of *AtTIP2;1*, also showed a decline of g_s during the drought phase in both experiments (Figure 34 and Figure 38). Since research in grapevine and other crop species also pointed at a strong relationship between gene expression of *TIP2;1* and stomatal conductance or drought

responses (Pou *et al.* 2013; Shaar-Moshe *et al.* 2015), the observation made here contributes to establishing a link between *TIP2;1* gene expression and stomatal conductance. Since AtTIP2;1 is localised to the tonoplast, it could be implicated in hydraulic buffering and therefore maintain a more stable g_s in well-watered plants. This could be the case during fluctuations of vapour pressure deficit. Since AtTIP2;1 was also shown to transport ammonia (Loque *et al.* 2005; Kirscht *et al.* 2016), I hypothesised in Chapter 2 that ammonia could serve as a gas signal from droughted to well-watered plants that could cause the observed decline in g_s in well-watered plants during the drought phase. I speculated that down-regulation of *AtTIP2;1* gene expression could release more ammonia that is produced during photorespiration in droughted plants (Voss *et al.* 2013), which would usually be trapped in the acidic vacuole by an acid-trap mechanism. While this could happen in droughted plants, AtTIP2;1 could also be important for signal perception and/or response in well-watered plants.

Identification of additional overexpression lines of AtTIP2;1 will be needed to confirm these results. Since an even a stronger correlation between gene expression of *AtTIP2;2* and stomatal conductance was found in Chapter 2, it will be interesting to find overexpression lines for this gene and compare. Also overexpression lines for AtTIP2;3 need to be tested in that regard. Moreover, it needs to be resolved why stomatal conductance of well-watered controls mimicked the drought response of the droughted plants.

3.4.5. Conclusion

Transgenic lines that constitutively express *AtTIP2;1*, *AtTIP2;2*, or *AtTIP2;3* in *Arabidopsis thaliana* confirmed protein localisation to the tonoplast. Promoter activity for the same genes, as assessed by promoter-GUS fusions, was highest around vascular tissues. Interestingly, *AtTIP2;1* promoter activity was also observed in guard cells. While this needs to be confirmed, this observation should be investigated since previous research has shown a strong relationship between gene expression of *TIP2;1* and stomatal conductance. Interestingly, overexpression of *AtTIP2;1* in this study modified stomatal sensitivity in well-watered plants causing a more stable stomatal conductance throughout the experiment. Whether this is connected to hydraulic buffering due to higher water permeability of the tonoplast or decreased sensitivity to some sort of signal need to be investigated. Further research also needs to be done for overexpression lines of *AtTIP2;2* and *AtTIP2;3*.

4. PLANT GENOME EDITING FOR TARGETED KNOCKOUTS OF *At*TIP2 AQUAPORIN ISOFORMS

4.1. Introduction

The study of knockdown or knockout mutants for specific genes is a commonly used reverse genetics technique (Alonso and Ecker 2006). Comparisons between the phenotype of the wild-type and the modified plants can give clues about the function of specific genes and/or their interaction with other genes.

Aquaporins are integral membrane proteins which form channels that facilitate transport of water and other small solutes across membranes (Tyerman *et al.* 1999). They belong to the gene family of major intrinsic proteins (MIPs), which has 35 members in *Arabidopsis thaliana* (Johanson *et al.* 2001). Two major sub-families are called plasma membrane intrinsic proteins (PIPs), which have been shown to localise mainly to the plasma membrane, and tonoplast intrinsic proteins (TIPs), which have been shown to localise mainly to the tonoplast. Other subfamilies include NOD-26 like intrinsic proteins (NIPs) and small intrinsic proteins (SIPs). Proteins from the largest subfamily, PIPs, which has 13 members, are the main focus of many studies (Martre *et al.* 2002; Fetter *et al.* 2004; Sade *et al.* 2014b). Their localisation on the plasma membrane, which is the primary barrier of cells, has often a strong effect on transport of water of various small molecules (Chaumont and Tyerman 2014). Recently however, studies on TIPs, a sub-family with 10 members, have shown their potential involvement in leaf gas exchange (Sade *et al.* 2009; Pou *et al.* 2013; Maurel *et al.* 2016) and lateral root development (Reinhardt *et al.* 2016). Moreover, transport of ammonia has been shown for TIP2 aquaporins (Holm *et al.* 2005; Loque *et al.* 2005; Bertl and Kaldenhoff 2007; Kirscht *et al.* 2016). Hence, the focus of this study will be the TIP2 isoforms *AtTIP2;1*, *AtTIP2;2*, and *AtTIP2;3*.

To establish the role of TIP aquaporins in lateral root development, observations of shorter roots and less lateral roots in knockdown mutants were of pivotal importance (Reinhardt *et al.* 2016). In this particular case, insertion lines from public collections were used. While for many genes, insertion lines exist in public collections (Alonso *et al.* 2003), some genes don't have any suitable insertion mutations which would cause a knockdown or knockout. Research has shown that T-DNA insertions are not randomly distributed (Li *et al.* 2006). According to the research, T-DNA insertions are more likely to be found in intergenic regions than in exons of genes, and T-DNA insertion depends on the existence of suitable restriction sites and is less likely in low expressed genes. If a certain knockout or knockdown is deleterious to plant health, viable plants and seeds can also sometimes not be obtained. Moreover, even with many seed collections available, it is not always easy to find the right lines even if they exist. In this case, a popular technique

which has been used in many studies is gene silencing by antisense RNA or RNA interference (RNAi) (Kaldenhoff *et al.* 1998; Martre *et al.* 2002; Ma *et al.* 2004; Sade *et al.* 2014b). Antisense RNA of a target gene is expressed driven by a constitutive promoter and inhibits translation of target genes by base pairing to the mRNA and double stranded RNA (dsRNA) cleavage by Argonaute 2 (Ago2) (Ecker and Davis 1986). For RNA interference, a microRNA complementary to the target gene of interest is expressed in plants. The microRNA becomes part of an RNA-induced silencing complex, which binds to its target mRNA, and causes the degradation of this mRNA (Baulcombe 2004). Since the binding of antisense RNA or microRNAs is not strictly specific, one microRNA can be used to target several genes at once, as demonstrated for PIP1 knockdowns used to study their function in bundle sheath hydraulic regulation (Sade *et al.* 2014b). However, this non-specificity makes functional studies of of single genes difficult. In the same study, a significant reduction of *AtPIP2;1* was also observed even though this gene was not intended to be targeted. Another example is a study that used RNAi to silence *AtTIP1;1* to varying degrees (Ma *et al.* 2004). Phenotypes that were observed led to the conclusion that *AtTIP1;1* is pivotal for plant survival and that loss of this aquaporin isoform would lead to cell and plant death. However, a subsequent study which used a transposon insertion line for *AtTIP1;1* found that even the complete loss of this protein would not have any strong effect on plant growth (Schüssler *et al.* 2008). They hypothesised that the RNAi may have had off-target effects.

Early in this project, no publically available, suitable insertion lines were known for *AtTIP2;1*, *AtTIP2;2*, and *AtTIP2;3* to study the effect of gene knockout for these particular aquaporins. Only later the role of *AtTIP2;1* in lateral root development was published using a knockout mutant (Reinhardt *et al.* 2016). This knockout mutant was identified by the authors in the SLAT collection (Tissier *et al.* 1999) and seeds were obtained from the NASC. However, no suitable knockout lines exist for *AtTIP2;2* and *AtTIP2;3* to our knowledge. Since gene knockdown through techniques like RNA interference can have known issues as discussed above, it was decided to test the creation of knockouts by CRISPR-Cas genome editing.

CRISPR-Cas genome editing was introduced as a new promising reverse genetics tool in 2011 (Deltcheva *et al.* 2011). CRISPR stands for Clustered Regularly Interspaced Short Palindromic Repeats and Cas proteins are endonucleases. This tool allows the modification of gene sequences *in vivo* with a high degree of specificity (Schiml and Puchta 2016). While gene editing is not a new technique, CRISPR-Cas is making the process easier and more economical. Previously, three other engineered nucleases have been used for genome editing: meganucleases, zinc finger nucleases (ZFNs), transcription activator-like effector-based nucleases (TALEN) (Sprink *et al.* 2015). As part of a prokaryotic immune system, a target specific CRISPR RNA binds to the target sequence (foreign DNA like viruses) and forms a complex with a Cas endonuclease that cleaves the target sequence (Marraffini 2015). Foreign targets are disabled through error-prone non-homologous end-joining (NHEJ), which causes insertions or deletions when

these cleaved DNA strands are repaired (Shuman and Glickman 2007). This system can be customised by modifying the target specific CRISPR RNA, which is called single guide RNA (sgRNA), to target the desired location within the genome. This is much easier compared to the other genome editing systems that require engineering of the amino acid sequence of specific sequences within the genome. The CRISPR-Cas genome editing system used in this study was designed by Fauser *et al.* (2014). It consists of two vectors: pEn-Chimera and pDe-CAS9. The first vector, pEn-Chimera, contains a chimeric single guide RNA (sgRNA), consisting of the short CRISPR RNA (crRNA) and transactivating CRISPR RNA (tracrRNA) fused by a linker. This sgRNA needs to be fused with a 20 bp gene specific protospacer element forming a complex with the Cas9 endonuclease to guide it to the target sequence for cleavage. The protospacer sequence can be custom designed using online-tools (Heigwer *et al.* 2014; Lei *et al.* 2014; Xie *et al.* 2014) to target a specific gene of interest. The only requirement is that the target site must contain a protospacer adjacent motif (PAM) sequence (NGG, where N is any nucleobase) directly next to the protospacer sequence. The protospacer oligos are synthesised and fused into pEn-Chimera. Then a recombination reaction is used to transfer the sgRNA into pDe-CAS9. This vector is then transformed into *Arabidopsis thaliana* using disarmed *Agrobacterium tumefaciens* via floral dipping (Clough and Bent 1998). In the plants both sgRNA and Cas9 endonuclease are expressed and target the gene(s) of interest.

The aquaporin genes *AtTIP2;1*, *AtTIP2;2*, and *AtTIP2;3* were chosen as targets, since not much is known about the specific function of these genes. Reinhardt *et al.* (2016) found that *AtTIP2;1* is of major importance in lateral root development. During lateral root emergence, *AtTIP2;1* expression is up-regulated in specific cells at the base of the lateral root primordia, which could help to direct water movement to the lateral root primordia for cell expansion according to the authors. Interestingly, also a very good correlation between gene expression of *AtTIP2;1* and changes in stomatal conductance was found in grapevine (*Vitis Vinifera*) during drought and rehydration (Pou *et al.* 2013). In *Arabidopsis thaliana* there was still a good correlation, but about 40 % of all MIPs would also have a significant positive correlation with stomatal conductance during drought (Chapter 2). The highest correlation was found for *AtTIP2;2* with r = 0.85, while *AtTIP2;1* had a correlation coefficient of r = 0.68; these coefficients were lower when the rehydration phase was included. Correspondent with this, *TIP2;1* was identified as being significantly down-regulated under drought in Arabidopsis, Barley, Rice and Wheat in a cross-species meta-analysis on drought-adaptive genes (Shaar-Moshe *et al.* 2015). In tomato the overexpression of *SlTIP2;2* caused increased transpiration and changed the plants from an isohydric behaviour to a more anisohydric behaviour (Sade *et al.* 2009). The protein sequence of *SlTIP2;2* is most similar to *AtTIP2;1* in *Arabidopsis thaliana* (76.5 %). Both *AtTIP2;1* and *AtTIP2;3* were found to transport ammonia in yeast and *Xenopus* oocytes (Holm *et al.* 2005; Loque *et al.* 2005). Transgenic Arabidopsis plants with constitutive expression of *AtTIP2;1* didn't show any difference in ammonium uptake, however (Loque *et al.* 2005). For *AtTIP2;1* a crystal structure was reported recently (Kirscht *et al.* 2016). The authors found an extended

selectivity filter for ammonia defined by a conserved arginine (Arg 200) in helix E. Ammonia transport was also shown for the wheat aquaporin *TaTIP2;2* (Bertl and Kaldenhoff 2007). For *AtTIP2;1* it remains unclear, how transport of ammonia relates to its role in lateral root emergence and why its gene expression is highly responsive to drought.

These results from previous research suggest multiple function for TIP2 aquaporins. Since no knockout mutants exist for *AtTIP2;2* and *AtTIP2;3*, genome editing does offer a unique chance to create these mutants and investigate their function. Moreover, it would be the first time that CRISPR-Cas is applied to aquaporins to create gene specific changes. Off-target analysis will have to be done to investigate how specific the CRISPR-Cas system is, since the coding sequence similarity between the related TIP2 aquaporins is as high as 81%.

4.2. Materials and Methods

4.2.1. Design of single guide RNAs

Single guide RNAs (sgRNA) were designed to target the genes *AtTIP2;1*, *AtTIP2;2*, and *AtTIP2;3* using the CRISPR DESIGN web tool (crispr.mit.edu) in 2015. Two guide sequences with a high score (low off-target chance) were chosen per gene that target within an exon close to the 5'-end. In 2017, these guides were re-evaluated using the more recent CRISPR-P web tool (cbi.hzau.edu.cn/crispr/) for improved *in silico* off-target testing (Table 6).

4.2.2. Preparation of CRISPR-Cas vectors

A dual vector Gateway®-compatible CRISPR-Cas system designed by Fauser *et al.* (2014) was used with the custom designed guide sequences. Briefly, guide sequences were synthesized as desalted oligos to form complementary sequences, called protospacer, with vector-specific adaptors: FW (5'-ATTG + protospacer), REV (5'-AAAC + rev-com protospacer). The double stranded protospacers were obtained by resuspending the desalted oligos in ddH_2O and mixing them to a final concentration of 2 µM in a 50 µL reaction. For annealing, the reactions were heated to 95 °C for 5 min with subsequent slow cooling at room temperature for 20 min. The entry vector pEN-Chimera (Supplementary Figure S11a) was digested with the restriction enzyme *Bbs*I-HF (New England Biolabs) at 37°C overnight (Supplementary Table S9). Restriction products were purified using the illustra GFX PCR DNA and Gel Band Purification Kit (GE Healthcare) following manufacturer's instructions. Double stranded protospacers were ligated into the purified open vector using T4 Ligase (New England Biolabs) at 16 °C overnight (Supplementary Table S10). Ligation products were transformed into homemade DH5α *E.coli* competent cells. Transformed cells

were grown on selective LB plates (100 µg/mL Ampicillin (Amp)) at 37 °C overnight. Five colonies per construct were re-grown in 5 mL liquid LB + Amp (100 µg/mL) at 37 °C overnight. Ligations were evaluated by liquid culture PCR (Supplementary Table S11) using to protospacer-specific forward + SS42 primers (Supplementary Table S12). The cycling conditions were 3 min at 98 °C initial denaturation, followed by 30 cycles of 5 sec at 98 °C denaturation, 30 sec at 56 °C annealing, 15 sec at 72°C extension, and 1 min at 72 °C final extension. PCR products were examined by gel electrophoresis at 100 V for 45 min in a 1.2 % (w/v) agarose gel in 0.5 x TAE buffer with GelRed™ DNA stain (Biotium) and purified using the GenElute PCR Clean-Up Kit (Sigma-Aldrich). Plasmid DNA was extracted from two positive cultures per construct using the GenElute™ Plasmid Miniprep Kit (Sigma-Aldrich). The correct insertion of the protospacers into pEn-Chimera was confirmed using Sanger Sequencing of PCR products generated by SS42 primer (Supplementary Table S12, Supplementary Table S13) from eluted plasmids. LR Recombination Reactions (Supplementary Table S14) between pEn-Chimera-sgRNA and the destination vector pDe-CAS9 (Supplementary Figure S11b) were performed. After incubation overnight at room temperature, the LR reaction was stopped by Proteinase K treatment (0.5 µL/reaction, 10 min at 37 °C). Ligation products were transformed into Stellar™ Competent Cells (Clontech) as per manufacturer's instructions and cultures were grown on selective LB plates (100 µg/mL Spectinomycin (Spec)) at 37 °C overnight. Three colonies per construct were re-grown in 5 mL liquid LB + Spec (100 µg/mL) at 37 °C overnight. Efficiency of the ligation/transformation reactions was evaluated by liquid culture PCR (Supplementary Table S11) using the SS42 and SS43 primers (Supplementary Table S12). The cycling conditions were 3 min at 98 °C initial denaturation, followed by 35 cycles of 30 sec at 98 °C denaturation, 1 min at 60 °C annealing, 1 min 15 sec at 72°C extension, and 1 min 15 sec at 72 °C final extension. PCR products were examined by gel electrophoresis at 100 V for 45 min in a 0.8 % (w/v) agarose gel in 0.5 x TAE buffer with GelRed™ DNA stain (Biotium) and purified using the GenElute PCR Clean-Up Kit (Sigma-Aldrich). Plasmid DNA from cultures presenting the expected 1070 bp PCR product was extracted using the GenElute™ Plasmid Miniprep Kit (Sigma-Aldrich) following manufacturer's instructions. Subsequently, constructs were checked by restriction digest with *Afl*II and *Nhe*I (New England Biolabs) for 3 hrs at 37 °C (Supplementary Table S15); positive reactions generated 5.9 kb, 5.0 kb and 3.8 kb restriction products (Supplementary Figure S12).

4.2.3. Plant Material

Arabidopsis (*Arabidopsis thaliana*) ecotype Col-0 seeds from own laboratory stock were sown on solid, half-strength Murashige and Skoog medium (Murashige and Skoog 1962) (Supplementary Table S16). After vernalisation at 4 °C for 3 days in the dark, plates were transferred to a walk-in growth chamber at The Plant Accelerator® Adelaide, Australia (34° 58' 17'' S, 138° 38' 23'' E). Plants were grown under long-day conditions (16 h light/ 8 h dark, photosynthetically active radiation of ~150 µmol m^{-2} s^{-1}, 21 °C) for 7

d until they were transferred to soil (85 % (v/v) Seedling Substrate Plus+, Bord na Móna; 15 % (v/v) Horticultural Sand, Debco Pty Ltd). For floral dip transformations, 3 – 5 plants were grown per pot. Once flowering started, initial inflorescences were cut after one week to induce more inflorescences. At the peak of flowering, floral dip transformations were performed.

4.2.4. Agrobacterium transformation

Constructs of pDe-CAS9-sgRNA were transformed into chemically-competent *Agrobacterium tumefaciens* cells as outlined in the Supplementary Methods. Transformations were grown on 2YT plates (Supplementary Table S16) + Rif (50 µg/mL) + Spec (100 µg/mL) for 2 – 3 days at 28 °C.

Three colonies per construct were re-grown in 5 mL 2YT Broth + Rif (50 µg/mL) + Spec (100 µg/mL) overnight at 28 °C and 200 rpm. Constructs in *Agrobacterium* were evaluated by liquid culture PCR (Supplementary Table S11) using to protospacer-specific forward + SS43 primers (Supplementary Table S11). The cycling conditions were 3 min at 95 °C initial denaturation, followed by 35 cycles of 30 sec at 95 °C denaturation, 30 sec at 59 °C annealing, 1 min at 72°C extension, and 1 min at 72 °C final extension. PCR products were examined by gel electrophoresis at 100 V for 45 min in a 1.2 % (w/v) agarose gel in 0.5 x TAE buffer with GelRed™ DNA stain (Biotium) and purified using the GenElute PCR Clean-Up Kit (Sigma-Aldrich).

For floral dip transformations, 250 mL 2YT Broth + Rif (25 µg/mL) + Spec (100 µg/mL) were inoculated with 4 mL of the starter culture and grown overnight at 28 °C and 200 rpm. Floral dip transformations were carried out by dipping 3-5 plants per construct as described in Supplementary Methods. Plants were grown to seed and seeds were collected when mature (T_1).

4.2.5. Selection procedure

For selection of transformed T_1 plants, about 200 mg T_1 seed were uniformly sown on soil in a tray (30 x 40 cm) and vernalised at 4 °C for 3 days in the dark. A control with *Arabidopsis thaliana* Col-0 wild-type seed was included. Subsequently, trays were transferred to a walk-in growth chamber and grown under long-day conditions (as detailed above) for 5 days under a cover. Selection was carried out using Basta® herbicide (Bayer Crop Science) at a working concentration of 300 µM according to Weigel and Glazebrook (2006). Seedlings were sprayed three times at a three-day interval. Effectiveness of selection was evaluated by observing the response of *Arabidopsis thaliana* Col-0 wild-type seedlings. Twenty five survivors were transplanted from each line into the ARASYSTEM (BETATECH) and grown to seed (T_2). One line for one CRISPR construct per target were taken further for selection (i.e. AtTIP2;1 Guide#2, AtTIP2;2 Guide#1, AtTIP2;3 Guide#2). These guides were chosen since they were located closest to the first NPA-motif in each of the aquaporin genes.

For selection of transformed T_2 plants, T_2 seed were sterilised with chlorine gas according to Supplementary Methods. For each line, about 150 seed were sown on solid, half-strength Murashige and Skoog medium (Murashige and Skoog 1962) (Supplementary Table S16) supplemented with 10 mg/L (50 µM) glufosinate ammonium (Sigma-Aldrich). After vernalisation at 4 °C for 3 days in the dark, plates were transferred to the Plant Accelerator® Adelaide and grown under long-day conditions for 7 days (as above), or until selection was clearly visible. The ratio of resistant to sensitive seed was evaluated for each line. Only lines which had a 3:1 ratio (resistant:sensitive), and hence most likely only a single insertion of the CRISPR system, were used for further selection. Eight seedlings for each selected line were transplanted to the ARASYSTEM and 30 mg of leaf tissue were sampled per plant for genotyping into 1.3 ml Autotubes (Adelab) with two 3 mm glass beads and frozen in liquid nitrogen. Plant were grown to seed (T_3). Genotyping was done by High Resolution Melt (HRM) to evaluate CRISPR-Cas induced InDels in the target genes. Sanger Sequencing was performed of the samples confirmed as positive by HRM analysis (detailed below). CRISPR-Cas target regions were pre-amplified by PCR using gene specific primer pairs (Seq_TIP21_F/R, Seq_TIP22_F/R, Seq_TIP23_F/R; Supplementary Table S12) and Phusion® High-Fidelity DNA Polymerase (New England Biolabs) as described in Supplementary Table S19. The thermocycler was programmed to 30 sec at 98 °C initial denaturation, followed by 35 cycles of 10 sec at 98 °C denaturation, 15 sec at 60 °C annealing, 15 sec at 72 °C extension, and 5 min at 72 °C final extension. PCR products were examined by gel electrophoresis at 100 V for 45 min in a 1.2 % (w/v) agarose gel in 0.5 x TAE buffer with GelRed™ DNA stain (Biotium) and purified using the GenElute PCR Clean-Up Kit (Sigma-Aldrich). Sanger Sequencing reaction were prepared according to Supplementary Table S13 with only the forward primers for each target.

Lines which were positive for InDels in the target genes continued in the selection process. For selection of T_3 plants, which harbour InDels in the targeted genes but have outcrossed the CRISPR-Cas construct, T_3 seed were sterilised with chlorine gas according to Supplementary Methods. For each line, about 100 seed were sown on two plates with solid, half-strength Murashige and Skoog medium (Murashige and Skoog 1962) (Supplementary Table S16), one plate supplemented with 10 mg/L (50 µM) glufosinate ammonium (Sigma-Aldrich) for selection and one plate without selection. After vernalisation at 4 °C for 3 days in the dark, plates were transferred to the Plant Accelerator® Adelaide and grown under long-day conditions for 7 days, or until selection was clearly visible on the first plate. Lines for which a 1:3 segregation was observed would contain plants without the CRISPR-Cas construct. These plants were selected against on the selective plates, but would still grow on the plates without selection. All plants from the plates without selection were transplanted to soil and grown for 5 days. From each plant a small leaf (~ 4 mm diameter) was collected for the homemade Glufosinate Assay (Supplementary Methods) to predict which plants had outcrossed the CRISPR-Cas construct and were sensitive to glufosinate

ammonium. To confirm the observations, leaf punches were collected from sensitive plants using 1 µL Pipette Tips for genotyping with the Phire Plant Direct PCR Kit (ThermoFisher Scientific) as shown in Supplementary Table S20. The thermocycler was programmed to 5 min at 98 °C initial denaturation, followed by 40 cycles of 5 sec at 98 °C denaturation, 5 sec at 60 °C annealing, 30 sec at 72 °C extension, and 1 min at 72 °C final extension. PCR products were examined by gel electrophoresis at 100 V for 45 min in a 1.2 % (w/v) agarose gel in 0.5 x TAE buffer with GelRed™ DNA stain (Biotium). Plants from which no product for the CRISPR-Cas construct (SS42/SS43 primer pair) was amplified were transplanted to the ARASYSTEM. From each plant, 30 mg of leaf tissue were sampled for genotyping into 1.3 ml Autotubes (Adelab) with two 3 mm glass beads and frozen in liquid nitrogen. Plant were grown to seed (T_4). Genotyping was done by High Resolution Melt (HRM) to screen for homozygous CRISPR-Cas induced InDels in the target genes followed by Sanger Sequencing.

4.2.6. High Resolution Melt genotyping

Frozen leaf samples were ground to a fine powder using the 2010 Geno/Grinder® (SPEX® SamplePrep) for 2 x 30 sec at 1500 rpm. Genomic DNA extraction was carried out in 96-well format on the oKtopure™ robot platform (LGC Ltd) with sbeadex™ mini plant extraction chemistry (LGC Ltd) as described in the Supplementary Methods. Genomic DNA was quantified on a NanoDrop™ spectrophotometer (Thermo Scientific™). DNA concentrations were adjusted to 10 ng/µL in 30 µL final volume in a new 96-well plate using the CAS-1200 liquid handling system (Corbett Research). NanoDrop™ adjusted concentrations were validated using the QuantiNova SYBR Green PCR Kit (QIAGEN) on a RotorGene 6000 Real-Time PCR Instrument (Corbett Research). Pipetting instructions are shown in Supplementary Table S17. Gene-specific primer pairs (HRM_TIP21_F/R, HRM_TIP22_F/R, HRM_TIP23_F/R) for HRM and a reference primer pair (GAPDH_F/R) for SYBR qPCR were designed in NCBI Primer-Blast (Ye *et al.* 2012) according to manufacturer's instructions for the Type-it HRM PCR Kit (QIAGEN). Products were evaluated in the web-tool *mfold* (Rouillard *et al.* 2003) for secondary structures, since these can impact the HRM results. For the QuantiNova SYBR Green PCR the RotorGene 6000 Real-Time PCR Instrument was programmed for 2 min at 95 °C initial denaturation, followed by 40 cycles of 5 sec at 95 °C denaturation and 10 sec at 60 °C annealing and extension. A series of 1:10 dilutions was included for a standard curve. Subsequently, the genomic DNA concentration of all samples were adjusted using the Ct-values. HRM reactions were run using the Type-it HRM PCR Kit (QIAGEN) with pipetting instructions in Supplementary Table S18. In each run, 4-6 controls of genomic DNA from wild-type plants were included. For the HRM reactions the RotorGene 6000 Real-Time PCR Instrument was programmed for 5 min at 95 °C initial denaturation, followed by 40 cycles of 10 sec at 95 °C denaturation, 30 sec at 55 °C annealing, and 10 sec at 72 °C extension. The cycling was followed by a HRM gradient from 65 – 95 °C with 0.1 °C/step and 2 sec wait/step. Data analysis was conducted in Rotor-Gene 6000 Series Software 1.7 (QIAGEN).

4.2.7. Phenotyping

Arabidopsis (*Arabidopsis thaliana*) ecotype Col-0 wild-type seed and seed of the null mutant for *AtTIP2;3* were sown on solid (5 g/L Phytagel), half-strength Murashige and Skoog medium (Murashige and Skoog 1962) (Supplementary Table S16). After vernalisation at 4 °C for 3 days in the dark, plates were transferred to a walk-in growth chamber (details above). Plants were grown under long-day conditions (as above) for 8 days either in a horizontal or vertical position. For imaging purposes, seedlings were transferred to fresh plates with solid, half-strength Murashige and Skoog medium and roots were stretched-out. Images were taken on a Combo Scanner (MP C5503, RICOH).

4.3. Results

4.3.1. Transformation vector construction

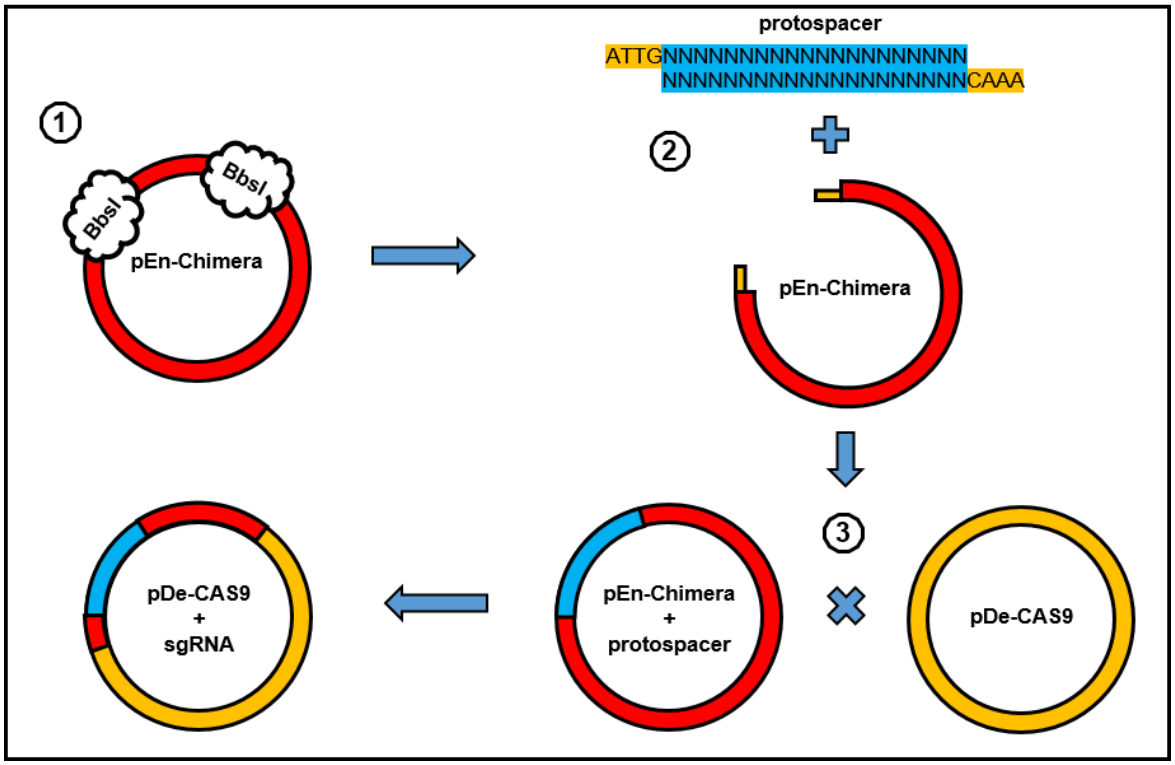

Figure 41. Molecular cloning of gene specific guide sequences as protospacers into the dual vector Gateway®-compatible CRISPR-Cas system designed by Fauser et al. (2014). (1) The entry vector pEn-Chimera is cut using the resitriction enzyme *BbsI*. (2) A protospacer sequence is ligated into pEn-Chimera to create the sgRNA. (3) The sgRNA is transferred to the destination vector pDe-CAS9 by LR reaction.

Molecular cloning techniques were used to construct a destination vector for transformation into Arabidopsis to express sgRNAs and the CAS9 endonuclease for targeted genome editing (Figure 41).

For each of the three target genes (*AtTIP2;1*, *AtTIP2;2*, and *AtTIP2;3*), two guide sequences were chosen (Table 6) that recognise the genes towards their 5' end using the CRISPR DESIGN web tool

(crispr.mit.edu). Since the CRISPR DESIGN web tool did not have any information on the genetic structure of *Arabidopsis thaliana* and, hence, would not correctly predict if off-targets are located in genes, a plant specific web tool, CRISPR-P (cbi.hzau.edu.cn/crispr/), was used to check off-targets for the chosen guide sequences later into the project (Table 6). CRISPR-P did not predict any off-targets for constructs containing guides AtTIP2;1 Guide#1 and AtTIP2;3 Guide#1, while for AtTIP2;1 Guide#2 three off-targets were predicted, for AtTIP2;2 Guide#1 and Guide#2 one and seven off-targets were predicted respectively, and for AtTIP2;3 Guide#2 three off-targets were predicted. Since genes in the aquaporin family have a high level of similarity, AtTIP2;1 Guide#2 has also a low probability of targeting *AtTIP3;2* (Off-target#2: AT1G17810), and AtTIP2;3 Guide#2 has also a low probability of targeting *AtTIP2;1* (Off-target#1: AT3G16240). With CRISPR-P, multiple unique sequences (without off-targets) were found for *AtTIP2;1* (3), *AtTIP2;2* (3), and *AtTIP2;3* (6), but most of them are localised towards the 3' end of the genes. All off-targets predicted by CRISPR-P had 3 – 4 mismatches with the chosen guide sequences.

Table 6. Guide sequences (with PAM) and corresponding predicted off-targets for CRISPR-Cas to target the aquaporin genes *AtTIP2;1*, *AtTIP2;2*, and *AtTIP2;3* in *Arabidopsis thaliana*. The scoring (higher score = better targeting) and off-target prediction was carried out using the CRISPR-P (cbi.hzau.edu.cn/crispr/) online tool. The intended targets are shaded in grey and followed by their predicted off-targets without shading. The PAM is indicated by green shading. Mismatches between the sgRNAs and their off-targets are indicated by red letters. For the off-targets, "Region" specifies the locus either as coordinates or Gene ID if localised within a gene.

Target site	Sequence	Info
AtTIP2;1 Guide#1	ACCGCGATGGCCACTAGTCCCGG	Score: 100 Predicted off-targets: none
AtTIP2;1 Guide#2	AAGTGACGGCTGGGTTCACATGG	Score: 99 Predicted off-targets: 3
- Off-target #1	CAGTGACATCTGGGTTGACATGG	Score: 0.4 Region: intergenic (3:+16238383)
- Off-target #2	AAGTGACAGCGGGGTTGACGTGG	Score: 0.1 Region: exon (AT1G17810)
- Off-target #3	AAGTTACGGCTTGGTTGATATGG	Score: 0.1 Region: intergenic (4:+15964996)
AtTIP2;2 Guide#1	GTGACACTCGGTCTCGCCGTCGG	Score: 99 Predicted off-targets: 1
- Off-target #1	GTGACACTCTGTTTCGTTGTGGG	Score: 0 Region: exon (AT5G38210)
AtTIP2;2 Guide#2	CGAGACCGAGTGTCACGGCGGGG	Score: 99 Predicted off-targets: 7
- Off-target #1	CGAGGTTGAGTGACACGGCGAGG	Score: 0.2 Region: exon (AT1G38185)
- Off-target #2	CAAAACCGAGTGCCTCGGCGTGG	Score: 0.2 Region: exon (AT5G54200)

- Off-target #3	GTAGACCGAGGGTGACGGCGGGG	Score: 0.1 Region: exon (AT2G25810)
- Off-target #4	CGAGATCGAGTTTCAAGGCGGAG	Score: 0.1 Region: exon (AT2G44230)
- Off-target #5	AGAGACCGAATGTGACGGAGGAG	Score: 0.1 Region: exon (AT4G25835)
- Off-target #6	GGAGACCGAGTAAAACGGCGGAG	Score: 0 Region: exon (AT2G46210)
- Off-target #7	CGAGACCGAGTGTTCCGGTAAGG	Score: 0 Region: exon (AT3G21890)
AtTIP2;3 Guide#1	GGCTCCATCAGAGGTTAGTTTGG	Score: 100 Predicted off-targets: none
AtTIP2;3 Guide#2	CAAGGCCAAGAGTCACGGCTGGG	Score: 99 Predicted off-targets: 3
- Off-target #1	CAAGACCAAAAGTGACGGCTGGG	Score: 0.4 Region: exon (AT3G16240)
- Off-target #2	CAAGGCCAAGACTCAAAGCTGAG	Score: 0.1 Region: intergenic (3:+16743871)
- Off-target #3	CAAGGACCAGATTCAGGGCTGAG	Score: 0.1 Region: intron (AT1G17060)

The guide sequence recognition sites for the gene *AtTIP2;1* were located in the second exon, since the first exon is short. In the genes *AtTIP2;2* and *AtTIP2;3*, the guide sequence recognition sites were located in the first exon (Figure 42).

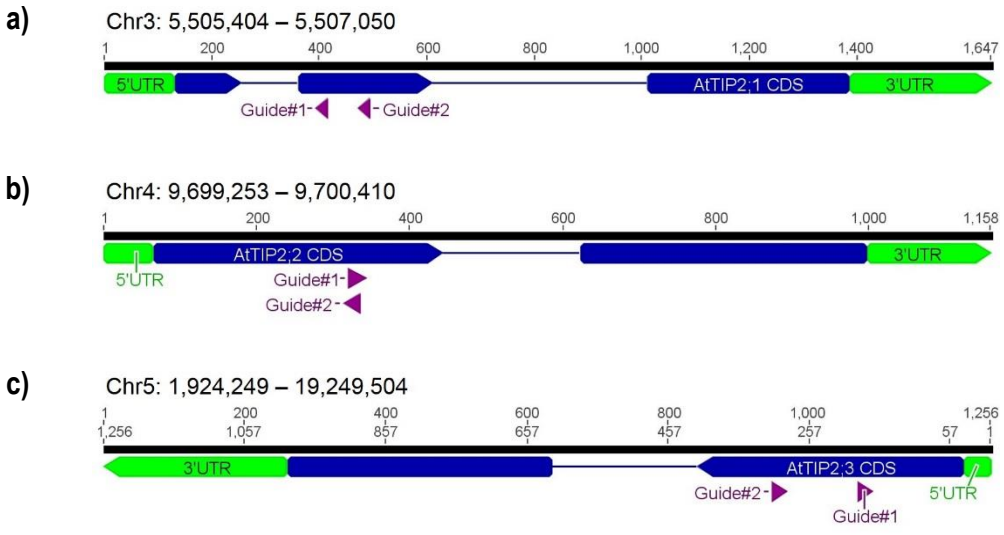

Figure 42. Localisation of the single guide RNA target loci within the genes (a) *AtTIP2;1*, (b) *AtTIP2;2*, and (c) *AtTIP2;3* in *Arabidopsis thaliana*. The 5' and 3' UTRs are shown in green, while the coding sequences with introns are shown in blue. Positions of the single guide RNA target loci are shown in purple.

4.3.2. Selection of plants with CRISPR-Cas induced mutations

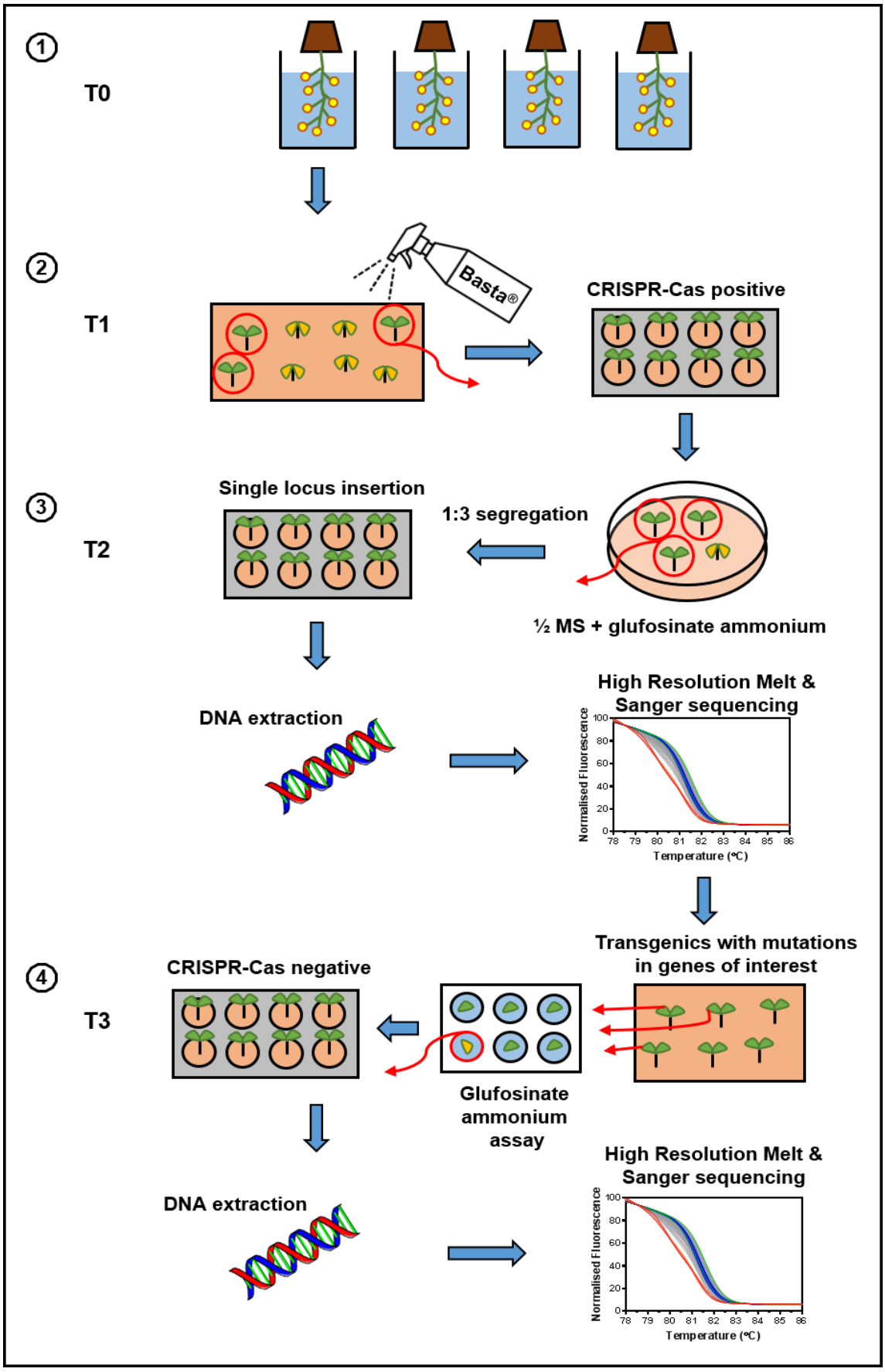

Figure 43. Workflow scheme for selection of plants with CRISPR-Cas induced mutations. (1) Floral dip transformation of pDe-CAS9-sgRNA vectors into *Arabidopsis thaliana*. (2) Selection of transgenic T_1 plants using Basta®. (3) Segregation analysis of

T_2 plants to select plants with single locus insertion of CRISPR-Cas constructs. DNA extraction for High Resolution Melt and Sanger sequencing to find plants which show mutations in genes of interest induced by CRISPR-Cas. (4) Offspring from plants with predicted mutations are grown and leaves are used in a glufosinate ammonium assay to find CRISPR-Cas negative plants. DNA extraction from CRISPR-Cas negative plants for High Resolution Melt and Sanger sequencing to find homozygous mutations.

After guide sequences were chosen and transformation vectors constructed, CRISPR-Cas constructs were transformed into plants of *Arabidopsis thaliana* Col-0 by floral dip (Figure 43). The selection procedure was designed to find plants with the CRISPR-Cas construct inserted in a single locus, so it could be removed after subsequent generations. High Resolution Melt and Sanger sequencing were used to find plants with CRISPR-Cas induced mutations in the genes of interest. In the third generation of offspring, CRISPR-Cas negative plants were selected by screening leaves for glufosinate ammonium sensitivity. These CRISPR-Cas free plants were genotyped for homozygous mutations in the genes of interest.

First, glufosinate ammonium (applied as Basta® herbicide spray) selection of T_1 plants was carried out on offspring from two independent transformation events each.

For each target gene, one CRISPR-Cas construct was chosen first, and, if no induced mutations were detected, the second construct was tested as well. Up to 26 glufosinate ammonium resistant T_1 plants were grown to seed. T_2 offspring were germinated on media with glufosinate ammonium and segregation ratios were determined (Table 7). Between 40 – 70% of T_1 lines were found with a 1:3 segregation of T_2 offspring, which indicates that the CRISPR-Cas construct inserts were located in a single locus; a prerequisite to be able to outcross the CRISPR-Cas construct in successive generations.

Table 7. Single locus frequency of CRISPR-Cas construct insert observed for T_1 lines. Segregation ratios are determined in T_2 offspring germinated on medium with glufosinate ammonium.

Target	Line	Lines tested	Lines with 1:3 segregation	Single locus freq. (%)
AtTIP2;1	TIP21sgRNA1 #3	20	10	50.0
	TIP21sgRNA1 #4	20	9	45.0
	TIP21sgRNA2 #1	25	15	60.0
	TIP21sgRNA2 #2	26	17	65.4
AtTIP2;2	TIP22sgRNA1 #1	7	3	42.9
	TIP22sgRNA1 #2	15	8	53.3
	TIP22sgRNA1 #3	15	6	40.0
	TIP22sgRNA1 #4	15	7	46.7

AtTIP2;3	TIP23sgRNA2 #2	25	17	68.0
	TIP23sgRNA2 #3	26	16	61.5

High Resolution Melt (HRM) analysis indicated that mutations were successfully induced in the target genes by CRISPR-Cas constructs AtTIP2;1 Guide#1 (Figure 44), AtTIP2;2 Guide#1 (Figure 46), and AtTIP2;3 Guide#2 (Figure 47), while no mutations were found in plants with AtTIP2;1 Guide#2 (Figure 45). Plants with the constructs AtTIP2;2 Guide#2 and AtTIP2;3 Guide#1 were not tested.

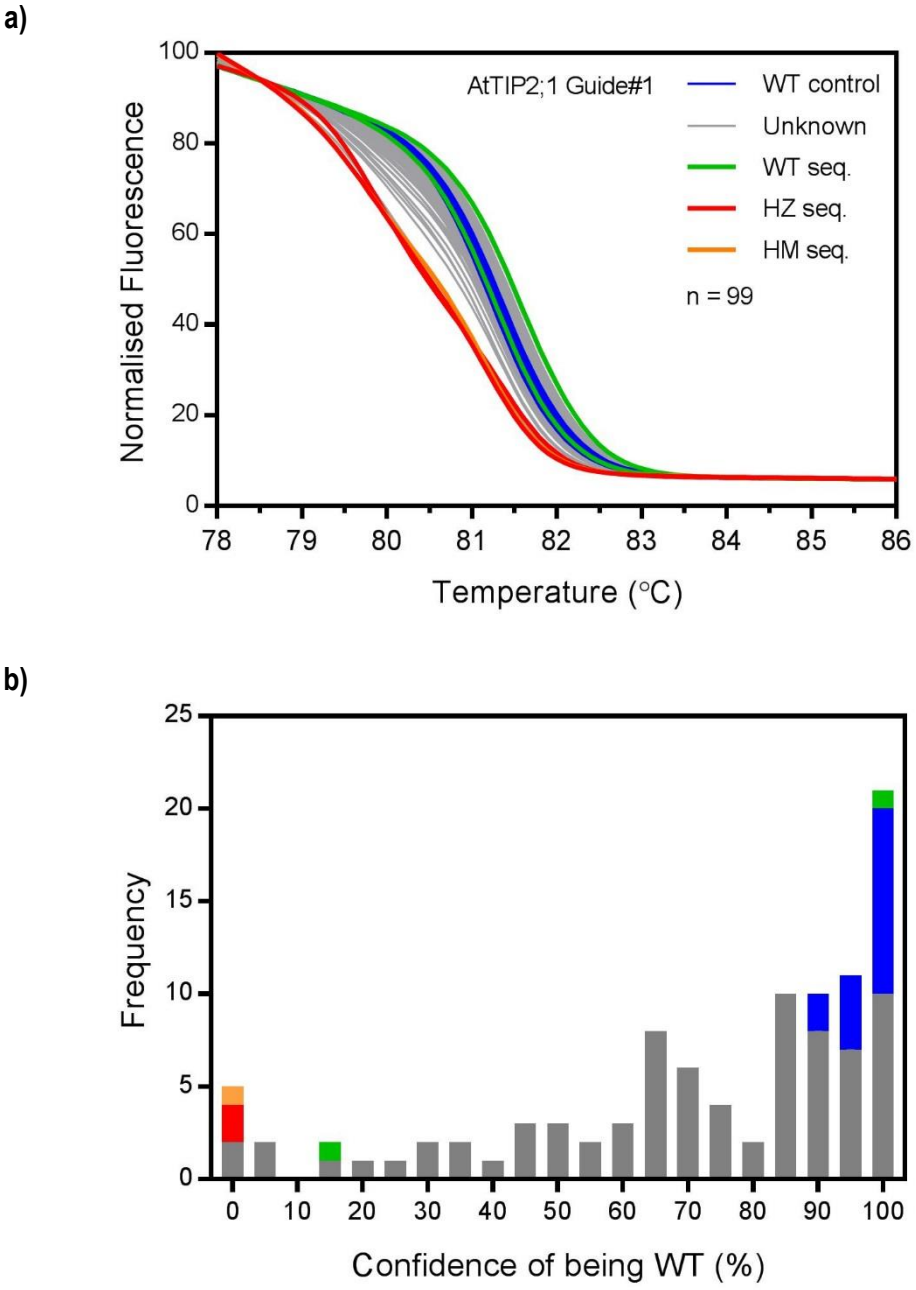

Figure 44. High Resolution Melt analysis of *AtTIP2;1* target locus for mutations induced by CRISPR-Cas AtTIP2;1 Guide#1. a) Normalised melt curves of 82 bp PCR amplicon spanning the CRISPR target site. Data between 78-79 °C and 85-86 °C were used to normalize the fluorescence. Melt curves of PCR amplicons from *Arabidopsis thaliana* Col-0 WT control samples are shown in blue and all unknown samples from CRISPR-Cas transformed plants are shown in grey. Five of the unknown

samples were genotyped by Sanger Sequencing: wild-type sequence (green), heterozygous mutations (red), homozygous mutation (orange). n = 99 plants (including 16 WT controls). b) Histogram of the predicted confidence of being a wild-type for each sample. Each curve was compared to the known wild-type controls and a confidence was calculated of how likely the unknown samples is from a wild-type plant. Bin width = 5%, bar height indicates the total number of samples in each bin. Same colour code as above; different colours show how many samples in each bin are unknown, known wild-type, or predicted to be heterozygous or homozygous.

HRM analysis of plants expressing the CRISPR-Cas AtTIP2;1 Guide#1 showed a range of different melt curves for the target region (Figure 44a), some of which had an earlier melt compared to the WT controls and some with a later melt. Melt curves of WT controls identified as wild-type with a confidence level > 87.5% (Figure 44b). Genotyping by Sanger Sequencing showed that one sample which had a higher melt temperature compared to the wild-type (green curve, Confidence of being WT: 15.5%) had still the wild-type alleles. Two samples with a lower melt temperature (orange curves, Confidence of being WT: 0.01% and 0.02%) were identified to have heterozygous mutations and a third sample with lower melt temperature (red curve, Confidence of being WT: 0.02%) was identified to have a one base homozygous insertion (166_167insA) in the coding sequence which is 4 bp downstream of the PAM (Supplementary Figure S13).

a)

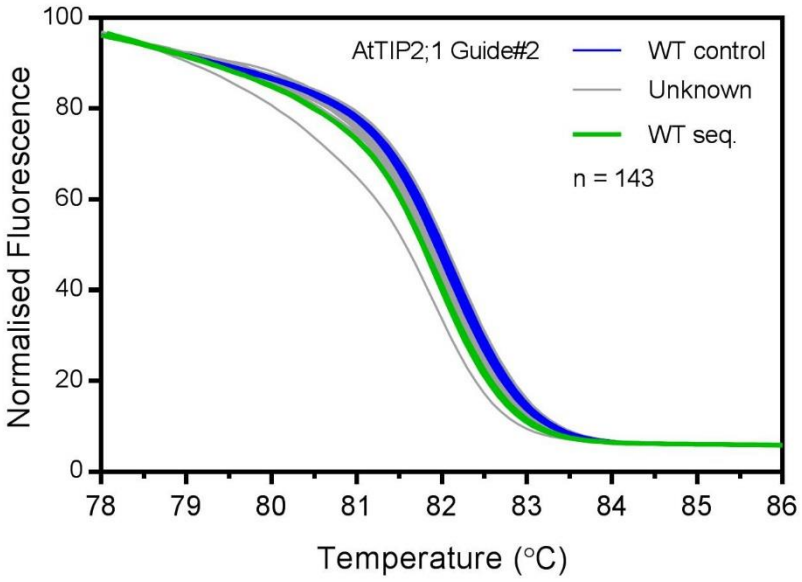

b)

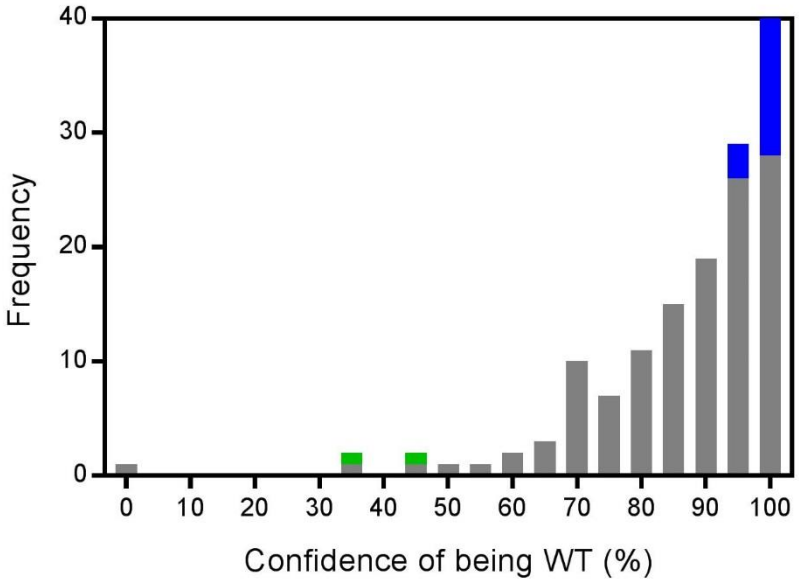

Figure 45. High Resolution Melt analysis of *AtTIP2;1* target locus for mutations induced by CRISPR-Cas AtTIP2;1 Guide#2. a) Normalised melt curves of 87 bp PCR amplicon spanning the CRISPR target site. Data between 78-79 °C and 85-86 °C were used to normalize the fluorescence. Curves from three different HRM runs were temperature shifted by using the WT control curves as reference. Each run included five independent WT control reactions. Melt curves of PCR amplicons from *Arabidopsis thaliana* Col-0 WT control are shown in blue and all unknown samples from CRISPR-Cas transformed plants are shown in grey. Two of the unknown samples were genotyped by Sanger Sequencing: wild-type sequence (green). n = 143 plants (including 15 WT controls). b) Histogram of the predicted confidence of being a wild-type for each sample. Each curve was compared to the known wild-type controls and a confidence was calculated of how likely the unknown samples is from a wild-type plant. Bin width = 5%, bar height indicates the total number of samples in each bin. Same colour code as above; different colours show how many samples in each bin are unknown, known wild-type, or predicted to be heterozygous or homozygous.

Little differences in melt curves for the target region of CRISPR-Cas AtTIP2;1 Guide#2 were observed for T_2 plants expressing this construct (Figure 45a). WT control samples were identified as wild-type with a confidence > 90% (Figure 45b). Two samples which were genotyped by Sanger Sequencing (green curves, Confidence of being WT: 36% and 46%) were identified as wild-type (Supplementary Figure S14). Only one sample had a low (< 30%) confidence of being a WT, but was not sequenced.

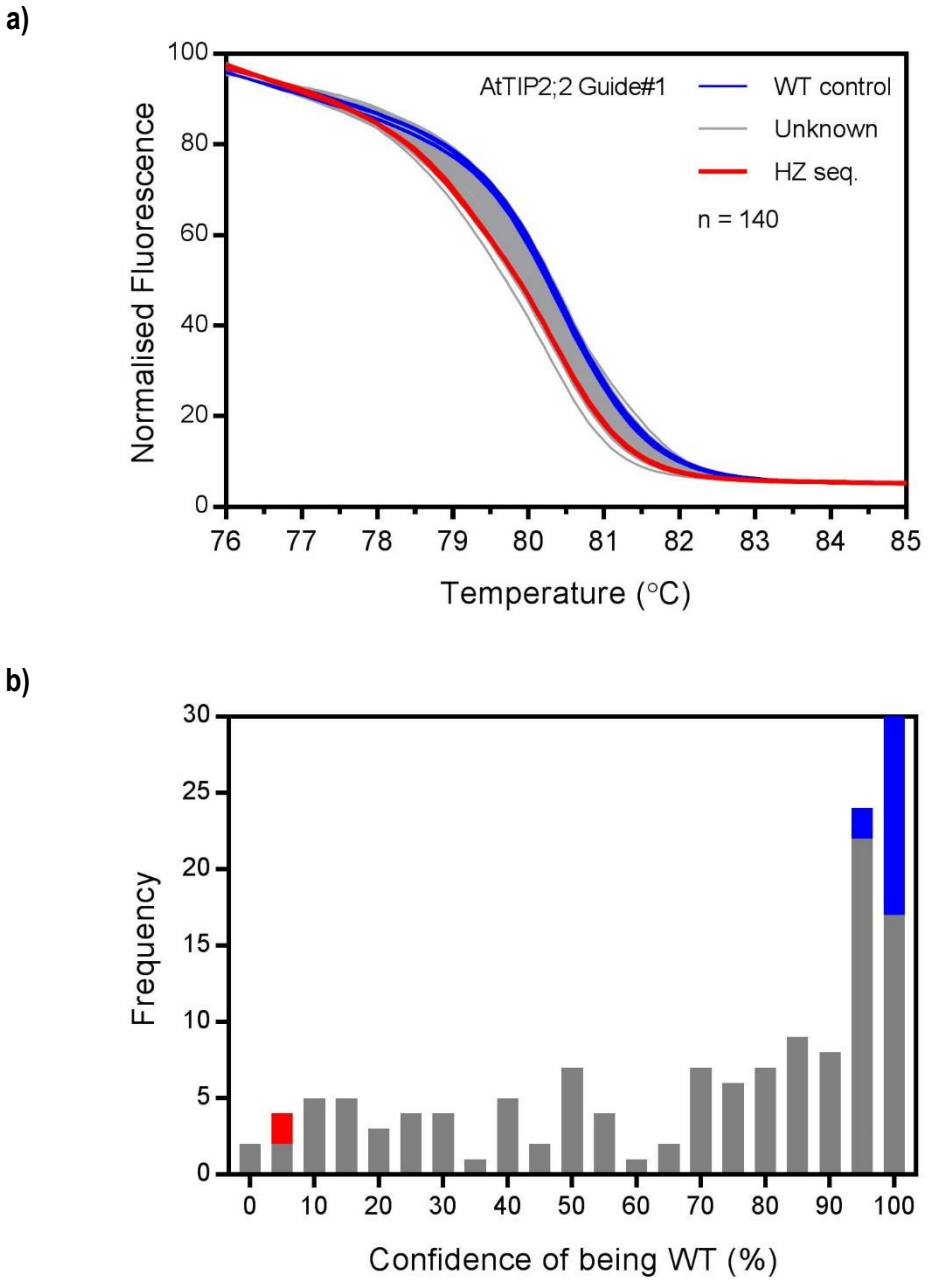

Figure 46. High Resolution Melt analysis of *AtTIP2;2* target locus for mutations induced by CRISPR-Cas AtTIP2;2 Guide#1. a) Normalised melt curves of 89 bp PCR amplicon spanning the CRISPR target site. Data between 76-77 °C and 84-85 °C were used to normalize the fluorescence. Curves from three different HRM runs were temperature shifted by using the WT control curves as reference. Each run included five independent WT control reactions. Melt curves of PCR amplicons from *Arabidopsis thaliana* Col-0 WT control are shown in blue and all unknown samples from CRISPR-Cas transformed plants are shown in grey. Two of the unknown samples were genotyped by Sanger Sequencing and identified with heterozygous mutations (red). n = 140 plants (including 15 WT controls). b) Histogram of the predicted confidence of being a wild-type for each sample. Each curve was compared to the known wild-type controls and a confidence was calculated of how likely the unknow samples is from a wild-type plant. Bin width = 5%, bar height indicates the total number of samples in each bin. Same colour code as above; different colours show how many samples in each bin are unknown, known wild-type, or predicted to be heterozygous or homozygous.

Similar to AtTIP2;1 Guide#1, a range of melt curves was observed for the target sequence of AtTIP2;2 Guide#1 in T_2 plants expression the CRISPR-Cas construct (Figure 46a). WT controls were identified as wild-types with a confidence > 90% (Figure 46b). The distribution of observed confidence was also very similar to AtTIP2;1 Guide#1 (Figure 44). Two samples with confidence of 4.2% and 5.2% of being a WT (red curves) were identified as heterozygous mutants by Sanger Sequencing (Supplementary Figure S15).

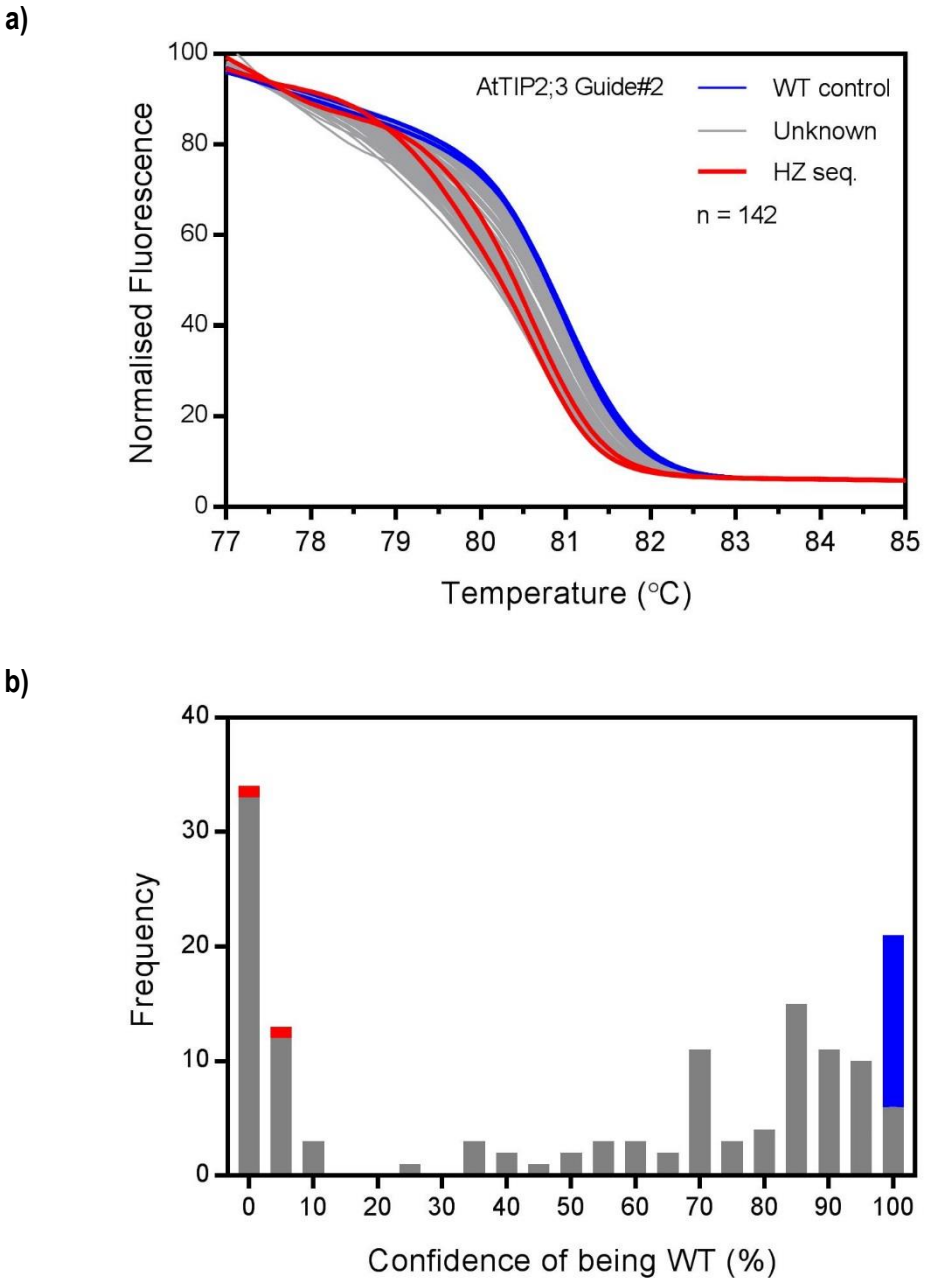

Figure 47. High Resolution Melt analysis of *AtTIP2;3* target locus for mutations induced by CRISPR-Cas AtTIP2;3 Guide#2. a) Normalised melt curves of 87 bp PCR amplicon spanning the CRISPR target site. Data between 78-78 °C and 84-85 °C were used to normalize the fluorescence. Curves from three different HRM runs were temperature shifted by using the WT control curves as reference. Each run included five independent WT control reactions. Melt curves of PCR amplicons from *Arabidopsis thaliana* Col-0 WT control are shown in blue and all unknown samples from CRISPR-Cas transformed plants are

shown in grey. Two of the unknown samples were genotyped by Sanger Sequencing and identified with heterozygous mutations (red). n = 142 plants (including 15 WT controls). b) Histogram of the predicted confidence of being a wild-type for each sample. Each curve was compared to the known wild-type controls and a confidence was calculated of how likely the unknown samples is from a wild-type plant. Bin width = 5%, bar height indicates the total number of samples in each bin. Same colour code as above; different colours show how many samples in each bin are unknown, known wild-type, or predicted to be heterozygous or homozygous.

T_2 plants expressing the AtTIP2;3 Guide#2 showed a high proportion of target sequences with a lower melt temperature compared to the WT controls (Figure 47). WT controls were also identified with a higher confidence as wild-type (> 95%) compared to the other constructs. Two samples (Confidence of being WT: 0.1% and 2.5%) which were genotyped by Sanger Sequencing were identified as heterozygous mutants (Supplementary Figure S16).

Since always eight offspring (T_2) per T_1 plant were characterised by HRM, it emerged that usually multiple offspring from the same mother plant show a low probability of being a WT, or all of them have a high probability of being a WT. Sanger Sequencing of a few samples also demonstrated that the majority of T_2 plants have heterozygous mutations (Figures 12, 14, 15).

Sanger Sequencing chromatograms can be used to predict the size and location of different indels (Figure 48). Plants that harbour heterozygous mutations induced by CRISPR-Cas showed an abrupt loss of base call quality from the location of the mutation (Figure 48a). By using two primers to sequence the amplicon from opposing directions, could indicate the location of the mutation. This was always within the target sequence site of the corresponding CRISPR-Cas guide RNA.

a)

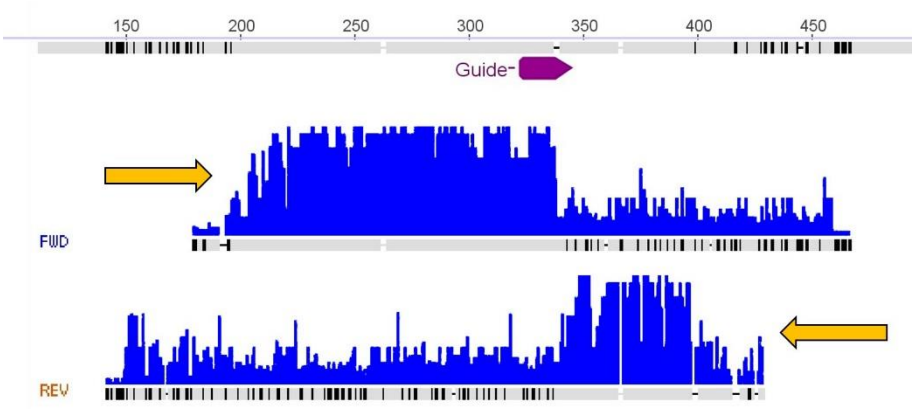

b)

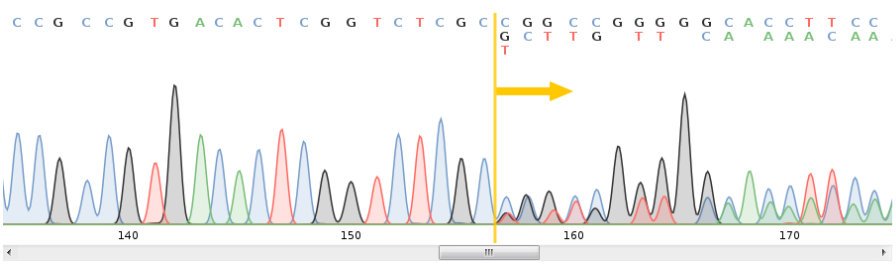

c)

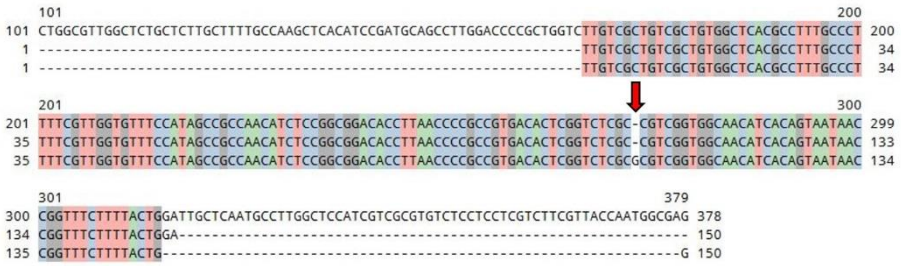

Figure 48. Sequence decomposition of Sanger Sequencing chromatograms to predict indels of heterozygous mutations induced by CRISPR-Cas. a) Alignment of two Sanger Sequencing chromatograms (FWD: forward primer; REV: reverse primer) with the wild-type sequence. Yellow arrows show the direction of sequencing. The blue areas show quality scores of the sequencing and black lines below the chromatograms indicate disagreements between sequencing results and wild-type sequence. The position of the CRISPR-Cas guide target site is shown in purple. b) Sequence decomposition using the web-tool CRISP-ID (http://crispid.gbiomed.kuleuven.be). The yellow line and arrow indicate were multiple signals start in the chromatogram. The assignment is shown above. c) Alignment of the sequence decomposition in CRISP-ID. The red arrow indicates the predicted position of an insertion (G).

Convoluted peaks in the chromatogram were analysed using the online tool CRISP-ID (Figure 48b). The decomposed sequences were aligned to the wild-type sequence and mostly showed single base insertions for one allele and the wild-type sequence for the other allele (Figure 48c). The predicted heterozygous mutations and homozygous mutations detected by Sanger Sequencing are shown in Figure 49. Except for two lines with predicted deletions (AtTIP2;1 #4-17-4 and AtTIP2;2 #2-2-5-12), all other mutations were single base insertions 4 bases downstream of the PAM within the guide sequence target site.

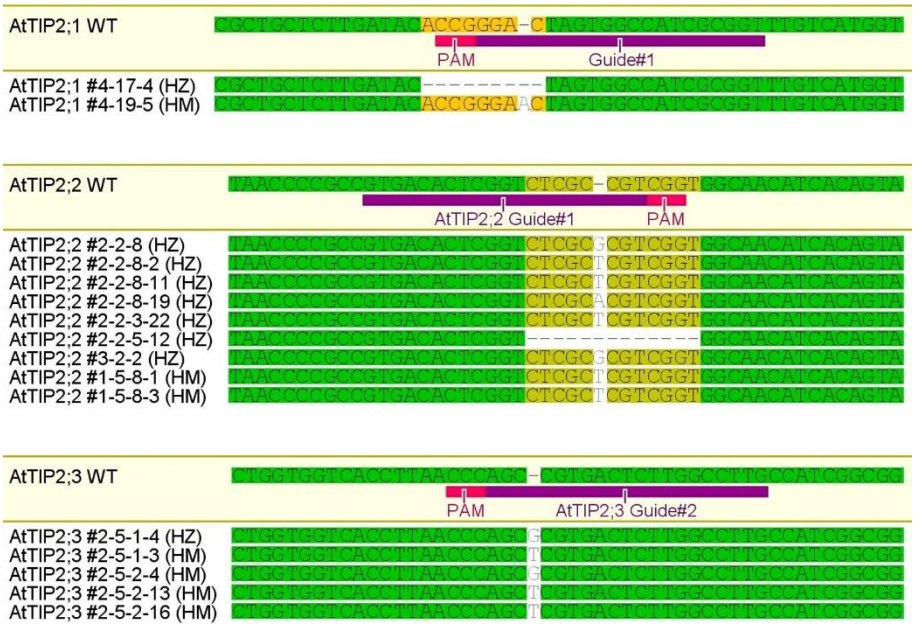

Figure 49. Sequence alignments show different types of mutations in the genes *AtTIP2;1*, *AtTIP2;2*, and *AtTIP2;3* induced by gene specific CRISPR-Cas constructs. All sequences are aligned against the corresponding wild-type (WT). A purple box indicates the position of the CRISPR-Cas target sequences including the PAM (pink). Sequences marked as "HZ" were

predicted from heterozygous mutations using the web-tool CRISP-ID, while sequences marked as "HM" were homozygous for the mutation. All mutations were observed in T_2 and T_3 plants.

Leaves from sensitive T_3 seedlings, which had supposedly outcrossed the CRISPR-Cas, showed bleaching in 300 µM glufosinate ammonium solution as early as three days, while leaves from resistant seedlings remained green (Figure 50).

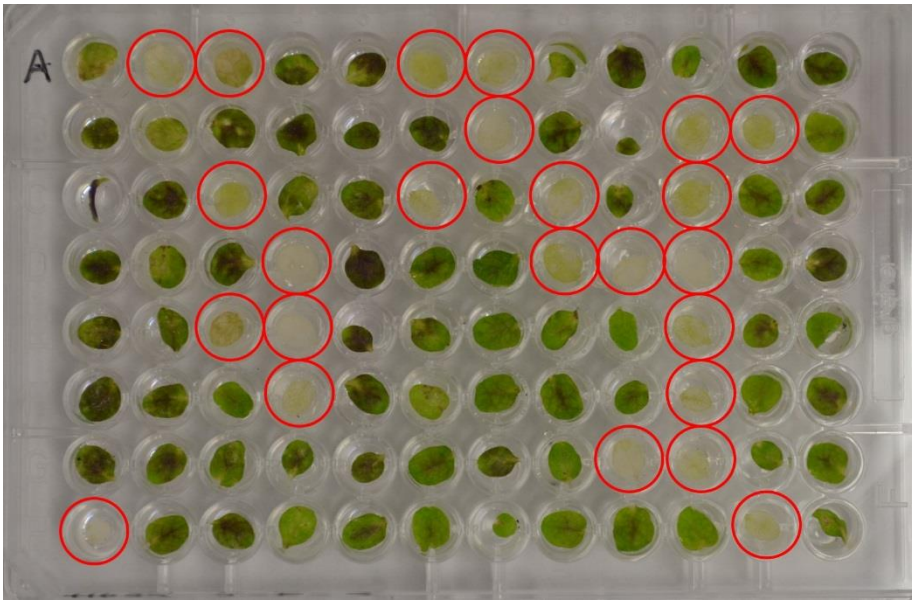

Figure 50. Genotyping of T_3 plants using a homemade glufosinate ammonium assay. Leaves of 2-week old seedlings were floated on ½ MS medium with 300 µM glufosinate ammonium for up to 1 week. Red circles indicate leaves from seedlings that are sensitive (bleached leaves) to glufosinate ammonium, and hence, should have outcrossed the CRISPR-Cas construct.

Seedlings that had shown sensitivity to glufosinate ammonium were validated by PCR, using CRISPR-Cas specific primers, to calculate a false positive rate for the glufosinate ammonium assay (Table 8). A false positive rate < 10% was observed for most lines, except AtTIP2;2 #1-5-8. The segregation ratio of sensitive/resistant was observed to be close to 1:3 (25% sensitive).

Table 8. Selection ratios of T_3 seedlings observed in the homemade glufosinate ammonium assay with the aim to select sensitive plants that have outcrossed the CRISPR-Cas construct. Seedlings showing a sensitive phenotype in the Glufosinate assay were genotyped by PCR and a false positive rate was calculated; no test for false negatives. The final ratio of sensitive/resistant plants was calculated.

Parent line	Plants tested	Leaves sensitive (Glufosinate assay)	False positives (PCR tested)	False positive rate	Ratio of sensitive/resistant
AtTIP2;2 #1-5-8	96	23	9	39%	15%
AtTIP2;2 #2-2-3	95	23	0	0%	24%

AtTIP2;2 #2-2-5	96	23	2	9%	22%
AtTIP2;2 #2-2-8	89	27	1	4%	29%
AtTIP2;3 #2-5-1	96	28	1	4%	28%
AtTIP2;3 #2-5-2	96	24	2	8%	23%
AtTIP2;3 #2-5-6	95	19	1	5%	19%
AtTIP2;3 #2-5-8	96	32	0	0%	33%
AtTIP2;3 #3-6-1	92	24	2	8%	24%
AtTIP2;3 #3-6-6	92	22	0	0%	24%

HRM analysis and Sanger Sequencing analysis identified homozygous mutations (one base insertions) in six lines (AtTIP2;2 #1-5-8-1, AtTIP2;2 #1-5-8-3, AtTIP2;3 #2-5-1-3, AtTIP2;3 #2-5-2-4, AtTIP2;3 #2-5-2-13, and AtTIP2;3 #2-5-2-16 (Figure 49). Offspring from the heterozygous T_2 parent line AtTIP2;3 #2-5-2 showed segregation of guanine/thymine single base insertions at position 254_255 in the coding sequence of *AtTIP2;3* (Figure 51). Offspring with a homozygous insertion of guanine showed a higher melting temperature compared to the wild-type, while offspring with a homozygous insertion of thymine showed a lower melting temperature (Figure 51a) as predicted by the online-tool *uMelt*^{SM} (Figure 51b). Since no heterozygous (G/T) offspring were sequenced, the *uMelt*^{SM} was used to predict the shape of the curve. Similar curves were also found the in the actual HRM analysis, which can be assumed to be heterozygous.

a)

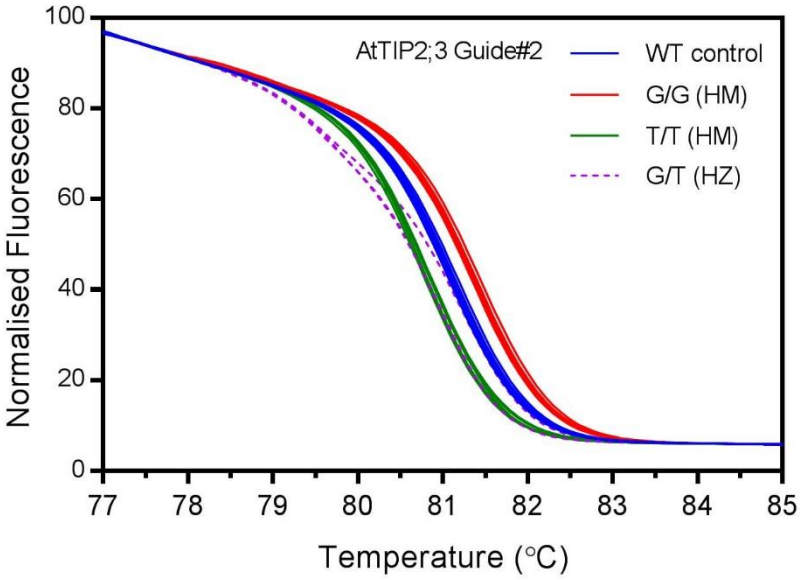

b)

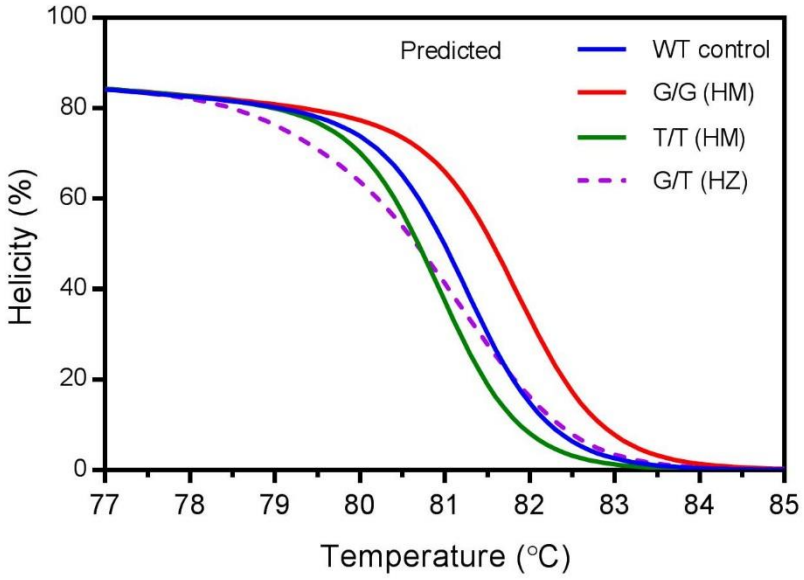

Figure 51. Comparison of High Resolution Melt (HRM) curves obtained from offspring T_3 seedlings, originating from a T_2 plant with heterozygous mutations induced by CRISPR-Cas, and *in silico* predicted melt curves for the same sequences. a) HRM curves from multiple segregating T_3 seedlings of an 87 bp PCR amplicon spanning the CRISPR target site for Guide#2 in *AtTIP2;3*. Data between 78-78 °C and 84-85 °C were used to normalize the fluorescence. Wild-type controls (WT control) are shown in blue, T_3 seedlings which are predicted to have a homozygous insertion of guanine (G) are red, T_3 seedlings which are predicted to have a homozygous insertion of thymine (T) are green, and heterozygous T_3 seedlings which are predicted to have both variants of insertions (G/T) are dashed purple. b) *In silico* predicted melt curves for the sequences with the same mutations using uMelt^{SM} (https://www.dna.utah.edu/umelt/umelt.html). Melt curves were temperature shifted relative to the WT control from the *in vitro* melt.

Translation of the coding sequence from homozygous mutants of *AtTIP2;2* and *AtTIP2;3* showed that the insertions caused a frame-shift and premature stop (Figure 52). The protein sequence starts to change from position 92 and 86 in mutants of *AtTIP2;2* and *AtTIP2;3*. While both wild-type proteins have a length of 250 amino acids, the mutants have only 140 and 123.

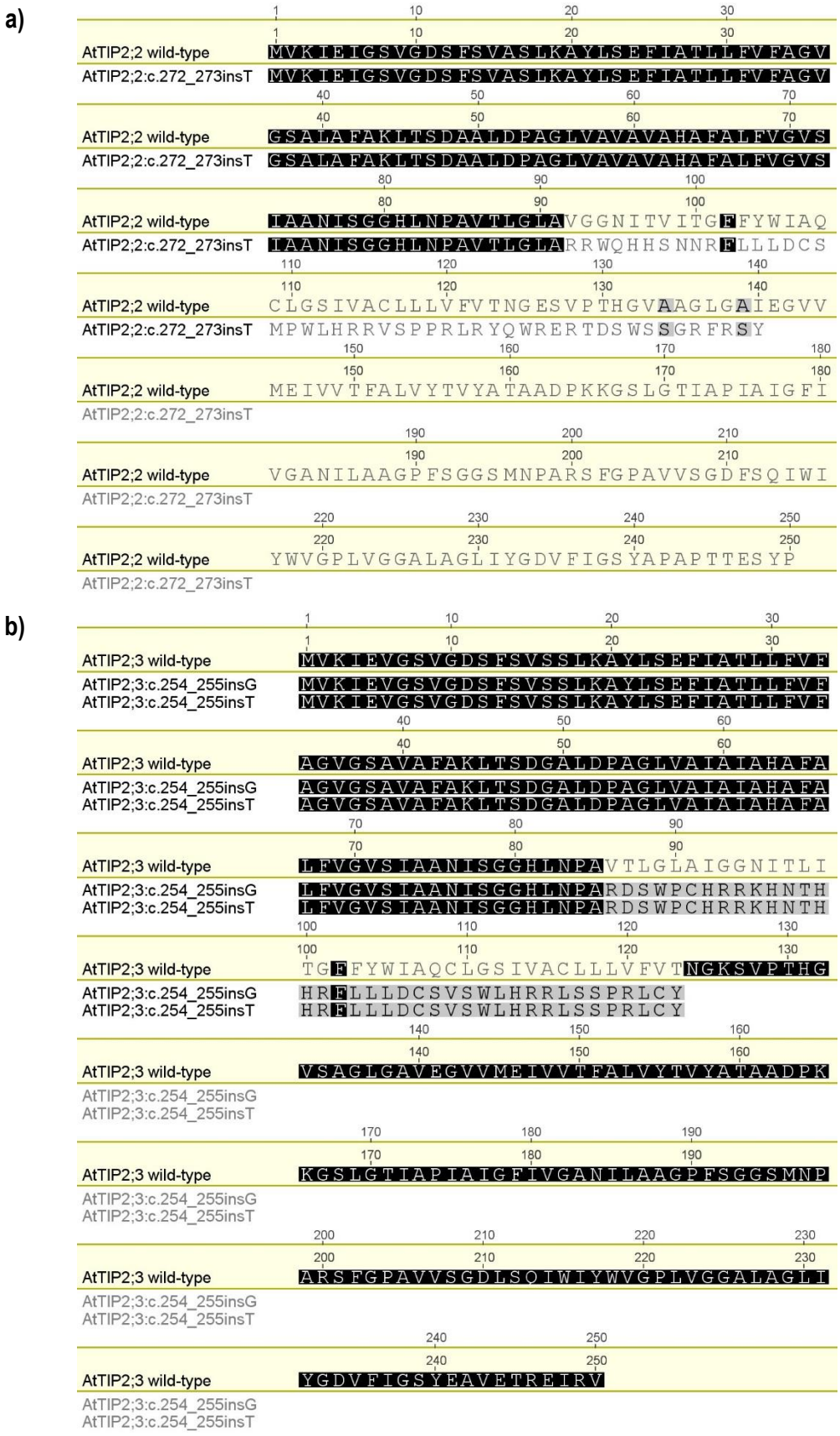

Figure 52. Protein translation and sequence comparison for null mutants of *AtTIP2;2* and *AtTIP2;3* in *Arabidopsis thaliana*. a) For *AtTIP2;2* a single base insertion of thymine between position 272_273 in the coding sequence of the gene causes a change of protein sequence from position 92 and a pre-mature stop after 140 amino acids. b) For *AtTIP2;3* a single base insertion of

either guanine or thymine between position 254_255 in the coding sequence of the gene causes a change of protein sequence from position 86 and a pre-mature stop after 123 amino acids.

4.3.2. Phenotyping of a putative *AtTIP2;3* null mutant

Phenotyping of null mutants of *AtTIP2;3* showed a conditional phenotype (Figure 53). Seedlings grown on vertical plates had a slightly shorter root compared to the wild-type (Figure 53a). Growing the same seedlings on a horizontal plate instead enhanced this short root phenotype (Figure 53b).

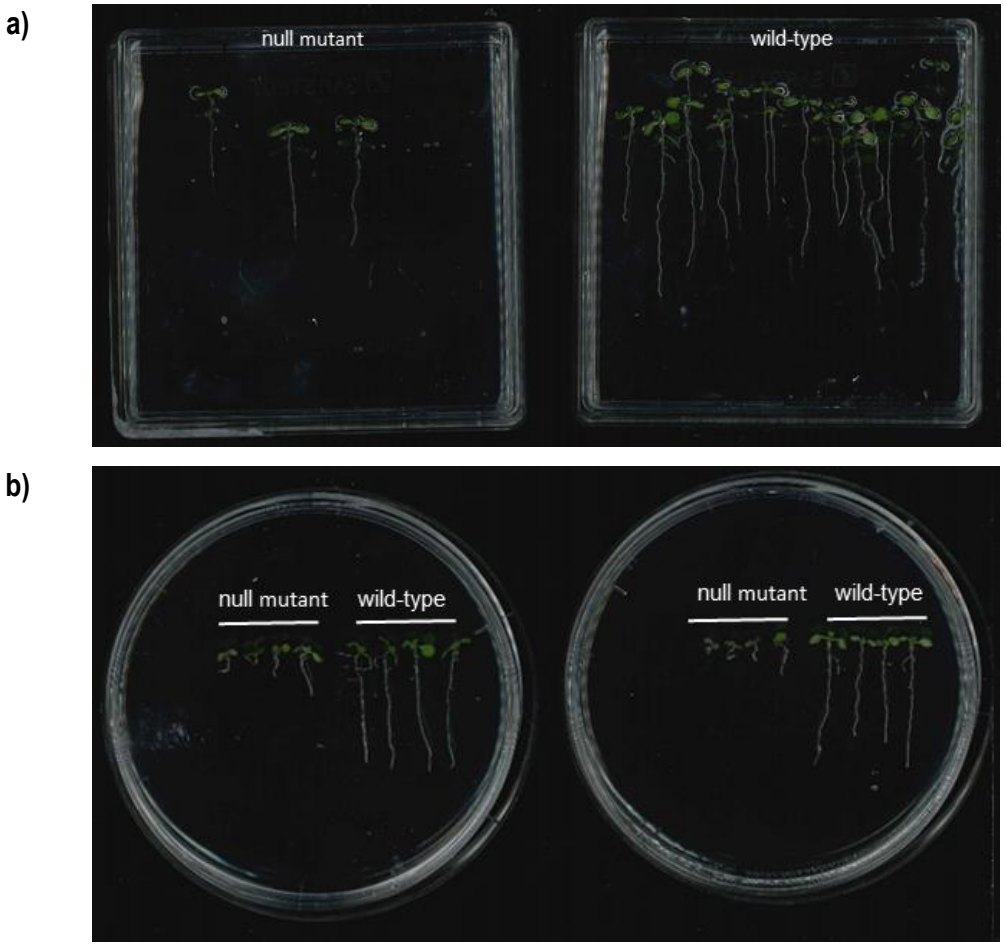

Figure 53. Comparison of root length between null mutant of *AtTIP2;3* and wild-type *Arabidopsis thaliana* Col-0. Seedlings were grown under long-day conditions (16 h light/ 8 h dark,PAR ~150 µmol m^{-2} s^{-1}, 21°C) on ½ MS media plates for 8 days. a) Seedlings grown in vertical position. b) Seedlings grown in horizontal position. They were transferred to new plates for imaging to stretch-out the roots.

4.4. Discussion

Targeted genome editing by CRISPR-Cas is a new, simple, and affordable technique to create knockout mutants for a reverse genetics strategy if no suitable lines exist in public collections. CRISPR-Cas constructs with gene specific guide RNAs can be easily assembled using standard molecular techniques (Schiml and Puchta 2016). The constructs are transformed into plants of *Arabidopsis thaliana* using disarmed *Agrobacterium tumefaciens* and floral dip (Clough and Bent 1998). Screening of CRISPR-Cas plants can be achieved with standard techniques such as PCR, mismatch cleavage assays, High Resolution Melt, and sequencing (Zischewski *et al.* 2017).

Here we present the successful identification of CRISPR-Cas induced single base insertions in the genes *AtTIP2;1*, *AtTIP2;2*, and *AtTIP2;3* (Figure 49). It demonstrates that this technique can precisely target individual genes in a large highly conserved gene family such as the major intrinsic proteins. Using this technique, a conditional short root phenotype was identified for the null mutant of *AtTIP2;3* (Figure 53). To identify mutated plants which have outcrossed the CRISPR-Cas construct faster and cheaper, a leaf glufosinate ammonium assay was developed (Figure 50).

4.4.1. Selection of guide sequences and segregation analysis for single locus insertions

One bottleneck of CRISPR-Cas is to find suitable, unique guide sequences for the genes of interest to avoid off-target mutations. Since genes in gene families have often very similar sequences, this can make this task challenging; i.e. the similarity between coding sequences of the TIP2 aquaporins in *Arabidopsis thaliana* is between 70 – 81%. However, CRISPR-P predicted at least three unique guide sequences for each *AtTIP2* gene. For the creation of null mutants, it is often more beneficial to choose guide sequences that are located closer to the 5' end of the gene. That way, small mutations in the DNA have a greater effect on the final protein sequence. However, this often means a compromise has to be made between localisation of the CRISPR target site and the number of potential off-targets. Current web-tools like CRISPR-P (Lei *et al.* 2014) give a detailed overview on potential off-targets. For this study, we chose guide sequence towards the 5' end of the gene (Table 6), for which some of them have potential *in silico* predicted off-target sites with 3 – 4 mismatches. Previous research in both human cells (Anderson *et al.* 2015) and in *Arabidopsis thaliana* (Peterson *et al.* 2016) suggest a low off-target activity. While *in planta* characterisation of predicted off-target sites has not been carried out yet, these sites need to be tested in the future to prove that phenotypes are due to the intended mutations and not due to off-target events.

Segregation analysis on plates using T_2 seedlings showed that about 40 – 70% of T_1 lines had a CRISPR-Cas insertion in a single locus (Table 7), which is an important requirement to be able to outcross the CRISPR-Cas construct in later generations, once the desirable mutations were induced. The insertion of

foreign genetic material into crops is one reason why they need to be labelled as GMO (Sprink *et al.* 2016). This led to a debate whether CRISPR-Cas induced mutations have to be considered as GMO or not if the CRISPR-Cas construct is removed after the process. New techniques such as cloning-free, *in vitro*, and DNA-free CRISPR-Cas are being developed to avoid the integration of foreign DNA into the target genome at all times of the process (Puchta 2017).

4.4.2. Identification of mutations by high resolution melt analysis and selection of CRISPR-Cas free T_3 plants by glufosinate ammonium assay

The second bottleneck is the identification of CRISPR-Cas induced mutations. High Resolution Melt (HRM) analysis was used successfully in discriminating plants with a high confidence of being wild-type from plants with a low confidence i.e. plants which are more likely to contain CRISPR-Cas induced mutations (Figures 12 - 15). Previously, HRM had been successfully used by the group who designed the CRISPR-Cas vectors used in this study (Fauser *et al.* 2014). Besides HRM, other methods like mismatch cleavage assays, different gel and capillary electrophoresis techniques, and Sanger or Next Generation Sequencing are in use to screen for CRISPR-Cas induced mutations (Zischewski *et al.* 2017). While PCR and gel electrophoresis techniques often do not have the required resolution to detect single base changes, capillary electrophoresis and sequencing techniques require specialised equipment and are costly. A popular technique are mismatch cleavage assays, however these cannot detect homozygous mutants easily (Vouillot *et al.* 2015). HRM offers a high throughput, closed-tube, low cost alternative, providing qPCR instrumentation with HRM capability is available. Closed-tube systems require less manual handling and have the advantage of reduced chance of contamination. If reactions are optimized, single base resolution can be achieved.

Several samples with a confidence ≤ 10% of being a wild-type were identified by HRM and confirmed as heterozygous or homozygous mutants by sequencing (Figure 44 - Figure 47). Since CRISPR-Cas can induce a number of different mutations (Fauser *et al.* 2014), it is difficult to use other known sequence variants as standards in HRM to compare against. Hence, the only way to predict whether a certain sample/plant has been mutated by CRISPR-Cas is to look for melt curves that are very different compared to the wild-type sequence melt curves. We showed that Sanger sequencing of a few samples can help to judge how different the melt curves of mutants are. Moreover, a different shape of the melt curve, i.e. two melt transitions as shown in Figure 51, can indicate the presence of heterozygous mutations (Montgomery *et al.* 2007).

For AtTIP2;3 Guide#2 (Figure 47), 30% of all tested (unknowns) plants had a confidence ≤ 10% of being a wild-type, while for the other CRISPR-Cas constructs (AtTIP2;1 Guide#1, AtTIP2;2 Guide#1) less than 10% had a confidence ≤ 10% of being a wild-type (Figure 44, Figure 46). Based on sequencing results of samples in this range, they could contain mutations, thus plant lines from these samples were chosen

to grow the next generation (T_3) of seedlings. In contrast, melt curves for plants with the AtTIP2;1 Guide#2 showed very low difference to the wild-type controls (Figure 45). These results indicate that different guide RNAs could have different efficiencies to induce mutations. This could be due to sequence differences of the guide RNAs, which could cause changes to the folding of the mature sgRNA. The sgRNA needs to have a certain structure to fit with the Cas9 endonuclease (Liang *et al.* 2016).

However, HRM data obtained in this study also demonstrated that curves from samples of unknowns that contain the wild-type sequence (confirmed by sequencing) are not necessarily identical to know wild-type control samples. For one sample, which was genotyped by sequencing after a significant higher melt temperature was detected compared to the wild-type controls, the calculated confidence of being a wild-type was only 16% even though the unknown sample contained the true wild-type sequence (Figure 44). This could have been due to differences in the salt concentration in the reaction and/or mistakes during the preparation of the reaction mixture. Melt curves which were generated from samples of known wild-type control plants showed however less variance. To avoid melting differences due to different concentrations of PCR product in each reaction, DNA concentrations were normalised so all samples would amplify within ± 1 Ct cycle (data not shown). The HRM™ manual of the Rotor-Gene™ 6000 instrument (Corbett) recommends to exclude samples with Cts of 30 or higher and samples which have a lower end-point fluorescence compared to most samples. While all samples in one run did amplify within ± 1 Ct cycle, different runs had an average Ct between 20 – 25 (data not shown). However, it was noticed that the end-point fluorescence showed some variance between samples. Schütz and von Ahsen (2009) found that melting curves are more influenced by differences in dye and salt concentration rather than differences in PCR product (duplex DNA). This points at the variance in fluorescence as one potential factor for the observed variation. Optimization of the reactions could improve this. Furthermore, it should be tested if differences in salt concentration could have influenced the melting profiles. It is possible that the elution buffer from the genomic DNA preparation is not optimal for HRM.

Most of the sequenced T_2 plants had heterozygous mutations (Figure 49) and contained single insertions (Figure 48), according to the prediction with CRISP-ID (Dehairs *et al.* 2016). This fits with the observations of Fauser *et al.* (2014), who also found a significantly higher frequency of insertions than deletions. They also found that most insertions would occur 3 or 4 bases downstream of the PAM sequence, which agrees with our findings.

To separate CRISPR-Cas free T_3 plants, which had outcrossed the CRISPR-Cas construct, form plants which still contained the construct, leaves of seedlings from segregating lines were tested in a novel, simple glufosinate assay. While leaf disc assays with herbicide application or to test stress tolerance have been done before (Biskup *et al.* 2009; Kumar *et al.* 2012), this assay has not been applied for CRISPR-

Cas screening. For most lines, we observed a low false positive rate (< 10%) by PCR validation and a typical 1:3 segregation (Table 8). Since only 25% of all plants do not contain the CRISPR-Cas construct, this simple assay can reduce the cost of screening significantly.

HRM data from T_3 plants showed a better separation within each individual line, if the parental plant was heterozygous for CRISPR-Cas induced mutations. This is demonstrated by HRM analysis on offspring for a line of AtTIP2;3 Guide#2 (Figure 51). Samples separated clearly for all three combinations, i.e. homozygous guanine insertion, homozygous thymine insertion, and heterozygous plants with a guanine insertion in one allele and a thymine insertion in the other allele. Sequencing of two samples allowed to identify both homozygous insertions. *In silico* melting in *uMelt*^{SM} (Dwight *et al.* 2011) confirmed the temperature difference observed between the homozygous mutants and also allowed prediction of melting of heterozygous samples that aligned with the observed curves. This shows that high throughput HRM in combination with sequencing of a few individuals can be used to characterise mutations, without the need to sequence every plant. Homozygous null mutants were also identified for the gene *AtTIP2;2* in the T_3 generation (Figure 49). For the gene *AtTIP2;1*, a homozygous null mutant was identified in the T_2 generation, however, these plants were not progressed into the T_3 generation due to time restrictions and, since, another *AtTIP2;1* insertion line became publically available (Reinhardt *et al.* 2016).

Translation of the coding sequences of *AtTIP2;2* and *AtTIP2;3* with the identified one base insertions showed that these insertions cause frameshift mutations and premature stop codons (Figure 52). We postulate that these changes will make the proteins non-functional.

4.4.3. Conditional short root phenotype for putative *AtTIP2;3* null mutant

Preliminary phenotypic observations of the putative *AtTIP2;3* null mutant revealed a conditional short root phenotype compared to Col-0 wild-type seedlings (Figure 53). Seedlings grown on vertical plates showed a better root elongation compared to seedlings on horizontal plates. The main difference between these two conditions is that roots on vertical plates can grow along the plate, whereas on horizontal plates roots will grow into the agar. This could indicate that null mutants of *AtTIP2;3* have difficulties to penetrate the media. The potential importance of *AtTIP2;3* in roots is supported by observation from the literature showing that *AtTIP2;3* is mainly expressed in the roots (Alexandersson *et al.* 2005; Reinhardt *et al.* 2016). However, promoter-GUS constructs for *AtTIP2;3* in Chapter 3 also indicated some expression in leaves around vascular tissue. In roots, GUS staining was observed in the stele and pericycle (Chapter 3, Figure 31). These results were in line with observations by Gattolin *et al.* (2009), who showed that the protein was localised to pericycle cells within the root by fluorescent microscopy. The pericycle has a main function in lateral root formation. Reinhardt *et al.* (2016) showed that a triple mutant of *AtTIP1;1*, *AtTIP1;2*, and *AtTIP2;1* had a significant reduction in lateral root emergence. They hypothesised that the spatio-

temporal expression of these aquaporins could be important to direct water flow for cell expansion during lateral root formation. While this does not explain the defect in root elongation, the expression pattern should have a significant effect on the function of *AtTIP2;3* in roots. Further experiments should aim to analyse if cell division is disturbed in roots of the putative mutant or if cell elongation could be inhibited due to low turgor pressure. Moreover, off-target analysis by sequencing needs to be performed for the *in silico* predicted off-target sites (Table 6). Off-target #1, which has 3 miss-matches to the CRISPR guide sequence, is located in the coding region of *AtTIP2;1*. While previous research found low off-target activity (Peterson *et al.* 2016), it needs to be confirmed that the observed phenotype is only due to non-functional *AtTIP2;3*.

4.4.4. Conclusion

Genome editing with CRISPR-Cas is a suitable technique to induce targeted mutations in individual aquaporin genes. Screening seedlings for mutations is the main bottleneck. High Resolution Melt analysis is a high-throughput technique enabling screening for mutations in a time and cost effective manner. However, variance between each reaction can make the interpretation of melting data difficult. Optimisation is required to use the full potential of the technique. Putative null mutants for both *AtTIP2;2* and *AtTIP2;3* with CRISPR-Cas induced single insertions were found. The putative null mutant of *AtTIP2;3* shows a strong root phenotype worthy of further investigation.

5. VITIS MANUSCRIPT

In the following chapter, research is presented on plant water relations and aquaporin gene expression in the contrasting *Vitis vinifera* cultivars Grenache (near-isohydric) and Syrah (anisohydric) during drought and rehydration. The research was a collaborative effort between multiple authors as outlined in the manuscript. Currently, this manuscript is being prepared for submission to the scientific journal “Plant, Cell & Environment”.

Statement of Authorship

Title of Paper	A comparison of root and shoot hydraulics, aquaporin expression and leaf gas exachange between isohydric and anisohydric Vitis vinifera cultivars reveals differences in hydraulic control mediated by aquaporins
Publication Status	☐ Published ☐ Accepted for Publication ☐ Submitted for Publication ☑ Unpublished and Unsubmitted w ork w ritten in manuscript style
Publication Details	List of authors: Silvina Dayer, Johannes Daniel Scharwies, Sunita Ramesh, Wendy Sullivan, Franziska Doerflinger, Vinay Pagay and Stephen D Tyerman The manuscript was prepared for intended submission to the journal "Plant, Cell & Environment"

Principal Author

Name of Principal Author (Candidate)	Johannes Daniel Scharwies		
Contribution to the Paper	Performed qPCR analysis with Sunita Ramesh. Conducted data analysis, interpretation, figure design, and wrote the manuscript with Silvina Dayer.		
Overall percentage (%)	30 %		
Certification:	This paper reports on original research I conducted during the period of my Higher Degree by Research candidature and is not subject to any obligations or contractual agreements with a third party that would constrain its inclusion in this thesis. I am the primary author of this paper.		
Signature		Date	27/09/2017

Co-Author Contributions

By signing the Statement of Authorship, each author certifies that:

i. the candidate's stated contribution to the publication is accurate (as detailed above);

ii. permission is granted for the candidate in include the publication in the thesis; and

iii. the sum of all co-author contributions is equal to 100% less the candidate's stated contribution.

Name of Co-Author	Silvina Dayer		
Contribution to the Paper	Conceived the project with Stephen D Tyerman and Vinay Pagay. Carried out the experiments in the glasshouse. Conducted data analysis, interpretation, figure design, and wrote the manuscript with Johannes Daniel Scharwies.		
Signature:		Date	2017-09-27

Name of Co-Author	Sunita Ramesh		
Contribution to the Paper	Performed qPCR analysis with Johannes Daniel Scharwies.		
Signature		Date	28/09/2017

Name of Co-Author	Wendy Sullivan		
Contribution to the Paper	Helped with experiments in the glasshouse and wet lab.		
Signature		Date	28.9.17.

Name of Co-Author	Franziska Doerflinger		
Contribution to the Paper	Helped with experiments in the glasshouse and wet lab.		
Signature		Date	30-9-17

Name of Co-Author	Vinay Pagay		
Contribution to the Paper	Conceived the project with Stephen D Tyerman and Silvina Dayer. Helped with experiments in the glasshouse, data interpretation, and gave feedback on the written manuscript. Will act as corresponding author.		
Signature		Date	29/9/17

Name of Co-Author	Stephen D Tyerman		
Contribution to the Paper	Conceived the project with Vinay Pagay and Silvina Dayer. Helped with experiments in the glasshouse, data analysis and interpretation, and gave feedback on the written manuscript. Will act as senior author.		
Signature		Date	28/9/17.

Please cut and paste additional co-author panels here as required.

A COMPARISON OF ROOT AND SHOOT HYDRAULICS, AQUAPORIN EXPRESSION AND LEAF GAS EXCHANGE BETWEEN ISOHYDRIC AND ANISOHYDRIC VITIS VINIFERA CULTIVARS REVEALS DIFFERENCES IN HYDRAULIC CONTROL MEDIATED BY AQUAPORINS

Silvina Dayer[3*], Johannes Daniel Scharwies[1*], Sunita Ramesh[1], Wendy Sullivan[1], Franziska Doerflinger[2], Vinay Pagay[2†#] and Stephen D Tyerman[1†]

[1]Australian Research Council Centre of Excellence in Plant Energy Biology, Waite Research Institute, School of Agriculture Food and Wine, The University of Adelaide, Waite Campus, PMB 1, Glen Osmond, SA 5064, Australia

[2]School of Agriculture Food and Wine, Waite Research Institute, The University of Adelaide, Waite Campus, PMB 1, Glen Osmond, SA 5064, Australia

[3] Bordeaux Sciences Agro, Institut des Sciences de la Vigne et du Vin, Ecophysiologie et Génomique Fonctionnelle de la Vigne, UMR 1287, F–33140 Villenave d'Ornon, France

*† These authors contributed equally.

[#] Corresponding Author

Corresponding Author

Vinay V. Pagay

email: vinay.pagay@adelaide.edu.au

Abstract

The hydraulic and gas exchange properties of plants that confer either isohydry or anisohydry are still relatively poorly understood. Here we explore how both root and shoot hydraulics, gas exchange, aquaporin expression and abscisic acid (ABA) may be involved and coordinated. A comparison was made between the near-isohydric grapevine cultivar Grenache and the anisohydric cultivar Syrah in a mild water deficit and ABA watering experiment. Grenache showed stronger adjustments of leaf, plant, and root hydraulic conductances to changes in soil moisture availability compared to Syrah. Stomatal conductance of Grenache showed a steeper correlation to ABA concentration in the xylem sap of leaves compared to Syrah. Under well-watered conditions, changes in vapour pressure deficit (VPD) had a strong influence on stomatal conductance in both cultivars with adjustments of leaf hydraulic conductance. Grenache was more sensitive to decreases in soil water availability compared to Syrah, which responded primarily to VPD under the same conditions. Stronger correlations between changes in gene expression of some aquaporin isoforms in leaves and roots and plant hydraulic parameters in Grenache indicates that hydraulic control in Grenache may be mediated via aquaporins. Overall, the results reinforce the hypothesis that both hydraulic and chemical signals significantly contribute to the differences in isohydric and anisohydric behaviour.

Introduction

The water status of the plants is constantly challenged by fluctuating environmental conditions, such as changes in soil water availability and atmospheric humidity. In order to prevent desiccation, plants have evolved complex adaptive mechanisms that allow them to absorb water and minerals from the soil and transport them to the transpiring leaf. These mechanisms are regulated in a dynamic fashion and are based on the interplay between i) the stomatal regulation of water loss during transpiration (Chaves *et al.* 2010); and ii) changes in the hydraulic conductivity of the vascular system, which regulates the flux of water entering the plant through the roots (known as root hydraulic conductivity; L_o; (Maurel *et al.* 2010)) and to the evaporating sites of the leaves (known as stem and leaf hydraulic conductivity, K_{leaf}; (Sack and Holbrook 2006)). In addition, water channel proteins, called aquaporins (AQPs), facilitate the exchange of water across cell membranes playing a key role in regulating the radial flow of water (Steudle 2000; Chaumont and Tyerman 2014). It has been established that AQPs can account for up to 95% of the water permeability of plant cell membranes, representing the most likely candidates for protein-mediated regulation of hydraulic conductance in roots and leaves (Maurel *et al.* 2008; Heinen *et al.* 2009). In grapevine (*Vitis vinifera*), two studies claimed the identification of 23 or 28 AQPs, respectively (Fouquet *et al.* 2008; Shelden *et al.* 2009). They belong to the family of major intrinsic proteins (MIPs). The largest sub-families are called plasma membrane intrinsic proteins (PIPs), which localise mainly to the plasma membrane, and tonoplast intrinsic proteins (TIPs), which localise mainly to the tonoplast.

Stomatal movements, resulting from changes in turgor of the guard cells, involve complex and still debated mechanisms that are mediated by chemical and/or hydraulic signals (Comstock 2002). It is well established that under soil and/or atmospheric water stress, i.e. soil drying or high vapour pressure deficit (VPD), the roots (and shoots) synthesize abscisic acid (ABA), a plant hormone, that is translocated to the leaf via the transpiration stream and reaches the guard cells where it induces stomatal closure (Tardieu and Simonneau 1998; Dodd 2005). Even though ABA signalling is seen as the main pathway for stomatal regulation, hydraulic and/or chemical signals other than ABA have been proposed to contribute significantly (Christmann *et al.* 2007; Wilkinson *et al.* 2007) including the recently reported γ-aminobutyric acid (GABA; (Mekonnen *et al.* 2016)). Evidence for the involvement of a hydraulic root-to-shoot signal has been provided by experiments where wild-type tomato plants were grafted on ABA-deficient roots (Holbrook *et al.* 2002). Despite the inability of the roots to produce ABA, stomata still showed the wild-type response to water deficit. Furthermore, Christmann *et al.* (2007) demonstrated in *Arabidopsis thaliana* that changes in turgor pressure of mesophyll cells in leaves occurred within minutes of root-induced water stress and elicited activation of ABA biosynthesis and signalling required for stomatal closure (Christmann *et al.* 2007). These observations still support a role of ABA in stomatal closure but

question whether it may act as a primary-long distance signal of water stress. Hydraulic mediation of stomatal closure is also supported by studies where large diurnal fluctuations of stomatal conductance (g_s) and leaf water potential (Ψ_{leaf}) were observed without substantial changes in the soil water content (Salleo *et al.* 2000). The co-variation of g_s and Ψ_{leaf} has been interpreted as a mechanism to protect the plant from severe dehydration and consequently, xylem cavitation and loss of hydraulic conductivity (M T Tyree and Sperry 1989). Other studies have suggested the presence of a hydraulic signals after positive correlations between leaf hydraulic conductance and g_s at a relatively constant Ψ_{leaf} (Nardini *et al.* 2001). Recent studies in grapevine suggested that g_s was regulated to a greater degree by hydraulic rather than chemical signals during the early phases of water stress, while ABA seemed to have an additive effect involved in the long-term maintenance of stomatal closure under prolonged water stress (Tombesi *et al.* 2015). According to these studies, the involvement of both hydraulic and chemical signals seems to be a more likely explanation in the regulation of g_s under water stress.

The overall leaf hydraulic conductance comprises the axial and radial flows of water along or between xylem vessels, and the transcellular transport (across cell membranes) in vascular bundles and mesophyll cells (Heinen *et al.* 2009). In certain species, the transcellular path can play a major role as it is efficiently facilitated by aquaporins, contributing to a large extent to the leaf hydraulic conductance (Prado and Maurel 2013). Rapid and reversible changes in K_{leaf} involving AQPs have been observed under fluctuating environmental conditions such as radiation (Prado *et al.* 2013), water stress (Galmes *et al.* 2007) and in response to exogenous application of ABA (Shatil-Cohen *et al.* 2011; Pantin *et al.* 2013). For example in grapevine, K_{leaf} decreased by about 30% under water stress concomitantly with a decrease of expression of some PIPs and TIPs aquaporin isoforms (Pou *et al.* 2013). Furthermore, the authors found significant positive correlations between g_s, K_{leaf} and leaf AQP expression, suggesting a contribution of AQPs in regulating the flow of water under drought and rehydration. In *Arabidopsis*, xylem-fed ABA reduced the inner leaf water transport (K_{leaf}) by specifically decreasing the water permeability of vascular bundle sheath cells, putatively through inactivation of PIPs (Shatil-Cohen *et al.* 2011). In line with that study, Pantin *et al.* (2013) confirmed those observations and proposed a model in which ABA close stomata via its already known chemical effect on guard cells (Simonneau *et al.* 1998), but also via an indirect hydraulic action through a decrease in leaf water permeability triggered within vascular tissues (Pantin *et al.* 2013). According to these findings, the hydraulic signal induced by ABA may be an important component in the mechanisms used by different species to regulate the stomatal conductance under water stress.

In addition to stomatal conductance and K_{leaf} variations, other responses to drought include changes in root hydraulic conductance (L_o; normalized to root dry weight). In contrast to the commonly observed reduction in K_{leaf}, ABA application and water stress have usually opposite effects on L_o: while water stress reduces L_o, ABA increases it in most studies (Aroca *et al.* 2006; Thompson *et al.* 2007; Parent *et al.* 2009).

The increase in L_o by ABA can be interpreted as a mechanism to improve the water supply to the shoot, helping to maintain the water continuum in the plant under soil or atmospheric water stress (Kudoyarova *et al.* 2011; Pantin *et al.* 2013). The opposite effect of ABA on L_o under well-watered and water deficit conditions indicates the action of other unknown regulatory mechanisms. Diurnal changes in L_o have also been observed under well-watered conditions concomitantly with changes in shoot transpiration (Vandeleur *et al.* 2009). In general, these variations correlate with the transcript abundance of root aquaporins suggesting that the water transport across the roots is regulated by AQPs to meet the transpirational demand of the shoots (Sakurai-Ishikawa *et al.* 2011; Laur and Hacke 2013; Vandeleur *et al.* 2014). Accordingly, these studies support the hypothesis of shoot-to-root signalling via the xylem (either chemical or hydraulic) that regulates L_o in response to transpiration and that is modulated by aquaporins (Vandeleur *et al.* 2014). Positive correlations between L_o, g_s and leaf transpiration have also been observed in grapevine exposed to exogenous ABA applications suggesting a connection between ABA-mediated root and leaf conductances that requires further examination (DeGaris 2016).

The leaf bundle sheath and root endodermis cells (and other xylem parenchyma cells) are thought to be important sites regulating the water supply of leaves and roots, respectively (Sack and Holbrook 2006; Shatil-Cohen *et al.* 2011). While changes in K_{leaf} and L_o have been examined in numerous studies, any coordination between them has received less attention. The hydraulic and chemical (ABA-mediated) mechanisms, described before, that operate between roots and leaves to control g_s are particularly important in understanding the iso/anisohydric behaviors reflecting the strategies of various species and even cultivars to cope with water stress (Pantin *et al.* 2013). In isohydric plants, leaf water potential (Ψ_{leaf}) is maintained relatively constant under declining soil moisture availability through a tight regulation of stomatal aperture (Simonneau *et al.* 1998). In contrast, anisohydric plants maintain g_s to prioritize photosynthesis, which is related to a more variable Ψ_{leaf}. These differences in the regulation of g_s are apparently associated with differences in the perception of ABA (Simonneau *et al.* 1998). For instance, Grenache, a cultivar described as near-isohydric (Schultz 2003), showed a higher sensitivity of g_s to changes in vapour pressure deficit (VPD) that were correlated with higher levels of ABA in the xylem sap (Soar *et al.* 2006). In contrast, Syrah described as anisohydric and considered less drought tolerant that Grenache, did not show this sensitivity. Therefore, isohydric behavior has been linked to an interaction between hydraulic and chemical (ABA) information, whereas anisohydric behaviour has not been related to such interaction (Simonneau *et al.* 1998). Changes in plant hydraulic conductance and the expression of AQPs in leaves and roots, has also been correlated with the degree of iso/anisohydry (Lovisolo *et al.* 2010). Differences in the hydraulic conductance of petioles were suggested to underlie the different stomatal behaviour displayed by two grapevine cultivars (Schultz 2003). Under water stress, the root hydraulic conductance in Grenache was reduced in a greater extent than in Chardonnay paralleling the drop of stomatal conductance (Vandeleur *et al.* 2009). However, only Chardonnay, the less drought

tolerant cultivar, seemed to compensate for that reduction by increasing the expression of AQPs (Vandeleur *et al.* 2009). Those studies revealed that in isohydric plants, the roots adjust the water conductance in concert with leaf stomata to maintain a more constant water potential.

The present study aims to elucidate how the iso/anisohydric behaviour displayed by two grapevine cultivars is related with their hydraulic responses of roots and leaves in relation to stomatal regulation. Accordingly, a comparative study was conducted in Grenache (near-isohydric) and Syrah (anisohydric) to evaluate the relationships between g_s, K_{leaf} and L_o, under mild water deficit and recovery (potentially resulting in endogenous ABA biosynthesis), and exogenous application of ABA. In addition, the expression of PIP and TIP aquaporins in roots and leaves were quantified to determine the extent to which these proteins contributed to the different water use strategies of these cultivars. We hypothesized that the more isohydric Grenache regulates its stomata under water stress and/or exogenous ABA application by decreasing L_o concomitantly with g_s and K_{leaf} to maintain a more constant Ψ_{leaf}. This behaviour is mediated by a down-regulation of leaf AQPs. In contrast, the relatively anisohydric Shiraz maintains L_o under water deficit through an up-regulation of root AQPs in order to maintain g_s and K_{leaf}.

Materials and Methods

Experimental site and plant material

The experiments were carried out in 2015 and 2016 at The Plant Accelerator®, University of Adelaide, Waite Campus located in Urrbrae (Adelaide), South Australia (34° 58' 17'' S, 138° 38' 23'' E). One-year-old rootlings of own rooted grapevines (*Vitis vinifera* L.) cvs. Grenache and Syrah were planted in 4.5 L pots containing a mixture of 50 % vermiculite and perlite and 50 % of UC soil mix (61.5 L sand, 38.5 L peat moss, 50 g calcium hydroxide, 90 g calcium carbonate and 100 g Nitrophoska® (12:5:1, N:P:K plus trace elements; Incitec Pivot Fertilisers, Southbank, Vic., Australia) per 100 L at pH 6.8. Plants were grown for two months in a temperature-controlled glasshouse (day/night: approx. 25/20 °C) and irrigated to field capacity every three days from December 21st 2015. The vines were pruned to two shoots 10 days after bud burst (January 10th, 2016) and oriented upright during their development using wooden stakes. A liquid soil fertiliser (Megamix 13:10:15 N:P:K plus trace elements; Rutec, Tamworth, Australia) at a concentration of 1.6 mL L^{-1} was applied as required to bring all plants to approximately equal size. The fertiliser was applied weekly for three weeks once the plants had developed the first adult leaves. On the 25th February 2016, all vines were moved from the greenhouse and transferred to a DroughtSpotter (Phenospex, Netherlands) automated gravimetric watering platform where individual pots were automatically weighed continuously (15 min intervals) and watered twice daily (0600 h, 1600 h) based on the plant weight loss by transpiration. All plants were irrigated to their field capacity weights (determined the previous days) daily until the start of the experiment. Day and night temperatures in the DroughtSpotter glasshouse were kept at 25/20 ºC, respectively.

Treatments

Grenache and Syrah vines were used to examine the effects of water deficit (WD) and recovery by re-watering (REC) on stomatal conductance (g_s) and root hydraulic conductance (L_o; normalized to root dry weight). A set of vines were kept as control (well-watered; WW), irrigated to field capacity and weight to replace the amount of water consumed by transpiration daily. Water deficit was imposed by reducing the amount of irrigation until a defined value of leaf maximum daily g_s of approx. 50 mmol H_2O m^{-2} s^{-1} (Medrano *et al.* 2002) was reached. After maintaining g_s at about 50 mmol m^{-2} s^{-1} for three days, vines were rehydrated by irrigating the pots to field capacity and recovery from water stress was examined after seven days. An additional treatment consisting of an exogenous application of ABA was simultaneously carried out on a separate set of vines from both cultivars. In this treatment, the vines were root-fed by applying 50 µM of ABA (Valent Biosciences Corporation, Libertyville, IL, USA) daily to the root system concurrently with irrigation. The selected concentration of ABA application was based on prior experiments, which showed that 50 µM of ABA applied to the root system of potted vines is required to

have a significant effect on g_s (DeGaris et al., 2015). All the pots were covered with a thick layer of perlite to minimize evaporation from the soil.

The night before each measurement day, selected vines from each treatment were moved from the DroughtSpotter glasshouse to an adjacent glasshouse with identical environmental conditions for physiological measurements and tissue sampling for gene expression analysis. The measurement days were: i) well-watered (WW) vines only on the day before the experiment commenced (Day 0); ii) WW and WD vines the day water deficit and ABA treatments achieved a stomatal conductance of ~50 mmol H_2O m^{-2} s^{-1} (Day 5); iii) WW, WD, and ABA vines three days after g_s reached ~50 mmol m^{-2} s^{-1} and was held constant in WD and ABA vines (Day 7); and, iv) WW and REC vines seven days after rewatering was performed in REC vines (Day 14). At each time point, three to five WW vines were used as 'controls' to compare against the specific treatment(s).

Physiological measurements

Leaf gas exchange

In order to track stomatal conductance (g_s) and establish the desired stress level in WD and ABA treatments, daily measurements of g_s were performed in all vines on the DroughtSpotter platform on fully-expanded leaves (estimated minimum leaf age: [Leaf Plastochron Index >10]) in the basal section of the shoots using a porometer (SC-1, Decagon Devices, Pullman, WA, USA). Measurements were performed every day at mid-morning (10:30-11:30 h) on two leaves per treatment and replicate.

On the specific sampling dates, leaf net assimilation rate (A), g_s and transpiration (E) were measured concomitantly with the rest of physiological measurements between 10:00 and 11:00 h. Measurements were performed on two fully-expanded, healthy leaves using an open system infrared gas analyzer (LI-6400XT, LI-COR Biosciences Inc., Lincoln, NE, USA) with a 6 cm^2 cuvette. An external LED light source (LI-6400 -02B) attached to the cuvette was used at a fixed PAR value of 1500 µmol m^{-2} s^{-1} due to the non-saturating light levels in the glasshouse for photosynthesis (approx. 200 µmol m^{-2} s^{-1}). After gas exchange measurements were performed, the same leaf was excised to determine Ψ_{leaf}.

Leaf water potential and sap collection for ABA analysis

Predawn, leaf and stem water potentials were measured on adult, primary leaves of vines on the specific sampling dates. Predawn leaf water potential (Ψ_{PD}) was measured before sunrise (04:00-05:00 h), and leaf (Ψ_{leaf}) and stem (Ψ_{stem}) water potentials around midday (11:00-12:00 h). Stem water potential was measured after leaves had been sealed in aluminum foil and plastic bags for two hours, to allow equilibration of water potentials. One leaf per plant was measured from three to five plants per group using a Scholander-type pressure chamber (PMS Instruments Co, Albany, OR, USA).

After recording leaf water potential values, an overpressure of 0.5 MPa was applied to the encapsulated leaf for xylem sap collection (approx. 35 µL). Sap was collected from the cut surface of the protruding petiole using a micropipette and transferred to a pre-weighed and labelled micro tube before snap freezing in liquid nitrogen. Samples were stored at -80 °C until subsequent analysis of ABA.

ABA analysis of xylem sap

ABA concentration in xylem sap samples ($[ABA]_{xylem}$) was analysed as described in (Speirs *et al.* 2013). Briefly, the volume of each sample was measured using a pipette for normalisation. Each sample was mixed with 30 µL of deuterated standard (Plant Biotechnology Institute, Saskatoon, SK, Canada) containing deuterium-labelled analogues of ABA, phaseic acid (PA), dihydrophaseic acid (DPA) and the glucose ester of ABA (ABA-GE) at a concentration of 100 ng mL^{-1} each. Solids were precipitated in a centrifuge at 12,470 × g for 5 min. From each sample, 20 µL supernatant was transferred to a LC/MS tube and analysed by liquid chromatography/mass spectrometry (Agilent 6410 Triplequadroplope LC-MS/MS with Agilent 1200 series HPLC, Agilent Technologies Inc. Santa Clara, USA). A Phenomenex C18(2) column (75 mm × 4.5 mm × 5 µm; Phenomenex, Torrance, CA, USA) was used at 40 °C and samples were eluted with a 15 min linear gradient of 10 % to 90 % acetonitrile. Nanopure water and acetonitrile were both mixed with 0.05% acetic acid. Compounds were identified by retention times and mass/charge ratio.

Hydraulic conductance of leaves, plant and roots

Leaf and whole plant hydraulic conductance (K_{leaf} and K_{plant}) were determined using the evaporative flux method (Flexas et al. 2013). This measurement is based on the relationship between the driving leaf transpiration rate (E) and the water potential gradient ($\Delta\Psi$) when leaf water potential reaches a steady state. In this case hydraulic conductance is calculated as follows: $K_{leaf}=E/(\Psi_{stem} - \Psi_{leaf})$ and $K_{plant}=E/(\Psi_{PD} - \Psi_{leaf})$.

The hydraulic conductance of the entire root system was measured for the same plants using a High Pressure Flow Meter (Dynamax, Houston, TX, USA) as previously described in Vandeleur et al. (2009). This is a destructive technique whereby the stem of the vine is cut above the soil surface, covered with filtered deionized water and the stump connected to the High Pressure Flow Meter with a water-tight seal as quickly as possible, typically within 1 min. A transient ramp in pressure with simultaneous recording of flow rate was used to calculate hydraulic conductance and normalized by dividing the conductance by the total root dry weight (L_o). All measurements were conducted with 5 minutes of shoot excision. The soil was washed from the roots before drying at 60 °C for more than 48 h prior to weighing.

AQPs expression in roots and leaves

Samples of leaves and roots were collected from vines immediately after physiological measurements for subsequent analysis of AQP transcript abundance by quantitative reverse transcription PCR (RT-qPCR). Leaves were immediately immersed in liquid nitrogen and stored at -80 °C until analysis. Roots were carefully selected from the bottom and upper parts of the pot in order to get the thinner, white and more functional roots. The root samples were quickly washed to remove soil particles and dried with tissue paper before being submerged in liquid nitrogen.

Leaf and root material was ground to a fine powder in liquid nitrogen using a mortar and pestle. For leaves, total RNA was extracted from 100 mg of fine frozen powder using the Spectrum Plant Total RNA extraction Kit (Sigma-Aldrich, St. Louis, MO, USA). DNA contamination was avoided by digestion with the On-Column DNase I Digestion Set (Sigma-Aldrich, St. Louis, MO, USA) during RNA extraction according to manufacturer recommendations. For roots, RNA extractions were performed as described by Vandeleur et al. (2014). RNA was extracted from 200 mg of fine frozen powder with a 20 mL sodium perchlorate extraction buffer (5 M sodium perchlorate, 0.2 M Tris pH 8.3, 8.5 % (w/v) polyvinylpolypyrrolidone, 2 % PEG 6000, 1 % (w/v) SDS, 1 % (v/v) *β*-mercapto-ethanol) for 30 min at room temperature. The lysate was filtered through a glass wool filter and mixed with 30 mL of cold absolute ethanol before precipitation at -20 °C overnight. After centrifugation at 3500 rpm for 20 min at 4 °C, the pellets were washed with cold ethanol and purified using the Spectrum Plant Total RNA Extraction Kit with on-column DNase digestion as described for leaves. Concentration and purity of total RNA were determined on a NanoDrop™ 1000 Spectrophotometer (Thermo Fisher Scientific Inc., MA, USA). Agarose gel electrophoresis (1.2 % agarose) was done to visualize the integrity of RNA.

For cDNA synthesis, 1 µg of total RNA was reverse transcribed using iScript™ cDNA Synthesis Kit for RT-qPCR (Bio-Rad, CA, USA) according to manufacturer instructions.

Gene expression analysis was carried out by quantitative reverse transcription PCR (RT-PCR) (QuantStudio™ 12K Flex; ThermoFisher Scientific Inc., MA, USA). For standard curves, 1:10 serial dilutions of purified PCR products were made in the range of 10^6 to 10 copies/reaction. RT-qPCR was performed in a 10 µL reaction volume containing 1 µL of either the serial dilution or undiluted cDNA, 5 µL KAPA SYBR® FAST Master Mix (2X) Universal (Kapa Biosystems Inc., MA, USA), 100 nM of gene-specific primers, and 0.2 µL of ROX Reference Dye Low (50X). The thermal cycling conditions were: one cycle of 3 min at 95 °C followed by 40 cycles of 16 s at 95 °C and 20 s at 60 °C. Subsequently, melting curves were recorded from 60 to 95 °C at a ramp rate of 0.05°C/s. Normalized relative quantities (NRQ) of gene expression were calculated between the gene of interest (goi) and two reference genes (ELF, GAPDH) taking differences in PCR efficiency (E^{Ct}) into account (Pfaffl 2001; Hellemans *et al.* 2007):

$$NRQ = \frac{E_{goi}^{Ct,goi}}{\sqrt{E_{ELF}^{Ct,ELF} * E_{GAPDH}^{Ct,GAPDH}}} \quad (1)$$

Overall, a mean NRQ value and standard error were calculated from five independent biological replicates. The absence of non-specific products was confirmed by analysis of the melt curves. Sequences for the gene-specific primers were used from Tashiro *et al.* (2016) (*GAPDH*) and Shelden (2008) (*ELF, PIP1;1, PIP2;2, PIP2;3, TIP1;1*) or designed using NCBI Primer-Blast (Ye *et al.* 2012) (*PIP2;1, TIP2;1*) (Supplementary Table 1). Log_2 ratios for the heatmap were calculated between the mean NRQ of the WW controls and the mean NRQ of WD, ABA or REC.

Statistical Analyses

Analysis of variance (ANOVA) was performed using Infostat software (version 1.5; National University of Córdoba, Córdoba, Argentina). The means were compared using Fisher's multiple range test ($p \leq 0.05$) when appropriate, and significant interactions between treatments are indicated and described in the text. Pearson correlation coefficients and multiple linear regressions were calculated in the statistical language R (R Core Team, 2017). Correlation maps were constructed using the R package *corrplot* (Wei and Simko, 2016). Only correlations which were significant at $p \leq 0.05$ are shown in the correlation maps. Linear regressions and Mann-Whitney test were performed using GraphPad Prism version 7.00 for Windows (GraphPad Software, La Jolla California USA). Figures, except correlation maps, were created in GraphPad Prism.

Results

Water relations of mild water deficit and ABA watered vines

Potted vines of the near-isohydric grape cultivar Grenache and the anisohydric cultivar Syrah were subjected to four different treatments on the DroughtSpotter platform and g_s was monitored using a porometer. Well-watered (WW) vines were maintained at a constant soil water content for maximum g_s (Fig. 1); mild water deficit vines (WD) were not watered until g_s reached approx. 50 mmol m^{-2} s^{-1} (Fig. 1a, Day 4), after which the same deficit was maintained for two more days (Fig. 1b, Day 6); ABA watered (ABA) vines that were watered with 50 µM ABA solution until g_s reached approx. 50 mmol m^{-2} s^{-1} as well (Fig. 1b, Day 6), and d) recovery (REC) vines originated from the WD treatment that were re-watered after Day 6 to WW levels (Fig. 1c, Day 13).

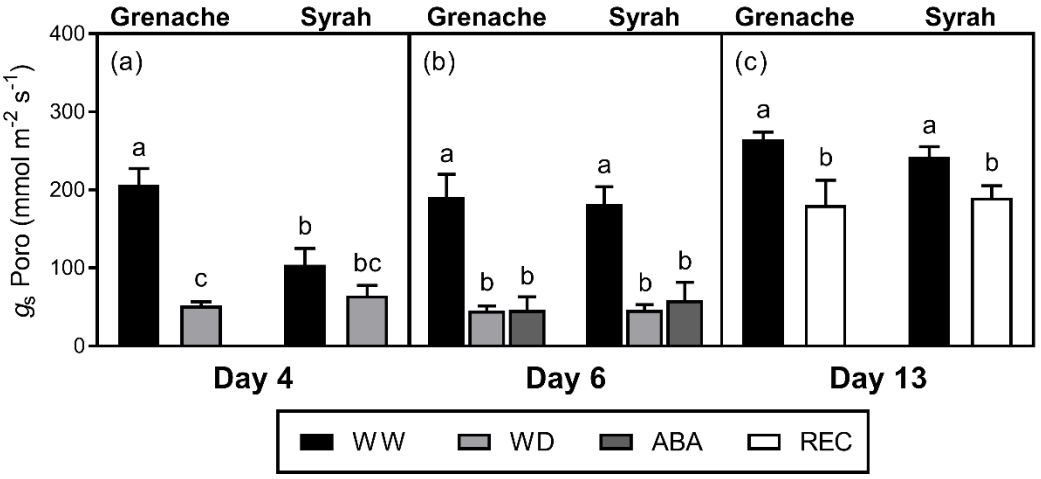

Figure 1. Stomatal conductance as measured with a porometer (g_s Poro; a-c) in Grenache and Syrah grapevines under mild water deficit (WD), exogenous application of abscisic acid (ABA) and recovery from water stress (REC) at different sampling days along the experiment. Well-watered (WW) vines were measured at each time point and used as control. The WD vines were first sampled at Day 4 when the desired g_s value was achieved (~50 mmol m^{-2} s^{-1}) and at Day 7 after the stress was sustained for three days. Recovery vines were sampled after seven days of re-watering at WW levels. Values are means ±SE (n=5). Different letters indicate statistically significant differences between treatments and cultivars ($p \leq 0.05$) by Fisher's LSD test.

Due to significant differences in vapour pressure deficit (VPD) between sampling days when physiological measurements were made (Supplementary Fig. S1), g_s measured by infrared gas analysis (IRGA) varied somewhat, therefore relative g_s was calculated for the treatments WD, ABA, and REC relative to the WW controls on the same days (Fig. 2a-c). The WD vines of the near-isohydric cultivar Grenache showed a significantly larger reduction in g_s compared to the anisohydric cultivar Syrah on Day 5 (Fig. 2a), while no

differences in soil and plant water status (Ψ_{PD}, Ψ_{leaf}, Ψ_{stem}) were observed between WD vines of both cultivars (Fig. 2d, g, j). However, significantly lower Ψ_{PD}, Ψ_{leaf}, and Ψ_{stem} were measured in WD vines of both cultivars compared to WW vines. A range of Ψ_{PD}, which is an estimate of soil water potential, from -0.2 to -0.5 MPa was measured in WD vines for days 5 and 7 (Fig. 2d, e). On Day 7, WD vines from both cultivars showed a similar reduction of g_s relative to WW plants after being exposed to the same deficit for 3 days (Fig. 2b), however a significantly lower Ψ_{PD} was measured for WD vines of Syrah compared to Grenache. At the same time, WD vines of Syrah also had a lower Ψ_{leaf} compared to Grenache, while Ψ_{stem} was not significantly different (Fig. 2h, k). The ABA vines, which had a g_s of approximately 50 mmol m^{-2} s^{-1} on Day 6 (Fig.1b) and was not significantly different from the WD vines, showed a significantly larger reduction of g_s relative to the WW and WD vines on Day 7 (Fig. 2b). ABA-treated Grenache vines had significantly lower relative g_s compared to ABA-treated vines of Syrah. Despite adequate soil moisture, ABA-treated vines of both cultivars had a similar Ψ_{leaf} and Ψ_{stem} to that of WD vines (Fig. 2h, k). When WD vines were recovered (REC) for seven days, they showed no significant differences in vine water status compared to the WW vines (Fig. 2c, i, l).

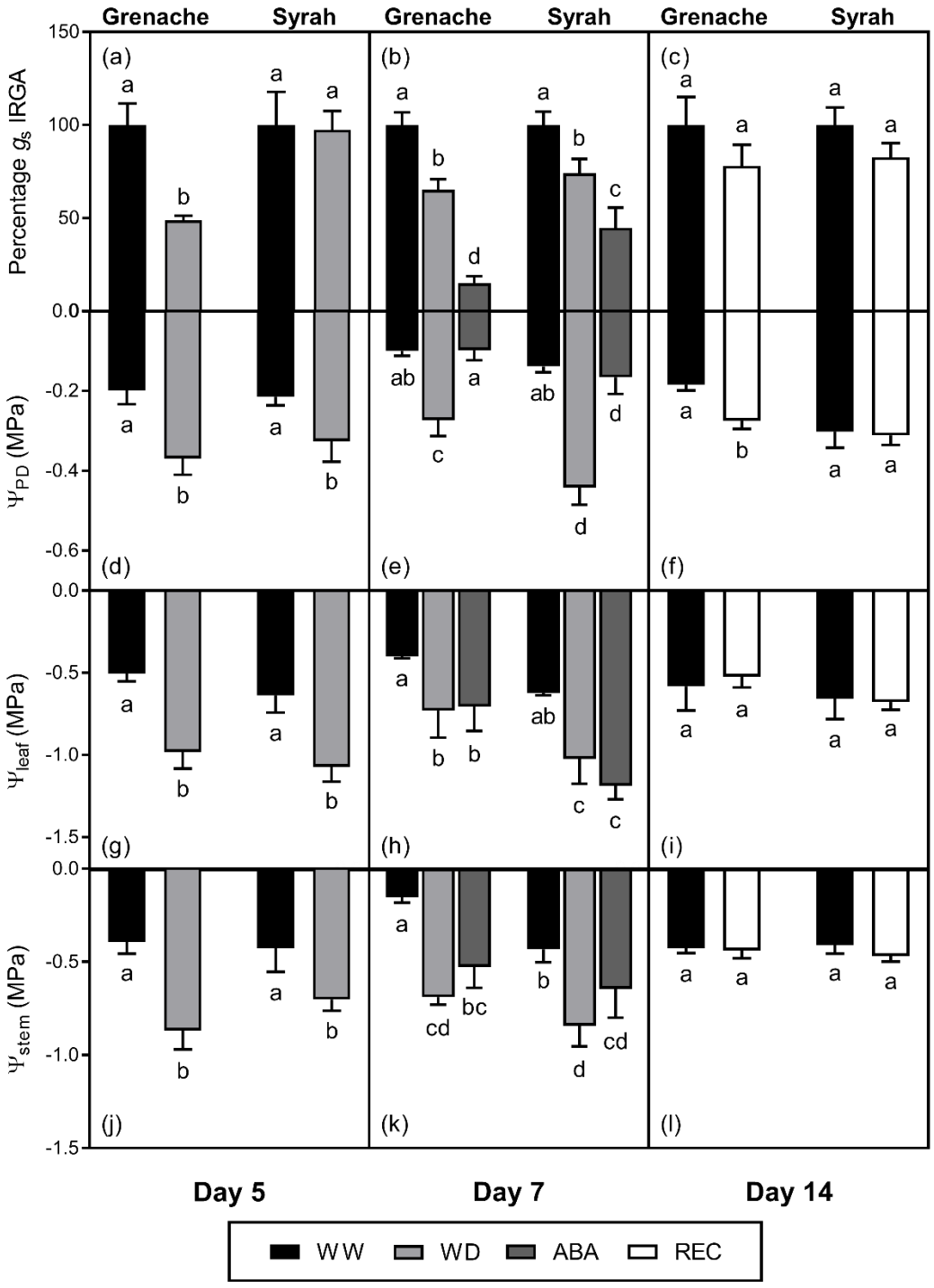

Figure 2. Stomatal conductance relative to WW controls measured with the IRGA (g_s IRGA; a-c), pre-dawn (Ψ_{PD}; d-f), leaf (Ψ_{leaf}; g-i) and stem (Ψ_{stem}; j-l) water potentials in Grenache and Syrah grapevines under mild water deficit (WD), exogenous application of abscisic acid (ABA) and recovery from water stress (REC) at different sampling days along the experiment. Values are means ±SE (n=5). Different letters indicate statistically significant differences across all treatments and cultivars within the day ($p \leq 0.05$) by Fisher's LSD test.

Correlations between physiological parameters and aquaporin gene expression

The statistical relationship between the measured plant physiological parameters and gene expression of selected aquaporins is shown in the split correlogram for WW vines in Fig. 3a and for the combination of WW and WD vines in Fig. 3b. The data for Grenache are shown in the upper triangle and data for Syrah are shown in the lower triangle of each correlogram divided by a black diagonal line. Specific categories of columns (col) are labelled along the bottom (A to F) and rows (row) on the right hand side (1 to 6) to enable reference (e.g. col A, row 1) to relevant sets of correlations.

Since environmental conditions, like vapour pressure deficit (VPD, Supplementary Fig. S1) changed significantly between different days of the experiment, measurements on WW vines were also variable. A correlogram for WW vines only (Fig. 3a) was used to explore the primary sources and effects of this variability in the data, by excluding all other treatments. Within the recorded physiological parameters (upper left black box), some were significantly correlated to VPD_{leaf}. Gas exchange parameters, g_s and *E,* were positively correlated to VPD_{leaf} for well-watered vines in both cultivars (col A, row 6, Fig. 3a). Additionally, K_{leaf} and K_{plant} were positively correlated to VPD_{leaf} for well-watered vines of Grenache (col D, row 6, Fig. 3a) but not for K_{plant} in Syrah (col A, row 3). No significant correlation was found between root hydraulic conductance (L_o), and VPD_{leaf}. Also, expression of some AQP genes was correlated to VPD_{leaf}. Gene expression of *PIP2;2* in roots was positively correlated to VPD_{leaf} in well-watered vines of Grenache (col F, row 6), while in well-watered vines of Syrah, *PIP2;3* in leaves and *PIP1;1* in roots were negatively and positively correlated to VPD_{leaf}, respectively (col A, rows 2,1). While g_s and *E* increased with increasing VPD_{leaf} for both cultivars, only Syrah showed negative correlations with Ψ_{leaf} and Ψ_{stem} (col A, row 4; Fig. 3a). ABA concentration in the xylem of leaves from well-watered plants ($[ABA]_{xylem}$) showed very few significant correlations to other parameters in general (col B and row 5, Fig. 3a). None of the gas exchange and hydraulic conductance parameters correlated to xylem ABA concentration $[ABA]_{xylem}$, however $[ABA]_{xylem}$ of WW vines from Grenache (143.5 ± 25.26 ng mL^{-1}, n=13) was higher (p = 0.0019) compared to leaves of WW vines from Syrah (43.77 ± 3.731 ng mL^{-1}, n=11).

Data from WW and WD vines were combined and a second correlogram was developed to investigate the relationships between plant physiological parameters and root and leaf AQP gene expression during the transition from well-watered to water deficit conditions (Fig. 3b). In contrast to WW vines only, g_s was not significantly correlated to VPD_{leaf} for both cultivars once data of WD vines were included, but negative correlations were observed to $[ABA]_{xylem}$ (col A, row 5 and col B, row 6; Fig. 3b). This correlation was stronger in Grenache where g_s also correlated with Ψ_{PD} and Ψ_{stem} (col C, row 6, Fig. 3b) unlike Syrah. VPD_{leaf} correlated positively to *E* only in Syrah but not in Grenache. K_{leaf} and K_{plant} (col D row 6, Fig. 3b) also showed correlations to g_s and *E* in the cultivar Grenache. While K_{leaf} was not correlated to $[ABA]_{xylem}$ in both cultivars, K_{plant} (r = -0.60, p = 0.005) was negatively correlated to $[ABA]_{xylem}$ for both cultivars (col

D row 5 & col B row 3, Fig. 3b). L_o was positively correlated with E, g_s, Ψ_{leaf} and Ψ_{stem} only for Grenache where it was also negatively correlated to $[ABA]_{xylem}$ (col D, rows 3-6).

The expression of AQPs showed different patterns between the two cultivars (compare top right quadrant for Grenache (cols E-F, rows 3-6) with bottom left quadrant for Syrah (cols A-D, rows 1-2, Fig. 3b). Notable differences are: the absence in Grenache of the negative correlations between leaf *TIP1;1* and gas exchange parameters in Syrah (col A, row 2), and the absence in Syrah of the positive correlations between leaf *TIP2;1* and g_s and E in Grenache (col E row 6). However, leaf *TIP2;1* in Syrah was more positively correlated with Ψ_{leaf} (col C row 2). In Grenache, expression of leaf *PIP2;2* was positively correlated to E, water potentials and K_{plant} (col E rows 3-6), while for Syrah positive correlations with g_s, E, K_{leaf} and K_{plant} (cols A-D row 2) were observed.

The two most highly expressed aquaporins in roots (*PIP1;1* and *PIP2;2*) also showed differences between the two cultivars (cols A-D row 1 and col F rows 3-6). Root *PIP1;1* for Grenache was positively correlated with g_s, E and K_{plant} while Syrah showed no significant correlations for these parameters. Similar to leaves, expression of *PIP2;2* in roots of Grenache was positively correlated to g_s and E, water potentials and K_{plant} (col F rows 3-6), but not to L_o. In Syrah these were notably absent except for a positive correlation with Ψ_{PD}. Root *TIP2;1* showed positive correlations to g_s, E, Ψ_{stem} and K_{plant} in Grenache, but only positive correlations to water potentials in Syrah (similar to leaf *TIP2;1*). In both cultivars, root *PIP2;2* and *TIP2;1* were negatively correlated to $[ABA]_{xylem}$ (col B row 1 and col F row 5). Interestingly, no significant correlations were found between any aquaporins and L_o.

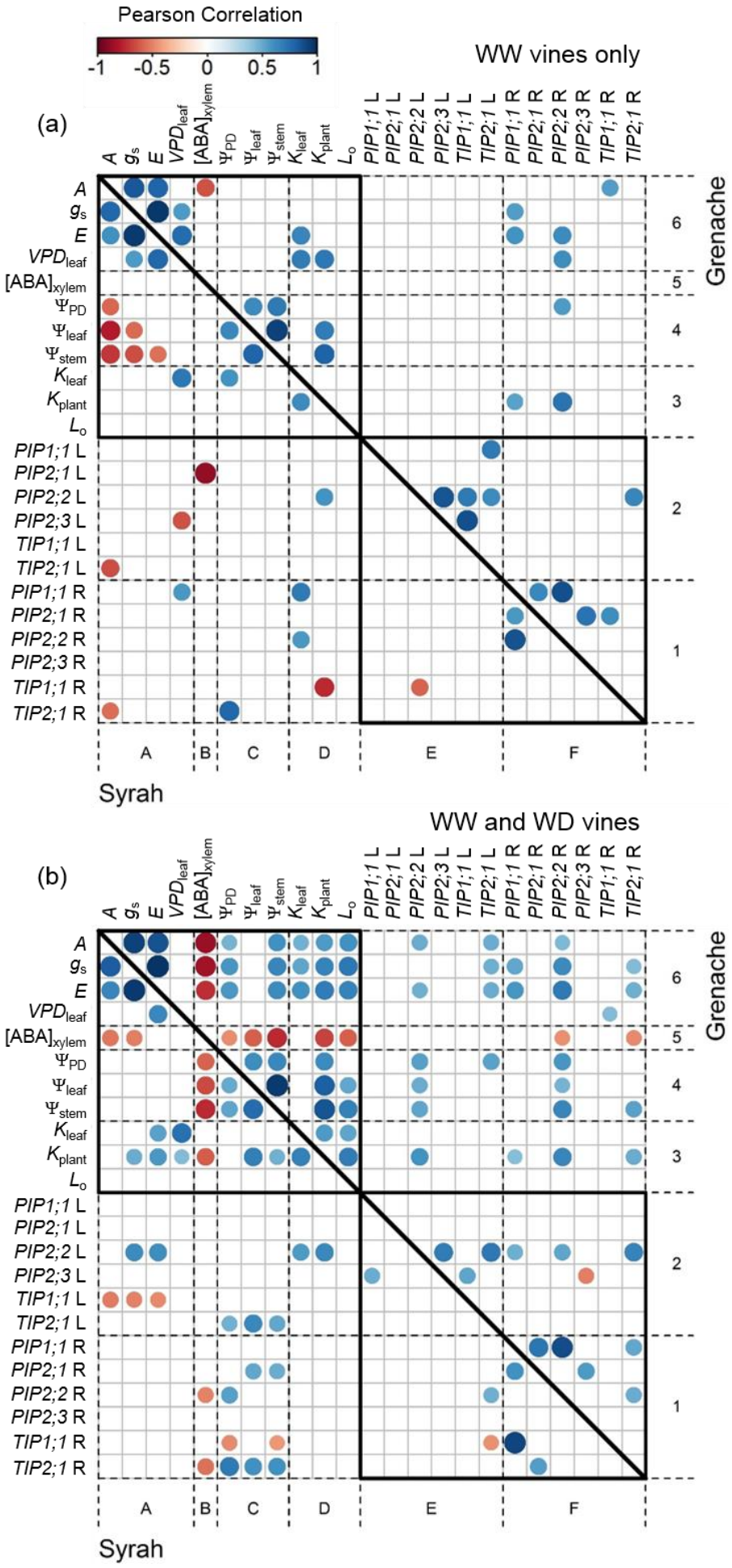
Pearson Correlation
-1
-0.5
0
0.5
1
(a)
WW vines only
Grenache
Syrah
(b)
WW and WD vines
Grenache
Syrah
A
gs
E
VPDleaf
[ABA]xylem
ΨPD
Ψleaf
Ψstem
Kleaf
Kplant
Lo
PIP1;1 L
PIP2;1 L
PIP2;2 L
PIP2;3 L
TIP1;1 L
TIP2;1 L
PIP1;1 R
PIP2;1 R
PIP2;2 R
PIP2;3 R
TIP1;1 R
TIP2;1 R
6
5
4
3
2
1
A
B
C
D
E
F

Figure 3. Correlation maps (correlograms) of plant physiological parameters and gene expression in leaves and roots of the cultivars Grenache (upper triangle) and Syrah (lower triangle). (a) Correlations based on data from well-watered vines (WW) only and (b) correlations based on combined data from well-watered (WW) and mild water deficit (WD) vines. The exogenous ABA treated vines and recovery from mild water deficit (REC) treatments were excluded from the analysis. Only significant Pearson correlations coefficients ($p \leq 0.05$) are shown. Significant positive correlations are shown in blue, while significant negative correlations are shown in red. $[ABA]_{xylem}$ was log10 transformed before the analysis. Expression of aquaporin genes measured in leaves are denoted with an "L" (e.g. *PIP1;1* L), while expression in roots are denoted with an "R" (e.g. *PIP1;1* R).

Influence of changes in VPD on well-watered vines

A closer examination of the correlation between g_s and VPD_{leaf} (Fig. 3a) in WW vines of Grenache ($r = 0.57$, $p = 0.034$) and Syrah ($r = 0.56$, $p = 0.036$) revealed a similar response of increasing g_s with increasing VPD in the range of 2 to 3 kPa, but significantly higher g_s in Grenache compared to Syrah (Fig. 4).

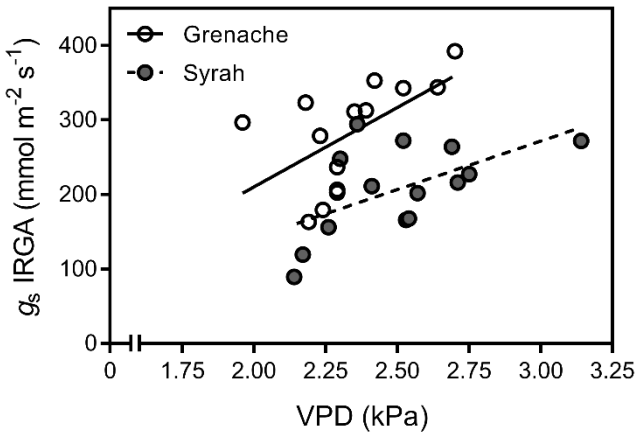

Figure 4. Relationship between stomatal conductance and VPD for well-watered vines (Days 0, 5, 7, 14) during the experiment (both measured with the IRGA). The slopes for both linear regressions are significantly positive ($p \leq 0.05$), but not significantly different between the two cultivars. However, the elevations are significantly different ($p = 0.0002$).

While the correlogram for WW vines (Fig. 3a) showed that K_{leaf} was only positively correlated to E in the cultivar Grenache, linear regressions show that data from both Grenache and Syrah fall on the same line (Fig. 5). The correlation between K_{leaf} and E is just short of being significantly positive ($p = 0.052$). Grenache had a significantly higher K_{leaf} relative to Syrah under well-watered conditions (insert Fig.5).

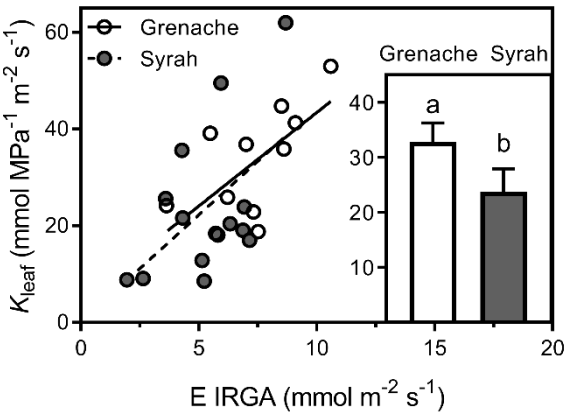

Figure 5. Relationship between K_{leaf} and E for well-watered vines. For both cultivars, the points fall on the same line. In Grenache, this positive correlation is significant ($r^2 = 0.65$, $p = 0.030$) while in Syrah it is almost significant ($r^2 = 0.53$, $p = 0.052$). Insert: comparing the mean K_{leaf} between the two cultivars showed that Grenache had a significantly higher K_{leaf} compared to Syrah ($p = 0.04$, Mann-Whitney test).

Similar to K_{leaf}, significant higher K_{plant} were measured for the cultivar Grenache, compared to Syrah (Gr.: 18.5 ± 2.2 mmol MPa^{-1} m^{-2} s^{-1}, n=14; Sy.: 11.1 ± 1.0 mmol MPa^{-1} m^{-2} s^{-1}, n=14; $p = 0.0058$) and L_o (Gr.: 7.3 x 10^{-6} ± 1.0 x 10^{-6} kg s^{-1} MPa^{-1} g^{-1}, n=11; Sy.: 1.7 x 10^{-6} ± 5.3 x 10^{-7} kg s^{-1} MPa^{-1} g^{-1}, n=12; $p = 0.0002$). Correlations between E and K_{plant} were not significant at $p \leq 0.05$, but correlation coefficients were positive for both Grenache ($r = 0.50$, $p = 0.067$), which was close to being significant, and Syrah ($r = 0.37$, $p = 0.194$). The correlations between E and L_o were also not significant at $p \leq 0.05$, but for Grenache ($r = 0.51$, $p = 0.108$) a positive correlation coefficient was found, while for Syrah ($r = -0.08$, $p = 0.796$) the correlation coefficient was close to zero. The water potential gradient between stem and leaf ($\Psi_{stem} - \Psi_{leaf}$) did not show any significant change in well-watered vines of both cultivars in relation to changes in E ($r < 0.15$, $p > 0.6$).

Effects of mild water deficit and ABA treatment in Grenache and Syrah

A multiple linear regression model developed for each cultivar indicated that in Grenache, the soil water availability, given by Ψ_{PD}, is the main factor that explains changes in g_s and overrides any effect of changes in VPD. In contrast, changes in g_s in Syrah are primarily explained by VPD (Table 1).

Table 1. Multiple linear regression model to predict changes in stomatal conductance (g_s) in response to environmental changes like vapour pressure deficit (VPD_{leaf}) and predawn water potential (Ψ_{PD}), which reflects the soil water availability. Model formula = $g_s \sim VPD_{leaf} + \Psi_{PD}$. Input: all data pooled from well-watered, water deficit, and recovery vines from the cultivars Grenache and Syrah. The variables VPD_{leaf} and Ψ_{PD} were centred before running the multiple linear regression.

	Grenache			**Syrah**		
	Estimate	**Std. Error**	**P value**	**Estimate**	**Std. Error**	**P value**
(Intercept)	223.76	15.06	< 0.001 ***	177.15	10.76	< 0.001 ***
***VPD*leaf**	16.46	74.07	0.826	85.94	40.81	0.046 *
Ψ_{PD}	557.36	160.06	0.002 **	84.81	107.89	0.440

The two cultivars were compared for the relationship between g_s and $[ABA]_{xylem}$ in Fig. 6. The decline in g_s with increasing $[ABA]_{xylem}$ for Syrah was significantly (p = 0.0005) lower than that for Grenache. Note the logarithmic transformation for $[ABA]_{xylem}$ indicating that the relationship is not linear but exponential. Vines that were treated with ABA instead of water deficit, showed the same relationship between $[ABA]_{xylem}$ of leaves and g_s for both cultivars, and these data are included as squared symbols in Fig. 6. The slopes of the linear regression lines were very similar for data from well-watered and water deficit vines (Grenache: -150.3 ± 26.2 mmol MPa^{-1} m^{-2} s^{-1} ng^{-1} mL; Syrah: -45.6 ± 22.2 mmol MPa^{-1} m^{-2} s^{-1} ng^{-1} mL) and additionally with data from ABA treated vines included (Grenache: -166.4 ± 23.9 mmol MPa^{-1} m^{-2} s^{-1} ng^{-1} mL; Syrah: -53.3 ± 18.3 mmol MPa^{-1} m^{-2} s^{-1} ng^{-1} mL).

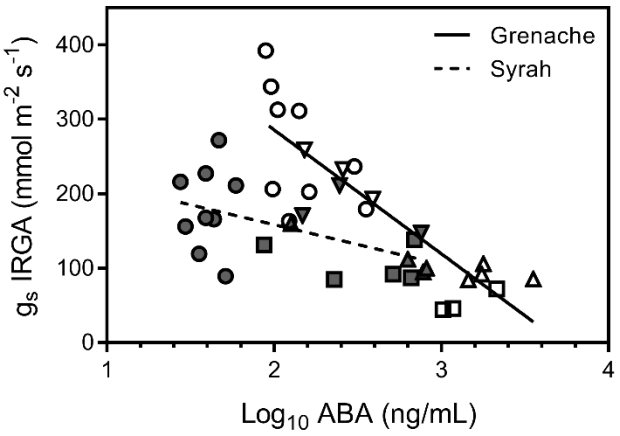

Figure 6. Relationship between $[ABA]_{xylem}$ and g_s measured for well-watered (circles), water deficit (Day 5: triangles up, Day 7: triangles down), and ABA treated vines (squares) from the cultivars Grenache (open symbols) and Syrah (filled symbols). A significant slope (p < 0.001) was predicted for Grenache, while the slope for Syrah was not significant (p = 0.069). Significant negative regressions were predicted for Grenache (g_s = -166.4 ± 23.9 x $\log_{10}([ABA]_{xylem})$ + 618.7 ± 63.1; $p \leq 0.0001$) and Syrah (g_s = -53.3 ± 18.3 x $\log_{10}([ABA]_{xylem})$ + 265 ± 40.7; p = 0.009).

Simple linear regressions showed that K_{leaf} and K_{plant} changed similar in Grenache and Syrah in response to changes in E (Fig. 7a, b). ABA treatment (squared symbols) caused a similar response in K_{leaf}, K_{plant}, and E and, hence, data did fit on the same regression lines. In contrast, linear regressions between E and L_o showed a significantly positive response in Grenache, but no response in Syrah (Fig. 7c). Interestingly, L_o remained stable in Syrah despite changes in E. L_o in Syrah was at all times similar to L_o in water deficit or ABA treated vines of Grenache.

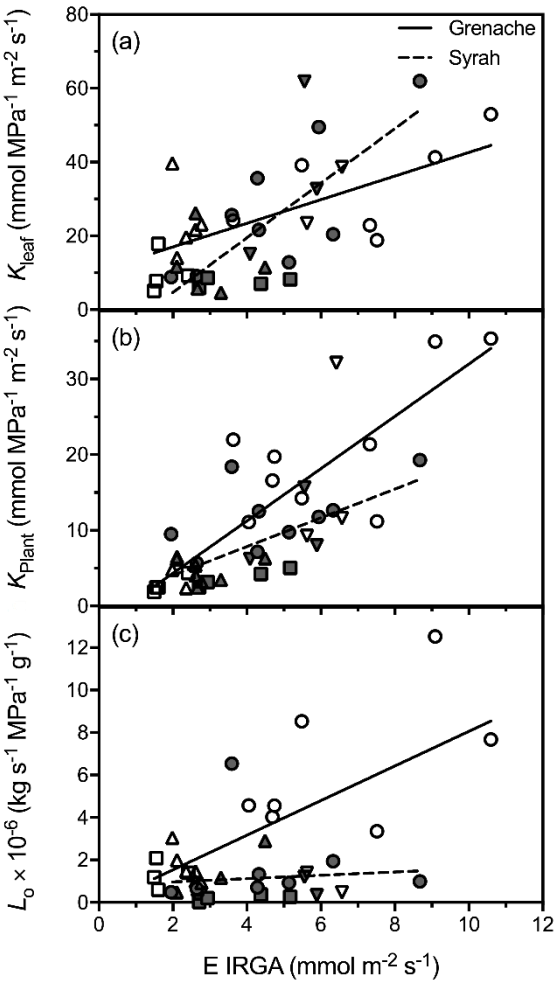

Figure 7. Relationship between E and K_{leaf}, K_{plant}, or L_o for well-watered (circles), water deficit (Day 5: triangles up, Day 7: triangles down), and ABA treated vines (squares) from the cultivars Grenache (open symbols) and Syrah (filled symbols). (a) K_{leaf} was significantly positive correlated to E for both Grenache (K_{leaf} = 3.2 ± 0.84 x E + 10.61 ± 4.41; p = 0.0018) and Syrah (K_{leaf} = 7.39 ± 1.76 x E - 10.07 ± 7.98; p = 0.0005). The slopes were significantly different (p = 0.0321). (b) K_{plant} was positively correlated to E for both Grenache (K_{plant} = 3.45 ± 0.512 x E - 2.56 ± 2.66; p < 0.0001) and Syrah (K_{plant} = 1.899 ± 0.5402 x E + 0.2659 ± 2.448; p = 0.0023) as well. The slopes were not significantly different. (c) L_o was significantly positively correlated to E only in the cultivar Grenache (L_o = 0.815 ± 0.2142 x E - 0.09383 ± 1.081; p = 0.0016), but not in Syrah (p = 0.6992).

A heatmap of relative gene expression for selected root and leaf AQP genes shows the Log_2 expression ratio relative to well-watered controls (Fig. 8). Most of the genes measured were down-regulated during water deficit, ABA treatment, and also recovery. The strongest down-regulation was measured for *TIP2;1* in roots of Syrah under WD (Fig. 8b). Only *TIP1;1* was consistently up-regulated in water deficit relative to well-watered vines (Fig. 8). In most cases, gene expression was similarly regulated by water deficit and ABA treatment.

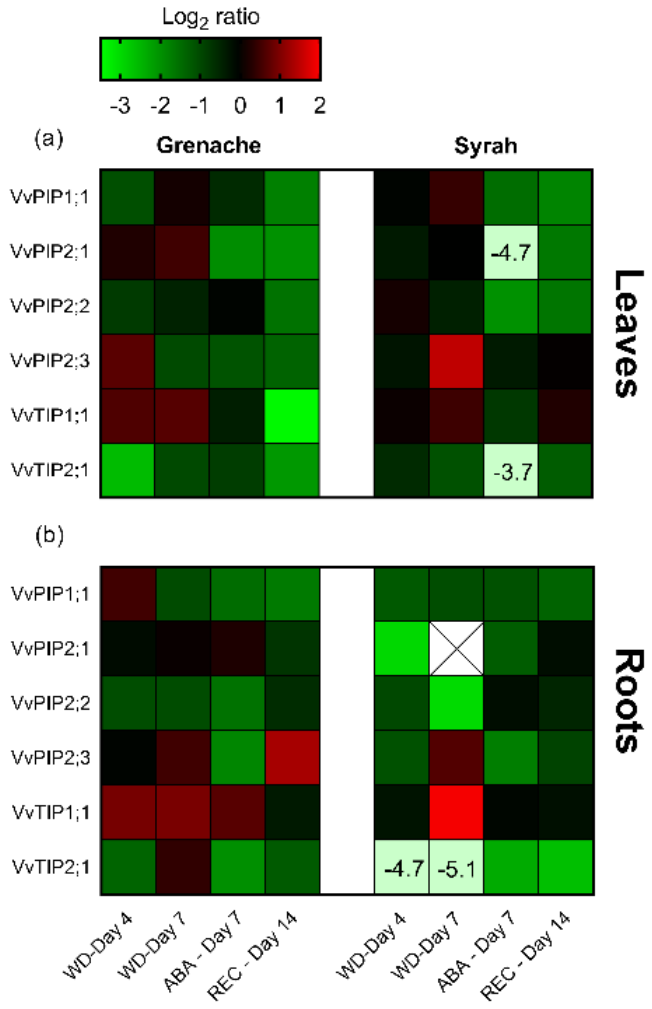

Figure 8. Relative expression of selected aquaporin genes in leaves (a) and roots (b) of water deficit (WD), abscisic acid treated (ABA), and recovery (REC) vines of the cultivars Grenache and Syrah in comparison to well-watered vines. Log_2 ratios are shown as mean of 2 – 5 biological replicates. Missing data are marked with X. Expression ratios of strongly down-regulated genes are shown as numbers on light green background. The double gradient colour legend shows log_2 ratios from -3.5 to 2.0.

Discussion

Isohydric behavior of plants under water deficit is characterized by a limited decline in Ψ_{leaf} by closure of stomata, while anisohydric behavior is characterized by maintenance of high g_s and consequently a greater reduction in Ψ_{leaf}. There is much interest in these different behaviors since agriculturally important plants with different degrees of isohydry/anisohydry can have very different water demands under certain environmental conditions and hence require different management strategies. The hydraulics and gas exchange properties of plants that confer either isohydry or anisohydry are still relatively poorly understood though there is evidence to indicate that the response of K_{leaf} to ABA may be a key feature (Coupel-Ledru *et al.* 2017). In this study, we investigated additional features of the mechanisms that may account for the differences in isohydry by exploring how both, roots and shoot hydraulics, gas exchange, AQP expression and ABA may be involved. We used two *V. vinifera* cultivars, Grenache and Syrah, which have previously been shown to exemplify these differences (Schultz 2003). Schultz concluded that Grenache was more isohydric than Syrah as a result of stronger control over g_s and K_{leaf}. Grapevine has since served as an important model plant to study iso/anisohydric behaviors and several studies have used the cultivars Grenache and Syrah as models for isohydric and anisohydric behavior, respectively (Schultz 2003; Soar *et al.* 2006; Prieto *et al.* 2010; Coupel-Ledru *et al.* 2014; Gerzon *et al.* 2015; Scharwies and Tyerman 2016; Coupel-Ledru *et al.* 2017).

Isohydric and anisohydric behaviour and stomatal sensitivity to ABA

Anisohydric behavior of Syrah was observed in the present study by the significantly lower Ψ_{PD} and Ψ_{leaf} on Day 7 of the experiment compared to Grenache (Figure 2e, h), while both cultivars showed a similar relative g_s (Figure 2b). A higher sensitivity of g_s to changes in Ψ_{PD} for Grenache could also be deduced from the correlogram, where g_s and E were positively correlated to Ψ_{PD} only in Grenache. In contrast, g_s of Syrah was more sensitive to changes in VPD during the mild water deficit experiment as it was observed from the multiple linear regression (Table 1). In the Schultz (2003) experiment, drought stress resulted in a range of Ψ_{PD} comprised between -0.8 and -1.4 MPa contrasting to the milder and more typical Ψ_{PD} achieved in the present study of -0.3 and -0.5 MPa.

Interestingly, stomata from the cultivar Grenache showed a higher sensitivity to ABA in the xylem of leaves compared to Syrah (Figure 6). This fits with a higher sensitivity of K_{leaf} to ABA fed via the petiole in Grenache compared to Syrah, as observed by Coupel-Ledru *et al.* (2017), although we did not observe a relationship between K_{leaf} and $[ABA]_{xylem}$. Tardieu and Simonneau (1998) suggested that isohydric behaviour could be related to stomatal sensitivity to ABA being modulated by Ψ_{leaf} or E, while anisohydric behaviour could be due to a single relationship between g_s and ABA. They showed that stomata of maize (isohydric) were more sensitive to ABA at lower Ψ_{leaf}. In a leaf dehydration assay on different grapevine

genotypes, Hopper *et al.* (2014) found that leaves of Syrah had a higher water loss rate and lower number of stomata per unit area compared to Grenache, which suggested a lower response of stomata to dehydration in Syrah. However, stomata of Syrah showed a quicker response to ABA fed via the petiole to detached leaves compared to Grenache, which was opposite to that expected (Hopper *et al.* 2014). This may be explained by the effect of Ψ_{leaf} on ABA sensitivity in Grenache. Leaves in the assay would have had a water potential approaching zero, since they would be equilibrating to the feeding solution. Therefore, ABA sensitivity may have been at its lowest in Grenache. Exogenous ABA application in the present study, which was done on intact plants, resulted in the same relationship between g_s and $[ABA]_{xylem}$ compared to ABA responses generated by the mild water deficit (Figure 6, square symbols). It is important to note that Ψ_{leaf} and Ψ_{stem} were the same with ABA treatment and water deficit for both cultivars (Figure 2h) indicative of a hydraulic restriction within the plant due to ABA treatment. The down-regulation in response to ABA of several AQPs and the decrease of hydraulic conductances in leaves, root, and whole plant as shown in Figure 7 (squared symbols) could explain this. Thus ABA treatment virtually mimicked water deficit treatment even though there was no soil water deficit with ABA treatment (Figure 7).

It should also be considered that Grenache may produce more ABA or Syrah could have a higher rate of ABA catabolism. The maximum ABA in the xylem sap of leaves measured during the experiment was higher in Grenache compared to Syrah (Figure 6). Rossdeutsch *et al.* (2016) found higher average ABA concentrations in the xylem sap of Grenache shoots during drought stress as compared to Syrah, but they were not significantly different. However, they measured significantly higher concentrations of dihydrophaseic acid (DPA), a degradation product of ABA, in Syrah compared to Grenache. This may indicate that Syrah has a higher catabolism of ABA, which may regulate its responsiveness to water deficit, and results of the present study support this hypothesis. We observed that water-stressed Syrah vines had nearly three-fold higher DPA concentration in the xylem sap of leaves compared to WW vines as well as all Grenache vines (data not shown). The higher DPA levels suggest greater cumulative water stress in Syrah compared to Grenache as ABA catabolism results in accumulation of DPA and phaseic acid (PA) over time. The higher ABA sensitivity of stomata we observed in Grenache fits with the hypothesis that isohydric behavior relates to tighter stomatal regulation, possibly through ABA sensitivity. Future research could aim to test the stomatal sensitivity to ABA in Grenache and Syrah at different Ψ_{leaf} to verify the hypothesis by Tardieu and Simonneau (1998).

VPD effects on stomatal conductance in well-watered vines

As previously observed for several woody and herbaceous species (Franks *et al.* 2007) and grapevines (Schultz 1996; Soar *et al.* 2006; Prieto *et al.* 2010), positive relationships between g_s and VPD were observed under well-watered conditions for both cultivars. A positive relationship as observed for changes

of VPD in the range of 2-3 kPa in this study was also shown by Rogiers *et al.* (2011). For higher values of VPD, a negative effect on g_s should be expected under WD conditions. The VPD has been reported to be one of the main sources of variation in g_s in grapevines (Schultz and Stoll 2010). However, it is not known which mechanisms (passive feedback, active feedback, feedforward, or some combination of these) coordinate g_s and leaf water balance when changes in Ψ_{leaf} are solely due to VPD (Monteith 1995; Buckley 2005; Franks *et al.* 2007). The response of g_s to VPD seems to differ between field or laboratory experiments, and between isohydric and anisohydric plants (Tardieu and Simonneau 1998). VPD and consequently, E, is usually higher in the field than in the laboratory, where a 'midday depression' of g_s is traditionally attributed to high VPD (Correia *et al.* 1995; Chaves *et al.* 2010). Such decrease in g_s during the afternoon was mostly observed when plants were under mild water deficit, particularly isohydric plants (Tardieu and Simonneau 1998). In contrast to our observations on Syrah, g_s of anisohydric species were reported to be similar in the morning and afternoon regardless of VPD suggesting no direct effect of VPD on stomatal control (Tardieu and Simonneau 1998). Based on a study on the anisohydric cultivar Semillon, Rogiers *et al.* (2012) suggested that stomatal sensitivity to VPD could be higher in dry soils due to the increased levels of ABA. This hypothesis is also supported by results from partial root zone drying in Syrah (Collins *et al.* 2010). Possibly, VPD effects are dominant in anisohydric cultivars up to a certain point when the soil becomes very dry and stomata then respond more to soil water deficit. Since isohydric cultivars are more sensitive to changes in soil water availability, VPD may have only a significant effect during well-watered conditions. In the present study, we found that both cultivars responded to VPD, but Grenache had a higher g_s at any given VPD under well-watered conditions and the correlation was less strong than that for Shiraz.

Although g_s responds to multiple plant signals triggered in general by the environment, hydraulic conductance of the plant plays a key role in the response of g_s to changes in leaf water relations (Sperry *et al.* 2002). In our experiment, K_{leaf} from both cultivars and K_{plant} in Grenache, responded to VPD but no response was observed for L_o. These observations agree with the findings by Ocheltree *et al.* (2014) who observed that K_{leaf} but not L_o was correlated to changes in E caused by changes in VPD. Similarly, K_{leaf} in Arabidopsis increased when the plants were transferred to low humidity conditions, and root AQPs were suggested to play a role in the response (Levin *et al.* 2007). In our experiment, significant positive correlations were found between the gene expression of *PIP1*;*1* and *PIP2*;*2* in roots of Grenache and E, VPD, and K_{plant} (Figure 3a). This may indicate that these AQPs had an influence on K_{plant} through actions in the root. In Syrah, K_{leaf} positively correlated with the same two AQP isoforms in roots, but no correlation was found with K_{plant} or L_o. As proposed by Simonin *et al.* (2015), changes in E are synchronized with changes in K_{leaf} to balance the water potential gradient (Ψ_{stem}-Ψ_{leaf}). While both cultivars in our study showed a similar response of K_{leaf} to E, only Grenache showed trends to changes in K_{plant} and L_o suggesting that this near-isohydric cultivar had tighter control of its internal hydraulic conductances

relative to Syrah. In this respect, a higher L_o could minimize the water potential gradient from soil to leaf (Ψ_{PD}-Ψ_{leaf}) at increased VPD, allowing plants to maintain higher rates of g_s and preventing a decline in E in response to increasing VPD (Pantin *et al.* 2013). L_o, however, deserves further investigation for its role in the response of E to higher values of VPD in both cultivars.

Divergent strategies for hydraulic control of plant water relations

Control of hydraulic conductivities in roots, stems and leaves is believed to be another important aspect of isohydric and anisohydric behaviour. Schultz (2003) suggested differences in K_{leaf} between Grenache and Syrah could be the origin of their isohydric and anisohydric behaviour, respectively. In the present study, K_{leaf} was higher in Grenache, which could be explained by its larger xylem vessels (Gerzon *et al.* 2015), compared to Syrah, however, xylem vessel sizes were not measured in this study. Stronger positive correlations between gas exchange parameters and hydraulic conductances in the near-isohydric cultivar Grenache compared to the anisohydric cultivar Syrah suggest that hydraulic pathways inside isohydric plants are more adaptive to changes in E (Figure 3b). Significant differences in the response of L_o to changes in E separated the two cultivars (Figure 7c), which is an important new finding since little is known about root hydraulics in isohydric and anisohydric cultivars (Lovisolo *et al.* 2010). Distinct differences in L_o were previously linked to different expression patterns of AQPs hypothesized to be via a xylem-mediated hydraulic signal (Vandeleur *et al.* 2009). The linear regressions between E and L_o calculated in this study for Grenache were similar to the linear regressions shown by Vandeleur *et al.* (2009). Interestingly, Coupel-Ledru *et al.* (2017) found that K_{leaf} of detached leaves fed with solutions of different ABA concentration decreased with increasing ABA concentration in Grenache, but no change in K_{leaf} was observed in Syrah. This response is similar to what we observed in roots (Figure 7c). While K_{leaf} in this study showed a significant positive relationship with E for both cultivars (Figure 7a), no significant correlations were found to $[ABA]_{xylem}$ (Figure 3b). Different results may be due to the different behavior of leaves when detached from the plant.

Simonin *et al.* (2015) suggested that a positive correlation between changes in E and K_{leaf} could help to stabilize the gradient between Ψ_{stem} and Ψ_{leaf} for hydraulic transport to the leaf. This would cause less variation in Ψ_{leaf}, which is a feature of isohydric behavior, and maximise g_s and, therefore, CO_2 uptake for photosynthesis. At the whole plant level, our results showed no significant changes in gradient between Ψ_{PD} and Ψ_{leaf} in relation to changes in E for both cultivars despite differences in hydraulic regulation, a behavior termed 'isohydrodynamic' by Franks *et al.* (2007). The coordination between E and hydraulic conductances could be important for plants to maintain water potential gradients especially when E is reduced by low g_s. It is interesting in this respect how ABA application to roots resulted in lower Ψ_{stem} and Ψ_{leaf} despite stomatal closure and no soil water deficit. If E is reduced in response to water deficit, e.g. through a reduction of g_s, and hydraulic conductances from the soil to the leaves remain constant, the

gradient for water flow (i.e. Ψ_{PD} - Ψ_{leaf}) would decrease. Since isohydric plant species or cultivars like Grenache have a more sensitive stomatal regulation to water deficit, the mechanism of decreasing hydraulic conductance with decreasing *E* could be more important. In contrast, decreasing hydraulic conductance in anisohydric plants like Syrah, which maintain a higher g_s and *E*, would cause a stronger drop in Ψ_{leaf}.

Aquaporins could play a major role in the regulation of hydraulic conductances. As suggested by Vandeleur *et al.* (2014), AQPs are most likely involved in the regulation of L_o in response to changes in *E*. Pou *et al.* (2013) found that in grapevine expression of leaf *TIP2;1* was well-correlated to changes in g_s during drought and rehydration. In this study, we also found that *TIP2;1* and *PIP2;2* were positively correlated to *E* and g_s in roots and leaves of the cultivar Grenache, but not in Syrah (Figure 3b). They were also positively correlated to K_{plant}, but not to K_{leaf} or L_o. This difference between Grenache and Syrah could explain different responses in hydraulic conductance to changes in *E*. It is surprising that no correlation was found between K_{leaf} and L_o, but there may be other factors that influence this relationship. Clearly, expression of most genes in this study was down-regulated during drought and even ABA treatment (Figure 8). The down-regulation in response to ABA could explain the decrease of hydraulic conductance in leaves, root, and whole plant as shown in Figure 7 (squared symbols). Contrary to our hypothesis, relative gene expression of AQP isoforms in this study was similar between both cultivars (Figure 8). Therefore, stronger hydraulic control in Grenache was not directly related to a stronger regulation of AQPs. However, more significant correlations between AQP gene expression, *E*, and K_{plant} in Grenache could indicate that AQPs were more relevant in this cultivar. Overexpression of *SlTIP2;2* in tomato resulted in higher *E* in mutant plants and made them more anisohydric (Sade *et al.* 2009). The authors suggested that increase membrane permeability for water, i.e. increased hydraulic conductance, could be the cause for the observed increase in *E*. Pantin *et al.* (2013) proposed a hydraulic feed-forward signal for stomatal regulation, which could be mediated by AQPs, as shown by Shatil-Cohen *et al.* (2011). According to their research, AQPs would modulate K_{leaf}, e.g. via the bundle sheath-mesophyll-continuum, which would send a feed-forward signal to stomata. Hence, two different hypotheses exist for the connection between *E* and hydraulic conductance. Either (i) changes in *E* affect hydraulic conductance through the function of AQPs, or, (ii) a hydraulic feed-forward signal mediated by AQPs affects g_s. In the first case, different stomatal behavior between isohydric and anisohydric plants could require alternative hydraulic regulation via AQPs. In the second case, alternative hydraulic regulation by AQPs, potentially via ABA, could affect the isohydric and anisohydric behavior through feed-forward signaling to stomata. Future research could aim to understand which model is more likely.

Acknowledgements

We would like to thank Trevor Garnett (Plant Accelerator) for support with the DroughtSpotter, and Everard Edwards and Annette Boetcher (CSIRO) for assistance with the ABA analysis.

Supplementary Materials

Supplementary Table S1. Sequences of gene-specific primers to amplify reference and aquaporin genes in RT-qPCR.

Vitis Gene	Sequence
ELF	Forward; 5'-CGGGCAAGAGATACCTCAAT-3'
	Reverse; 5'-AGAGCCTCTCCCTCAAAAGG-3'
GAPDH	Forward; 5'-TTCTCGTTGAGGGCTATTCCA-3'
	Reverse; 5'-CCACAGACTTCATCGGTGACA-3'
PIP1;1	Forward; 5'-TGGTGCGGGTGTAGTGAAGG-3'
	Reverse; 5'-AGACAGTGTAGACAAGGACGAAGG-3'
PIP2;1	Forward; 5'-GGCATTTCTGGGGGACACAT-3'
	Reverse; 5'-CTTTGACGAGACCCACACCA-3'
PIP2;2	Forward; 5'-AAAGTTTGGGACGACCAGTG-3'
	Reverse; 5'-TTTTTAGTTGGTGGGGTTGC-3'
PIP2;3	Forward; 5'-GCCATTGCAGCATTCTATCA-3'
	Reverse; 5'-TCCTACAGGGCCACAAATTC-3'
TIP1;1	Forward; 5'-CATTGCCGCCATCATCTAC-3'
	Reverse; 5'-AGAAATCTCAACCCCACCAG-3'
TIP2;1	Forward; 5'-TTAACCCTGCGGTGACCTTC-3'
	Reverse; 5'-TCAATGACTCCAACCCCAGC-3'

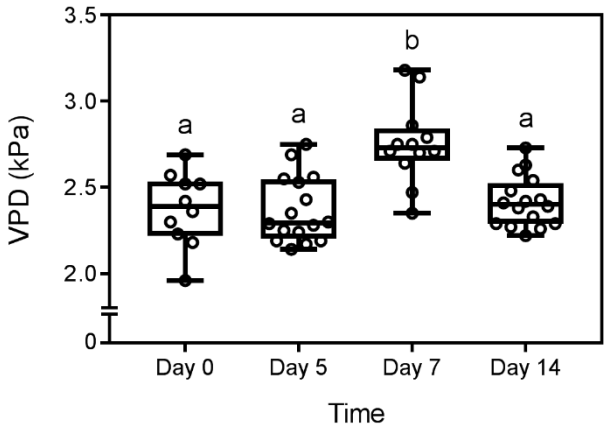

Supplementary Figure S1. VPD_{leaf} measured by the IRGA during the different days of the experiment. Significant differences (One-way ANOVA and Tukey's HSD test) are indicated by different letters.

References

Aroca, R, Ferrante, A, Vernieri, P, Chrispeels, MJ (2006) Drought, abscisic acid and transpiration rate effects on the regulation of PIP aquaporin gene expression and abundance in Phaseolus vulgaris plants. *Annals of Botany* **98**, 1301-10.

Buckley, TN (2005) The control of stomata by water balance. *New Phytologist* **168**, 275-92.

Chaumont, F, Tyerman, SD (2014) Aquaporins: highly regulated channels controlling plant water relations. *Plant Physiology* **164**, 1600-1618.

Chaves, MM, Zarrouk, O, Francisco, R, Costa, JM, Santos, T, Regalado, AP, Rodrigues, ML, Lopes, CM (2010) Grapevine under deficit irrigation: hints from physiological and molecular data. *Annals of Botany* **105**, 661-676.

Christmann, A, Weiler, EW, Steudle, E, Grill, E (2007) A hydraulic signal in root-to-shoot signalling of water shortage. *The Plant Journal* **52**, 167-174.

Collins, MJ, Fuentes, S, Barlow, EWR (2010) Partial rootzone drying and deficit irrigation increase stomatal sensitivity to vapour pressure deficit in anisohydric grapevines. *Functional Plant Biology* **37**, 128-138.

Comstock, JP (2002) Hydraulic and chemical signalling in the control of stomatal conductance and transpiration. *Journal of Experimental Botany* **53**, 195-200.

Correia, MJ, Pereira, JS, Chaves, MM, Rodrigues, ML, Pacheco, CA (1995) ABA xylem concentrations determine maximum daily leaf conductance of field-grown Vitis vinifera L. plants. *Plant, Cell & Environment* **18**, 511-521.

Coupel-Ledru, A, Lebon, É, Christophe, A, Doligez, A, Cabrera-Bosquet, L, Péchier, P, Hamard, P, This, P, Simonneau, T (2014) Genetic variation in a grapevine progeny (Vitis vinifera L. cvs Grenache×Syrah) reveals inconsistencies between maintenance of daytime leaf water potential and response of transpiration rate under drought. *Journal of Experimental Botany* **65**, 6205-6218.

Coupel-Ledru, A, Tyerman, S, Masclef, D, Lebon, E, Christophe, A, Edwards, EJ, Simonneau, T (2017) Abscisic acid down-regulates hydraulic conductance of grapevine leaves in isohydric genotypes only. *Plant Physiology* EPub.

DeGaris, KA (2016) Direct and indirect influences of water deficit on salt uptake, ion accumulation and root-shoot interactions of grapevines. The University of Adelaide.

Dodd, IC (2005) Root-to-shoot signalling: Assessing the roles of 'up' in the up and down world of long-distance signalling in planta. *Plant and Soil* **274**, 251-270.

Fouquet, R, Leon, C, Ollat, N, Barrieu, F (2008) Identification of grapevine aquaporins and expression analysis in developing berries. *Plant Cell Reports* **27**, 1541-1550.

Franks, PJ, Drake, PL, Froend, RH (2007) Anisohydric but isohydrodynamic: seasonally constant plant water potential gradient explained by a stomatal control mechanism incorporating variable plant hydraulic conductance. *Plant, Cell & Environment* **30**, 19-30.

Galmes, J, Pou, A, Alsina, MM, Tomas, M, Medrano, H, Flexas, J (2007) Aquaporin expression in response to different water stress intensities and recovery in Richter-110 (Vitis sp.): relationship with ecophysiological status. *Planta* **226**, 671-81.

Gerzon, E, Biton, I, Yaniv, Y, Zemach, H, Netzer, Y, Schwartz, A, Fait, A, Ben-Ari, G (2015) Grapevine anatomy as a possible determinant of isohydric or anisohydric behavior. *American Journal of Enology and Viticulture* **66**, 340-347.

Heinen, RB, Ye, Q, Chaumont, F (2009) Role of aquaporins in leaf physiology. *Journal of Experimental Botany* **60**, 2971-2985.

Hellemans, J, Mortier, G, De Paepe, A, Speleman, F, Vandesompele, J (2007) qBase relative quantification framework and software for management and automated analysis of real-time quantitative PCR data. *Genome Biology* **8**, R19.

Holbrook, NM, Shashidhar, VR, James, RA, Munns, R (2002) Stomatal control in tomato with ABA-deficient roots: response of grafted plants to soil drying. *Journal of Experimental Botany* **53**, 1503-14.

Hopper, DW, Ghan, R, Cramer, GR (2014) A rapid dehydration leaf assay reveals stomatal response differences in grapevine genotypes. *Horticulture Research* **1**, 2.

Kudoyarova, G, Veselova, S, Hartung, W, Farhutdinov, R, Veselov, D, Sharipova, G (2011) Involvement of root ABA and hydraulic conductivity in the control of water relations in wheat plants exposed to increased evaporative demand. *Planta* **233**, 87-94.

Laur, J, Hacke, UG (2013) Transpirational demand affects aquaporin expression in poplar roots. *Journal of Experimental Botany* **64**, 2283-93.

Levin, M, Lemcoff, JH, Cohen, S, Kapulnik, Y (2007) Low air humidity increases leaf-specific hydraulic conductance of Arabidopsis thaliana (L.) Heynh (Brassicaceae). *Journal of Experimental Botany* **58**, 3711-3718.

Lovisolo, C, Perrone, I, Carra, A, Ferrandino, A, Flexas, J, Medrano, H, Schubert, A (2010) Drought-induced changes in development and function of grapevine (Vitis spp.) organs and in their hydraulic and non-hydraulic interactions at the whole-plant level: a physiological and molecular update. *Functional Plant Biology* **37**, 98-116.

M T Tyree, a, Sperry, JS (1989) Vulnerability of xylem to cavitation and embolism. *Annual Review of Plant Physiology and Plant Molecular Biology* **40**, 19-36.

Maurel, C, Simonneau, T, Sutka, M (2010) The significance of roots as hydraulic rheostats. *Journal of Experimental Botany* **61**, 3191-8.

Maurel, C, Verdoucq, L, Luu, DT, Santoni, V (2008) Plant aquaporins: Membrane channels with multiple integrated functions. *Annual Review of Plant Biology* **59**, 595-624.

Medrano, H, Escalona, JM, Bota, J, Gulias, J, Flexas, J (2002) Regulation of photosynthesis of C3 plants in response to progressive drought: stomatal conductance as a reference parameter. *Annals of Botany* **89**, 895-905.

Mekonnen, DW, Flugge, UI, Ludewig, F (2016) Gamma-aminobutyric acid depletion affects stomata closure and drought tolerance of Arabidopsis thaliana. *Plant Sci* **245**, 25-34.

Monteith, JL (1995) A reinterpretation of stomatal responses to humidity. *Plant, Cell & Environment* **18**, 357-364.

Nardini, A, Tyree, MT, Salleo, S (2001) Xylem cavitation in the leaf of Prunus laurocerasus and its impact on leaf hydraulics. *Plant Physiology* **125**, 1700-1709.

Ocheltree, TW, Nippert, JB, Prasad, PVV (2014) Stomatal responses to changes in vapor pressure deficit reflect tissue-specific differences in hydraulic conductance. *Plant, Cell & Environment* **37**, 132-139.

Pantin, F, Monnet, F, Jannaud, D, Costa, JM, Renaud, J, Muller, B, Simonneau, T, Genty, B (2013) The dual effect of abscisic acid on stomata. *New Phytologist* **197**, 65-72.

Parent, B, Hachez, C, Redondo, E, Simonneau, T, Chaumont, F, Tardieu, F (2009) Drought and abscisic acid effects on aquaporin content translate into changes in hydraulic conductivity and leaf growth rate: a trans-scale approach. *Plant Physiology* **149**, 2000-2012.

Pfaffl, MW (2001) A new mathematical model for relative quantification in real-time RT–PCR. *Nucleic Acids Research* **29**, 2002-2007.

Pou, A, Medrano, H, Flexas, J, Tyerman, SD (2013) A putative role for TIP and PIP aquaporins in dynamics of leaf hydraulic and stomatal conductances in grapevine under water stress and re-watering. *Plant, Cell & Environment* **36**, 828-843.

Prado, K, Boursiac, Y, Tournaire-Roux, C, Monneuse, JM, Postaire, O, Da Ines, O, Schaffner, AR, Hem, S, Santoni, V, Maurel, C (2013) Regulation of Arabidopsis leaf hydraulics involves light-dependent phosphorylation of aquaporins in veins. *Plant Cell* **25**, 1029-39.

Prado, K, Maurel, C (2013) Regulation of leaf hydraulics: from molecular to whole plant levels. *Front Plant Sci* **4**, eCollection.

Prieto, JA, Lebon, É, Ojeda, H (2010) Stomatal behavior of different grapevine cultivars in response to soil water status and air water vapor pressure deficit. *2010* **44**, 12.

Rogiers, SY, Greer, DH, Hatfield, JM, Hutton, RJ, Clarke, SJ, Hutchinson, PA, Somers, A (2012) Stomatal response of an anisohydric grapevine cultivar to evaporative demand, available soil moisture and abscisic acid. *Tree Physiol* **32**, 249-61.

Rogiers, SY, Greer, DH, Hutton, RJ, Clarke, SJ (2011) Transpiration efficiency of the grapevine cv. Semillon is tied to VPD in warm climates. *Annals of Applied Biology* **158**, 106-114.

Rossdeutsch, L, Edwards, E, Cookson, SJ, Barrieu, F, Gambetta, GA, Delrot, S, Ollat, N (2016) ABA-mediated responses to water deficit separate grapevine genotypes by their genetic background. *Bmc Plant Biology* **16**, 91.

Sack, L, Holbrook, NM (2006) Leaf hydraulics. *Annual Review of Plant Biology* **57**, 361-381.

Sade, N, Vinocur, BJ, Diber, A, Shatil, A, Ronen, G, Nissan, H, Wallach, R, Karchi, H, Moshelion, M (2009) Improving plant stress tolerance and yield production: is the tonoplast aquaporin SlTIP2;2 a key to isohydric to anisohydric conversion? *New Phytologist* **181**, 651-661.

Sakurai-Ishikawa, J, Murai-Hatano, M, Hayashi, H, Ahamed, A, Fukushi, K, Matsumoto, T, Kitagawa, Y (2011) Transpiration from shoots triggers diurnal changes in root aquaporin expression. *Plant Cell and Environment* **34**, 1150-63.

Salleo, S, Nardini, A, Pitt, F, Gullo, MAL (2000) Xylem cavitation and hydraulic control of stomatal conductance in Laurel (Laurus nobilis L.). *Plant, Cell & Environment* **23**, 71-79.

Scharwies, JD, Tyerman, SD (2016) Comparison of isohydric and anisohydric Vitis vinifera L. cultivars reveals a fine balance between hydraulic resistances, driving forces and transpiration in ripening berries. *Functional Plant Biology* **44**, 322–336.

Schultz, HR (1996) Water relations and photosynthetic responses of two grapevine cultivars of different geographical origin during water stress. *Proceedings of the 6th International Symposium on Kiwifruit, Vols 1 and 2* 251-266.

Schultz, HR (2003) Differences in hydraulic architecture account for near-isohydric and anisohydric behaviour of two field-grown *Vitis vinifera* L. cultivars during drought. *Plant Cell and Environment* **26**, 1393-1405.

Schultz, HR, Stoll, M (2010) Some critical issues in environmental physiology of grapevines: future challenges and current limitations. *Australian Journal of Grape and Wine Research* **16**, 4-24.

Shatil-Cohen, A, Attia, Z, Moshelion, M (2011) Bundle-sheath cell regulation of xylem-mesophyll water transport via aquaporins under drought stress: a target of xylem-borne ABA? *Plant Journal* **67**, 72-80.

Shelden, MC (2008) A comparison of water stress-induced xylem embolism in two grapevine cultivars, Chardonnay and Grenache, and the role of aquaporins. University of Adelaide.

Shelden, MC, Howitt, SM, Kaiser, BN, Tyerman, SD (2009) Identification and functional characterisation of aquaporins in the grapevine, Vitis vinifera. *Functional Plant Biology* **36**, 1065-1078.

Simonin, KA, Burns, E, Choat, B, Barbour, MM, Dawson, TE, Franks, PJ (2015) Increasing leaf hydraulic conductance with transpiration rate minimizes the water potential drawdown from stem to leaf. *Journal of Experimental Botany* **66**, 1303-1315.

Simonneau, T, Barrieu, P, Tardieu, F (1998) Accumulation rate of ABA in detached maize roots correlates with root water potential regardless of age and branching order. *Plant, Cell & Environment* **21**, 1113-1122.

Soar, CJ, Speirs, J, Maffei, SM, Penrose, AB, McCarthy, MG, Loveys, BR (2006) Grape vine varieties Shiraz and Grenache differ in their stomatal response to VPD: apparent links with ABA physiology and gene expression in leaf tissue. *Australian Journal of Grape and Wine Research* **12**, 2-12.

Speirs, J, Binney, A, Collins, M, Edwards, E, Loveys, B (2013) Expression of ABA synthesis and metabolism genes under different irrigation strategies and atmospheric VPDs is associated with stomatal conductance in grapevine (Vitis vinifera L. cv Cabernet Sauvignon). *Journal of Experimental Botany* **64**, 1907-16.

Sperry, JS, Hacke, UG, Oren, R, Comstock, JP (2002) Water deficits and hydraulic limits to leaf water supply. *Plant Cell and Environment* **25**, 251-263.

Steudle, E (2000) Water uptake by plant roots: an integration of views. *Plant and Soil* **226**, 45-56.

Tardieu, F, Simonneau, T (1998) Variability among species of stomatal control under fluctuating soil water status and evaporative demand: modelling isohydric and anisohydric behaviours. *Journal of Experimental Botany* **49**, 419-432.

Tashiro, RM, Philips, JG, Winefield, CS (2016) Identification of suitable grapevine reference genes for qRT-PCR derived from heterologous species. *Molecular Genetics and Genomics* **291**, 483-492.

Thompson, AJ, Andrews, J, Mulholland, BJ, McKee, JMT, Hilton, HW, Horridge, JS, Farquhar, GD, Smeeton, RC, Smillie, IRA, Black, CR, Taylor, IB (2007) Overproduction of abscisic acid in tomato increases transpiration efficiency and root hydraulic conductivity and influences leaf expansion. *Plant Physiology* **143**, 1905-1917.

Tombesi, S, Nardini, A, Frioni, T, Soccolini, M, Zadra, C, Farinelli, D, Poni, S, Palliotti, A (2015) Stomatal closure is induced by hydraulic signals and maintained by ABA in drought-stressed grapevine. *Scientific Reports* **5**, 12449.

Vandeleur, RK, Mayo, G, Shelden, MC, Gilliham, M, Kaiser, BN, Tyerman, SD (2009) The role of plasma membrane intrinsic protein aquaporins in water transport through roots: diurnal and drought stress responses reveal different strategies between isohydric and anisohydric cultivars of grapevine. *Plant Physiology* **149**, 445-460.

Vandeleur, RK, Sullivan, W, Athman, A, Jordans, C, Gilliham, M, Kaiser, BN, Tyerman, SD (2014) Rapid shoot-to-root signalling regulates root hydraulic conductance via aquaporins. *Plant, Cell & Environment* **37**, 520-538.

Wilkinson, S, Bacon, MA, Davies, WJ (2007) Nitrate signalling to stomata and growing leaves: interactions with soil drying, ABA, and xylem sap pH in maize. *Journal of Experimental Botany* **58**, 1705-16.

Ye, J, Coulouris, G, Zaretskaya, I, Cutcutache, I, Rozen, S, Madden, TL (2012) Primer-BLAST: A tool to design target-specific primers for polymerase chain reaction. *BMC Bioinformatics* **13**, 134-134.

6. GENERAL DISCUSSION, LIMITATIONS, AND FUTURE DIRECTIONS

6.1. General discussion

6.1.1. Introduction

Aquaporins are of significant importance in regulating transport of water and other small molecules through membranes in animals and plants (Gomes *et al.* 2009). In plants, water uptake from the soil and transport to the shoot is of pivotal importance to balance water loss by transpiration. Major gatekeepers to regulate transpiration in plants are stomata, which can be actively regulated to control water loss (Jones 1998). Also, plant internal hydraulic conductance and water flow across membranes plays an important role in regulation of water flow to growing tissues (Ludevid *et al.* 1992; Ehlert *et al.* 2009; Reinhardt *et al.* 2016), maintenance of gradients (Vandeleur *et al.* 2014; Simonin *et al.* 2015), and possibly feed-forward signalling in hydraulic control of stomatal conductance (Sade *et al.* 2014b).

PIP aquaporins have been at the centre of previous research due to their localisation to the plasma membrane, which is the primary barrier for symplastic and transcellular water flow. It has been shown that PIP aquaporins have significant roles in regulating root hydraulic conductance (Javot *et al.* 2003; Vandeleur *et al.* 2009). It was suggested that PIP aquaporins could be essential in recovery from drought, since double antisense plants for knock-down of PIPs recovered slower than control plants (Martre *et al.* 2002). In leaves, PIP aquaporin expression in bundle sheath cells have been proposed to control the bundle sheath-mesophyll hydraulic continuum and could send a hydraulic feed-forward signal for stomatal control (Sade *et al.* 2014b). The PIP isoform *At*PIP2;1 has also been directly connected to stomatal control due to its function in hydrogen peroxide transport, which is involved in ABA mediated stomatal closure (Grondin *et al.* 2015; Rodrigues *et al.* 2017).

Different hydraulic strategies of plants, i.e. isohydric and anisohydric behaviour (Tardieu and Simonneau 1998; Schultz 2003), could also be determined by differences in aquaporin expression and/or activity (Sade *et al.* 2009; Vandeleur *et al.* 2009; Coupel-Ledru *et al.* 2017). Sade *et al.* (2009) showed that overexpression of the TIP aquaporin isoform *SlTIP2;2* in tomato caused higher transpiration in well-watered and droughted transgenic plants. They argued that overexpression transformed the transgenic plants to be more anisohydric. These observations indicate that TIP aquaporins may be linked to the control of leaf gas exchange. Likewise, gene expression of TIP isoform *VvTIP2;1* in grapevine was significantly correlated to changes in stomatal conductance during a drought and rehydration experiment (Pou *et al.* 2013). In a cross species meta-analysis of gene expression in Arabidopsis, barley, rice, and

wheat, *TIP1;1* and *TIP2;1* were identified to be significantly down-regulated during drought (Shaar-Moshe *et al.* 2015).

The control of plant hydraulic behaviour and stomatal conductance are interesting breeding targets, since water availability and the need for irrigation are a big challenge in agriculture (Rosegrant *et al.* 2009; Langridge and Reynolds 2015). For example, modification of stomatal density in plants has been explored to make plants more drought tolerant (Hepworth *et al.* 2015). Hence, understanding the role of TIP aquaporins in leaf gas exchange could offer new opportunities for improving water use efficiency of crop plants.

6.1.2. Aquaporin gene expression during drought and rehydration revealed varied degrees of correlation between expression and stomatal conductance across isoforms

Overexpression of the TIP aquaporin isoform *SlTIP2;2* in tomato increased transpiration of transgenic plants significantly (Sade *et al.* 2009). Also, a very good correlation was found between gene expression of the TIP isoform *VvTIP2;1* and changes in stomatal conductance during drought and rehydration in grapevine (Pou *et al.* 2013). Hence, the aim was to explore if a similar relationship between aquaporin expression and stomatal conductance could also be found in the model plant *Arabidopsis thaliana*.

Similar to observations by Alexandersson *et al.* (2005), gene expression of most aquaporin isoforms in leaves of Arabidopsis was down-regulated during drought and increased again when plants were rehydrated (Chapter 2, Figure 8a). Only gene expression of the isoforms *AtPIP1;4*, *AtPIP2;4*, *AtPIP2;5*, and *AtPIP2;6* was significantly up-regulated. While down-regulation of aquaporin expression could cause a decline of leaf hydraulic conductance and help to prevent water loss (Schultz 2003; Sade *et al.* 2014b), up-regulation during recovery could facilitate faster rehydration of the tissue (Martre *et al.* 2002). Interestingly, the same experiment in grapevine showed that gene expression of the TIP isoform *TIP1;1* was up-regulated during drought (Chapter 5, Figure 8a), which was opposite to Arabidopsis. Increased expression of *VvTIP1;1* in grapevine was in line with previous observations by (Pou *et al.* 2013). In contrast, *TIP1;1* was identified to be significantly down-regulated during drought in Arabidopsis, barley, rice, and wheat (Shaar-Moshe *et al.* 2015). This shows that differences in aquaporin regulation during drought and rehydration may exist in different species.

In Arabidopsis, the best correlations between aquaporin gene expression and stomatal conductance were found for the isoforms *AtPIP1;1*, *AtPIP1;2*, *AtPIP2;2*, and *AtTIP2;2* (Chapter 2, Figure 10 and Figure 11). A positive correlation was also found between gene expression of *AtTIP2;1* and g_s. In grapevine, the only significant positive correlation between gene expression in leaves and g_s was found for *VvTIP2;1* (Chapter

5, Figure 3) and it was only found in the near-isohydric cultivar Grenache. Gene expression of *VvPIP2;2* in leaves was positively correlated with transpiration (E) but not g_s, and *VvPIP1;1* showed no correlation at all. While the results from grapevine were in line with observation by Pou *et al.* (2013), it remains unknown why these difference exist between Arabidopsis and grapevine. In Chapter 5, we hypothesised that the difference in correlations between the cultivars Grenache and Syrah could be involved in determining their near-isohydric and anisohydric behaviours, respectively. Alexandersson *et al.* (2010) showed that changes in aquaporin gene expression during drought was very similar when comparing five different accessions; only *AtPIP2;4* and *AtPIP2;6* were differentially regulated in two accessions. This could indicate that hydraulic behaviour is rather similar between different accessions of Arabidopsis.

While Alexandersson *et al.* (2005) found that gene expression of *AtPIP1;4* and *AtPIP2;5* was up-regulated during drought, research in Chapter 2 also found that their expression was significantly correlated to genes like *AtNCED3*, which is involved in ABA synthesis (Chapter 2, Figure 9a). Since previous research showed that *AtPIP1;4* facilitates hydrogen peroxide transport during biotic stress (Tian *et al.* 2016), this may link *AtPIP1;4* also to hydrogen peroxide signalling to mediate ABA induced stomatal closure during drought as demonstrated for *AtPIP2;1* (Rodrigues *et al.* 2017). Hence, further research is needed to investigate this link.

6.1.3. Abscisic acid may not mediate changes in aquaporin gene expression during drought

The plant hormone abscisic acid (ABA) is an important chemical signal that mediates stomatal closure during drought stress (Tardieu and Davies 1993). Jang *et al.* (2004) showed that ABA treatment of 2 weeks old Arabidopsis grown hydroponically induced gene expression of most PIP aquaporins, which is opposite to the down-regulation of gene expression during drought. Nevertheless, ABA could have a role in the regulation of aquaporin gene expression during drought. Therefore, the aim was to induce stomatal closure similar to closure during drought by watering plants with ABA solutions and observe changes in aquaporin gene expression.

Interestingly, no consistent significant response in aquaporin gene expression was found during the ABA watering experiment in Arabidopsis even though stomatal conductance was significantly reduced (Chapter 2, Figure 8b). This suggests that ABA may not be mediating the changes in gene expression observed during drought and rehydration in Arabidopsis. Results from the drought and rehydration experiment in Chapter 2 even suggest that aquaporin gene expression changed together with stomatal conductance (Chapter 2, Figure 10 and Figure 11) before significant changes in leaf ABA concentration were measured (Chapter 2, Figure 7a). This may point to a signal other than ABA that induces stomatal closure and changes in aquaporin expression during drought. Christmann *et al.* (2007) suggested a

hydraulic signal from roots to the shoot that would induce ABA production in leaves. In grapevine, it was also suggested that a hydraulic signal could be involved in the induction of stomatal closure during drought (Tombesi *et al.* 2015).

However, ABA supply to roots in grapevine (Chapter 5) showed a reduction of aquaporin gene expression and water potentials. While this is different to Arabidopsis, changes in water potentials may have also influenced aquaporin expression. Christmann *et al.* (2013) suggested that yet unknown potential sensors may be involved in translating hydraulic signals into chemical signals in the shoot. These may also regulate aquaporin expression. Again this showed that Arabidopsis and grapevine behave differently. Therefore, results obtained in one species may not translate directly to another species.

6.1.4. Constitutive expression of *AtTIP2;1* had significant influence on stomatal conductance in well-watered plants

Overexpression of the TIP isoform *SlTIP2;2* in tomato caused a significant increase in transpiration in transgenic plants (Sade *et al.* 2009). Similar to this, overexpression of *GmPIP2;6* caused an increase in transpiration of transgenic soybean plants (Zhou *et al.* 2014). The aim in Chapter 3 on constitutive expression of all three TIP2 isoforms in Arabidopsis was to find out whether increased transpiration could also be observed and if the response would be different for the different TIP2 isoforms.

So far, one *AtTIP2;1* overexpression line was found that showed a significantly different stomatal response in well-watered plants (Chapter 3, Figure 38 and Figure 40). While no general higher transpiration was observed in the overexpressor as shown in studies by Sade *et al.* (2009) and Zhou *et al.* (2014), well-watered overexpression plants had a more stable g_s during the experiment compared to control plants, which showed a decline in g_s similar to the drought treated plants. This may indicate that the overexpression line became less sensitive to what caused the changes in g_s of wild-type well-watered plants. Higher conductance of the tonoplast membrane could increase hydraulic buffering and keep stomatal conductance more stable. Activities of the TIP2 promoters were also shown to be highest around vascular tissue (Chapter 2, Figure 29 - Figure 31). Hence, TIP2 aquaporins could be similarly involved in controlling hydraulic feed-forward signals to stomata as suggested for PIP aquaporins (Sade *et al.* 2014b).

Additional, independent AtTIP2;1 overexpression lines need to be identified to confirm the results. Also, AtTIP2;2 and AtTIP2;3 overexpression lines need to be tested in drought and rehydration experiments to explore their effects on stomatal conductance.

6.1.5. CRISPR-Cas knock-out of AtTIP2;3 showed reduced root growth phenotype

The TIP aquaporin genes *AtTIP1;1*, *AtTIP1;2*, and *AtTIP2;1* have been shown to be important for lateral root emergence (Reinhardt *et al.* 2016). So far, no *AtTIP2;2* and *AtTIP2;3* knock-outs have been described in the literature. The aim was to create single knock-out mutants for all three TIP2 aquaporin isoforms and characterise them to understand whether knock-outs showed differences in growth and gas exchange.

Here we used CRISPR-Cas to induce point mutants in genes encoding the three TIP2 isoforms. The most common mutations were one base insertions (Chapter 4, Figure 49), which is in line with previous observations presented in the literature (Fauser *et al.* 2014). While off-target testing for the mutant lines is still outstanding and stomatal conductance has not been measured yet for these plants, a significant root growth phenotype was observed for a mutant line of the gene *AtTIP2;3* (Chapter 4, Figure 53). Alexandersson *et al.* (2005) observed that *AtTIP2;3* was mainly expressed in roots and promoter-GUS constructs for *AtTIP2;3* showed an exclusive expression in roots (Zhu *et al.* 2013). However, promoter-GUS constructs used in Chapter 3 showed also expression in leaves (Chapter 3, Figure 31). Nevertheless, predominant expression in roots could point at a role in root growth. A complementation could provide evidence whether the observed phenotype is due to the dysfunctional *AtTIP2;3* gene. Furthermore, knock-out lines will be tested for their transpiration and compared to the overexpression lines.

6.1.6. Stomatal responses in well-watered controls

Well-watered control plants were used in the drought-rehydration experiments for comparison. Interestingly, drought-like stomatal responses were observed even in well-watered plants during the course of the experiment (Chapter 2, Figure 4a). It is known that stomata respond to changes in humidity or vapour pressure deficit (VPD) (Levin *et al.* 2007). In the grapevine drought and rehydration experiment (Chapter 5), variability of stomatal conductance in well-watered plants was significantly correlated to differences in VPD (Chapter 5, Figure 3a), but in Arabidopsis no relationship between changes in g_s and VPD was found (Chapter 2, Supplementary Figure S8). While further research is needed to exclude the influence of VPD, a volatile signal from droughted plants could induce stomatal closure similar to the mechanisms that occur during herbivory (Paré and Tumlinson 1999). It also appeared as if well-watered plants from an overexpression line of AtTIP2;1 showed less variation in g_s compared to wild-type control plants.

Since experiments are often conducted in controlled environment rooms with little air exchange, volatile signals could confound results due to effects on control plants. Also, stressed plants in enclosed

horticulture could potentially limit productivity of other plants due to reduction in stomatal conductance. Hence, further experiments to test for a (volatile) signal would be important.

6.2. Limitations

Several limitations need to be considered in this research on the role of aquaporins during drought stress. The model plant *Arabidopsis thaliana* was chosen due to its wide use in molecular plant physiology, its small size, short generation time, and ease of transformation by floral dip (Clough and Bent 1998; Koornneef and Meinke 2010). While gene expression and simple plant physiological parameters can be easily measured in Arabidopsis, measurements of water potential and hydraulic conductance are very difficult due to the soft tissue and small size. However, a few studies measured rosette hydraulic conductivity (Prado *et al.* 2013) or root hydraulic conductivity (Pou *et al.* 2016). Nevertheless, model plants like grapevine, as used in Chapter 5, are more suitable for measurements of water potentials and hydraulic properties (Vandeleur *et al.* 2009; Coupel-Ledru *et al.* 2014; Scharwies and Tyerman 2016). In grapevine, isohydric and anisohydric cultivars were identified that can be used to study the influence of aquaporins on their different behaviour. However, for molecular physiology and genetic modification grapevine isn't very suitable.

In this research, gene expression was analysed to investigate relationships between aquaporin isoforms and plant physiological parameters. While gene expression analysis is common and often shows important connections (Jang *et al.* 2004; Alexandersson *et al.* 2005; Vandeleur *et al.* 2009), protein abundance and post-translational modifications need to be considered as well since they have significant effects on aquaporin function (Pietro *et al.* 2013; Prado *et al.* 2013; Vialaret *et al.* 2014). Gene expression was also measured from whole leaf extracts. Previous research has shown that aquaporin activity in specific tissues can define their function. For example PIP expression in bundle sheath cells may control hydraulic signals in leaves (Sade *et al.* 2014b) and TIP aquaporin expression in lateral root primordia may determine whether lateral root emergence can be initiated or not (Reinhardt *et al.* 2016). Likewise constitutive overexpression or knock-out, as used in Chapters 3 and 4, can help to identify functions of specific aquaporin isoforms, but may also cause side effects.

So far, only a single overexpression line (Chapter 3) and one knock-out line (Chapter 4) were identified and studied. While this was due to time constraints, it will be important to find additional lines to confirm the results. In particular for the CRISPR-Cas lines, off-target effects have been a discussion (Anderson *et al.* 2015; Peterson *et al.* 2016). Therefore, potential off-targets that were identified *in silico* need to be checked for mutations by sequencing.

6.3. Future directions

The gene expression analysis during drought-rehydration and ABA watering in Chapter 2 is close to complete and will be prepared for submission to a scientific journal. Also, the study on plant hydraulics and aquaporin expression in grapevine is currently being prepared for submission to the scientific journal "Plant, Cell & Environment".

Further gene expression analysis needs to be carried out to identify overexpression lines for TIP2 isoforms as presented in Chapter 3. It will be important to understand how overexpression of *AtTIP2;1* influenced the stomatal response in well-watered plants and if *AtTIP2;2* and *AtTIP2;3* have a similar effect. Measurements of hydraulic conductivity in leaves could be tested to evaluate whether overexpression increased the hydraulic conductivity. Also water potential measurements would be useful to test whether overexpression had a hydraulic buffering effect.

For the CRISPR-Cas knock-out lines, off-targets need to be tested by sequencing. Further research needs to be done on the short root phenotype of *AtTIP2;3* knock-out to understand why root elongation was inhibited. Also, changes in stomatal conductance need to be evaluated for the TIP2 knock-out lines.

APPENDICES

Supplementary information of Chapter 2

Supplementary Figures

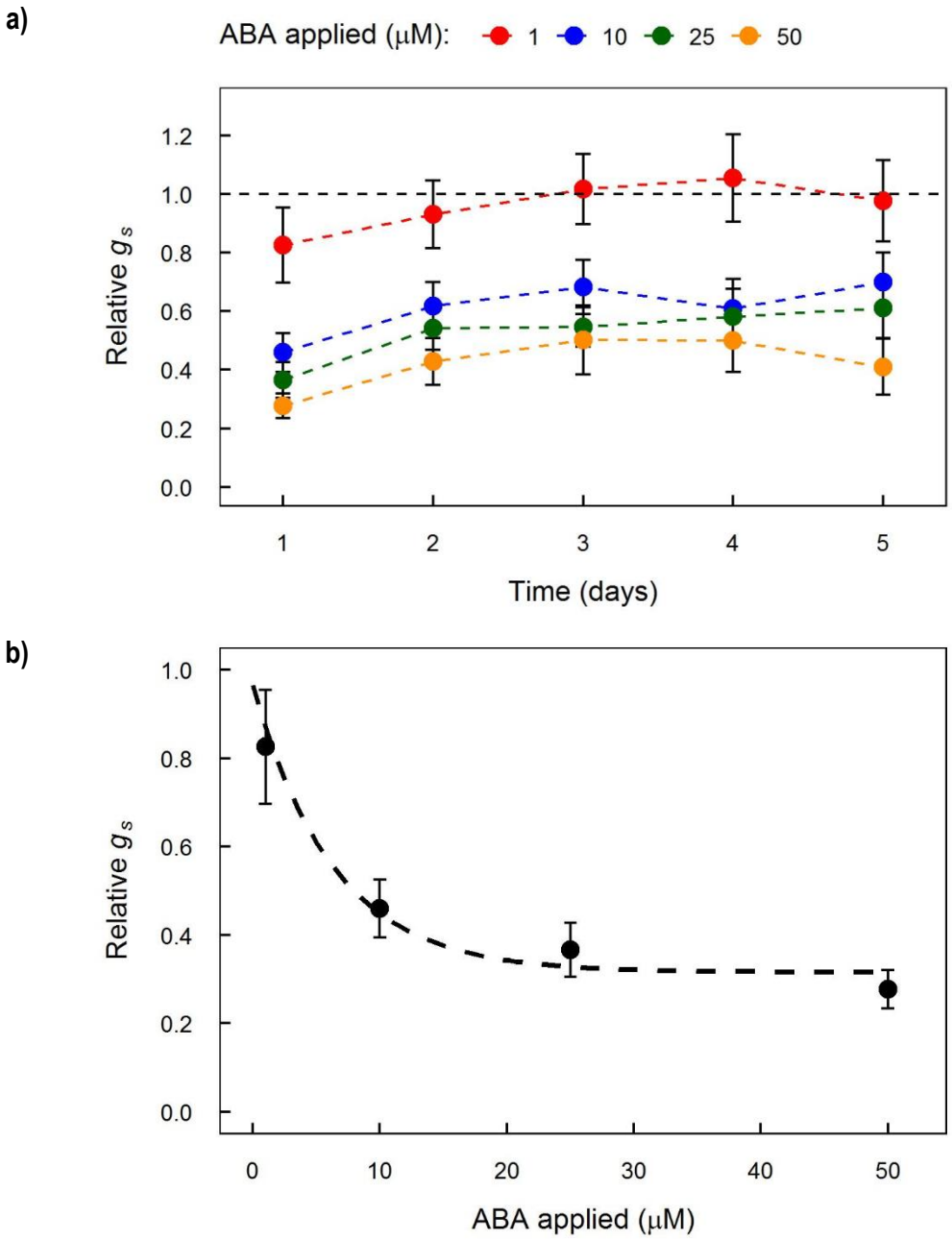

Supplementary Figure S2. Relative stomatal conductance (Relative g_s) measured on leaves of Arabidopsis plants (*Arabidopsis thaliana*) ecotype Col-0 which were daily watered with solutions containing different concentrations of abscisic acid (1, 10, 25, 50 µM) over five days. Relative g_s was calculated relative to the average stomatal conductance of control plants which were watered with a mock-control solution. a) Temporal changes of relative g_s when plants were watered with ABA solutions of the same strength each morning. Each point represents the mean ± SE of five independent plants on which g_s

was measured on two leaves each. b) Relationship between concentration of ABA applied and relative g_s for data from day 1. An exponential regression was fitted to the mean values (dashed line).

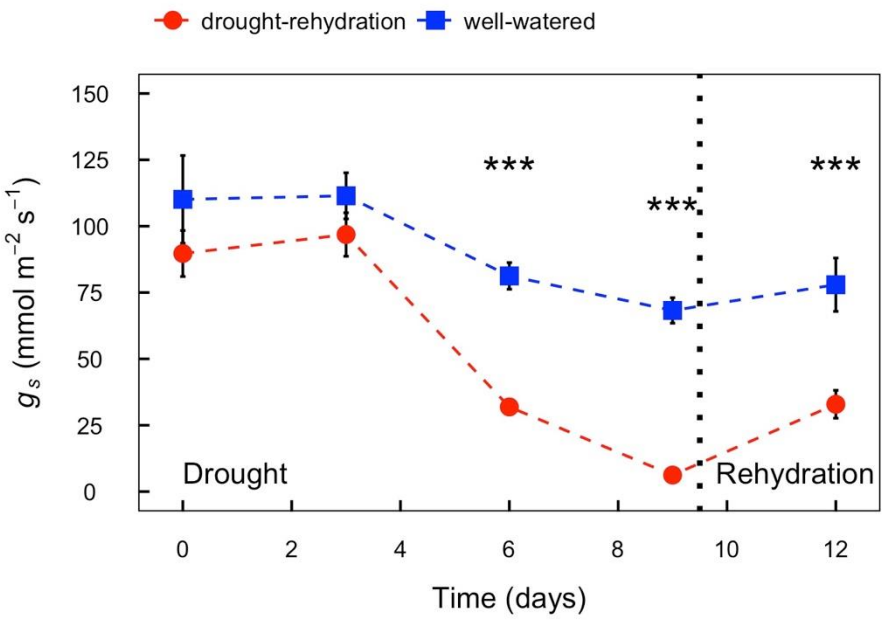

Supplementary Figure S3. Stomatal conductance (g_s) measured on leaves of Arabidopsis plants (*Arabidopsis thaliana*) ecotype Col-0 used in a trial drought – rehydration experiment. Each point represents the mean ± SE of five independent plants on which g_s was measured on four leaves each. Significant differences between the treated and control groups by ANOVA with Bonferroni post-tests are marked: *** for P ≤ 0.001. For plants of the "drought – rehydration" group (solid red circles) watering was withheld from day 1 till day 9 (wilting point), after which watering to field capacity was resumed. Plants of the "well – watered" group (solid blue squares) were watered to field capacity each day of the experiment.

a)

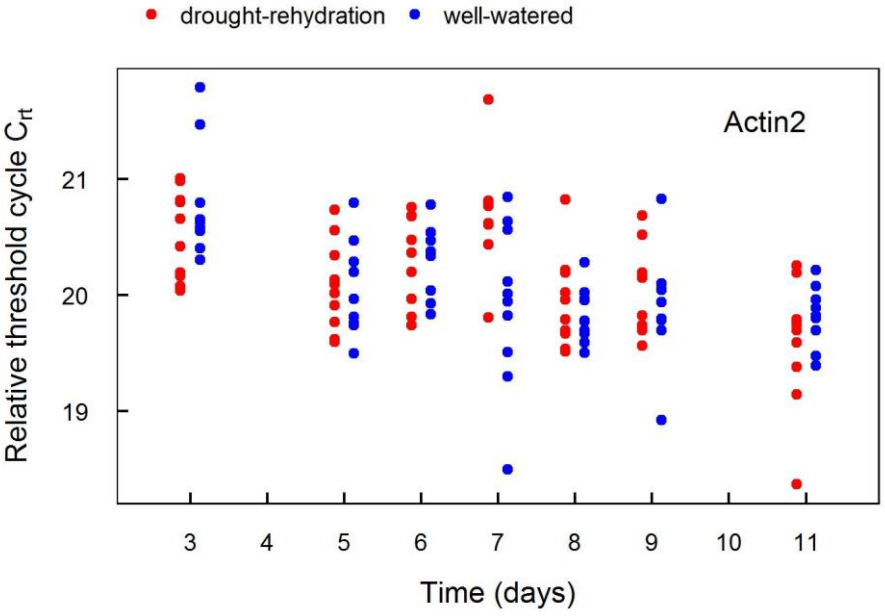

b)

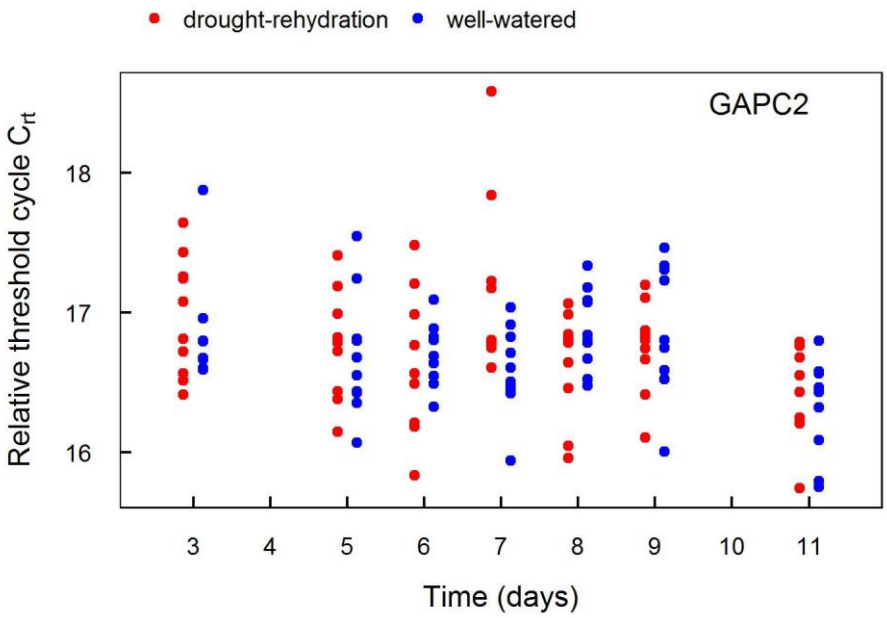

Supplementary Figure S4. Raw relative threshold cycles (C_{rt}) as measured by RT-qPCR for the reference genes a) Actin2 (AT3G18780) and b) GAPC2 (AT1G13440) in leaves of Arabidopsis plants (*Arabidopsis thaliana*) ecotype Col-0 used in the drought – rehydration experiment. RT-qPCR was performed using custom designed OpenArray® plates for the QuantStudio™ 12K Flex system (ThermoFisher). C_{rt} for the two reference genes was measured using cDNA produced from RNA which was extracted from two leaves of five independent plants per group (red: drought-rehydration; blue: well-watered).

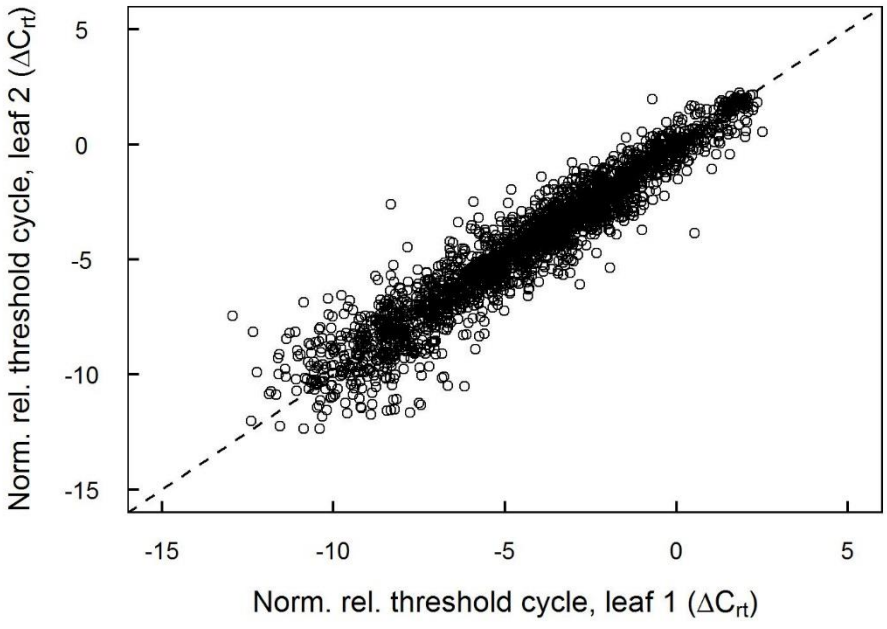

Supplementary Figure S5. Comparison of normalised relative threshold cycles (ΔC_{rt}) measured for the same targets on leaf 1 and 2 of individual Arabidopsis plants (*Arabidopsis thaliana*) ecotype Col-0 used in the drought – rehydration experiment. Relative threshold cycles were normalised against the reference genes Actin2 (AT3G18780) and GAPC2 (AT1G13440). RT-qPCR was performed using custom designed OpenArray® plates for the QuantStudio™ 12K Flex system (ThermoFisher).

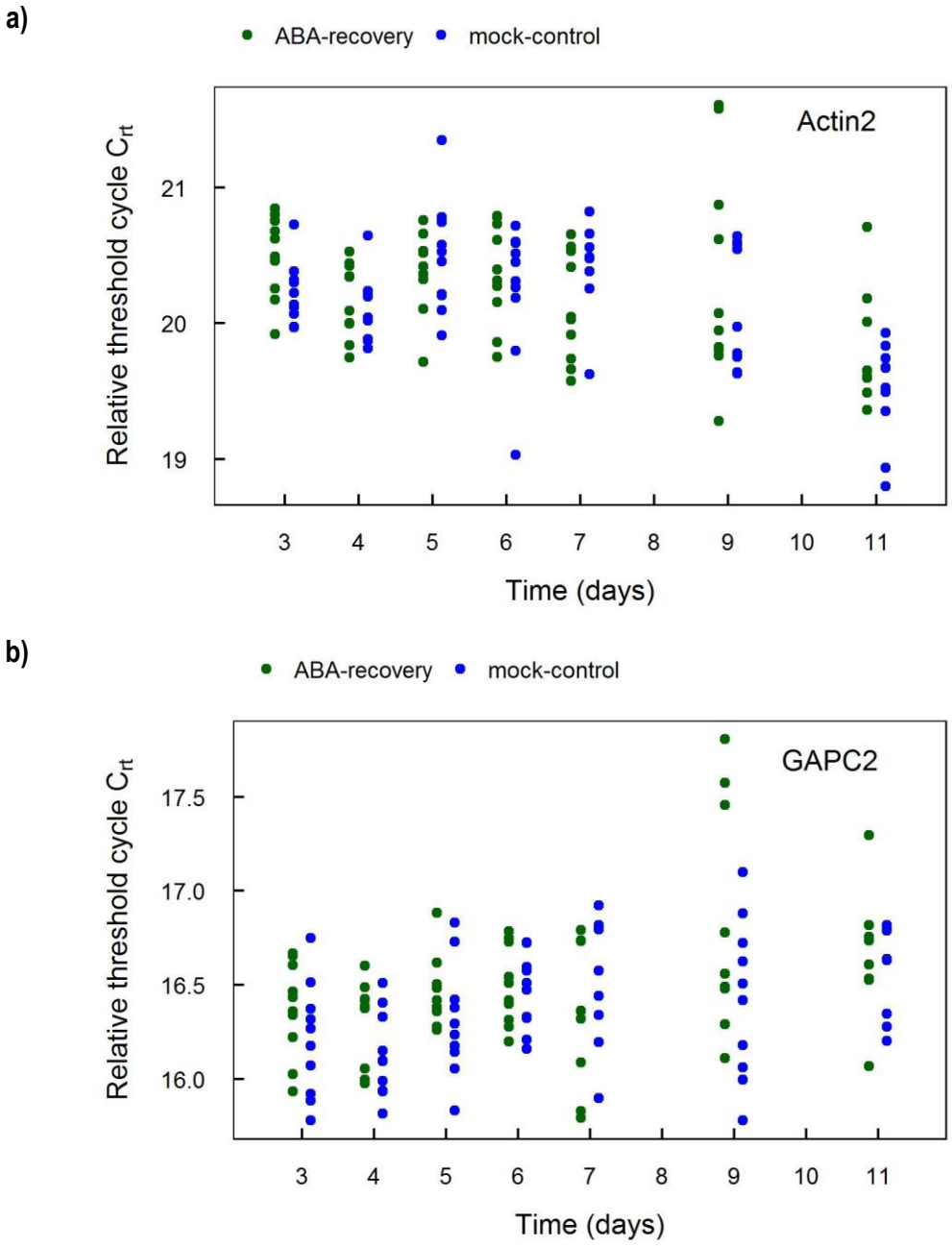

Supplementary Figure S6. Raw relative threshold cycles (C_{rt}) as measured by RT-qPCR for the reference genes a) Actin2 (AT3G18780) and b) GAPC2 (AT1G13440) in leaves of Arabidopsis plants (*Arabidopsis thaliana*) ecotype Col-0 used in the ABA watering experiment. RT-qPCR was performed using custom designed OpenArray® plates for the QuantStudio™ 12K Flex system (ThermoFisher). C_{rt} for the two reference genes was measured using cDNA produced from RNA which was extracted from two leaves of five independent plants per group (red: ABA-recovery; blue: mock-control).

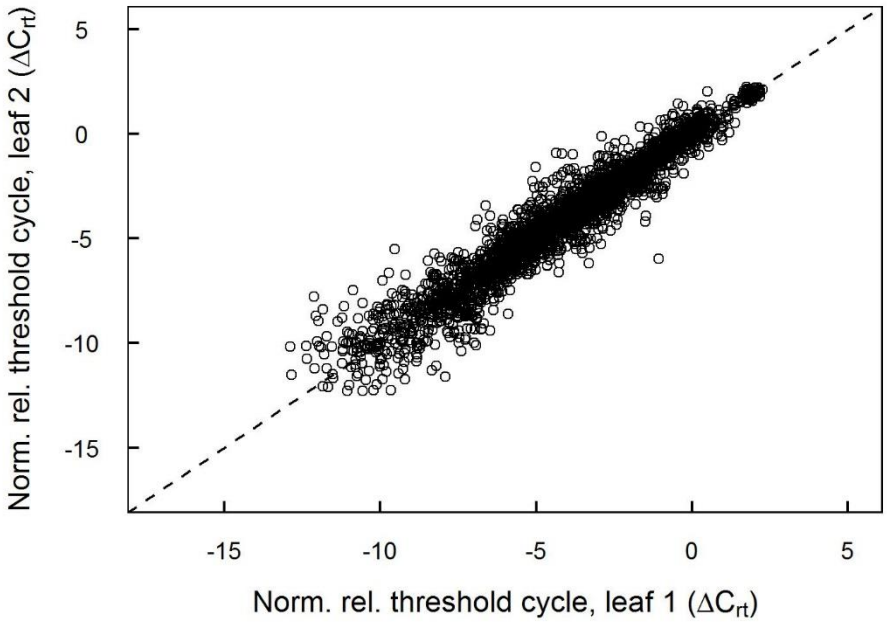

Supplementary Figure S7. Comparison of normalised relative threshold cycles (ΔC_{rt}) measured for the same targets on leaf 1 and 2 of individual Arabidopsis plants (*Arabidopsis thaliana*) ecotype Col-0 used in the ABA watering experiment. Relative threshold cycles were normalised against the reference genes Actin2 (AT3G18780) and GAPC2 (AT1G13440). RT-qPCR was performed using custom designed OpenArray® plates for the QuantStudio™ 12K Flex system (ThermoFisher).

a)

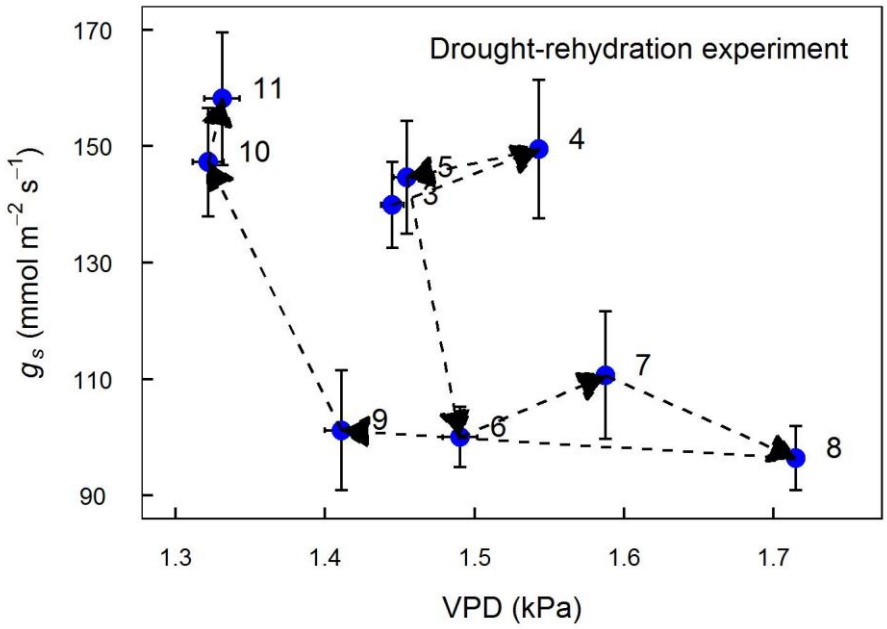

b)

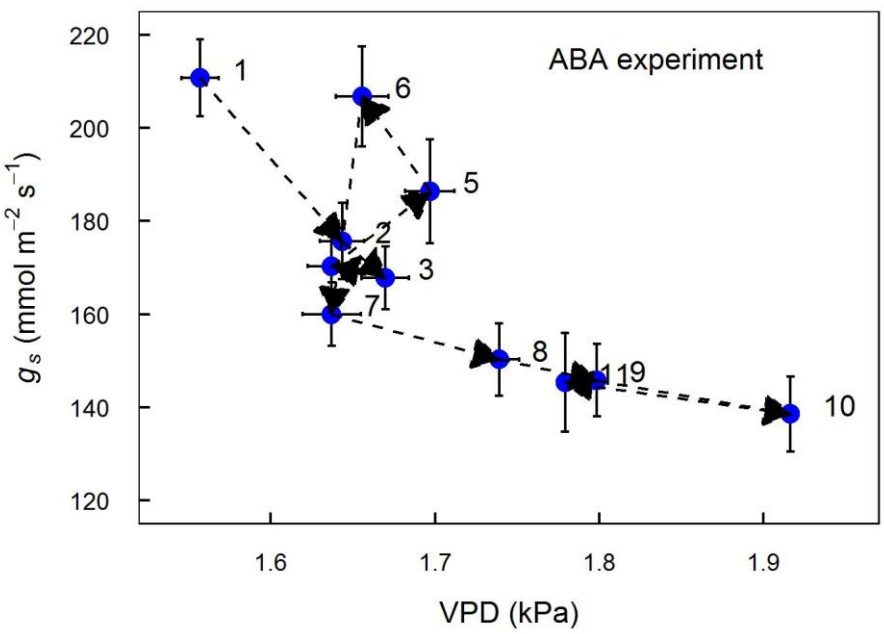

Supplementary Figure S8. Relationship between vapour pressure deficit (VPD) and stomatal conductance (g_s) of well-watered plants recorded during the a) drought-rehydration experiment and b) ABA watering experiment. VPD was calculated from temperature and relative humidity which were recorded close to the leaves of the plants in the experiment. Stomatal conductance were measured for the well-watered or mock-control Arabidopsis plants (*Arabidopsis thaliana*) ecotype Col-0. Data are shown as mean ± SE per day. The day is indicated by a number next to the symbol. Data points for successive days are connected by dashed lines and the directions are indicated by arrows.

Supplementary Tables

Supplementary Table S2. TaqMan® probes on custom designed TaqMan® OpenArray® Real-Time PCR Plates (56 assay format) for gene expression analysis of aquaporins and other drought stress related genes. TaqMan® OpenArray® Real-Time PCR Plates were manufactured by ThermoFisher Scientific. Context sequence refers to the TaqMan® probe. Where context sequence is #NA, details of the probes were not supplied by the manufacturer.

Gene name	Locus	Assay ID	Context sequence
AtABI1	AT4G26080	At02238783_g1	TTATCCGTTGACCATAAACCGGATA
AtACT2	AT3G18780	At02335270_gH	#NA
AtCCD1	AT3G63520	At02206714_g1	AACACAGGGAAATCATGCGTGACTG
AtCIPK16	AT2G25090	At02274390_m1	ATTGTACACGAAGATCTTCAAGGCG
AtELF	AT1G13950	At02337969_g1	#NA
AtERF058	AT1G22190	At02305348_s1	TTAGATGTTGCCATAGGGGTATTTT
AtGAPC2	AT1G13440	At02284911_gH	#NA
AtKAT1	AT5G46240	At02316701_g1	#NA
AtMYB2	AT2G47190	At02264149_g1	GTTCCTCTGGGCTAAAGCGAACTGG
AtNCED2	AT4G18350	At02223260_s1	TACCGTATGGGTTTCATGGCACATT
AtNCED3	AT3G14440	At02247253_s1	AGCTTGTAGCTTTTGGGCTGTAGGG
AtNCED4	AT4G19170	At02300341_s1	TCTTAATTACGTCCCGTACAACAAA
AtNCED5	AT1G30100	At02168304_s1	CCGTATGGTTTCCACGGCACTTTCG
AtNIP1;1	AT4G19030	At02336641_g1	GCTAATTGCCGCACCGGTATCGAGT
AtNIP1;2	AT4G18910	At02300159_g1	ATAATTGCCGGGCCGGTATCGGGAG

AtNIP2;1	AT2G34390	At02204681_g1	TTTCTTGCAAAAGCTCTTAGCGGAG
AtNIP3;1	AT1G31885	At02169592_g1	TTTTCTCCGGGCCAATTTCGGGAGC
AtNIP4;1	AT5G37810	At02337513_m1	GCCACCGATAATCGTGCGGTTGGAG
AtNIP4;2	AT5G37820	At02229735_gH	GTCGTGCGACTGGAGAATTAGCTGG
AtNIP5;1	AT4G10380	At02298958_m1	CACTCGCAAGCTTGGAGCCGAGTTC
AtNIP6;1	AT1G80760	At02290074_g1	ACTTATAGCTGGACCTGCAACTTCT
AtNIP7;1	AT3G06100	At02235993_g1	TACCGGACCGATTTCAGGAGGATCG
AtPIP1;1	AT3G61430	At02205472_g1	TCCTGGGATGACCACTGGGTGTTTT
AtPIP1;2	AT2G45960	At02263525_gH	GACTCTCATGTTCCTATTCTAGCAC
AtPIP1;3	AT1G01620	At02258569_gH	TGGAATCTCTGGTGGGCACATAAAC
AtPIP1;4	AT4G00430	At02207001_gH	CTGCTGGAATTTCAGGTGGACACAT
AtPIP1;5	AT4G23400	At02166390_g1	TTGGGATGACCATTGGATCTTCTGG
AtPIP2;1	AT3G53420	At02336003_g1	GCACCGCCGGTATCTCTGGTGGTCA
AtPIP2;2	AT2G37170	At02357614_s1	CCTTCAGAAGTGCAGCCAACGTTTG
AtPIP2;3	AT2G37180	At02338152_gH	CATGGGATGACCACTGGATATTCTG
AtPIP2;4	AT5G60660	At02269587_g1	TGGGACGACCAATGGATTTTTTGGG
AtPIP2;5	AT3G54820	At02189083_g1	GACCATCATTGGATATTCTGGGTGG
AtPIP2;6	AT2G39010	At02324320_g1	AAGGCTTGGGATGATCAGTGGATCT
AtPIP2;7	AT4G35100	At02255535_gH	TCTCACATCCCCGTTTTGGCTCCAC
AtPIP2;8	AT2G16850	At02171667_g1	CTCACGTCCCGGTTTTGGCTCCGTT
AtRAP2.4	AT1G78080	At02288270_s1	TTGTATTAGTCTCTCTGTGTCGGTC
AtRMA1	AT4G03510	At02209115_g1	TTCTCCACTCGATGGAGCTTATCTA
AtSIP1;1	AT3G04090	At02230039_mH	TACCTGCTCAGGCAATTGGTGCTGC
AtSIP1;2	AT5G18290	At02201653_g1	ATCCTGCCATTGCGTTTGGGTGGGC
AtSIP2;1	AT3G56950	At02190288_g1	GCATGAACCCTGCAGCTGTTATGGG
AtSIRK1	AT5G10020	At02272430_g1	TTAGCCATGCATCTTTACGAGACTA
AtSUT2	AT2G02860	At02162218_g1	TTCCCCAGATGATAGTATCACTTGG
AtSYP121	AT3G11820	At02240692_g1	CTGATTTCCACTGGAGAGAGTGAGA
AtSYP122	AT3G52400	At02187626_g1	TCTCCACAGGTGAAAGTGAAACATT
AtTIP1;1	AT2G36830	At02323140_g1	GCCACCGGTGGCTTGGCTGTGCCGG
AtTIP1;2	AT3G26520	At02280733_g1	CACCGGTGGCGAGCCAATTCCAGCG
AtTIP1;3	AT4G01470	At02207676_s1	TTTATCGGTGCAGCCATTGCAGCTA
AtTIP2;1	AT3G16240	At02252724_g1	TCTGCCATTGCCTACGCAAAGCTGA
AtTIP2;2	AT4G17340	At02222599_g1	TTACCAATGGCGAGAGCGTACCGAC
AtTIP2;3	AT5G47450	At02317512_gH	ACTAATGGCAAGAGCGTACCGACCC
AtTIP3;1	AT1G73190	At02228798_g1	CAACAAACGGCATGAGACCAGTTGG
AtTIP3;2	AT1G17810	At02157564_g1	CTAATGGCTTGAGACCAGTAGGTTT
AtTIP4;1	AT2G25810	At02274818_g1	GAGGAATGGGAACTCCGGTTCACAC
AtTIP5;1	AT3G47440	At02295610_g1	CCGTCATGGAACAGCACGTACCGAT
AtTUB5	AT1G20010	At02333375_gH	#NA
AtUBQ10	AT4G05320	At02358313_s1	#NA

Supplementary Table S3. Pipetting instructions for multi-reaction mix for TaqMan® OpenArray® Real-Time PCR Plates.

Component	**6 µL multi-reaction**
2X TaqMan® OpenArray® Real-Time PCR Master Mix	3 µL
ddH_2O	0.12 µL
cDNA (50 ng/µL)	2.88 µL

Supplementary information of Chapter 3

Supplementary Figures

a)

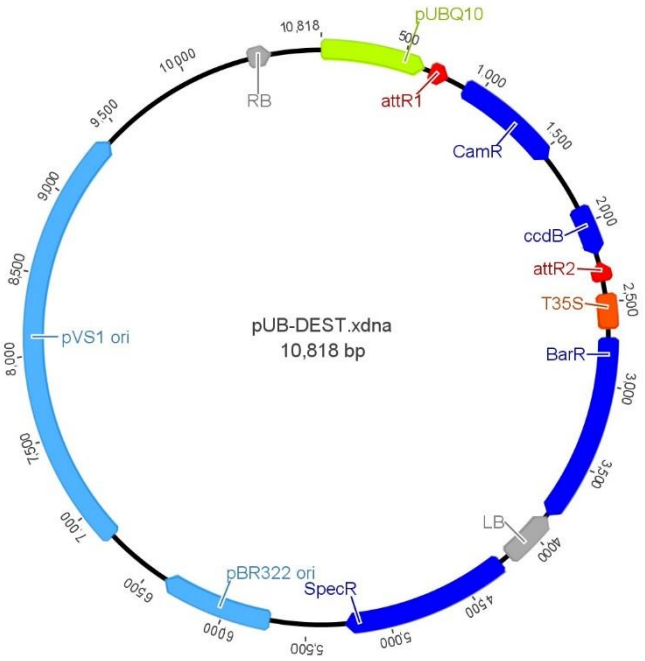

b)

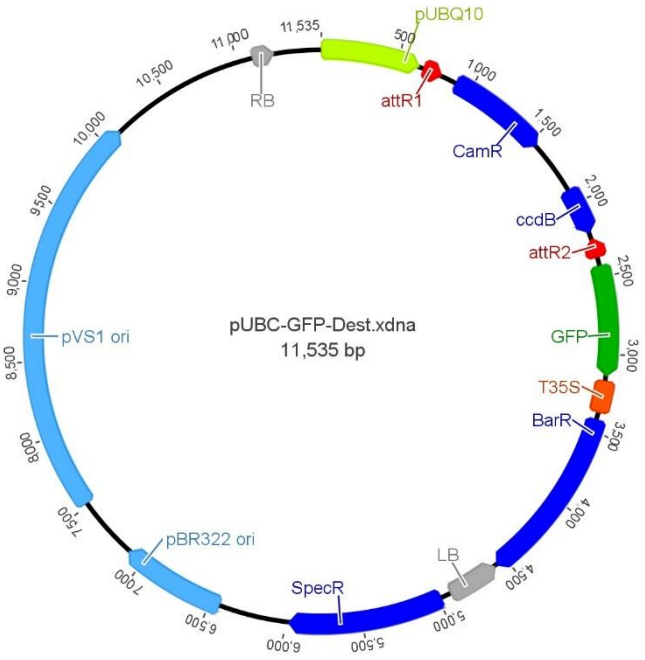

Supplementary Figure S9. Graphic maps of a) pUB-DEST and b) pUBC-GFP-DEST vectors for overexpression. The Ubiquitin10 vectors contain a UBQ10 promoter (light green) to drive a gene of interest. Additionally the pUBC-GFP-DEST vector (b) also contains a sequence for a fluorescent GFP tag (dark green), which will be attached to the protein. Transcription is terminated by a 35S terminator (orange). Three resistance genes (BarR, CamR, SpecR) provide a marker for selection. CamR is located with the ccdB gene for selection within the insertion site attR1 and attR2 (red). Both vectors also have a pVS1 and pBR322 origin of replication (light blue).

a)

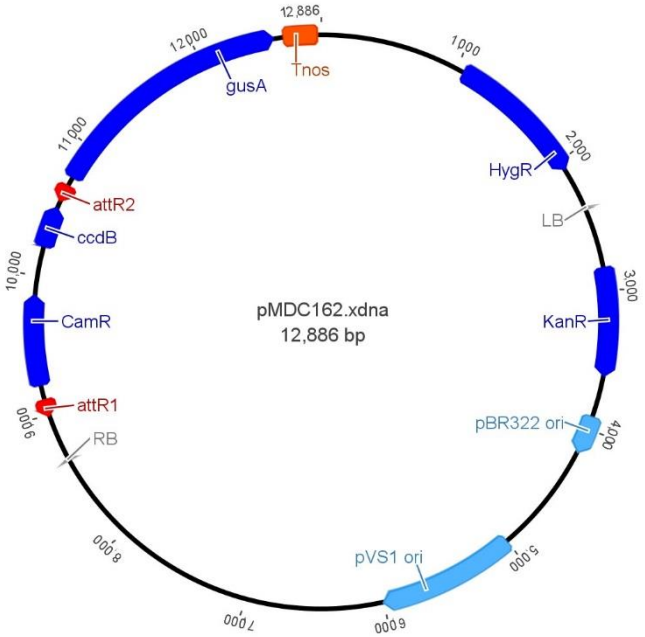

Supplementary Figure S10. Graphic map of the pMDC162 vector for GUS reporter studies. The vector contains the gusA gene (dark blue) which can be driven by a promoter of interest. Three resistance genes (CamR, HygR, KanR) provide a marker for selection. CamR is located with the ccdB gene for selection within the insertion site attR1 and attR2 (red). Transcription is terminated by a nos terminator (orange). The vector also has a pVS1 and pBR322 origin of replication (light blue).

Supplementary Tables

Supplementary Table S4. List of primer sequences used for the TIP2 overexpression project.

Primer	Oligo	Tm (°C)	Product size (bp)
TIP21_CACC-FL_F	forward: 5'-CACCATGGCTGGAGTTGCCTTTG-3'	72	757 or 754 (-stop)
TIP21_FL_R	reverse: 5'-TTAGAAATCAGCAGAAGCAAGAGGAACA-3'	69	
or			
TIP21_FL-STOP_R	reverse: 5'-GAAATCAGCAGAAGCAAGAGGAAC-3'	70	
TIP22_CACC-FL_F	forward: 5'-CACCATGGTGAAGATTGAGATA-3'	62	757 or 754 (-stop)
TIP22_FL_R	reverse: 5'-TCAAGGGTAGCTTTCTGTGG-3'	62	
or			
TIP22_FL-STOP_R	reverse: 5'-AGGGTAGCTTTCTGTGGTGG-3'	62	
TIP23_CACC-FL_F	forward: 5'-CACCATGGTGAAGATCGAAGTTG-3'	68	757 or 754 (-stop)
TIP23_FL_R	reverse: 5'-TTACACTCGGATCTCACGGGTTTC-3'	69	
or			
TIP23_FL-STOP_R	reverse: 5'-CACTCGGATCTCACGGGT-3'	64	
M13_F	forward: 5'-CAGGAAACAGCTATGAC-3'	58	variable
M13_R	reverse: 5'-CAGGAAACAGCTATGAC-3'	58	
pTIP21_CACC_F	forward: 5'-CACCACCGTTGCTGTGGTTCAATA-3'	63	2262
pTIP21_R	reverse: 5'-AGAATAAGGAAATGTTTTGAAGGG-3'	62	

pTIP22_CACC_F pTIP22_R	forward: 5'-CACCAACCAAAATTGACCGTGCATC-3' reverse: 5'-TGTGGTTTTGGGCATACTAAT-3'	66 61	3003
pTIP23_CACC_F pTIP23_R	forward: 5'-CACCGGTTTTAGAACGGACGGAGG-3' reverse: 5'-TTTCTGTTATTTGGGCTTTGTATG-3'	65 63	1244
SP1	forward: 5'-TGCAAGTCAACAGATCTAAAATTG-3'	58	variable
SP2	forward: 5'-TGTGATTTAATCGATCTAACAACTTT-3'	58	variable
SP3	forward: 5'-TCTGATCAAATCACTTGGAAAA-3'	58	variable
SP4	forward: 5'-AGGGGTTGGGTTGTAAGTTC-3'	58	variable
SP5	forward: 5'-TGGAGATTCTGGTTTTGAAAGT-3'	58	variable
SP6	forward: 5'-GGCAAATGAAATGAGTCTGG-3'	58	variable
SP7	forward: 5'-CGGTTTCGTATTGGTATTGG-3'	58	variable
SP8	forward: 5'-TAGAGCGAGAATTCGCAAAC-3'	58	variable
AtACT2_F AtACT2_R	forward: 5'-CTTGCACCAAGCAGCATGAA-3' reverse: 5'-ACCGATCCAGACACTGTACTTCCTT-3'	60 63	69
AtTIP2;1_F AtTIP2;1_R	forward: 5'-GCTGGAGTTGCCTTTGGTTC-3' reverse: 5'-TTTGACCACCGACAGCAAGA-3'	60 60	283

Supplementary Table S5. Pipetting instructions for PCR amplification of TIP2 coding and promoter sequences for cloning using the Phusion® High-Fidelity DNA Polymerase (New England Biolabs).

Component	50 µL reaction
ddH_2O	to 50 µL
5x Phusion® HF Buffer	10 µL
10 mM dNTPs	1 µL
10 µM primer forward	2.5 µL
10 µM primer reverse	2.5 µL
Template DNA	variable (pDNA: 1-10 ng, cDNA or gDNA: 50-250 ng)
Phusion® High-Fidelity DNA Polymerase	0.5 µL

Supplementary Table S6. Pipetting instructions for directional cloning using the pENTR/D-TOPO Cloning Kit (ThermoFisher Scientific).

Component	6 µL reaction
Sterile water	to 6 µL

Salt solution	1 µL
Purified PCR product	variable (1-5 ng of 1 kb PCR product)
pENTR/D-TOPO® vector	1 µL

Supplementary Table S7. Pipetting instructions for LR reactions using Gateway® LR Clonase® II enzyme mix (ThermoFisher Scientific).

Component	5 µL reaction
TE buffer [0.25X] pH = 8	2 µL
pENTR+insert (50-150 ng)	1 µL
pUB-DEST or pUBC-GFP-DEST or pMDC162 (50-150 ng)	1 µL
Gateway® LR Clonase® II enzyme mix	1 µL

Supplementary Table S8. Solutions for GUS assay (chemicals from Sigma Aldrich).

Solution	Components
90% Acetone	90% (v/v) Acetone, 10% (v/v) ddH_2O
10% Triton-X	10% (v/v) Triton-X, 90% (v/v) ddH_2O
0.1 M $NaPO_4$ Buffer	14% (v/v) 0.2 M $NaH_2PO_4 \cdot 2H_2O$, 36% (v/v) 0.2 M Na_2HPO4, 50% (v/v) ddH_2O, pH = 7.2
Staining Buffer	50% (v/v) 0.1 M NaPO4 Buffer, 2% (v/v) 10% Triton-X, 2% (v/v) 0.1 M Potassium ferrocyanide, 2% (v/v) 0.1 M Potassium ferricyanide, 44% (v/v) ddH_2O
FAA fixative	50% (v/v) Ethanol, 3.7% (v/v) Formaldehyde, 5% (v/v) Acetic acid, 41.3% (v/v) ddH_2O
0.1 M X-Gluc	100 mg X-Gluc, 1.9 mL DMF (N,N-Dimethylformamide); store in dark at -20°C

Supplementary Methods

Preparation of chemically competent E. coli DH5α cells

Inoculate 5 mL liquid LB medium with a single colony of E. coli DH5α or from a glycerol stock. Grow overnight at 200 rpm and 37 °C. The next morning, inoculate 150 mL liquid LB with 3.5 mL of the starter culture. Measure OD_{600}: Use LB Broth as blank; the start OD_{600} should be about 0.1. Grow culture for 1.5-3 hrs at 200 rpm and 37°C. Measure OD_{600} periodically until $OD_{600} \approx 0.5$. Transfer culture into multiple 50mL Conical Centrifuge Tubes and rest for 10 min on ice. Centrifuge at ≤ 4000 *x g* for about 3 min at 4 °C or until supernatant is clear. Decant supernatant and resuspend cells gently in 10 mL cold 0.1 M $CaCl_2$. Incubate on ice for 20 min. Centrifuge at ≤ 4000 *x g* for about 3 min at 4 °C or until supernatant is clear. Decant supernatant and resuspend cells gently in 5 mL cold 0.1 M $CaCl_2$ + 15 % Glycerol. Store on ice. Aliquot 300 µL each into 1.5 mL micro tubes (pre-chill at -20 °C) on ice and snap-freeze immediately in liquid nitrogen. Store competent cells at -80 °C.

Supplementary information of Chapter 4

Supplementary Figures

a)

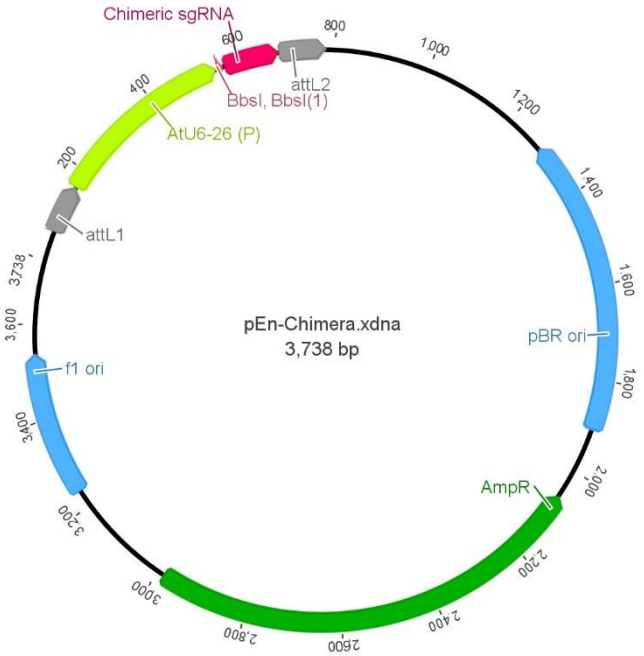

b)

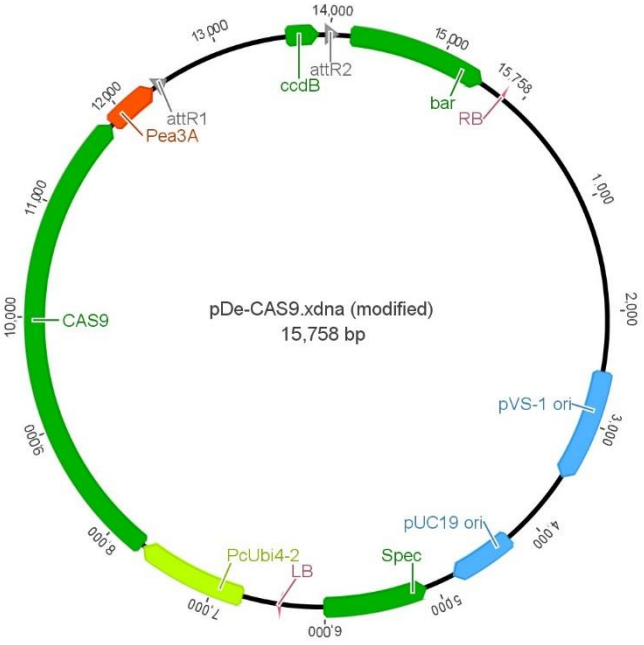

Supplementary Figure S11. Graphic maps of pEn-Chimera and pDe-CAS9 vectors. (a) The entry vector pEn-Chimera contains two origins of replication (blue), an Ampicillin resistance (dark green), AtU6-26 promoter (light green) to drive the expression of the single guide RNA, the chimeric sgRNA (red), restriction sites for *Bbs*I to open the vector for ligation with the guide sequence, and the attL1/attL2 sites (grey) for the LR reaction with the destination vector (pDe-CAS9). (b) The destination vector pDe-CAS9 contains two origins of replication (blue), a Phosphinothricin and Spectinomycin resistance (dark green), the nuclease CAS9 (dark green) which is driven by the PcUbi4-2 promoter (light green) and terminated by the Pea3A terminator

(orange), the attR1/attR2 sites (grey) for the LR reaction with the entry vector (pEn-Chimera), and the ccdB gene (dark green) for selection within this site.

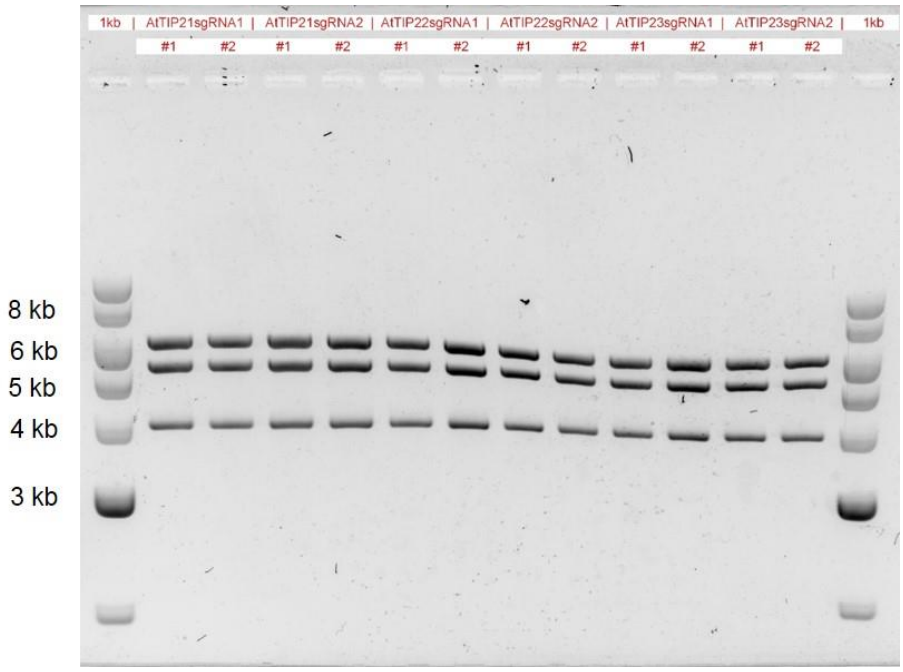

Supplementary Figure S12. Gel electrophoresis image of pDe-CAS9-sgRNA restriction digest with with *Afl*II and *Nhe*I. For each construct two samples are shown.

a)

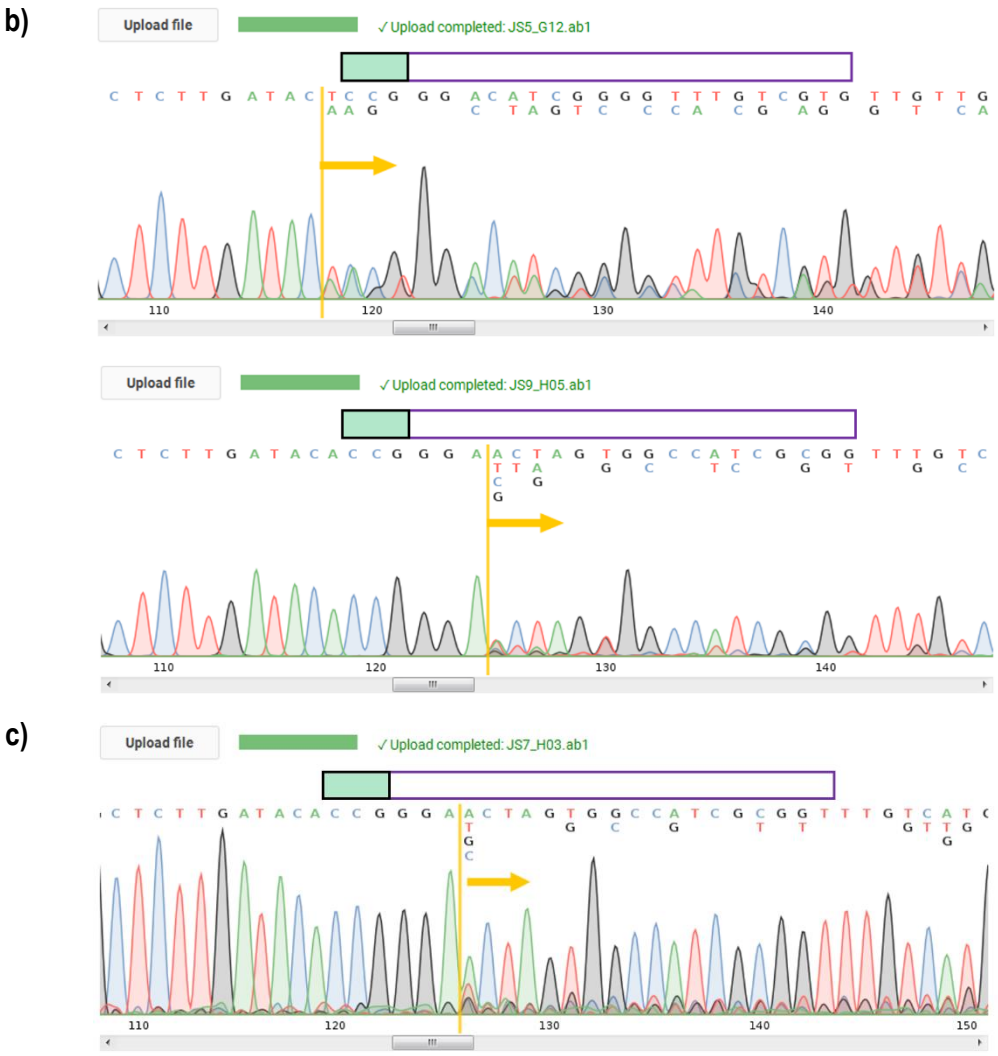

Supplementary Figure S13. Sequence decomposition of Sanger Sequencing chromatograms from selected samples of AtTIP2;1 Guide#1. The purple box indicates the position of the guide sequence target site and the green box the PAM. The predicted genetic sequence is shown as letter code and can have multiple layers where multiple signals were picked up. In this case the boxes for guide sequence and PAM are shown above the code. The yellow line and arrow indicate were multiple signals start in the chromatogram. Sequence decomposition was done using the web-tool CRISP-ID (http://crispid.gbiomed.kuleuven.be). a) Samples predicted as wild-type, b) samples predicted with heterozygous mutations, and c) sample predicted with potential homozygous mutation.

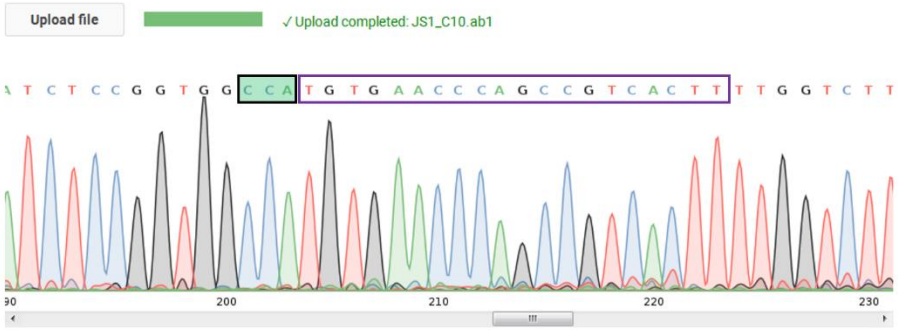

Supplementary Figure S14. Sequence decomposition of Sanger Sequencing chromatograms from selected samples of AtTIP2;1 Guide#2. The purple box indicates the position of the guide sequence target site and the green box the PAM. The predicted genetic sequence is shown as letter code. Sequence decomposition was done using the web-tool CRISP-ID (http://crispid.gbiomed.kuleuven.be). All samples were predicted to be wild-type.

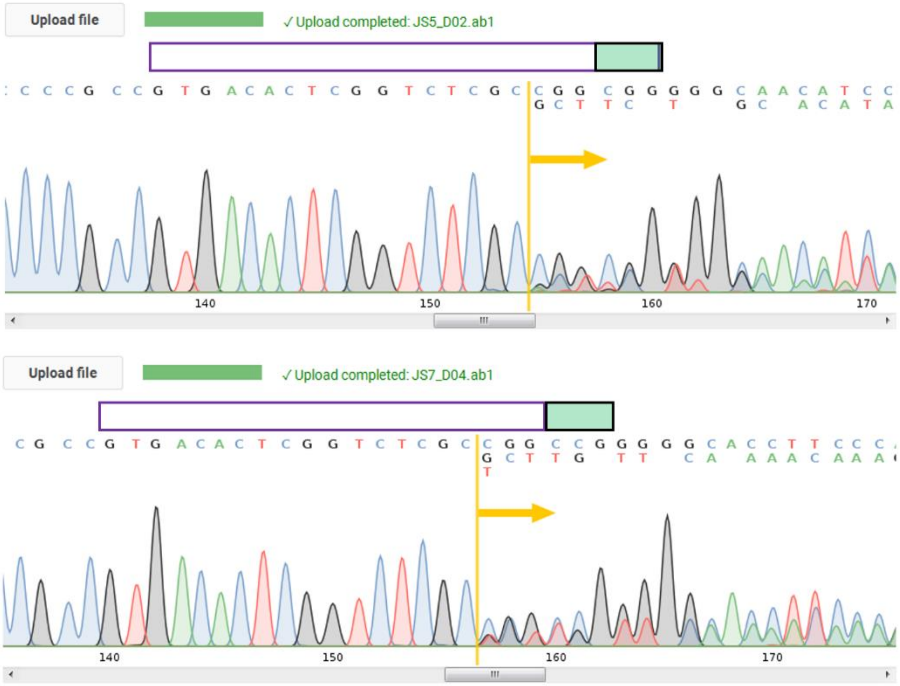

Supplementary Figure S15. Sequence decomposition of Sanger Sequencing chromatograms from selected samples of AtTIP2;2 Guide#1. The purple box indicates the position of the guide sequence target site and the green box the PAM. The predicted genetic sequence is shown as letter code and can have multiple layers where multiple signals were picked up. In this case the boxes for guide sequence and PAM are shown above the code. The yellow line and arrow indicate were multiple signals start in the chromatogram. Sequence decomposition was done using the web-tool CRISP-ID (http://crispid.gbiomed.kuleuven.be). All samples were predicted to have heterozygous mutations.

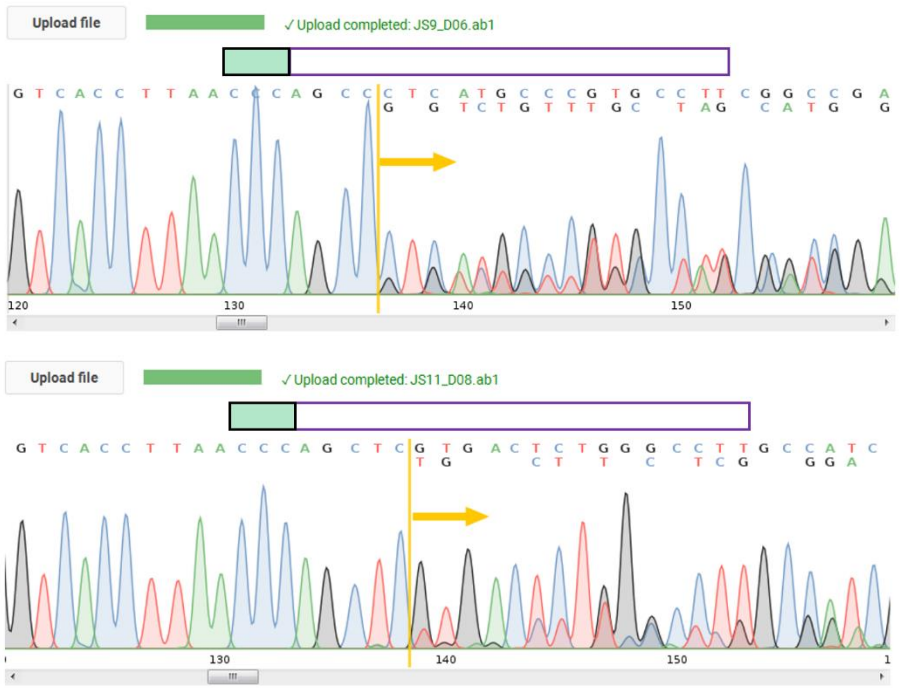

Supplementary Figure S16. Sequence decomposition of Sanger Sequencing chromatograms from selected samples of AtTIP2;3 Guide#2. The purple box indicates the position of the guide sequence target site and the green box the PAM. The predicted genetic sequence is shown as letter code and can have multiple layers where multiple signals were picked up. In this case the boxes for guide sequence and PAM are shown above the code. The yellow line and arrow indicate were multiple signals start in the chromatogram. Sequence decomposition was done using the web-tool CRISP-ID (http://crispid.gbiomed.kuleuven.be). All samples were predicted to have heterozygous mutations.

Supplementary Tables

Supplementary Table S9. Pipetting instructions for restriction digest of pEn-Chimera using the restriction enzyme *Bbs*I-HF (New England Biolabs).

Component	20 µL reaction
ddH_2O	7 µL
10 X NEB buffer 2.1	2 µL
pEn-Chimera (50 ng/µL)	10 µL
*Bbs*I-HF (New England Biolabs)	1 µL

Supplementary Table S10. Pipetting instructions for ligation of double stranded protospacer into pEn-Chimera using T4 Ligase (New England Biolabs).

Component	11 µL reaction
T4 Ligase buffer	5 µL
pEn-Chimera (5 ng/µL) digested by *Bbs*I-HF	2 µL
Double stranded protospacer	3 µL
T4 Ligase	1 µL

Supplementary Table S11. Pipetting instructions for liquid culture PCR using the Phire Hot Start II DNA Polymerase (Thermo Scientific). After overnight incubation, 5 µL of liquid culture with bacteria is diluted in 15 µL sterile H_2O and heated at 95°C for 6 min to break open cells. This dilution is directly added to the reaction mixture.

Component	20 µL reaction
ddH_2O	12.2 µL
5x Phire Reaction Buffer	4 µL
10 mM dNTPs	0.4 µL
10 µM primer forward	1 µL
10 µM primer reverse	1 µL
Dilute liquid culture	2 µL
Phire Hot Start II DNA Polymerase	0.4 µL

Supplementary Table S12. List of primer sequences used for the CRISPR-Cas project. Primers SS42, SS43, and SS61 were taken from Fauser *et al.* (2014).

Primer	Oligo	Tm (°C)	Product size (bp)
SS42	TCCCAGGATTAGAATGATTAGG	58	-
SS43	CGACTAAGGGTTTCTTATATGC	58	-
SS61	GAGCTCCAGGCCTCCCAGCTTTCG	69	-
GAPDH_F GAPDH_R	forward: 5'-CTGCCCCAAGCAAAGATGCG-3' reverse: 5'- AGCGTTGGAAACAATGTCAAGG-3'	63 60	86
HRM_TIP21_F HRM_TIP21_R	forward: 5'-CCGTTGCAATCGGAGCCAAC-3' reverse: 5'-TGACTGTGATTTGACCACCGA-3'	59 59	87

HRM_TIP22_F HRM_TIP22_R	forward: 5'-CCTTAACCCCGCCGTGACA-3' reverse: 5'-CAAGGCATTGAGCAATCCAGTAAA-3'	62 60	89
HRM_TIP23_F HRM_TIP23_R	forward: 5'-TTGGAGTTTCCATTGCGGCT-3' reverse: 5'-GTGTTATGTTTCCGCCGATGG-3'	64 60	87
Seq_TIP21_F Seq_TIP21_R	forward: 5'-CTCTGCCATTGCCTACGGT-3' reverse: 5'-TACCAATCCACCGGTGACG-3'	60 60	374
Seq_TIP22_F Seq_TIP22_R	forward: 5'-TTCTCTTTGTGTTTGCTGGCG-3' reverse: 5'-TTTGTGTACCTCGCCATTGGT-3'	60 60	302
Seq_TIP23_F Seq_TIP23_R	forward: 5'-TTCGTATTCGCAGGCGTTGG-3' reverse: 5'-CTCTGCAGCAAACCGGGAAA-3'	60 60	495

Supplementary Table S13. Pipetting instructions for Sanger Sequencing (PD service) with AGRF.

Component	12 µL reaction
ddH_2O	up to 12 µL
10 µM primer	1 µL
Purified plasmid DNA	250 ng

Supplementary Table S14. Pipetting instruction for Gateway® LR Recombination Reaction (Thermo Fisher Scientific) between the entry vector pEn-Chimera with sgRNA and the destination vector (pDe-CAS9).

Component	5 µL reaction
TE buffer [0.25X] pH = 8	2 µL
pEn-Chimera-sgRNA (75 ng)	1 µL
pDe-CAS9 (75 ng)	1 µL
Gateway® LR Clonase® II enzyme mix	1 µL

Supplementary Table S15. Pipetting instruction for restriction digest of final pDe-CAS9-sgRNA plasmid DNA using *Afl*II and *Nhe*I restriction enzymes (New England Biolabs).

Component	10 µL reaction
ddH_2O	up to 10 µL
CutSmart® Buffer (New England Biolabs)	1 µL
*Afl*II (20,000 U/mL)	0.1 µL
*Nhe*I (20,000 U/mL)	0.1 µL

pDe-CAS9-sgRNA plasmid DNA	~ 100 ng

Supplementary Table S16. General growth media and solutions. Chemicals were obtained from Sigma Aldrich unless stated otherwise.

Media/Solution	Components
Luria Broth (LB)	10 g/L Bacto™ Tryptone (BD Biosciences), 5 g/L Bacto™ Yeast (BD Biosciences), 10 g/L NaCl, pH = 7 with 1M NaOH, + 15 g/L Difco™ Agar (BD Biosciences) for solid media
2YT Broth	16 g/L Bacto™ Tryptone (BD Biosciences), 10 g/L Bacto™ Yeast (BD Biosciences), 5 g/L NaCl, pH = 7 with 1M NaOH, + 15 g/L Difco™ Agar (BD Biosciences) for solid media
Floral dip medium (make fresh)	50 g/L sucrose, 10 mM $MgCl_2$, 10 mM MES pH = 5.6, 150 µM acetosyringone, 0.05 % (v/v) Silwet L-77 (add last, mix by inversion, avoid foam, handle with care)
½ Murashige and Skoog (MS) medium	2.2 g/L Murashige and Skoog Basal Salt Mixture (Sigma-Aldrich), 0.5 g/L MES, 2.5 g/L sucrose, pH = 5.7 with 1M KOH, + 5 g/L Phytagel™ (Sigma-Aldrich) for solid media

Supplementary Table S17. Pipetting instructions for quantitative real-time PCR to adjust concentrations of genomic DNA using the QuantiNova SYBR Green PCR Kit (QIAGEN).

Component	10 µL reaction
2x QuantiNova SYBR Green PCR Master Mix	5 µL
ddH_2O	2.3 µL
10 µM primer mix (forward and reverse)	0.7 µL
Genomic DNA (10 ng/µL)	2 µL

Supplementary Table S18. Pipetting instructions for High Resolution Melt reactions using the Type-it HRM PCR Kit (QIAGEN).

Component	10 µL reaction
2x HRM PCR Master Mix	5 µL
ddH_2O	2.3 µL

10 µM primer mix (forward and reverse)	0.7 µL
Genomic DNA (10 ng/µL)	2 µL

Supplementary Table S19. Pipetting instructions for Sanger Sequencing pre-amplification PCR using the Phusion® High-Fidelity DNA Polymerase (New England Biolabs).

Component	20 µL reaction
ddH_2O	11.4 µL
5x Phusion® HF Buffer	4 µL
10 mM dNTPs	0.4 µL
10 µM primer forward	1 µL
10 µM primer reverse	1 µL
Genomic DNA (10 ng/uL)	2 µL
Phusion® High-Fidelity DNA Polymerase	0.2 µL

Supplementary Table S20. Pipetting instructions for genotyping CRISPR-Cas plants with Phire Plant Direct PCR Kit (ThermoFisher Scientific).

Component	20 µL reaction
ddH_2O	8.8 µL
2X Phire Plant Tissue PCR Buffer	10 µL
2.5 µM Universal Control Primer mix	0.4 µL
25 µM SS42/SS43 primer mix	0.4 µL
Template	Leaf punch from 1 µL Pipette Tip
Phire Hot Start II DNA Polymerase	0.4 µL

Supplementary Methods

Preparation of chemically-competent *Agrobacterium tumefaciens* cells

A modified method of Berberich *et al.* (2008) was used to prepare chemically-competent *Agrobacterium tumefaciens* cells.

Strike glycerol stock of *Agrobacterium* strain AGLI on 2YT plate + Rif (25 µg/mL) and grow at 28 °C for two days. Transfer one single colony into 5 mL liquid 2YT Broth + Rif (25 µg/mL) and grow for 1-2 days at 28 °C and 200 rpm to develop a starter culture.

Inoculate 250 mL of LB Broth + Rif (25 µg/mL) in a 500 mL conical flask with 2.5 mL of the starter culture and grow overnight at 28 °C and 200 rpm; keep incubation time ≤ 14 hrs. Measure OD_{600}: Use LB Broth + Rif as blank; dilute culture 1:10 for OD measurements (100 µL culture + 900 µL LB Broth + Rif); grow cells till OD_{600} = 0.8 – 1.0. Transfer culture into multiple 50mL Conical Centrifuge Tubes on ice and centrifuge at ≤ 4000 *x g* for about 40 min at 4 °C; check in between and stop once supernatant is clear. Discard supernatant and resuspend pellets in 5 mL ice-cold 150 mM NaCl each; mix by carefully pipetting up and down. Pool suspensions in one tube and chill on ice for 15 min. Centrifuge at ≤ 4000 *x g* for about 30 min at 4 °C until supernatant is clear. Discard supernatant and resuspend pellet in 5 mL ice-cold 20 mM $CaCl_2$ and store on ice. Aliquot 100 µL each into 1.5 mL micro tubes (pre-chill at -20 °C) on ice and snap-freeze immediately in liquid nitrogen. Store competent cells at -80 °C.

Transformation of chemically-competent *Agrobacterium tumefaciens* cells

Pre-heat heating block to 39 °C and 2YT plates + antibiotics at 28 °C; antibiotics: 50 µg/mL Rif + plasmid specific antibiotic (e.g. 100 µg/mL Spec). Take chemically-competent *Agrobacterium tumefaciens* cells from the -80 °C freezer and add 1µg of plasmid DNA (max. 10 µL) immediately. Incubate at 39 °C for 2 – 5 min; mix by gentle flicking after 1 min. Add 500 µL 2YT Broth to each tube and incubate at 28°C and 200 rpm for 4 hrs. Centrifuge cultures at 5400 *x g* for 30 sec. Remove about 150 µL of supernatant and resuspend by gentle pipetting. Plate total transformation on pre-warmed 2YT plates + antibiotics. Incubate for 2 – 3 days at 28 °C.

Agrobacterium floral dip transformation

Make fresh floral dip medium (Supplementary Table S16); about 400 mL per construct. Split overnight culture (250 mL) into 2 x ultracentrifuge bottle (125 mL each); use balance to adjust. Centrifuge at 4000 *x g* for 30 min at room temperature. Discard supernatant and carefully resuspend in 3 mL infiltration medium.

Fill resuspended culture into 400 mL beaker and fill up to 400 mL with floral dip medium. Use gloves since Silwet-77 dissolves skin. Label pots of flowering *Arabidopsis thaliana* plants with names of constructs. Carefully dip inflorescence (3 – 5 plants per pot) into cultures with floral dip medium and use twisting motion to suspend the whole inflorescence without breaking it for 2 min (stop-watch; no longer). After dipping, rest the pots flat on trays and cover with plastic wrap to reduce drying for 24 hrs in the shade. After 24 hrs, uncover pants and carefully put up.

Seed sterilisation with chlorine gas

Don't inhale chlorine gas! Extremely toxic!

An equivalent of 100 µL of seed are filled into 2 mL micro tubes which are labelled with a black permanent pen (use only black pen). The tubes are placed into a rack into a small desiccator in a fume hood; make sure fume hood is running. Fill 100 mL beaker will 90 mL bleach/sodium hypochlorite solution (chem-supply; about 7 % available chlorine) and place in desiccator. Add about 6 mL concentrated HCl to the solution or until good gas development is visible. Immediately seal desiccator and leave for 2-3 hrs. Afterwards, remove lid carefully and transfer rack with seed into clean bench for at least 3 hrs to remove the chlorine gas from the tubes. Seal and store dry.

oKtopure™ automated DNA extraction (sbeadex™ mini plant extraction chemistry)

Manual steps: Add 200 µL lysis buffer to each sample. Mix by inversion and incubate for 1 hr at 55 °C. Centrifuge at 4000 rpm for 5 mins. Add 200 µL of binding buffer in deep-well plates. Insert plates with samples and deep-well plates with binding buffer in robot platform.

Automated steps: Transfer of 100 µL supernatant from samples into binding buffer; mixing by pipetting up and down for 30 sec. Incubation for 7 mins. Magnet engages to capture beads; wait for 30 sec. Removal of liquid from wells. Addition of 140 µL Wash buffer 1; mixing by pipetting up and down for

15 sec. Incubation for 6 mins. Magnet engages to capture beads; wait for 30 sec. Removal of Wash Buffer 1 from wells. Addition of 140 µL Wash buffer 2; mixing by pipetting up and down for 15 sec. Incubation for 6 mins. Magnet engages to capture beads; wait for 30 sec. Removal of Wash Buffer 2 from wells. Addition of 100 µL elution buffer; mixing by pipetting up and down for 30 sec. Transfer of DNA solution to 96-well plate.

Manual steps: Place 96-well plate with DNA onto magnet to capture any leftover beads. Transfer DNA solution into new 96-well plate. Store at 4 °C or at -20 °C for long term storage.

Homemade Glufosinate Assay

For the glufonisate selection, 250 µL of liquid, half-strength Murashige and Skoog medium (Murashige and Skoog 1962) (Supplementary Table S6) supplemented with 300 µM glufosinate ammonium (Sigma-Aldrich) were added into 96-well plates. In each well, one leaf (~ 4mm diameter) of about 2 weeks old plants were floated on top of the solution (bottom side down); the plates were covered with lids and incubated under long-day conditions (16 h light/ 8 h dark, PAR ~150 µmol m–2 s–1, 21 °C). Images of the plates were taken each day for five days using an Olympus E520 digital camera (OLYMPUS). Leave were rated according to their change of color (green = resistant, yellow = sensitive).

BIBLIOGRAPHY

Alexandersson, E, Danielson, JÅH, Råde, J, Moparthi, VK, Fontes, M, Kjellbom, P, Johanson, U (2010) Transcriptional regulation of aquaporins in accessions of Arabidopsis in response to drought stress. *The Plant Journal* **61**, 650-660.

Alexandersson, E, Fraysse, L, Sjövall-Larsen, S, Gustavsson, S, Fellert, M, Karlsson, M, Johanson, U, Kjellbom, P (2005) Whole gene family expression and drought stress regulation of aquaporins. *Plant Molecular Biology* **59**, 469-484.

Alleva, K, Niemietz, CM, Maurel, C, Parisi, M, Tyerman, SD, Amodeo, G (2006) Plasma membrane of Beta vulgaris storage root shows high water channel activity regulated by cytoplasmic pH and a dual range of calcium concentrations. *Journal of Experimental Botany* **57**, 609-621.

Alonso, JM, Ecker, JR (2006) Moving forward in reverse: genetic technologies to enable genome-wide phenomic screens in Arabidopsis. *Nat Rev Genet* **7**, 524-536.

Alonso, JM, Stepanova, AN, Leisse, TJ, Kim, CJ, Chen, H, Shinn, P, Stevenson, DK, Zimmerman, J, Barajas, P, Cheuk, R, Gadrinab, C, Heller, C, Jeske, A, Koesema, E, Meyers, CC, Parker, H, Prednis, L, Ansari, Y, Choy, N, Deen, H, Geralt, M, Hazari, N, Hom, E, Karnes, M, Mulholland, C, Ndubaku, R, Schmidt, I, Guzman, P, Aguilar-Henonin, L, Schmid, M, Weigel, D, Carter, DE, Marchand, T, Risseeuw, E, Brogden, D, Zeko, A, Crosby, WL, Berry, CC, Ecker, JR (2003) Genome-wide insertional mutagenesis of Arabidopsis thaliana. *Science* **301**, 653-657.

Anderberg, HI, Danielson, JA, Johanson, U (2011) Algal MIPs, high diversity and conserved motifs. *BMC Evol Biol* **11**, 110.

Anderson, EM, Haupt, A, Schiel, JA, Chou, E, Machado, HB, Strezoska, Ž, Lenger, S, McClelland, S, Birmingham, A, Vermeulen, A, Smith, AvB (2015) Systematic analysis of CRISPR–Cas9 mismatch tolerance reveals low levels of off-target activity. *Journal of Biotechnology* **211**, 56-65.

Barkla, BJ, Vera-Estrella, R, Pantoja, O, Kirch, HH, Bohnert, HJ (1999) Aquaporin localization - how valid are the TIP and PIP labels? *Trends Plant Sci* **4**, 86-88.

Baulcombe, D (2004) RNA silencing in plants. *Nature* **431**, 356-363.

Beebo, A, Thomas, D, Der, C, Sanchez, L, Leborgne-Castel, N, Marty, F, Schoefs, B, Bouhidel, K (2009) Life with and without AtTIP1;1, an Arabidopsis aquaporin preferentially localized in the apposing tonoplasts of adjacent vacuoles. *Plant Molecular Biology* **70**, 193-209.

Benga, G, Popescu, O, Borza, V, Pop, VI, Muresan, A, Mocsy, I, Brain, A, Wrigglesworth, JM (1986a) Water permeability in human erythrocytes: identification of membrane proteins involved in water transport. *Eur J Cell Biol* **41**, 252-62.

Benga, G, Popescu, O, Pop, VI, Holmes, RP (1986b) P-(Chloromercuri)benzenesulfonate binding by membrane proteins and the inhibition of water transport in human erythrocytes. *Biochemistry* **25**, 1535-1538.

Berberich, T, Takahashi, Y, Saitoh, H, Terauchi, R (2008) High-throughput functional screening of genes in planta. In 'The Handbook of Plant Functional Genomics.' pp. 113-136. (Wiley-VCH Verlag GmbH & Co. KGaA: Berlin)

Bertl, A, Kaldenhoff, R (2007) Function of a separate NH3-pore in Aquaporin TIP2;2 from wheat. *Febs Letters* **581**, 5413-5417.

Besserer, A, Burnotte, E, Bienert, GP, Chevalier, AS, Errachid, A, Grefen, C, Blatt, MR, Chaumont, F (2012) Selective regulation of maize plasma membrane aquaporin trafficking and activity by the SNARE SYP121. *The Plant Cell* **24**, 3463-3481.

Bienert, GP, Moller, AL, Kristiansen, KA, Schulz, A, Moller, IM, Schjoerring, JK, Jahn, TP (2007) Specific aquaporins facilitate the diffusion of hydrogen peroxide across membranes. *J Biol Chem* **282**, 1183-92.

Biskup, B, Scharr, H, Fischbach, A, Wiese-Klinkenberg, A, Schurr, U, Walter, A (2009) Diel growth cycle of isolated leaf discs analyzed with a novel, high-throughput three-dimensional imaging method is identical to that of intact leaves. *Plant Physiology* **149**, 1452-1461.

Bomblies, K, Franks, RG (2007) 'GUS Protocol (fool-proof version).' Available at http://www4.ncsu.edu/~rgfranks/research/protocols.html [Accessed 27/10/2015].

Borstlap, AC (2002) Early diversification of plant aquaporins. *Trends Plant Sci* **7**, 529-30.

Boursiac, Y, Boudet, J, Postaire, O, Luu, DT, Tournaire-Roux, C, Maurel, C (2008) Stimulus-induced downregulation of root water transport involves reactive oxygen species-activated cell signalling and plasma membrane intrinsic protein internalization. *Plant Journal* **56**, 207-218.

Boursiac, Y, Chen, S, Luu, D-T, Sorieul, M, van den Dries, N, Maurel, C (2005) Early effects of salinity on water transport in Arabidopsis roots. Molecular and cellular features of aquaporin expression. *Plant Physiology* **139**, 790-805.

Broek, Bvd, Vanzi, F, Normanno, D, Pavone, FS, Wuite, GJL (2006) Real-time observation of DNA looping dynamics of Type IIE restriction enzymes NaeI and NarI. *Nucleic Acids Research* **34**, 167-174.

Buckley, TN (2005) The control of stomata by water balance. *New Phytologist* **168**, 275-92.

Buckley, TN (2015) The contributions of apoplastic, symplastic and gas phase pathways for water transport outside the bundle sheath in leaves. *Plant Cell and Environment* **38**, 7-22.

Buckley, TN, Mott, KA (2013) Modelling stomatal conductance in response to environmental factors. *Plant, Cell & Environment* **36**, 1691-1699.

Byrt, CS, Zhao, M, Kourghi, M, Bose, J, Henderson, SW, Qiu, J, Gilliham, M, Schultz, C, Schwarz, M, Ramesh, SA, Yool, A, Tyerman, S (2017) Non-selective cation channel activity of aquaporin AtPIP2;1 regulated by Ca2+ and pH. *Plant, Cell & Environment* **40**, 802-815.

Canny, M, Wong, SC, Huang, C, Miller, C (2012) Differential shrinkage of mesophyll cells in transpiring cotton leaves: implications for static and dynamic pools of water, and for water transport pathways. *Functional Plant Biology* **39**, 91-102.

Castro, A, Stulen, I, Posthumus, FS, De Kok, LJ (2006) Changes in Growth and Nutrient Uptake in Brassica oleracea Exposed to Atmospheric Ammonia. *Annals of Botany* **97**, 121-131.

Chahal, SS (2010) Evaluation of soil hydraulic limitations in determining plant-available-water in light textured soils. The University of Adelaide.

Chaumont, F, Barrieu, F, Wojcik, E, Chrispeels, MJ, Jung, R (2001) Aquaporins constitute a large and highly divergent protein family in maize. *Plant Physiology* **125**, 1206-15.

Chaumont, F, Tyerman, SD (2014) Aquaporins: highly regulated channels controlling plant water relations. *Plant Physiology* **164**, 1600-1618.

Chevalier, AS, Bienert, GP, Chaumont, F (2014) A new LxxxA motif in the transmembrane helix3 of maize aquaporins belonging to the Plasma Membrane Intrinsic Protein PIP2 group is required for their trafficking to the plasma membrane. *Plant Physiology* **166**, 125-138.

Christmann, A, Grill, E, Huang, J (2013) Hydraulic signals in long-distance signaling. *Current Opinion in Plant Biology* **16**, 293-300.

Christmann, A, Weiler, EW, Steudle, E, Grill, E (2007) A hydraulic signal in root-to-shoot signalling of water shortage. *The Plant Journal* **52**, 167-174.

Clough, SJ, Bent, AF (1998) Floral dip: a simplified method for Agrobacterium-mediated transformation of Arabidopsis thaliana. *Plant Journal* **16**, 735-43.

Coupel-Ledru, A, Lebon, É, Christophe, A, Doligez, A, Cabrera-Bosquet, L, Péchier, P, Hamard, P, This, P, Simonneau, T (2014) Genetic variation in a grapevine progeny (Vitis vinifera L. cvs Grenache×Syrah) reveals inconsistencies between maintenance of daytime leaf water potential and response of transpiration rate under drought. *Journal of Experimental Botany* **65**, 6205-6218.

Coupel-Ledru, A, Tyerman, S, Masclef, D, Lebon, E, Christophe, A, Edwards, EJ, Simonneau, T (2017) Abscisic acid down-regulates hydraulic conductance of grapevine leaves in isohydric genotypes only. *Plant Physiology* EPub.

Cutler, SR, Ehrhardt, DW, Griffitts, JS, Somerville, CR (2000) Random GFP::cDNA fusions enable visualization of subcellular structures in cells of Arabidopsis at a high frequency. *Proceedings of the National Academy of Sciences* **97**, 3718-3723.

Dainty, J (1963) Water relations of plant cells. *Advances in Botanical Research* **1**, 279-326.

Davuluri, RV, Sun, H, Palaniswamy, SK, Matthews, N, Molina, C, Kurtz, M, Grotewold, E (2003) AGRIS: Arabidopsis Gene Regulatory Information Server, an information resource of Arabidopsis cis-regulatory elements and transcription factors. *BMC Bioinformatics* **4**, 25.

De Buck, S, Van Montagu, M, Depicker, A (2001) Transgene silencing of invertedly repeated transgenes is released upon deletion of one of the transgenes involved. *Plant Molecular Biology* **46**, 433-45.

De Paepe, A, De Buck, S, Hoorelbeke, K, Nolf, J, Peck, I, Depicker, A (2009) High frequency of single-copy T-DNA transformants produced by floral dip in CRE-expressing Arabidopsis plants. *The Plant Journal* **59**, 517-527.

de Ruijter, NCA, Verhees, J, van Leeuwen, W, van der Krol, AR (2003) Evaluation and comparison of the GUS, LUC and GFP reporter system for gene expression studies in plants. *Plant Biology* **5**, 103-115.

Dehairs, J, Talebi, A, Cherifi, Y, Swinnen, JV (2016) CRISP-ID: decoding CRISPR mediated indels by Sanger sequencing. **6**, 28973.

Deltcheva, E, Chylinski, K, Sharma, CM, Gonzales, K, Chao, Y, Pirzada, ZA, Eckert, MR, Vogel, J, Charpentier, E (2011) CRISPR RNA maturation by trans-encoded small RNA and host factor RNase III. *Nature* **471**, 602-607.

Dixon, HH, Joly, J (1895) On the ascent of sap. *Philosophical Transactions of the Royal Society of London. B* **186**, 563-576.

Dodd, IC (2013) Abscisic acid and stomatal closure: a hydraulic conductance conundrum? *New Phytologist* **197**, 6-8.

Dwight, Z, Palais, R, Wittwer, CT (2011) uMELT: prediction of high-resolution melting curves and dynamic melting profiles of PCR products in a rich web application. *Bioinformatics* **27**, 1019-1020.

Dynowski, M, Schaaf, G, Loque, D, Moran, O, Ludewig, U (2008) Plant plasma membrane water channels conduct the signalling molecule H2O2. *Biochem J* **414**, 53-61.

Ecker, JR, Davis, RW (1986) Inhibition of gene expression in plant cells by expression of antisense RNA. *Proceedings of the National Academy of Sciences* **83**, 5372-5376.

Ehlert, C, Maurel, C, Tardieu, F, Simonneau, T (2009) Aquaporin-mediated reduction in maize root hydraulic conductivity impacts cell turgor and leaf elongation even without changing transpiration. *Plant Physiology* **150**, 1093-1104.

Eybishtz, A, Peretz, Y, Sade, D, Akad, F, Czosnek, H (2009) Silencing of a single gene in tomato plants resistant to Tomato yellow leaf curl virus renders them susceptible to the virus. *Plant Molecular Biology* **71**, 157-171.

Fauser, F, Schiml, S, Puchta, H (2014) Both CRISPR/Cas-based nucleases and nickases can be used efficiently for genome engineering in Arabidopsis thaliana. *Plant Journal* **79**, 348-359.

Ferro, M, Salvi, D, Brugiere, S, Miras, S, Kowalski, S, Louwagie, M, Garin, J, Joyard, J, Rolland, N (2003) Proteomics of the chloroplast envelope membranes from Arabidopsis thaliana. *Mol Cell Proteomics* **2**, 325-45.

Fetter, K, Van Wilder, V, Moshelion, M, Chaumont, F (2004) Interactions between plasma membrane aquaporins modulate their water channel activity. *Plant Cell* **16**, 215-228.

Finkelstein, R (2013) Abscisic acid synthesis and response. *The Arabidopsis Book / American Society of Plant Biologists* **11**, e0166.

Finn, RN, Cerda, J (2015) Evolution and functional diversity of aquaporins. *Biol Bull* **229**, 6-23.

Fishman, S, Genard, M (1998) A biophysical model of fruit growth: simulation of seasonal and diurnal dynamics of mass. *Plant Cell and Environment* **21**, 739-752.

Flexas, J, Ribas-Carbo, M, Hanson, DT, Bota, J, Otto, B, Cifre, J, McDowell, N, Medrano, H, Kaldenhoff, R (2006) Tobacco aquaporin NtAQP1 is involved in mesophyll conductance to CO2 in vivo. *Plant Journal* **48**, 427-39.

Flexas, J, Scoffoni, C, Gago, J, Sack, L (2013) Leaf mesophyll conductance and leaf hydraulic conductance: an introduction to their measurement and coordination. *Journal of Experimental Botany* **64**, 3965-3981.

Fouquet, R, Leon, C, Ollat, N, Barrieu, F (2008) Identification of grapevine aquaporins and expression analysis in developing berries. *Plant Cell Reports* **27**, 1541-1550.

Gattolin, S, Sorieul, M, Hunter, PR, Khonsari, RH, Frigerio, L (2009) In vivo imaging of the tonoplast intrinsic protein family in Arabidopsis roots. *Bmc Plant Biology* **9**, 133.

Gilliham, M, Dayod, M, Hocking, BJ, Xu, B, Conn, SJ, Kaiser, BN, Leigh, RA, Tyerman, SD (2011) Calcium delivery and storage in plant leaves: exploring the link with water flow. *Journal of Experimental Botany* **62**, 2233-50.

Głowacka, K, Kromdijk, J, Leonelli, L, Niyogi, KK, Clemente, TE, Long, SP (2016) An evaluation of new and established methods to determine T-DNA copy number and homozygosity in transgenic plants. *Plant, Cell & Environment* **39**, 908-917.

Gomes, D, Agasse, A, Thiebaud, P, Delrot, S, Geros, H, Chaumont, F (2009) Aquaporins are multifunctional water and solute transporters highly divergent in living organisms. *Biochimica Et Biophysica Acta-Biomembranes* **1788**, 1213-1228.

Gong, X, Liu, M, Zhang, L, Ruan, Y, Ding, R, Ji, Y, Zhang, N, Zhang, S, Farmer, J, Wang, C (2015) Arabidopsis AtSUC2 and AtSUC4, encoding sucrose transporters, are required for abiotic stress tolerance in an ABA-dependent pathway. *Physiol Plant* **153**, 119-36.

Grant, CD, Groenevelt, PH, Robinson, NI (2010) Application of the Groenevelt-Grant soil water retention model to predict the hydraulic conductivity. *Australian Journal of Soil Research* **48**, 447-458.

Grefen, C, Donald, N, Hashimoto, K, Kudla, J, Schumacher, K, Blatt, MR (2010) A ubiquitin-10 promoter-based vector set for fluorescent protein tagging facilitates temporal stability and native protein distribution in transient and stable expression studies. *The Plant Journal* **64**, 355-365.

Grondin, A, Rodrigues, O, Verdoucq, L, Merlot, S, Leonhardt, N, Maurel, C (2015) Aquaporins contribute to ABA-triggered stomatal closure through OST1-mediated phosphorylation. *The Plant Cell* **27**, 1945-1954.

Gustavsson, S, Lebrun, AS, Norden, K, Chaumont, F, Johanson, U (2005) A novel plant major intrinsic protein in Physcomitrella patens most similar to bacterial glycerol channels. *Plant Physiology* **139**, 287-295.

Hachez, C, Besserer, A, Chevalier, AS, Chaumont, F (2013) Insights into plant plasma membrane aquaporin trafficking. *Trends in Plant Science* **18**, 344-352.

Hachez, C, Veselov, D, Ye, Q, Reinhardt, H, Knipfer, T, Fricke, W, Chaumont, F (2012) Short-term control of maize cell and root water permeability through plasma membrane aquaporin isoforms. *Plant Cell and Environment* **35**, 185-98.

Harmer, SL, Hogenesch, LB, Straume, M, Chang, HS, Han, B, Zhu, T, Wang, X, Kreps, JA, Kay, SA (2000) Orchestrated transcription of key pathways in Arabidopsis by the circadian clock. *Science* **290**, 2110-2113.

Harrison, SJ, Mott, EK, Parsley, K, Aspinall, S, Gray, JC, Cottage, A (2006) A rapid and robust method of identifying transformed Arabidopsis thaliana seedlings following floral dip transformation. *Plant Methods* **2**,

Heigwer, F, Kerr, G, Boutros, M (2014) E-CRISP: fast CRISPR target site identification. *Nat Meth* **11**, 122-123.

Hepworth, C, Doheny-Adams, T, Hunt, L, Cameron, DD, Gray, JE (2015) Manipulating stomatal density enhances drought tolerance without deleterious effect on nutrient uptake. *New Phytologist* **208**, 336-341.

Hetherington, AM, Woodward, FI (2003) The role of stomata in sensing and driving environmental change. *Nature* **424**, 901-908.

Hobbs, SLA, Kpodar, P, DeLong, CMO (1990) The effect of T-DNA copy number, position and methylation on reporter gene expression in tobacco transformants. *Plant Molecular Biology* **15**, 851-864.

Holbrook, NM, Shashidhar, VR, James, RA, Munns, R (2002) Stomatal control in tomato with ABA-deficient roots: response of grafted plants to soil drying. *Journal of Experimental Botany* **53**, 1503-14.

Holm, LM, Jahn, TP, Møller, ALB, Schjoerring, JK, Ferri, D, Klaerke, DA, Zeuthen, T (2005) NH3 and NH4+ permeability in aquaporin-expressing Xenopus oocytes. *Pflügers Archiv* **450**, 415-428.

Hooijmaijers, C, Rhee, JY, Kwak, KJ, Chung, GC, Horie, T, Katsuhara, M, Kang, H (2012) Hydrogen peroxide permeability of plasma membrane aquaporins of Arabidopsis thaliana. *Journal of Plant Research* **125**, 147-53.

Hose, E, Steudle, E, Hartung, W (2000) Abscisic acid and hydraulic conductivity of maize roots: a study using cell- and root-pressure probes. *Planta* **211**, 874-882.

Hunter, PR, Craddock, CP, Di Benedetto, S, Roberts, LM, Frigerio, L (2007) Fluorescent reporter proteins for the tonoplast and the vacuolar lumen identify a single vacuolar compartment in Arabidopsis cells. *Plant Physiology* **145**, 1371-1382.

Jang, JY, Kim, DG, Kim, YO, Kim, JS, Kang, HS (2004) An expression analysis of a gene family encoding plasma membrane aquaporins in response to abiotic stresses in Arabidopsis thaliana. *Plant Molecular Biology* **54**, 713-725.

Jauh, G-Y, Phillips, TE, Rogers, JC (1999) Tonoplast Intrinsic Protein isoforms as markers for vacuolar functions. *The Plant Cell* **11**, 1867-1882.

Javot, H, Lauvergeat, V, Santoni, V, Martin-Laurent, F, Guclu, J, Vinh, J, Heyes, J, Franck, KI, Schaffner, AR, Bouchez, D, Maurel, C (2003) Role of a single aquaporin isoform in root water uptake. *Plant Cell* **15**, 509-22.

Johanson, U, Danielson, JAH (2008) Unexpected complexity of the Aquaporin gene family in the moss Physcomitrella patens. *Bmc Plant Biology* **8**, 45.

Johanson, U, Karlsson, M, I, J, Gustavsson, S, Sjovall, S, Fraysse, L, Weig, AR, Kjellbom, P (2001) The complete set of genes encoding major intrinsic proteins in arabidopsis provides a framework for a new nomenclature for major intrinsic proteins in plants. *Plant Physiology* **126**, 1358-1369.

Johnson, KD, Chrispeels, MJ (1992) Tonoplast-bound protein kinase phosphorylates tonoplast intrinsic protein. *Plant Physiology* **100**, 1787-1795.

Johnson, KD, Herman, EM, Chrispeels, MJ (1989) An abundant, highly conserved tonoplast protein in seeds. *Plant Physiology* **91**, 1006-1013.

Jones, HG (1998) Stomatal control of photosynthesis and transpiration. *Journal of Experimental Botany* **49**, 387-398.

Jones, MM, Turner, NC (1978) Osmotic adjustment in leaves of sorghum in response to water deficits. *Plant Physiology* **61**, 122-126.

Joshi, HJ, Christiansen, KM, Fitz, J, Cao, J, Lipzen, A, Martin, J, Smith-Moritz, AM, Pennacchio, LA, Schackwitz, WS, Weigel, D, Heazlewood, JL (2012) 1001 Proteomes: a functional proteomics portal for the analysis of Arabidopsis thaliana accessions. *Bioinformatics* **28**, 1303-1306.

Kaldenhoff, R, Grote, K, Zhu, JJ, Zimmermann, U (1998) Significance of plasmalemma aquaporins for water-transport in Arabidopsis thaliana. *Plant Journal* **14**, 121-8.

Kaldenhoff, R, Kolling, A, Richter, G (1996) Regulation of the Arabidopsis thaliana aquaporin gene AthH2 (PIP1b). *J Photochem Photobiol B* **36**, 351-4.

Kirscht, A, Kaptan, SS, Bienert, GP, Chaumont, F, Nissen, P, de Groot, BL, Kjellbom, P, Gourdon, P, Johanson, U (2016) Crystal Structure of an ammonia-permeable aquaporin. *PLoS Biol* **14**, e1002411.

Kiyosawa, K, Tazawa, M (1977) Hydraulic conductivity of tonoplast-free Chara cells. *The Journal of Membrane Biology* **37**, 157-166.

Knepper, MA, Nielsen, S (2004) Peter Agre, 2003 Nobel Prize winner in chemistry. *Journal of the American Society of Nephrology* **15**, 1093-1095.

Koornneef, M, Meinke, D (2010) The development of Arabidopsis as a model plant. *The Plant Journal* **61**, 909-921.

Kuchel, PW (2006) The story of the discovery of aquaporins: convergent evolution of ideas - but who got there first? *Cell Mol Biol (Noisy-le-grand)* **52**, 2-5.

Kumar, G, Panjabi-Sabharwal, V, Kumari, S, Joshi, R, Karan, R, Mittal, S, Pareek, SLS, Pareek, A (2012) Clustered metallothionein genes are co-regulated in rice and ectopic expression of OsMT1e-P confers multiple abiotic stress tolerance in tobacco via ROS scavenging. *Bmc Plant Biology* **12**, 107-107.

Kuwagata, T, Ishikawa-Sakurai, J, Hayashi, H, Nagasuga, K, Fukushi, K, Ahamed, A, Takasugi, K, Katsuhara, M, Murai-Hatano, M (2012) Influence of low air humidity and low root temperature on water uptake, growth and aquaporin expression in rice plants. *Plant and Cell Physiology* **53**, 1418-1431.

Langfelder, P, Zhang, B, Horvath, S (2008) Defining clusters from a hierarchical cluster tree: the Dynamic Tree Cut package for R. *Bioinformatics* **24**, 719-20.

Langridge, P, Reynolds, MP (2015) Genomic tools to assist breeding for drought tolerance. *Curr Opin Biotechnol* **32**, 130-5.

Laur, J, Hacke, UG (2014) The role of water channel proteins in facilitating recovery of leaf hydraulic conductance from water stress in Populus trichocarpa. *Plos One* **9**, e111751.

Lee, HK, Cho, SK, Son, O, Xu, Z, Hwang, I, Kim, WT (2009) Drought stress-induced Rma1H1, a RING membrane-anchor E3 ubiquitin ligase homolog, regulates aquaporin levels via ubiquitination in transgenic Arabidopsis plants. *Plant Cell* **21**, 622-41.

Lee, SH, Chung, GC, Jang, JY, Ahn, SJ, Zwiazek, JJ (2012) Overexpression of PIP2;5 aquaporin alleviates effects of low root temperature on cell hydraulic conductivity and growth in Arabidopsis. *Plant Physiology* **159**, 479-488.

Lee, SH, Zwiazek, JJ (2015) Regulation of aquaporin-mediated water transport in Arabidopsis roots exposed to NaCl. *Plant and Cell Physiology* **56**, 750-8.

Lei, Y, Lu, L, Liu, HY, Li, S, Xing, F, Chen, LL (2014) CRISPR-P: a web tool for synthetic single-guide RNA design of CRISPR-system in plants. *Mol Plant* **7**, 1494-6.

Leonhardt, N, Kwak, JM, Robert, N, Waner, D, Leonhardt, G, Schroeder, JI (2004) Microarray expression analyses of Arabidopsis guard cells and isolation of a recessive abscisic acid hypersensitive protein phosphatase 2C mutant. *The Plant Cell* **16**, 596-615.

Levin, M, Lemcoff, JH, Cohen, S, Kapulnik, Y (2007) Low air humidity increases leaf-specific hydraulic conductance of Arabidopsis thaliana (L.) Heynh (Brassicaceae). *Journal of Experimental Botany* **58**, 3711-3718.

Levin, M, Resnick, N, Rosianskey, Y, Kolotilin, I, Wininger, S, Lemcoff, JH, Cohen, S, Galili, G, Koltai, H, Kapulnik, Y (2009) Transcriptional profiling of Arabidopsis thaliana plants' response to low relative humidity suggests a shoot-root communication. *Plant Science* **177**, 450-459.

Li, Y, Rosso, MG, Ülker, B, Weisshaar, B (2006) Analysis of T-DNA insertion site distribution patterns in Arabidopsis thaliana reveals special features of genes without insertions. *Genomics* **87**, 645-652.

Liang, G, Zhang, H, Lou, D, Yu, D (2016) Selection of highly efficient sgRNAs for CRISPR/Cas9-based plant genome editing. **6**, 21451.

Lin, W, Peng, Y, Li, G, Arora, R, Tang, Z, Su, W, Cai, W (2007) Isolation and functional characterization of PgTIP1, a hormone-autotrophic cells-specific tonoplast aquaporin in ginseng. *Journal of Experimental Botany* **58**, 947-956.

Liu, C, Li, C, Liang, D, Ma, F, Wang, S, Wang, P, Wang, R (2013) Aquaporin expression in response to water-deficit stress in two Malus species: relationship with physiological status and drought tolerance. *Plant Growth Regulation* **70**, 187-197.

Loque, D, Ludewig, U, Yuan, LX, von Wiren, N (2005) Tonoplast intrinsic proteins AtTIP2;1 and AtTIP2;3 facilitate NH3 transport into the vacuole. *Plant Physiology* **137**, 671-680.

Lucas, WJ, Groover, A, Lichtenberger, R, Furuta, K, Yadav, SR, Helariutta, Y, He, XQ, Fukuda, H, Kang, J, Brady, SM, Patrick, JW, Sperry, J, Yoshida, A, Lopez-Millan, AF, Grusak, MA, Kachroo, P (2013) The plant vascular system: evolution, development and functions. *J Integr Plant Biol* **55**, 294-388.

Ludevid, D, Höfte, H, Himelblau, E, Chrispeels, MJ (1992) The expression pattern of the Tonoplast Intrinsic Protein γ-TIP in Arabidopsis thaliana is correlated with cell enlargement. *Plant Physiology* **100**, 1633-1639.

Ma, S, Quist, TM, Ulanov, A, Joly, R, Bohnert, HJ (2004) Loss of TIP1;1 aquaporin in Arabidopsis leads to cell and plant death. *The Plant Journal* **40**, 845-859.

Macey, RI (1984) Transport of water and urea in red blood cells. *Am J Physiol* **246**, C195-203.

Mahdieh, M, Mostajeran, A (2009) Abscisic acid regulates root hydraulic conductance via aquaporin expression modulation in Nicotiana tabacum. *Journal of Plant Physiology* **166**, 1993-2003.

Manzi, M, Lado, J, Rodrigo, MJ, Zacarias, L, Arbona, V, Gomez-Cadenas, A (2015) Root ABA accumulation in long-term water-stressed plants is sustained by hormone transport from aerial organs. *Plant and Cell Physiology* **56**, 2457-66.

Marraffini, LA (2015) CRISPR-Cas immunity in prokaryotes. *Nature* **526**, 55-61.

Martre, P, Morillon, R, Barrieu, F, North, GB, Nobel, PS, Chrispeels, MJ (2002) Plasma membrane aquaporins play a significant role during recovery from water deficit. *Plant Physiology* **130**, 2101-10.

Maurel, C, Boursiac, Y, Luu, DT, Santoni, V, Shahzad, Z, Verdoucq, L (2015) Aquaporins in plants. *Physiological Reviews* **95**, 1321-1358.

Maurel, C, Kado, RT, Guern, J, Chrispeels, MJ (1995) Phosphorylation regulates the water channel activity of the seed-specific aquaporin alpha-TIP. *Embo Journal* **14**, 3028-3035.

Maurel, C, Reizer, J, Schroeder, JI, Chrispeels, MJ (1993) The vacuolar membrane protein gamma-TIP creates water specific channels in Xenopus oocytes. *Embo Journal* **12**, 2241-7.

Maurel, C, Tacnet, F, Güclü, J, Guern, J, Ripoche, P (1997) Purified vesicles of tobacco cell vacuolar and plasma membranes exhibit dramatically different water permeability and water channel activity. *Proc Natl Acad Sci U S A* **94**, 7103-7108.

Maurel, C, Verdoucq, L, Luu, DT, Santoni, V (2008) Plant aquaporins: Membrane channels with multiple integrated functions. *Annual Review of Plant Biology* **59**, 595-624.

Maurel, C, Verdoucq, L, Rodrigues, O (2016) Aquaporins and plant transpiration. *Plant, Cell & Environment* **39**, 2580-2587.

McAdam, SA, Brodribb, TJ (2015) The evolution of mechanisms driving the stomatal response to vapor pressure deficit. *Plant Physiology* **167**, 833-43.

McAdam, SA, Brodribb, TJ, Ross, JJ (2016) Shoot-derived abscisic acid promotes root growth. *Plant Cell and Environment* **39**, 652-9.

McAdam, SAM, Brodribb, TJ (2012) Fern and Lycophyte guard cells do not respond to endogenous abscisic acid. *Plant Cell* **24**, 1510-1521.

McCarthy, MG (1999) Weight loss from ripening berries of Shiraz grapevines (*Vitis vinifera* L. cv. Shiraz). *Australian Journal of Grape and Wine Research* **5**, 10-16.

McCourt, RM, Delwiche, CF, Karol, KG (2004) Charophyte algae and land plant origins. *Trends in Ecology & Evolution* **19**, 661-666.

Merlot, S, Gosti, F, Guerrier, D, Vavasseur, A, Giraudat, J (2001) The ABI1 and ABI2 protein phosphatases 2C act in a negative feedback regulatory loop of the abscisic acid signalling pathway. *Plant Journal* **25**, 295-303.

Monneuse, J-M, Sugano, M, Becue, T, Santoni, V, Hem, S, Rossignol, M (2011) Towards the profiling of the Arabidopsis thaliana plasma membrane transportome by targeted proteomics. *PROTEOMICS* **11**, 1789-1797.

Montgomery, J, Wittwer, CT, Palais, R, Zhou, L (2007) Simultaneous mutation scanning and genotyping by high-resolution DNA melting analysis. *Nat. Protocols* **2**, 59-66.

Moshelion, M, Halperin, O, Wallach, R, Oren, R, Way, DA (2015) Role of aquaporins in determining transpiration and photosynthesis in water-stressed plants: crop water-use efficiency, growth and yield. *Plant Cell and Environment* **38**, 1785-1793.

Mott, KA, Berg, DG, Hunt, SM, Peak, D (2014) Is the signal from the mesophyll to the guard cells a vapour-phase ion? *Plant, Cell & Environment* **37**, 1184-1191.

Münch, E (1930) 'Material flow in plants. Translated 2003 by J. A. Milburn and K. H. Kreeb, Germany: University of Bremen.' (Gustav Fischer Verlag: Jena Germany)

Murashige, T, Skoog, F (1962) A revised medium for rapid growth and bio assays with tobacco tissue cultures. *Physiologia Plantarum* **15**, 473-497.

Omuto, CT, Gumbe, LO (2009) Estimating water infiltration and retention characteristics using a computer program in R. *Computers & Geosciences* **35**, 579-585.

Otto, B, Kaldenhoff, R (2000) Cell-specific expression of the mercury-insensitive plasma-membrane aquaporin NtAQP1 from Nicotiana tabacum. *Planta* **211**, 167-72.

Otto, B, Uehlein, N, Sdorra, S, Fischer, M, Ayaz, M, Belastegui-Macadam, X, Heckwolf, M, Lachnit, M, Pede, N, Priem, N, Reinhard, A, Siegfart, S, Urban, M, Kaldenhoff, R (2010) Aquaporin tetramer composition modifies the function of tobacco aquaporins. *Journal of Biological Chemistry* **285**, 31253-31260.

Palkova, Z, Janderova, B, Gabriel, J, Zikanova, B, Pospisek, M, Forstova, J (1997) Ammonia mediates communication between yeast colonies. *Nature* **390**, 532-6.

Pantin, F, Monnet, F, Jannaud, D, Costa, JM, Renaud, J, Muller, B, Simonneau, T, Genty, B (2013) The dual effect of abscisic acid on stomata. *New Phytologist* **197**, 65-72.

Pantin, F, Simonneau, T, Rolland, G, Dauzat, M, Muller, B (2011) Control of leaf expansion: a developmental switch from metabolics to hydraulics. *Plant Physiology* **156**, 803-15.

Paré, PW, Tumlinson, JH (1999) Plant volatiles as a defense against insect herbivores. *Plant Physiology* **121**, 325-332.

Parent, B, Hachez, C, Redondo, E, Simonneau, T, Chaumont, F, Tardieu, F (2009) Drought and abscisic acid effects on aquaporin content translate into changes in hydraulic conductivity and leaf growth rate: a trans-scale approach. *Plant Physiology* **149**, 2000-2012.

Park, JH, Saier, J, M.H. (1996) Phylogenetic characterization of the MIP family of transmembrane channel proteins. *The Journal of Membrane Biology* **153**, 171-180.

Patrick, JW (2013) Does Don Fisher's high-pressure manifold model account for phloem transport and resource partitioning? *Front Plant Sci* **4**, 184.

Pei, Z-M, Murata, Y, Benning, G, Thomine, S, Klusener, B, Allen, GJ, Grill, E, Schroeder, JI (2000) Calcium channels activated by hydrogen peroxide mediate abscisic acid signalling in guard cells. *Nature* **406**, 731-734.

Peng, Y, Lin, W, Cai, W, Arora, R (2007) Overexpression of a Panax ginseng tonoplast aquaporin alters salt tolerance, drought tolerance and cold acclimation ability in transgenic Arabidopsis plants. *Planta* **226**, 729-40.

Péret, B, Li, G, Zhao, J, Band, LR, Voß, U, Postaire, O, Luu, D-T, Da Ines, O, Casimiro, I, Lucas, M, Wells, DM, Lazzerini, L, Nacry, P, King, JR, Jensen, OE, Schäffner, AR, Maurel, C, Bennett, MJ (2012) Auxin regulates aquaporin function to facilitate lateral root emergence. *Nat Cell Biol* **14**, 991-998.

Perkins, JR, Dawes, JM, McMahon, SB, Bennett, DL, Orengo, C, Kohl, M (2012) ReadqPCR and NormqPCR: R packages for the reading, quality checking and normalisation of RT-qPCR quantification cycle (Cq) data. *Bmc Genomics* **13**, 296.

Peterson, BA, Haak, DC, Nishimura, MT, Teixeira, PJPL, James, SR, Dangl, JL, Nimchuk, ZL (2016) Genome-wide assessment of efficiency and specificity in CRISPR/Cas9 mediated multiple site targeting in Arabidopsis. *Plos One* **11**, e0162169.

Pfaffl, MW (2001) A new mathematical model for relative quantification in real-time RT–PCR. *Nucleic Acids Research* **29**, 2002-2007.

Pierce, M, Raschke, K (1981) Synthesis and metabolism of abscisic acid in detached leaves of Phaseolus vulgaris L. after loss and recovery of turgor. *Planta* **153**, 156-165.

Pietro, Md, Vialaret, J, Li, G, Hem, S, Prado, K, Rossignol, M, Maurel, C, Santoni, V (2013) Coordinated post-translational responses of aquaporins to abiotic and nutritional stimuli in Arabidopsis roots. *Molecular & Cellular Proteomics* **12**, 12.

Postaire, O, Tournaire-Roux, C, Grondin, A, Boursiac, Y, Morillon, R, Schaffner, AR, Maurel, C (2010) A PIP1 Aquaporin Contributes to Hydrostatic Pressure-Induced Water Transport in Both the Root and Rosette of Arabidopsis. *Plant Physiology* **152**, 1418-1430.

Pou, A, Jeanguenin, L, Milhiet, T, Batoko, H, Chaumont, F, Hachez, C (2016) Salinity-mediated transcriptional and post-translational regulation of the Arabidopsis aquaporin PIP2;7. *Plant Molecular Biology* **92**, 731-744.

Pou, A, Medrano, H, Flexas, J, Tyerman, SD (2013) A putative role for TIP and PIP aquaporins in dynamics of leaf hydraulic and stomatal conductances in grapevine under water stress and re-watering. *Plant, Cell & Environment* **36**, 828-843.

Prado, K, Boursiac, Y, Tournaire-Roux, C, Monneuse, JM, Postaire, O, Da Ines, O, Schaffner, AR, Hem, S, Santoni, V, Maurel, C (2013) Regulation of Arabidopsis leaf hydraulics involves light-dependent phosphorylation of aquaporins in veins. *Plant Cell* **25**, 1029-39.

Prak, S, Hem, S, Boudet, J, Viennois, G, Sommerer, N, Rossignol, M, Maurel, C, Santoni, V (2008) Multiple phosphorylations in the c-terminal tail of plant plasma membrane aquaporins: role in subcellular trafficking of AtPIP2;1 in response to salt stress. *Molecular & Cellular Proteomics* **7**, 1019-1030.

Preston, GM, Carroll, TP, Guggino, WB, Agre, P (1992) Appearance of water channels in Xenopus oocytes expressing red cell CHIP28 protein. *Science* **256**, 385-387.

Puchta, H (2017) Applying CRISPR/Cas for genome engineering in plants: the best is yet to come. *Current Opinion in Plant Biology* **36**, 1-8.

Pusztai, A, Croy, RRD, Stewart, JS, Watt, WB (1979) Protein body membranes of Phaseolus vulgaris L. cotyledons: Isolation and preliminary characterization of constituent proteins. *New Phytologist* **83**, 371-378.

Quigley, F, Rosenberg, JM, Shachar-Hill, Y, Bohnert, HJ (2002) From genome to function: the Arabidopsis aquaporins. *Genome Biology* **3**,

R Core Team (2017) 'R: A language and environment for statistical computing.' (R Foundation for Statistical Computing: Vienna, Austria)

Rae, L, Lao, NT, Kavanagh, TA (2011) Regulation of multiple aquaporin genes in Arabidopsis by a pair of recently duplicated DREB transcription factors. *Planta* **234**, 429-44.

Ray, PM (1960) On the theory of osmotic water movement. *Plant Physiology* **35**, 783-795.

Reinhardt, H, Hachez, C, Bienert, MD, Beebo, A, Swarup, K, Voss, U, Bouhidel, K, Frigerio, L, Schjoerring, JK, Bennett, MJ, Chaumont, F (2016) Tonoplast aquaporins facilitate lateral root emergence. *Plant Physiology* **170**, 1640-54.

Reizer, J, Reizer, A, Saier, MH (1993) The MIP family of integral membrane channel proteins - Sequence comparisons, evolutionary relationships, reconstructed pathway of evolution, and proposed functional-differentiation of the 2 repeated halves of the proteins. *Critical Reviews in Biochemistry and Molecular Biology* **28**, 235-257.

Rivera-Serrano, EE, Rodriguez-Welsh, MF, Hicks, GR, Rojas-Pierce, M (2012) A small molecule inhibitor partitions two distinct pathways for trafficking of tonoplast intrinsic proteins in Arabidopsis. *Plos One* **7**, e44735.

Rodrigues, O, Reshetnyak, G, Grondin, A, Saijo, Y, Leonhardt, N, Maurel, C, Verdoucq, L (2017) Aquaporins facilitate hydrogen peroxide entry into guard cells to mediate ABA- and pathogen-triggered stomatal closure. *Proceedings of the National Academy of Sciences* **114**, 9200-9205.

Rosegrant, MW, Ringler, C, Zhu, T (2009) Water for agriculture: maintaining food security under growing scarcity. *Annual Review of Environment and Resources* **34**, 205-222.

Rouillard, J-M, Zuker, M, Gulari, E (2003) OligoArray 2.0: design of oligonucleotide probes for DNA microarrays using a thermodynamic approach. *Nucleic Acids Research* **31**, 3057-3062.

Sade, D, Sade, N, Shriki, O, Lerner, S, Gebremedhin, A, Karavani, A, Brotman, Y, Osorio, S, Fernie, AR, Willmitzer, L, Czosnek, H, Moshelion, M (2014a) Water balance, hormone homeostasis, and sugar signaling are all involved in tomato resistance to Tomato Yellow Leaf Curl Virus. *Plant Physiology* **165**, 1684-1697.

Sade, N, Gebretsadik, M, Seligmann, R, Schwartz, A, Wallach, R, Moshelion, M (2010) The role of tobacco Aquaporin1 in improving water use efficiency, hydraulic conductivity, and yield production under salt stress. *Plant Physiology* **152**, 245-54.

Sade, N, Shatil-Cohen, A, Attia, Z, Maurel, C, Boursiac, Y, Kelly, G, Granot, D, Yaaran, A, Lerner, S, Moshelion, M (2014b) The role of plasma membrane aquaporins in regulating the bundle sheath-mesophyll continuum and leaf hydraulics. *Plant Physiology* **166**, 1609-1620.

Sade, N, Shatil-Cohen, A, Moshelion, M (2015) Bundle-sheath aquaporins play a role in controlling Arabidopsis leaf hydraulic conductivity. *Plant Signal Behav* **10**, e1017177.

Sade, N, Vinocur, BJ, Diber, A, Shatil, A, Ronen, G, Nissan, H, Wallach, R, Karchi, H, Moshelion, M (2009) Improving plant stress tolerance and yield production: is the tonoplast aquaporin SlTIP2;2 a key to isohydric to anisohydric conversion? *New Phytologist* **181**, 651-661.

Sakurai, J, Ishikawa, F, Yamaguchi, T, Uemura, M, Maeshima, M (2005) Identification of 33 rice aquaporin genes and analysis of their expression and function. *Plant and Cell Physiology* **46**, 1568-77.

Scharwies, JD, Tyerman, SD (2016) Comparison of isohydric and anisohydric Vitis vinifera L. cultivars reveals a fine balance between hydraulic resistances, driving forces and transpiration in ripening berries. *Functional Plant Biology* **44**, 322–336.

Schiml, S, Puchta, H (2016) Revolutionizing plant biology: multiple ways of genome engineering by CRISPR/Cas. *Plant Methods* **12**, 8.

Schneider, CA, Rasband, WS, Eliceiri, KW (2012) NIH Image to ImageJ: 25 years of image analysis. *Nat Meth* **9**, 671-675.

Schultz, HR (2003) Differences in hydraulic architecture account for near-isohydric and anisohydric behaviour of two field-grown *Vitis vinifera* L. cultivars during drought. *Plant Cell and Environment* **26**, 1393-1405.

Schüssler, MD, Alexandersson, E, Bienert, GP, Kichey, T, Laursen, KH, Johanson, U, Kjellbom, P, Schjoerring, JK, Jahn, TP (2008) The effects of the loss of TIP1;1 and TIP1;2 aquaporins in Arabidopsis thaliana. *The Plant Journal* **56**, 756-767.

Schütz, E, von Ahsen, N (2009) Influencing factors of dsDNA dye (high-resolution) melting curves and improved genotype call based on thermodynamic considerations. *Analytical Biochemistry* **385**, 143-152.

Secchi, F, Pagliarani, C, Zwieniecki, MA (2017) The functional role of xylem parenchyma cells and aquaporins during recovery from severe water stress. *Plant, Cell & Environment* **40**, 858-871.

Shaar-Moshe, L, Hubner, S, Peleg, Z (2015) Identification of conserved drought-adaptive genes using a cross-species meta-analysis approach. *Bmc Plant Biology* **15**, 111.

Shatil-Cohen, A, Attia, Z, Moshelion, M (2011) Bundle-sheath cell regulation of xylem-mesophyll water transport via aquaporins under drought stress: a target of xylem-borne ABA? *Plant Journal* **67**, 72-80.

Shuman, S, Glickman, MS (2007) Bacterial DNA repair by non-homologous end joining. *Nat Rev Microbiol* **5**, 852-61.

Simonin, KA, Burns, E, Choat, B, Barbour, MM, Dawson, TE, Franks, PJ (2015) Increasing leaf hydraulic conductance with transpiration rate minimizes the water potential drawdown from stem to leaf. *Journal of Experimental Botany* **66**, 1303-1315.

Soar, CJ, Speirs, J, Maffei, SM, Penrose, AB, McCarthy, MG, Loveys, BR (2006) Grape vine varieties Shiraz and Grenache differ in their stomatal response to VPD: apparent links with ABA physiology and gene expression in leaf tissue. *Australian Journal of Grape and Wine Research* **12**, 2-12.

Soto, G, Alleva, K, Amodeo, G, Muschietti, J, Ayub, ND (2012) New insight into the evolution of aquaporins from flowering plants and vertebrates: orthologous identification and functional transfer is possible. *Gene* **503**, 165-76.

Soto, G, Fox, R, Ayub, N, Alleva, K, Guaimas, F, Erijman, EJ, Mazzella, A, Amodeo, G, Muschietti, J (2010) TIP5;1 is an aquaporin specifically targeted to pollen mitochondria and is probably involved in nitrogen remobilization in Arabidopsis thaliana. *Plant Journal* **64**, 1038-1047.

Sperry, JS, Nichols, KL, Sullivan, JEM, Eastlack, SE (1994) Xylem embolism in ring-porous, diffuse-porous, and coniferous trees of Northern Utah and Interior Alaska. *Ecology* **75**, 1736-1752.

Sprink, T, Metje, J, Hartung, F (2015) Plant genome editing by novel tools: TALEN and other sequence specific nucleases. *Current Opinion in Biotechnology* **32**, 47-53.

Sprink, T, Metje, J, Schiemann, J, Hartung, F (2016) Plant genome editing in the European Union—to be or not to be—a GMO. *Plant Biotechnology Reports* **10**, 345-351.

Stanfield, RC, Hacke, UG, Laur, J (2017) Are phloem sieve tubes leaky conduits supported by numerous aquaporins? *American Journal of Botany* **104**, 719-732.

Steppe, K, Lemeur, R (2007) Effects of ring-porous and diffuse-porous stem wood anatomy on the hydraulic parameters used in a water flow and storage model. *Tree Physiol* **27**, 43-52.

Steudle, E, Jeschke, W (1983) Water transport in barley roots. *Planta* **158**, 237-248.

Steudle, E, Peterson, CA (1998) How does water get through roots? *Journal of Experimental Botany* **49**, 775-788.

Steudle, E, Tyerman, SD (1983) Determination of permeability coefficients, reflection coefficients, and hydraulic conductivity of Chara corallina using the pressure probe: Effects of solute concentrations. *The Journal of Membrane Biology* **75**, 85-96.

Sui, H, Han, B-G, Lee, JK, Walian, P, Jap, BK (2001) Structural basis of water-specific transport through the AQP1 water channel. *Nature* **414**, 872-878.

Sutka, M, Li, G, Boudet, J, Boursiac, Y, Doumas, P, Maurel, C (2011) Natural variation of root hydraulics in Arabidopsis grown in normal and salt-stressed conditions. *Plant Physiology* **155**, 1264-1276.

Taiz, L (1992) The plant vacuole. *Journal of Experimental Biology* **172**, 113-122.

Taiz, L, Zeiger, E (2010) 'Plant Physiology, Fifth Edition.' (Sinauer Associates: Sunderland, MA)

Tajkhorshid, E, Nollert, P, Jensen, MO, Miercke, LJ, O'Connell, J, Stroud, RM, Schulten, K (2002) Control of the selectivity of the aquaporin water channel family by global orientational tuning. *Science* **296**, 525-30.

Tang, W, Newton, RJ, Weidner, DA (2007) Genetic transformation and gene silencing mediated by multiple copies of a transgene in eastern white pine. *Journal of Experimental Botany* **58**, 545-554.

Tardieu, F, Davies, WJ (1993) Integration of hydraulic and chemical signalling in the control of stomatal conductance and water status of droughted plants. *Plant, Cell & Environment* **16**, 341-349.

Tardieu, F, Parent, B, Simonneau, T (2010) Control of leaf growth by abscisic acid: hydraulic or non-hydraulic processes? *Plant, Cell & Environment* **33**, 636-647.

Tardieu, F, Simonneau, T (1998) Variability among species of stomatal control under fluctuating soil water status and evaporative demand: modelling isohydric and anisohydric behaviours. *Journal of Experimental Botany* **49**, 419-432.

Thompson, AJ, Andrews, J, Mulholland, BJ, McKee, JMT, Hilton, HW, Horridge, JS, Farquhar, GD, Smeeton, RC, Smillie, IRA, Black, CR, Taylor, IB (2007) Overproduction of abscisic acid in tomato increases transpiration efficiency and root hydraulic conductivity and influences leaf expansion. *Plant Physiology* **143**, 1905-1917.

Tian, S, Wang, X, Li, P, Wang, H, Ji, H, Xie, J, Qiu, Q, Shen, D, Dong, H (2016) Plant aquaporin AtPIP1;4 links apoplastic H2O2 induction to disease immunity pathways. *Plant Physiology* **171**, 1635-50.

Tissier, AF, Marillonnet, S, Klimyuk, V, Patel, K, Torres, MA, Murphy, G, Jones, JDG (1999) Multiple independent defective suppressor-mutator transposon insertions in Arabidopsis: A tool for functional genomics. *The Plant Cell* **11**, 1841-1852.

Tombesi, S, Nardini, A, Frioni, T, Soccolini, M, Zadra, C, Farinelli, D, Poni, S, Palliotti, A (2015) Stomatal closure is induced by hydraulic signals and maintained by ABA in drought-stressed grapevine. *Scientific Reports* **5**, 12449.

Tornroth-Horsefield, S, Wang, Y, Hedfalk, K, Johanson, U, Karlsson, M, Tajkhorshid, E, Neutze, R, Kjellbom, P (2006) Structural mechanism of plant aquaporin gating. *Nature* **439**, 688-694.

Tournaire-Roux, C, Sutka, M, Javot, H, Gout, E, Gerbeau, P, Luu, D-T, Bligny, R, Maurel, C (2003) Cytosolic pH regulates root water transport during anoxic stress through gating of aquaporins. *Nature* **425**, 393-397.

Tyerman, SD, Bohnert, HJ, Maurel, C, Steudle, E, Smith, JAC (1999) Plant aquaporins: their molecular biology, biophysics and significance for plant water relations. *Journal of Experimental Botany* **50**, 1055-1071.

Tyerman, SD, Niemietz, CM, Bramley, H (2002) Plant aquaporins: multifunctional water and solute channels with expanding roles. *Plant Cell and Environment* **25**, 173-194.

Tyree, MT (1997) The Cohesion-Tension theory of sap ascent: current controversies. *Journal of Experimental Botany* **48**, 1753-1765.

Tyree, MT, Ewers, FW (1991) The hydraulic architecture of trees and other woody plants. *New Phytologist* **119**, 345-360.

Ueda, M, Tsutsumi, N, Fujimoto, M (2016) Salt stress induces internalization of plasma membrane aquaporin into the vacuole in Arabidopsis thaliana. *Biochem Biophys Res Commun* **474**, 742-746.

Uehlein, N, Lovisolo, C, Siefritz, F, Kaldenhoff, R (2003) The tobacco aquaporin NtAQP1 is a membrane CO2 pore with physiological functions. *Nature* **425**, 734-737.

Uehlein, N, Sperling, H, Heckwolf, M, Kaldenhoff, R (2012) The Arabidopsis aquaporin PIP1;2 rules cellular CO2 uptake. *Plant, Cell & Environment* **35**, 1077-1083.

Utsugi, S, Shibasaka, M, Maekawa, M, Katsuhara, M (2015) Control of the water transport activity of barley HvTIP3;1 specifically expressed in seeds. *Plant and Cell Physiology* **56**, 1831-1840.

Van Genuchten, MT (1980) A closed-form equation for predicting the hydraulic conductivity of unsaturated soils. *Soil Science Society of America Journal* **44**, 892-898.

Vandeleur, RK, Mayo, G, Shelden, MC, Gilliham, M, Kaiser, BN, Tyerman, SD (2009) The role of plasma membrane intrinsic protein aquaporins in water transport through roots: diurnal and drought stress responses reveal different strategies between isohydric and anisohydric cultivars of grapevine. *Plant Physiology* **149**, 445-460.

Vandeleur, RK, Sullivan, W, Athman, A, Jordans, C, Gilliham, M, Kaiser, BN, Tyerman, SD (2014) Rapid shoot-to-root signalling regulates root hydraulic conductance via aquaporins. *Plant, Cell & Environment* **37**, 520-538.

Vera-Estrella, R, Barkla, BJ, Bohnert, HJ, Pantoja, O (2004) Novel regulation of aquaporins during osmotic stress. *Plant Physiology* **135**, 2318-29.

Vialaret, J, Di Pietro, M, Hem, S, Maurel, C, Rossignol, M, Santoni, V (2014) Phosphorylation dynamics of membrane proteins from Arabidopsis roots submitted to salt stress. *PROTEOMICS* **14**, 1058-1070.

Vida, TA, Emr, SD (1995) A new vital stain for visualizing vacuolar membrane dynamics and endocytosis in yeast. *The Journal of Cell Biology* **128**, 779-792.

Voss, I, Sunil, B, Scheibe, R, Raghavendra, AS (2013) Emerging concept for the role of photorespiration as an important part of abiotic stress response. *Plant Biol (Stuttg)* **15**, 713-22.

Vouillot, L, Thélie, A, Pollet, N (2015) Comparison of T7E1 and Surveyor Mismatch Cleavage Assays to detect mutations triggered by engineered nucleases. *G3: Genes|Genomes|Genetics* **5**, 407-415.

Walton, DC, Harrison, MA, Cote, P (1976) The effects of water stress on abscisic-acid levels and metabolism in roots of Phaseolus vulgaris L. and other plants. *Planta* **131**, 141-4.

Wan, X, Steudle, E, Hartung, W (2004) Gating of water channels (aquaporins) in cortical cells of young corn roots by mechanical stimuli (pressure pulses): effects of ABA and of HgCl2. *Journal of Experimental Botany* **55**, 411-22.

Wang, L-L, Chen, A-P, Zhong, N-Q, Liu, N, Wu, X-M, Wang, F, Yang, C-L, Romero, MF, Xia, G-X (2014) The Thellungiella salsuginea tonoplast aquaporin TsTIP1;2 functions in protection against multiple abiotic stresses. *Plant and Cell Physiology* **55**, 148-161.

Wang, RS, Pandey, S, Li, S, Gookin, TE, Zhao, ZX, Albert, R, Assmann, SM (2011) Common and unique elements of the ABA-regulated transcriptome of Arabidopsis guard cells. *Bmc Genomics* **12**, 216.

Wang, Y, Li, R, Li, D, Jia, X, Zhou, D, Li, J, Lyi, SM, Hou, S, Huang, Y, Kochian, LV, Liu, J (2017) NIP1;2 is a plasma membrane-localized transporter mediating aluminum uptake, translocation, and tolerance in Arabidopsis. *Proc Natl Acad Sci USA* **114**, 5047-5052.

Wayne, R, Tazawa, M (1990) Nature of the water channels in the internodal cells of Nitellopsis. *J Membr Biol* **116**, 31-9.

Wei, T, Simko, V (2016) corrplot: Visualization of a correlation matrix. *CRAN*

Weig, A, Deswarte, C, Chrispeels, MJ (1997) The major intrinsic protein family of Arabidopsis has 23 members that form three distinct groups with functional aquaporins in each group. *Plant Physiology* **114**, 1347-1357.

Weig, AR, Jakob, C (2000) Functional identification of the glycerol permease activity of Arabidopsis thaliana NLM1 and NLM2 proteins by heterologous expression in Saccharomyces cerevisiae. *Febs Letters* **481**, 293-298.

Weigel, D, Glazebrook, J (2006) Glufosinate ammonium selection of transformed Arabidopsis. *Cold Spring Harbor Protocols* **2006**, pdb.prot4670.

Wendler, S, Zimmermann, U (1985a) Compartment analysis of plant cells by means of turgor pressure relaxation: I. Theoretical considerations. *The Journal of Membrane Biology* **85**, 121-132.

Wendler, S, Zimmermann, U (1985b) Compartment analysis of plant cells by means of turgor pressure relaxation: II. Experimental results on Chara corallina. *The Journal of Membrane Biology* **85**, 133-142.

Wickham, H (2017) tidyverse: easily install and load 'Tidyverse' packages. *CRAN*

Wu, XN, Rodriguez, CS, Pertl-Obermeyer, H, Obermeyer, G, Schulze, WX (2013) Sucrose-induced receptor kinase SIRK1 regulates a plasma membrane aquaporin in Arabidopsis. *Molecular & Cellular Proteomics* **12**, 2856-2873.

Wudick, MM, Luu, D-T, Maurel, C (2009) A look inside: localization patterns and functions of intracellular plant aquaporins. *New Phytologist* **184**, 289-302.

Xie, K, Zhang, J, Yang, Y (2014) Genome-wide prediction of highly specific guide RNA spacers for CRISPR-Cas9 mediated genome editing in model plants and major crops. *Molecular Plant* **7**, 923-926.

Xin, SC, Yu, GH, Sun, LL, Qiang, XJ, Xu, N, Cheng, XG (2014) Expression of tomato SlTIP2;2 enhances the tolerance to salt stress in the transgenic Arabidopsis and interacts with target proteins. *Journal of Plant Research* **127**, 695-708.

Xu, CH, Wang, M, Zhou, L, Quan, TY, Xia, GM (2013) Heterologous expression of the wheat aquaporin gene TaTIP2;2 compromises the abiotic stress tolerance of Arabidopsis thaliana. *Plos One* **8**,

Yaaran, A, Moshelion, M (2016) Role of aquaporins in a composite model of water transport in the leaf. *International Journal of Molecular Sciences* **17**, 1045.

Yang, H, Menz, J, Haussermann, I, Benz, M, Fujiwara, T, Ludewig, U (2015) High and low affinity urea root uptake: involvement of NIP5;1. *Plant and Cell Physiology* **56**, 1588-97.

Ye, J, Coulouris, G, Zaretskaya, I, Cutcutache, I, Rozen, S, Madden, TL (2012) Primer-BLAST: A tool to design target-specific primers for polymerase chain reaction. *BMC Bioinformatics* **13**, 134-134.

Ye, Q, Wiera, B, Steudle, E (2004) A cohesion/tension mechanism explains the gating of water channels (aquaporins) in Chara internodes by high concentration. *Journal of Experimental Botany* **55**, 449-461.

Zardoya, R, Ding, X, Kitagawa, Y, Chrispeels, MJ (2002) Origin of plant glycerol transporters by horizontal gene transfer and functional recruitment. *Proc Natl Acad Sci U S A* **99**, 14893-6.

Zelazny, E, Borst, JW, Muylaert, M, Batoko, H, Hemminga, MA, Chaumont, F (2007) FRET imaging in living maize cells reveals that plasma membrane aquaporins interact to regulate their subcellular localization. *Proc Natl Acad Sci USA* **104**, 12359-64.

Zelazny, E, Miecielica, U, Borst, JW, Hemminga, MA, Chaumont, F (2009) An N-terminal diacidic motif is required for the trafficking of maize aquaporins ZmPIP2;4 and ZmPIP2;5 to the plasma membrane. *Plant Journal* **57**, 346-55.

Zhang, J, Schurr, U, Davies, WJ (1987) Control of stomatal behaviour by abscisic acid which apparently originates in the roots. *Journal of Experimental Botany* **38**, 1174-1181.

Zhao, S, Guo, Y, Sheng, Q, Shyr, Y (2014) Advanced heat map and clustering analysis using Heatmap3. *BioMed Research International* **2014**, 6.

Zhou, L, Wang, C, Liu, R, Han, Q, Vandeleur, R, Du, J, Tyerman, S, Shou, H (2014) Constitutive overexpression of soybean plasma membrane intrinsic protein GmPIP1;6 confers salt tolerance. *Bmc Plant Biology* **14**, 181.

Zhou, Y, Setz, N, Niemietz, C, Qu, H, Offler, CE, Tyerman, SD, Patrick, JW (2007) Aquaporins and unloading of phloem-imported water in coats of developing bean seeds. *Plant, Cell & Environment* **30**, 1566-1577.

Zhu, D, Wu, Z, Cao, G, Li, J, Wei, J, Tsuge, T, Gu, H, Aoyama, T, Qu, L-J (2013) TRANSLUCENT GREEN, an ERF family transcription factor, controls water balance in Arabidopsis by activating the expression of aquaporin genes. *Molecular Plant* **4**, 601-615.

Zischewski, J, Fischer, R, Bortesi, L (2017) Detection of on-target and off-target mutations generated by CRISPR/Cas9 and other sequence-specific nucleases. *Biotechnology Advances* **35**, 95-104.

Zwieniecki, MA, Brodribb, TJ, Holbrook, NM (2007) Hydraulic design of leaves: insights from rehydration kinetics. *Plant Cell and Environment* **30**, 910-21.

Zwieniecki, MA, Melcher, PJ, Holbrook, NM (2001) Hydrogel control of xylem hydraulic resistance in plants. *Science* **291**, 1059-1062.